An integrated study of the magmatic products linked to the Cumbre Nueva Collapse, La Palma

IN SUBMISSION FOR PHD GEOLOGY – DEPT. EARTH AND PLANETARY SCIENCES, BIRKBECK, UNIVERSITY OF LONDON

An integrated study of the magmatic products linked to the Cumbre Nueva Collapse, La Palma

Simon Groom

I declare that the work presented in this thesis is my own.

……..

Simon Groom

ABSTRACT

The eruptive sequences linked to the *Cumbre Nueva Collapse* of La Palma's *Taburiente* volcano provide ideal material for a study that integrates field volcanology, geochronology, lava petrology and whole rock magmatic geochemistry. Lavas exposed in *Taburiente's El Time* region and on the post-collapse *Bejenado* volcano bracket the collapse and record this period's magmatic processes. Their integrated study allows us to reconstruct how a collapse interacted with the magma supply system. By studying the same lava flows using multiple techniques that address successively deeper parts of the magma supply we present an unusually well-constrained interpretation of the processes at depth.

Results of field and $^{40}Ar/^{39}Ar$ geochronological study indicate that the collapse (≈530 ka) ended a typical period of volcanic re-surfacing at *Taburiente's Paleo-Cumbre Nueva Rift.* It was followed by focused volcanism within the collapse structure producing the *Bejenado* volcano. This was a major, rapid, volcanic episode that included explosive phreatomagmatic activity as well as of voluminous, effusive lava emplacement. Its physical volcanology was in part controlled by magmatic evolution, with products ranging from basanites to tephri-phonolites.

Petrological study indicates that dynamic collapse-related processes took place within the magma reservoir system throughout this period, in reservoirs located in the lithospheric mantle. Reservoir processes included the disruption of cumulates, super-saturated crystallisation of feldspar and clinopyroxene, mixing between primitive and evolved magmas, and assimilation of amphibole-bearing lithologies.

Whole rock elemental and isotope (Sr, Nd, Pb) geochemistry results indicate that most of *Bejenado's* eruptive products were hybrids between two magma batches with contrasting source signatures in a major ongoing reservoir process. The more primitive of these batches had an unusually depleted isotope signature for La Palma lavas, while the more evolved, HIMU-dominated, magma had high incompatible element contents. The unusual depleted signature indicates that the collapse affected the deepest part of the magma-supply system.

ACKNOWLEDGEMENTS

Three figures have been central in shaping this thesis. First and foremost, I would like to express my gratitude to my primary supervisor Prof. Hilary Downes for her support, training and passion for the petrology of primitive magmatic rocks. The breadth of her experience in basaltic magmatism has been invaluable. Second is Dr. Andreas Klügel of the University of Bremen, a major authority on the petrology of La Palma's eruptive products, who chose to collaborate with a student who was working at a different university in a different country. Third is Prof. Gerald Roberts, Head of Birkbeck's Earth and Planetary Science Department. He helped steer my path through 21st century academia and made sure things got done.

A number of institutions provided key support in implementing this research. I would like to thank Birkbeck, University of London for funding my Graduate Teaching Assistantship and research. I would like to thank the Parque Nacional de la Caldera de Taburiente and its director Ángel Martínez who provided access, sampling permission, field assistance and local knowledge while working on *Bejenado*. I would like to thank NERC for the award of two grant-in-kinds allowing research access to SUERC, East Kilbride and NIGL, Keyworth. I would like to thank the Geological Society of London and Mineralogical Society of Great Britain and Ireland for funding my initial fieldwork, and Birkbeck's Tim Newling Fund for supporting later fieldwork. Topographic data used in this thesis was sourced from Spain's Instituto Geográfico Nacional.

Components of this study owe their existence to key individuals. Conny Spelbrink's logistical support and expert local knowledge of La Palma, including its volcanology, was essential in implementing all three field campaigns. Dr. Dan Barfod of SUERC and Dr. Ian Millar of NIGL have both collaborated on analytical portions of this project, and will be credited with co-authorship on any papers that result. Dr. Simon Drake came to La Palma on my second field campaign, bringing his boundless enthusiasm for field volcanology to basaltic magmatism.

I am grateful to the facilities where analytical work was conducted. I'd like to thank Dr. Andrew Beard (who was also my second supervisor from the project's second year), Hank Sombroek, Maz Iqbal, Prof. Matthew Thirlwall and Dr. Christina Manning for technical support while working in Birkbeck, University of London, UCL, and Royal Holloway, University of London's laboratories. Thanks also to Dr. Thor Hansteen and Dr. Julie Prytulak for insights and comments on the submitted thesis.

I would like to thank family and friends who provided editorial and personal support, particularly in the project's later stages. Lindsay Groom (my mother) and Daniella Bowker both proof-read this thesis and made significant contributions while it was in draft. Dr. David Kossoff and my fellow residents of Birkbeck office 6.11b provided for countless scientific discussions. Finally, I would like to thank Carla Groom, Miranda Kenny, Emma Liu and Candice Pettifer.

CONVENTIONS:

Certain conventions have been used throughout this thesis to aid comprehension. These are detailed below:

- Italics have been used for regional place names, allowing key localities and their descriptions to be found in body text at a glance. Where a geological feature has taken its name from a specific locality, the whole feature name has been italicised.
- This document has been written in Microsoft Word using an adapted version of its "Distinctive" stylesheet.
- Elsevier Harvard reference format in the Zotero referencing software has been used. One feature of this format is that in-line references are in alphabetical order of first author name rather than chronological order.
- The results chapters of this thesis have been written as separate academic papers ready for journal submission. This has resulted in some duplication of introductory material.

TABLE OF CONTENTS

TABLE OF FIGURES

Chapter 1 : INTRODUCTION

1.1 WHY STUDY THE GEOLOGY OF THE CANARY ISLANDS?

Whereas the Hawaiian chain has provided the key case study for investigating oceanic island volcanism in the Pacific region (Morgan, 1971; Wilson, 1963), in the Atlantic this role has been filled by the Canary Islands. Both are the product of intra-oceanic-plate magmatism, a category of igneous activity which includes the formation of seamounts and marine plateau, the products of all of which are typically described as Oceanic Island Basalts (OIB) in terms of their petrogenesis and geochemistry. However, in spite of the superficial similarities of the two archipelagos, there are significant differences between their tectonic settings, with the Canaries being the product of an environment with slower moving plates and lower magma supply rates (Carracedo et al., 1998).

During their shield-stage, the volcanic edifices that form individual Canary Islands are primarily composed of primitive lava flows. Such lavas are exceptionally information-rich geological materials, for example: 1) the complex morphologies and surface textures of individual lava flows provide a record of the conditions on the volcano during their emplacement, 2) porphyritic lavas are common and their phenocrysts provide significant petrographic and chemical information about crystallisation conditions and reservoir processes, 3) the whole rock trace element and isotope geochemistry of lavas provides a record of the processes occurring in the deepest part of the magma supply system.

During their shield-stage, the edifices of Canary Islands are primarily composed of primitive lava flows which are exceptionally information-rich geological materials. For example: 1) the complex morphologies and surface textures of individual lava flows provide a record of the conditions on the volcano during their emplacement, 2) porphyritic lavas are common and their phenocrysts provide significant petrographic and chemical information about crystallisation conditions and reservoir processes, 3) the whole rock trace element and isotope geochemistry of lavas provides a record of the processes occurring in the deepest part of the magma supply system.

Thus each of the many lava flows that together make up the island can potentially provide a detailed record of conditions from the period from mantle partial melting until magmatic emplacement as a lava flow. Furthermore, by taking samples of key lavas, the history of the island and the changing conditions in its magma supply system can be determined. Canary Island volcanoes can therefore provide us with tangible, physical materials and evidence allowing us to explore some of the deepest geologically accessible processes occurring within the Earth.

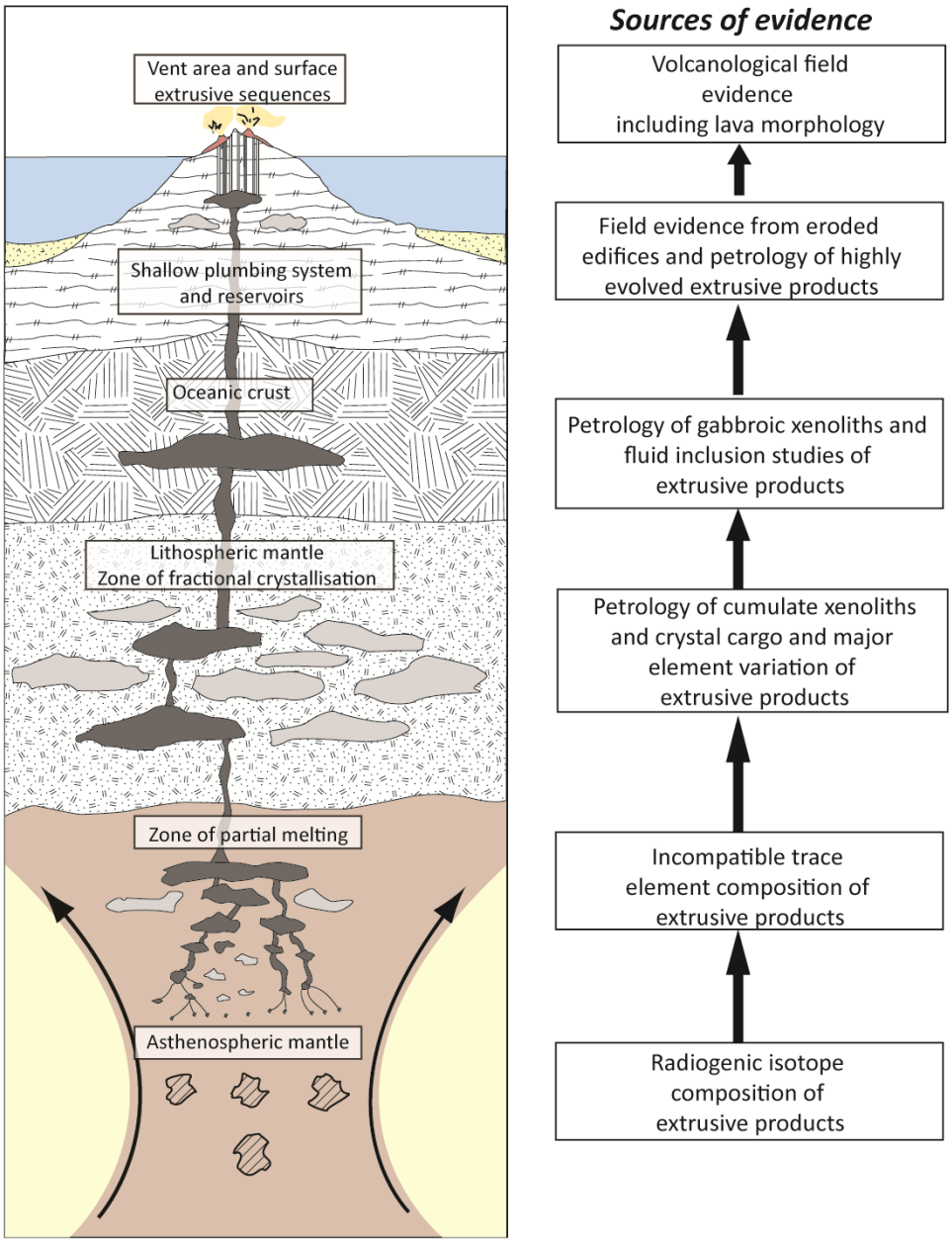

Figure 1-1 A schematic diagram of the magma supply system of the type of oceanic island common in the Atlantic, accompanied by a flowchart of the direct, non-geophysical, sources of evidence used to study its workings. The diagram is based on thermobarometric studies of characteristic islands (Klügel et al., 2005, Manconi et al., 2009).

1.2 The limitations of separate study of an oceanic island's field relations, petrology and magmatic geochemistry

Three sub-disciplines address an island's igneous system by studying direct, physical, sources of evidence (Figure 1-1): 1) the volcano and the uppermost part of the magma supply system are addressed by field volcanology, 2) the deeper reservoir system and processes within the lithosphere are the subject of igneous petrology, and 3) the zone of melt production in the asthenosphere is addressed by mantle geochemistry. There is considerable overlap between these sub-disciplines,

particularly between igneous petrology and the parts of the system that bracket the magmatic reservoirs from above and below, but they are nonetheless treated as distinct. However, in spite of these distinctions, much of this research is focused on extrusive igneous rocks (lava flows and pyroclastic deposits), with the same flows often treated in very different ways by studies that aim to address different parts of the system.

There are technical reasons why these disciplinary distinctions persist in spite of superficially addressing the same topic, particularly in terms of each approach's sample size requirements. Physical volcanology tends to focus on individual eruptions while broader field relations on oceanic islands are often highly complex, so such studies tend to address a sub-set of the total eruptive sequences in a given area. Conversely, in order for studies of mantle geochemistry to investigate subtle distinctions in the asthenospheric source it requires the analysis of moderate to large numbers (typically >25) of samples from separate lava flows. The trace element and isotopic results of these samples must all then be plotted against each other to allow differences between groups to be determined. However, such an approach is limited by the resolution at which an island has previously been geologically mapped. In the field, identifying and sampling lava flows that are demonstrably from different magma batches requires them to have already been characterised as discrete stratigraphic units. This comes up against the limitation that an oceanic island is the product of thousands of lava flows erupted from many vents, making fieldwork at this stratigraphic scale very demanding. Thus studies of mantle geochemistry rely either on lava samples from across a sufficiently wide area of the island to allow geochemists to confidently assume that the samples originated from separate eruptions, or requires high quality field relations covering the period of interest. The contrast in scales between volcanological and geochemical approaches often means that geochemical work only begins after other field studies are completed. An igneous petrological study, with its focus between these two extremes, often requires taking multiple samples from one eruption or thoroughly studying a small number of eruptions and in the process tends to bridge the requirements of the two approaches. In this sub-discipline whole rock geochemistry, petrography and mineral chemistry have traditionally been used to provide insights into the magma reservoir system.

Each of these approaches benefits to some extent from precise age determinations which can provide an absolute geochronological context. However, interpreting such data is acutely dependant on the quality of local field relations. Thus these two sub-disciplines are particularly closely related, and obtaining new geochronological data is often treated as an essential component of field studies.

Despite the technical issues, there are potential benefits to an approach that combines these separate fields. For example, differences in the phenocryst contents between lavas are the result of magmatic crystallisation and these differences are extremely useful for distinguishing lava units in the field. Understanding the petrological origin of these differences therefore has an impact on

planning and implementing field studies of a volcano. Furthermore, the radiogenic isotope composition of a magmatic rock provides the most fundamental fingerprint of its episode of melt production, and therefore has value in discriminating different phases of an island's activity.

This thesis attempts to provide an integrated study of an entire magma supply system, implementing these approaches concurrently, with the intention that together they will provide a more complete understanding of the system. The results are presented as sequential chapters in a vertical progression through an island's plumbing system, starting with surface observations, progressing through petrological constraints to source characteristics.

1.3 Giant landslides as an opportunity for integrated study

In order to make best use of such an approach it is preferable that the area studied should provide well exposed lavas with good preservation, that these lavas should be petrologically complex, and that they should have measurable variation in magmatic geochemistry. Such complexity is difficult to determine prior to analysis, but it is reasonable to suggest that periods when there are major changes in the whole island's structure are among the best to study for changes in the magma supply. The structural evolution of Canary Island volcanoes has been a focus of Juan Carlos Carracedo's landmark body of work (Carracedo, 1994, 1999, Carracedo et al., 1999b, 2001; Carracedo and Troll, 2013), and he has presented a qualitative model for how these edifices change over time (Carracedo, 1994).

In Carracedo's model, a Canary Island's main shield-building phase involves long periods of island growth as frequent discrete eruptions lead to the accretion of lava flows and pyroclastic deposits onto its flanks. Such steady growth phases are then punctuated by giant landslides, termed lateral collapses, which remove large parts of the volcanic edifice. These collapses are produced by within-island processes, with the vertical growth of lava flows and the lateral wedging from the intrusions that feed these eruptions together leading to an increase in edifice instability until eventually the volcano undergoes flank failure. The resulting collapse structures are among the most dramatic features of these islands, forming embayments with diameters on the order of 15 km.

Flank collapses allow us to study a volcano's inner workings. Firstly, the collapse embayment allows direct access to the shallow plumbing system, exposing the linear dyke swarms that feed an island's radial rift systems (Carracedo, 1994). Furthermore, a single collapse embayment results from the mass-wasting of ≈10-250 km³ of edifice (Carracedo et al., 1999b) and this leads to major changes to the volcano's stress distribution and the structure of its rift system, and with them it is likely to affect the magma supply system. There is no other period over the course of an island's growth when there is such a rapid and significant change in its conditions.

Studies of other Canary Islands such as El Hierro and Tenerife (Longpré et al., 2008, 2009; Manconi et al., 2009) indicate that these lateral collapses can be followed by the eruption of lavas that show marked changes in mineral content and petrology when compared to the lavas typically observed at that locality. Such changes indicate that the effects of the collapse extend at least into the reservoir system where fractional crystallisation and magmatic evolution take place. Such variation in island structure and lava composition is extremely desirable when planning an integrated interdisciplinary study of the type described above.

1.4 Why La Palma is an ideal case study for this approach.

Of the seven Canary Islands, the western island of La Palma is one of the youngest and has been subject to some of the least erosion. It therefore has one of the most complete geological records of all the islands. It is still within its shield-building stage (it last erupted in 1971), and the most common eruptive products observed here are sub-aerial lava flows, as opposed to the silicic ignimbrites common on Gran Canaria or on Tenerife's *Teide*.

The topography of the island is extremely steep, except in the island's central western region where the *Valle de Aridane* plain is surrounded by a major escarpment with 750m-scale cliffs (Figure 1-2). To the north of this region is the island's old *Taburiente* shield-volcano, to its south is the currently active *Cumbre Vieja* ridge-volcano. Previous research indicates that at "about 560 ka" (Carracedo et al., 2001) *Taburiente's* most active, southern, rift (the *Cumbre Nueva Rift*) underwent a giant landslide that removed its western flank and crest, mostly ending activity at *Taburiente*. The resulting collapse amphitheatre was then the site of the brief, rapid, growth of the post-collapse *Bejenado* volcano, following which eruptive activity ended in this part of the island.

This *Cumbre Nueva Collapse* provides a good case study for using lava flows to address changes in an island's magma supply system across the period of a giant landslide. Lavas exposed on the remains of the *Cumbre Nueva Rift* provide an opportunity to study the period immediately before the collapse, and a compositional baseline for any changes immediately afterwards in the lavas of the post-collapse *Bejenado* volcano. Because eruptive activity ended so soon after both the pre-collapse and the post-collapse phases, lavas from both sequences comprise young, fresh, well exposed flow-fields, providing an ideal opportunity for comprehensive field study and sampling. On other Canary Islands, such flows would typically have been buried by subsequent eruptions or destroyed by erosion.

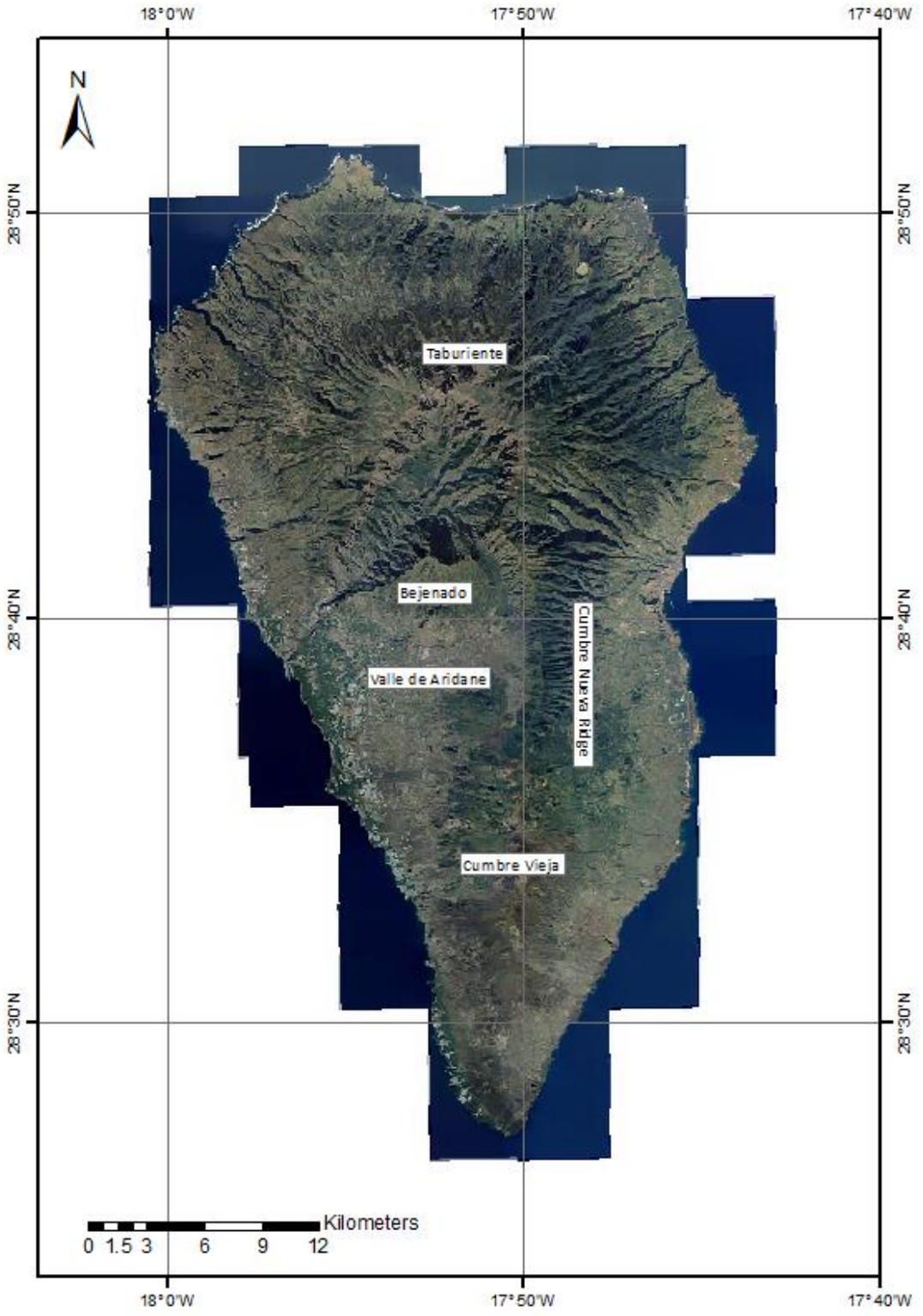

Figure 1-2 A composite satellite image of La Palma, data sourced from the Instituto Geográfico Nacional. The central western part of the island is ringed by major escarpments interpreted to result from the *Cumbre Nueva Collapse* of the *Taburiente* volcano and the erosional processes that followed it. This region is the focal case study for this thesis.

1.5 Aims and Objectives

This thesis aims to determine how La Palma's magma supply system responded to the changes in its volcanic edifice over the period of the *Cumbre Nueva Collapse.* This will be investigated through an exploratory study of the island's erupted products from the periods before and after its collapse. Within this aim the study has been designed to address unresolved issues in the geological evolution of La Palma.

By addressing multiple sub-disciplines in the process of doing this, this thesis aims to determine whether an integrated study provides a greater insight into the period and deeper parts of the magma supply than would be obtained through separate studies of each part of the system.

The objectives of this thesis are:

- To improve the understanding of the stratigraphy and physical volcanology of the post-collapse *Bejenado* volcano through extensive fieldwork.
- To use new $^{40}Ar/^{39}Ar$ dates to improve the geochronological constraints on the period prior to and following the *Cumbre Nueva Collapse*, including the duration of activity at *Bejenado* and bracketing the date of the *Cumbre Nueva Collapse*.
- To study the petrology and crystal cargos of *Bejenado's* lava flow fields to determine processes in the magma reservoir system in the period after the collapse.
- To compare the whole rock elemental and radiogenic isotope geochemistry of suites of pre-collapse and post-collapse lava flows to determine whether the collapse is accompanied by changes in the asthenospheric source signature.

Chapter 2 : LITERATURE REVIEW – WIDER CONTEXT

IGNEOUS PROCESSES IN THE CANARY ISLANDS AND THE SIGNIFICANCE OF LATERAL COLLAPSES

2.1 INTRODUCTION

This literature review is presented in two chapters, Chapter 2 is a *statement of problem* focused on theory and reviews the main forms of physical evidence from the Canary Islands, while Chapter 3 addresses the work directly relevant to our case study, central La Palma, and its magma supply and mantle source. Since this study aims to integrate different approaches to Canary Island volcanism, it is necessary to identify how the different sub-disciplines fit together. Chapter 2 therefore includes sections on geology, petrology, and mantle geochemistry and then discusses how they are all likely to be affected by the central event of this study: a major lateral collapse.

2.2 THE GEODYNAMIC SETTING OF THE CANARY ISLANDS

The hotspot model was first developed as an explanation of the Hawaiian island chain (Wilson, 1963), but its proposal was followed by persistent debates about how applicable it was to the Canary Islands (Anguita and Hernán, 2000; Carracedo, 1999; Zaczek et al., 2015). The mantle plume hypothesis of Morgan (1971) developed from the hotspot model and this provided a broader geodynamic explanation for many igneous processes located away from plate margins. This hypothesis allowed an ocean island chain to be treated as the product of two primary controls: 1) plate movement rates, and 2) exotic asthenospheric conditions (particularly elevated temperatures and unusual mantle source compositions). Together, these could explain the broad characteristics of island structure and magmatic composition as observed in the Hawaiian archipelago. There were obvious parallels to this scenario in the Canary Island chain (Figure 2-1), where the seven islands also formed a line, and along which there was an age progression between the oldest in the east to the youngest to the west (Abdel-Monem et al., 1972).

However, Anguita and Hernán (1975) presented key differences between the settings of the two island chains: 1) the African plate appeared to be stationary, unlike the rapidly moving Pacific plate 2) that the Canary Islands were in close proximity to the African passive margin, unlike the remote central Pacific of Hawaii and 3) that the role of this continental material would be exacerbated by the Moroccan Atlas Mountains (the largest range in Africa) which were nearby. Together these observations allowed them to propose that there were key tectonic differences between the Canary Islands' setting and the Central Pacific of Hawaii. To explain these features they proposed an alternative model where the Canary Islands resulted from a fracture propagating westward through the lithosphere. However, while this model was consistent with existing data, it largely failed to provide a superior explanation for any observations left unexplained by the hotspot model.

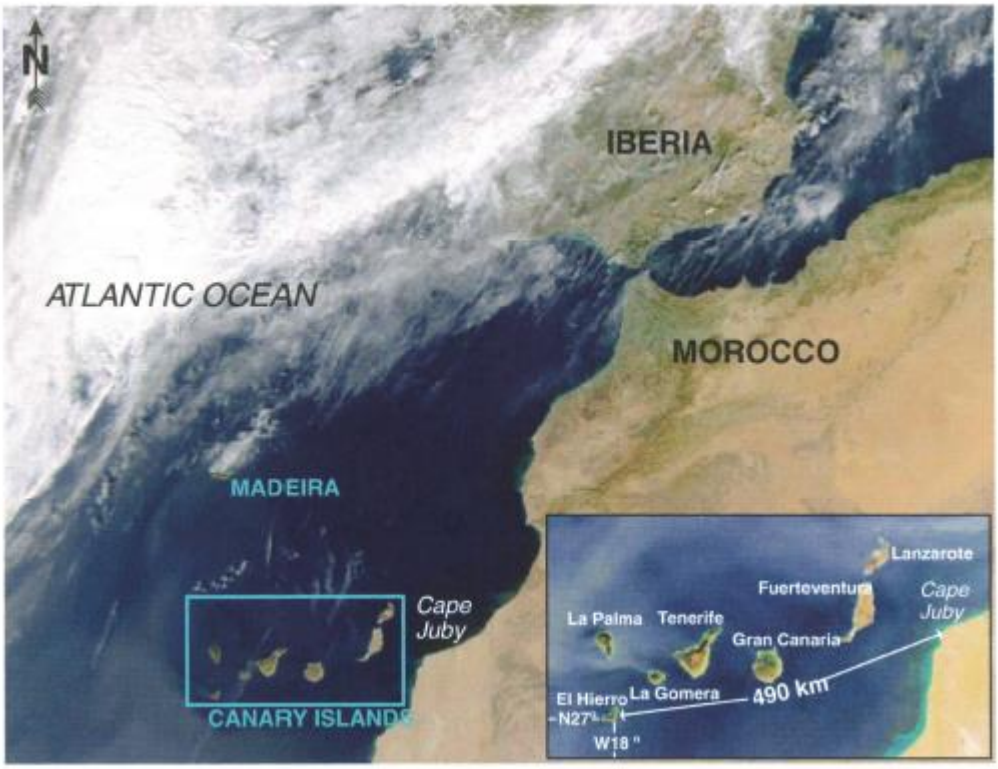

Figure 2-1 A satellite image of the Canary Islands archipelago and its position on the African continent's passive margin (from Carracedo et al., 2013).

In the 1990s a series of papers fine-tuned the hotspot model for the Canary Islands' specific setting (Carracedo et al., 1998; Carracedo, 1999; Carracedo et al., 1999b). In the preceding years the geology of islands in the Hawaiian chain had been characterised in terms of an internal evolutionary model and some key newly identified features (Clague and Dalrymple, 1988) in individual Canary islands provided useful parallels (Carracedo, 1999). In both chains an individual island's lifecycle was described as a staged evolutionary progression: 1) an initial effusive-dominated shield-building stage after each island emerged sub-aerially, 2) a following gap period of little eruptive activity during which erosion dominated, 3) a post-erosional phase when volcanism was rejuvenated but in which eruption rates and total eruptive volumes were lower than in the shield-building stage. In both chains this late stage was accompanied by a change in the composition of erupted magmas, with eruptions on Hawaiian islands changing from tholeiitic to more alkalic compositions, and in the Canary Islands this period was the first to be dominated by the eruption of highly differentiated magmas.

These studies took the tectonic contrasts of the two setting into account when interpreting these observations, specifically the differences between the African passive margin relative to the central Pacific. The Canary Islands are situated on old, thick, Jurassic, oceanic crust, leading to very low subsidence rates when compared to the Hawaiian islands, where rapid island growth is typically followed by isostatic subsidence (Carracedo, 1999). Furthermore, the Canaries are very close to the African continental margin and with it the sub-continental mantle provided a convenient

explanation for the complexities observed in magmatic composition[1], with new models of sub-continental edge-driven convection explaining the composition of lavas in the Eastern islands (King and Ritsema, 2000).

The strongest evidence in favour of a hotspot model for the Canaries was provided by the growing body of geochronological data (Abdel-Monem et al., 1972; Geldmacher et al., 2005; Geldmacher and Hoernle, 2000; Guillou et al., 2001). In the Hawaiian chain the shield-building stage of a given island typically lasted about 1 Ma (Carracedo, 1999) after which focused volcanism tended to migrate to a new centre. This was inferred to be more proximal to the proposed hotspot, and therefore a result of displacement of the Pacific plate. In the Canaries the early focused phase on each island appeared to last much longer (Figure 2-2A): the edifice-building stage on Tenerife had been ongoing since at least 8 Ma (Thirlwall et al., 2000), while the eastern island of Lanzarote emerged at 15.5 Ma and yet was subject to a major basaltic eruption in historic time (Thomas et al., 1999).

The volcanic focus of the Canary Islands appeared to have been progressing westward from the African coast for 20 Ma, but the rate of its migration was much slower than at Hawaii and after the long shield-building stage finished, an island's last low-activity eruptive phase continued almost indefinitely (Carracedo et al., 1998). A systematic geochronological study (Geldmacher et al., 2005) attempted to resolve this by including neighbouring island chains and dredge samples from local seamounts. This concluded that activity in the Canaries had been ongoing since 68 Ma, and that the distribution of local islands and seamounts over this period resulted from a stationary mantle source and the African plate rotating (0.20° ±0.05°/Ma ENE) above a single Euhler pole (Figure 2-2B). The distribution of islands within other chains on the African plate (Tristan de Cunha, St Helena) was also found to be consistent with this model of rotation.

In light of these studies, the Canary Islands are best described as a hotspot island chain from an environment with little plate movement and a lower productivity asthenospheric source than that beneath Hawaii. This interpretation was compatible with the growing amount of data on regional magmatic geochemistry. This tectonic setting and resulting style of oceanic island volcanism is not unique, and has parallels with Tristan de Cunha, Madeira, the Cape Verde islands and St Helena, which will be referred to as "Canarian-type" oceanic islands in this thesis. Without rapid plate movement, other controls need to be invoked to explain the lifecycle of the islands and some of their key features, such as why the volcanic focus appears to move between them erratically.

[1] 2.5 Mantle geochemistry of the Canary Islands. pp.31-36.

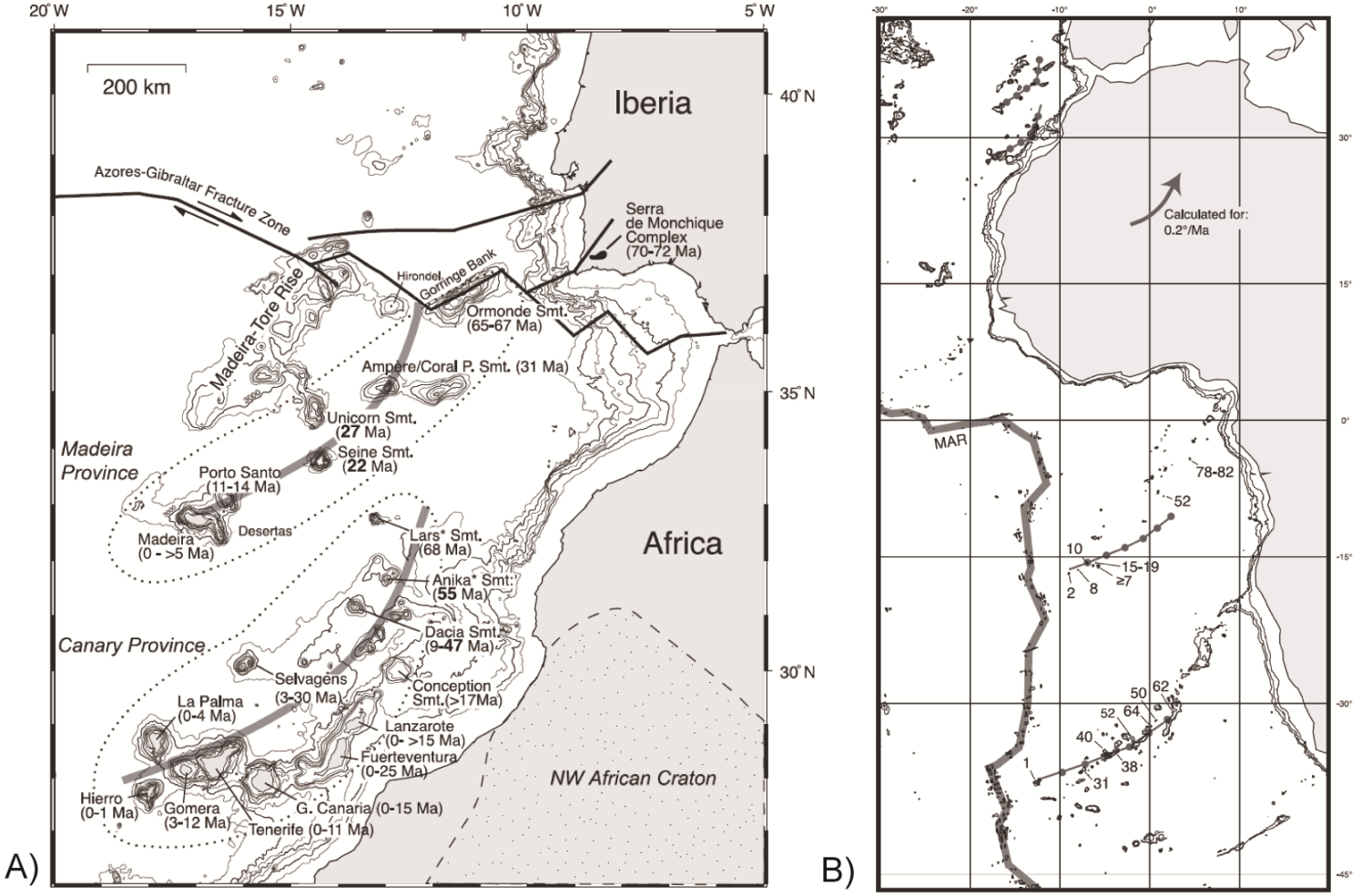

Figure 2-2 A) Published age ranges of representative dated rocks sampled from the Canary Islands, local marine volcanic edifices, and neighbouring island chains. B) Directions of inceasing age progressions of hotspot tracks on the African Plate, with resulting composite rotatonal trend of the entire plate over this period. Illustrations from Geldmacher et al. (2005).

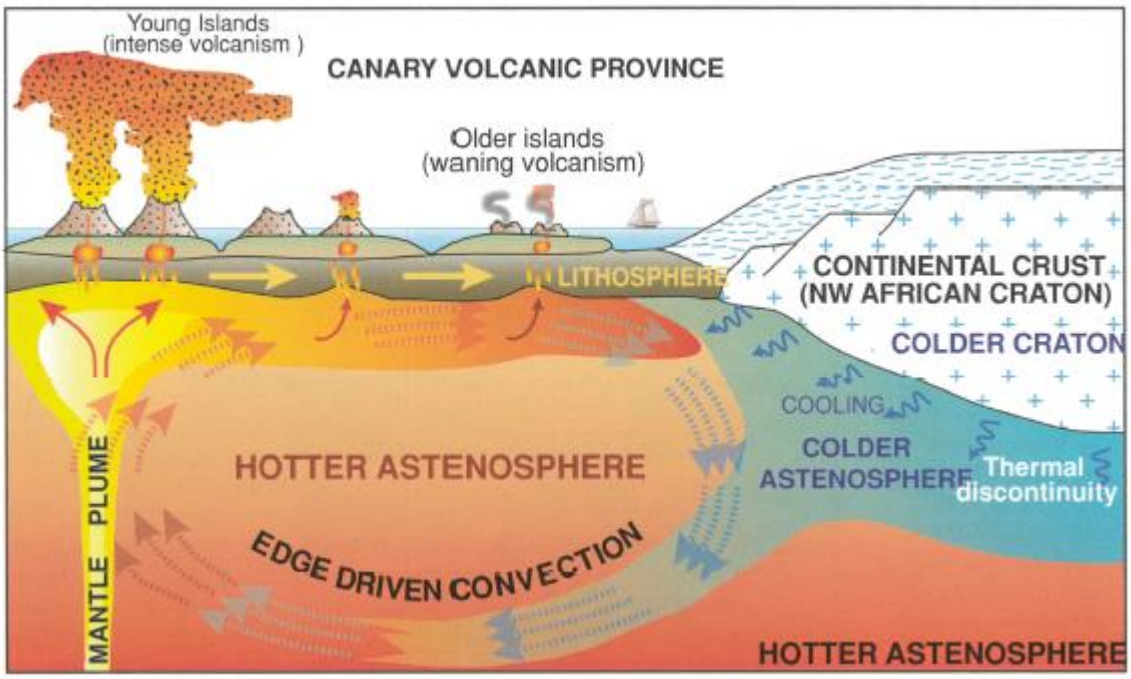

Figure 2-3 A composite geodynamic model invoking both hotspot activity and edge-driven convection to explain the primary features of oceanic island volcanism in the tectonic setting of the Canary Islands, the spelling of "asthenosphere" is as it was in the source publication of the diagram (Carracedo et al., 2013).

2.3 The evolution of volcanic edifices on Canarian-type oceanic islands

Carracedo (1994) proposed an endogenous model for how edifice morphology controls volcanism during the shield-building stage of a Canarian-type oceanic island, based on observations largely taken from the western Canary Islands. He observed that dyke swarms are a characteristic feature of Canary Island volcanism. The Canary Islands have a well-developed network of groundwater mines (gallerias) and within them suites of parallel dykes were often observed, as well as in an island's deeply eroded areas (notably on La Palma and Fuerteventura). Furthermore, the trend of these dyke swarms was found (on La Palma, Tenerife, El Hierro and Lanzarote) to run parallel to the main trend along which volcanic vents were distributed. These vents tended to be arranged in prominent lines and were situated on top of polygenetic volcanic ridges. It was proposed that together these features represented a form of volcanic rift system and that once such a system had developed it would become a major control on the morphology of the island. Canarian-type islands were often found to exhibit a triangular morphology (Tenerife, El Hierro), and this was interpreted as resulting from the intersection of multiple rift zones.

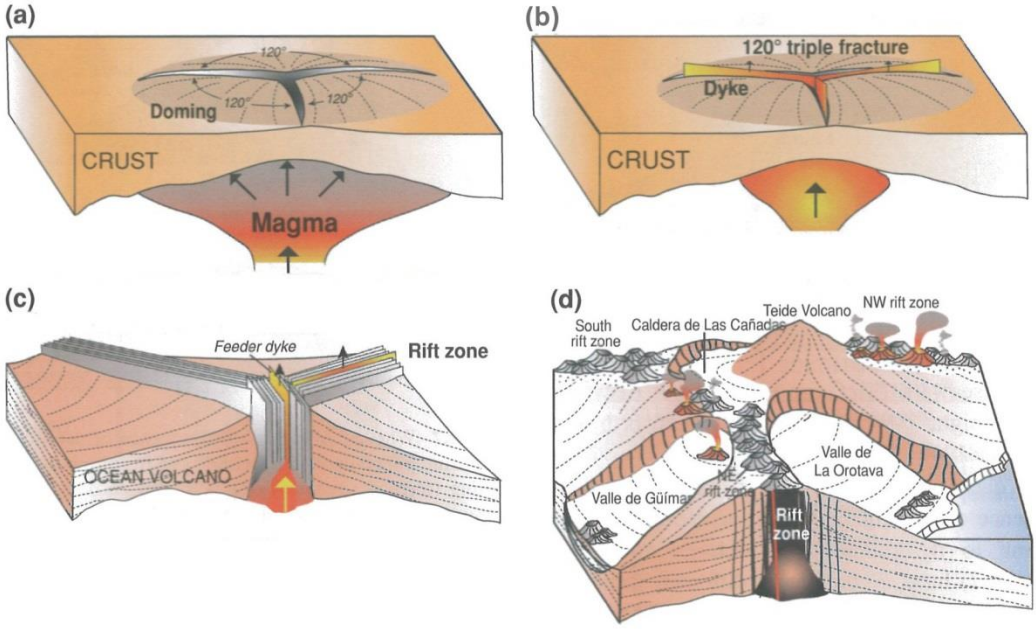

Figure 2-4 A schematic model for the development of the three-armed rift systems, each spaced at ≈120°, that are common in the Canary Islands, presented by Carracedo (1994), figure adapted from Carracedo & Troll (2013). The sequence involves: A) impinging of the hotspot on oceanic crust produces uplift and doming which results in 3 primary planes of weakness, B) initial dyke injection follows these planes of weakness, C) ongoing volcanism leads to the development of a planar dyke swarm, which constrains subsequent magma migration and results in volcanism focusing at rifts, d) the resulting oceanic island possesses a three armed structure, with lateral collapses taking place perpendicular to these rifts.

Carracedo (1994) (Figure 2-4) proposed that the rifts formed as a result of the initial distribution of extensional stresses in a domed or conical edifice, which would be expected to align in a least-effort arrangement and intersecting at 120°. Eruption-feeding dykes would be injected parallel to these planes and this trend would lead the edifice to become progressively more anisotropic with each dyke injection reinforcing this structure. Eventually dykes would need to be injected as blades between sheets in order for magma to ascend to the top of the edifice. This model was subjected to extensive synthetic analogue modelling through fluid injection experiments on gelatine cones (Walter and Troll, 2003) and, while the initial dyke orientations that resulted were found to be largely radial rather than triple-armed, the authors of the study argued in support of the model.

Carracedo also attempted to explain the vast escarpments found in the western Canary Islands within his model. These escarpments tended to be horseshoe-shaped, with kilometre-scale headwalls and tens of kilometres in length. Examples of these structures had been identified on La Palma (*Valle de Aridane*), Tenerife (*Guimar, Orotava*) and El Hierro (*El Golfo*) and in each case they were situated perpendicular to a pre-existing polygenetic ridge. Carracedo (1994) invoked a mechanism where a giant gravitational landslide produced such a structure by removing the unstable flank of an active rift zone. Within the rift-zone model, ongoing eruptions would cause the flank instability of individual rift zones to increase over time as lavas accreted to its walls and feeder dykes wedged apart its axis.

In addressing both the distribution of vents and dykes as well as the common escarpments, Carracedo's model appeared to explain much of the morphological features of shield-stage Canarian-type Islands. As an edifice matured its rift zones would become increasingly defined and a growing number of collapse structures would be visible on its flanks.

This interpretation was not universally accepted, with debate initially focused on how particular escarpments formed in the western Canary Islands. An alternative explanation for the *Las Cañadas Caldera* on Tenerife (Martí et al., 1997; Martí and Gudmundsson, 2000) was proposed where a collapse caldera formed as a result of the evacuation of a shallow magma chamber, with the *Teide* stratovolcano then infilling the resulting cavity. However, such a scenario would be expected to lead to an associated major sequence of highly differentiated explosive deposits and these were not as common as would be expected (Carracedo et al., 2007). Furthermore, more and more escarpments across the islands seemed to fit the giant landslide model when studied in detail (Carracedo et al., 1999b, 2001). This was supported by offshore bathymetric studies (Hunt et al., 2011, 2013a, 2013b; Masson, 1996; Urgeles et al., 1999) which identified debris avalanche fans on the ocean floor extending out from these proposed collapse structures.

Recent reviews (Carracedo and Troll, 2013) have continued to support Carracedo (1994). In particular it has proved robust in providing an explanation of the period between an oceanic island's earliest collapses and when it reaches peak volume. However, it does not explain all the major characteristic features of these islands, such as why there is an erosional gap period when volcanism briefly stops, or why after this central stratovolcanoes form from sequences of highly differentiated explosive deposits. These stratovolcanoes are primary features of Gran Canaria and Tenerife. Whether such later features result from endogenous controls of a similar type to the rift system (Carracedo et al. (2013) invokes a density filter as the cause of the differentiated stratovolcanoes) or from larger scale tectonic-type processes, they nonetheless indicate there are some significant unknown controls acting over the course of the growth of Canarian-type islands.

2.4 THE MAGMA TRANSPORT AND RESERVOIR SYSTEMS OF CANARIAN-TYPE OCEANIC ISLANDS

Since the beginning of the 21st century, research focusing on the evolution of the magma transport and reservoir system of active volcanoes has significantly expanded. This has largely addressed dynamic processes as opposed to simple fractional crystallisation (Cashman and Sparks, 2013). For example, increasingly accurate volcano seismology has allowed the detailed three dimensional reconstruction of the magma movement pathways (Paulatto et al., 2012) that contributed to individual eruptions, while rapid improvements in the microanalysis of crystal cargoes have allowed magma storage conditions to be decrypted for specific eruptive units. Such approaches have provided quantitative constraints on processes occurring during crystal growth, such as depths and pressures of rim formation from clinopyroxene-melt (cpx-melt) thermobarometry (Masotta et al.,

2013; Putirka, 1999; Putirka et al., 2003), magmatic $_{P}H_2O$ from plagioclase composition (Waters and Lange, 2015) or magma-mixing timescales from uranium series disequilibrium (Johansen et al., 2005) of the whole crystal population of a lava. Used in combination, volcano seismology and quantitative petrology have allowed volcano igneous plumbing systems to be treated as a combined area for new research.

Unfortunately, the low eruption frequency characteristic of Canarian-type volcanism has meant that this combined approach can only be applied in rare, opportunistic, circumstances such as the recent 2012 eruption on El Hierro (Longpré et al., 2014) in the Canaries or the 2014 -2015 eruption on Fogo in the Cape Verdes (González et al., 2015). As a result this combined-seismic approach has largely been used to confirm magma plumbing models developed from historic and pre-historic lava flows (Klügel et al., 2015). In the western Canary Islands, the most commonly applied quantitative petrological techniques are: 1) cpx-melt thermobarometry and 2) fluid inclusion thermobarometry (Hansteen et al., 1998). These two barometric techniques routinely yield different average depths (Galipp et al., 2006; Hildner et al., 2012; Klügel et al., 2005) which have been interpreted as depths of long-term magma crystallisation and short-term ponding and stagnation, respectively. There has been a growing consensus (Klügel et al., 2015) that the main reservoir system exists as a horizon of small volume sills in the lower oceanic crust and upper lithospheric mantle, at depths of between 8 and 20km (Figure 2-5). An implicit feature of this model of small volume sills emptied in the course of infrequent eruptions is that each flow-field will be the product of a discrete sequence of individual events from melt formation, through ponding and onto eruption. Furthermore, seismic data indicate that there is considerable potential for lateral magma movement at this depth during an eruption's onset.

However, despite this increasingly well constrained model of depth, transport and reservoir geometry, relatively little recent work has been focused on visualising the magmatic processes occurring within these reservoirs. For understanding such systems traditional petrological studies of cumulate xenoliths (Barker et al., 2015; Klügel, 1998; Schmincke et al., 1998) remain the best current source of evidence. Unfortunately, in the western Canary Islands previous work has emphasised oceanic crustal xenoliths (Schmincke et al., 1998), or treated mantle xenoliths mainly as a host vehicle for fluid inclusions (Hansteen et al., 1998; Klügel et al., 1997). Nonetheless, a major population of mafic cumulate xenoliths is being identified and described on La Palma (Barker et al., 2015) and may provide insights into the production of evolved melts.

2.5 Mantle geochemistry of the Canary Islands

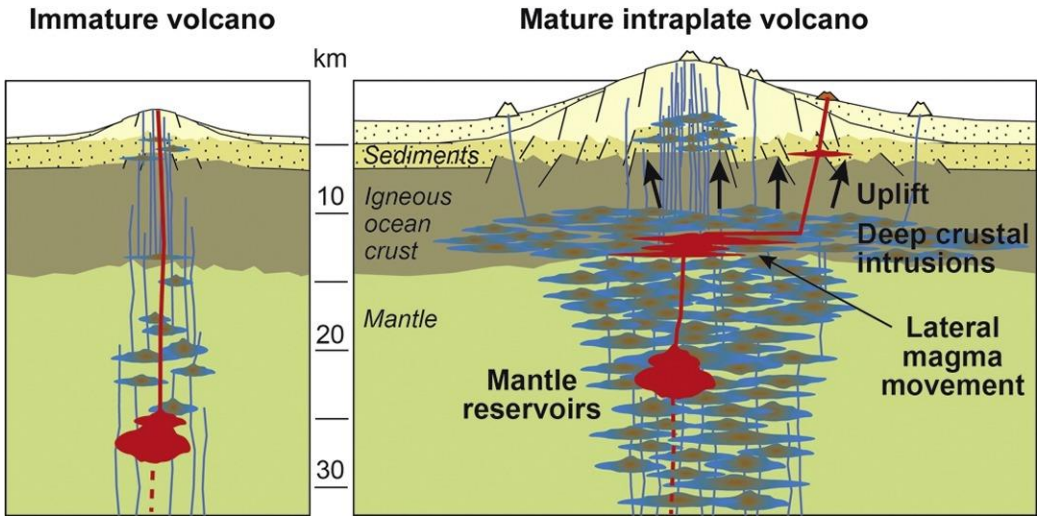

Figure 2-5 A model (Klügel et al., 2015) for the magma reservoir system and transport pathways of a low-eruption frequency Canarian-type oceanic island, visualised as a network of ephemeral small volume sills. Seamounts are assumed to be immature, while subaerial Canary Island volcanoes are all classed as mature intraplate volcanoes.

AN INTRODUCTION TO MANTLE GEOCHEMISTRY

Since 1980 the amount of data from studies of magmatic geochemistry has grown dramatically, and a geodynamic interpretation has developed for what the composition of intra-plate lavas tells us about asthenospheric processes and convecting mantle-plumes (Zindler and Hart, 1986). Within a magmatic system the ratios of an element's radiogenic and non-radiogenic isotopes (eg $^{87}Sr/^{86}Sr$) are believed to be invariant over the course of partial melting and magmatic crystallisation. The ratios of such isotopes within a lava therefore provide the best signature of the mantle source rock from which its magma partially melted. Of the possible isotope systems, Sr, Nd and Pb were among the first to become routine for the analysis of magmatic rocks and their ratios were interpreted as dimensions in multi-element radiogenic isotope ratio space. This provided a virtual field in which all rocks could be interpreted.

Interpreting analyses from world-wide oceanic island basalts, the variation in isotopic compositions could be resolved into the product of five vectors in this isotope ratio space. These vectors were interpreted as end-members in the mantle and were described by Zindler and Hart (1986) as:

1) DMM – Depleted MORB Mantle: a source depleted in radiogenic isotopic components that is likely to be located at shallow depths. This is interpreted as the result of long term, large-scale, melt-production at mid-ocean ridges.
2) PREMA/FOZO – Prevalent Mantle: a very common intermediate mixture residing between all other components, that has typically been interpreted as the mantle's dominant composition.
3) HIMU – High μ: a component with high initial $^{238}U/^{204}Pb$ (μ) ratios, resulting in extreme time integrated enrichment in radiogenic Pb, interpreted as the product of the isotopic evolution of ancient oceanic crust subducted at 1.5-2.0 Ga.

4) EM I – Enriched Mantle 1: the first of two distinct components which resemble the bulk composition of continental lithosphere, exhibiting enrichment in radiogenic isotopic components. This is typically interpreted as the product of assimilation of material from the lower continental crust into the melt source.
5) EM II – Enriched Mantle 2: the second of the enriched, continental lithospheric, components. This is typically interpreted as the product of magmatic recycling of continentally derived sediment.

These mantle-components are considered to be large-scale physical reservoirs located separately within the mantle. The isotopic compositions of individual magmas would result from partially melting various mixtures of these components. The differences in isotopic composition between these reservoirs would have originated in stages since their paths each began to diverge from that of the early chondritic Earth, with each component subsequently following a separate path of time-integrated isotopic evolution (Zindler and Hart, 1986). Convective mantle plumes were invoked in the origin of the latter four components.

As analytical techniques improved and new radiogenic isotope systems became available (radiogenic Os (Marcantonio et al., 1995) and Hf (Geldmacher et al., 2010) were soon added to the model) these components were still found to describe global compositional variation. Additionally, analyses of stable isotope (O) and noble gas isotopic compositions (He, Ar) of magmatic phenocrysts (Hilton et al., 2000; Thirlwall et al., 1997) were soon used in combination with this framework to determine the significance of primodial mantle processes and provide evidence of crustal recycling. However, the coupling of such phenocryst-hosted isotope systems to the whole-rock radiogenic isotope based end-members was not quite as robust due to the possibile role of xenocrystic material and magma-mixing in their origin. Incompatible trace elements had long provided a major source of information about mantle geochemistry, and when united with radiogenic isotope data they provided a detailed insight into the composition of these components (Hofmann, 1988; Sun and McDonough, 1989). The ratios of such elements are mostly invariant over the course of magmatic evolution, comparable with isotope ratios, but their subtle chemical differences allowed them to also be used as a tracer of partial melting processes.

Mantle geochemistry of the Canary Islands

Analyses of the Pb, Sr and Nd isotopic composition of Canary Island lava flows have been found to form arrays between three of the proposed end-members (Gurenko et al., 2006). Geographically at the centre of the chain is Tenerife and its lava compositions are dominated by the HIMU component (Simonsen et al., 2000). Analyses of lavas taken from the islands to Tenerife's east and west form two separate mixing trends with two other end-members. Towards the African margin magmatic compositions show increasing evidence of HIMU mixing (Thirlwall et al., 1997) with the EM I component (proposed to be continentally-derived), while to the west (towards the Central Atlantic)

the compositions show involvement of a depleted DMM component (Gurenko et al., 2009b; Praegel and Holm, 2006).

The HIMU component found throughout the Canary Islands was the focus of a significant body of research (Hoernle et al., 1995; Simonsen et al., 2000; Thirlwall, 1997). Hoernle et al. (1995) used seismic imaging, regional tectonics and isotope geochemistry to propose a common origin for the volcanism across a much larger region that included the Canary Islands, neighbouring Madeira, the Western Mediterranean and Italy, and even sub-alpine France and Germany's Central European Volcanic Province. All this region's volcanism was interpreted as the product of a widespread, sheet-like, body of hot upwelling mantle that could be identified in tomographic images, and all magmatic compositions from this region were shown to converge on a common HIMU-type component. Thirlwall (1997) suggested that the global HIMU component was more complex than previously believed. While it was traditionally ascribed to a single source originating from the isotopic evolution of oceanic crustal slabs subducted at 1.5-2.0 Ga (Hofmann and White, 1982), it could equally result from an ongoing process involving the later subduction of younger slabs (as young as 400 Ma) that retained an element of this component through recycling. Such an origin would only be identifiable by the presence of anomalously low $^{207}Pb/^{204}Pb$ ratios, and this was demonstrated to be the case for Canary Island lavas (Simonsen et al., 2000) among those of other Atlantic regions. Widom et al. (1999) demonstrated that across the Canary Islands this "young-HIMU" component was accompanied by an Os isotope signature that was among the most radiogenic found globally, consistent with the subduction recycling of young oceanic crust.

The combined database of isotopic analyses from Canary Island magmatic rocks subsequently grew largely through two types of studies: 1) cross-archipelago comparisons with small numbers of samples per island (Day et al., 2010; Geldmacher et al., 2010; Gurenko et al., 2006; Widom et al., 1999), and 2) within-island studies with multiple samples from several edifices aimed at determining an island's internal variation (Galipp, 2005; Praegel and Holm, 2006; Simonsen et al., 2000; Thirlwall, 1997). In general, the isotopic variation identified between islands (Gurenko et al., 2006, 2009b) was found to be of a larger scale than that exhibited over the course of an individual island's growth (Day et al., 2010).

Multiple studies of Gran Canaria focused on the Canary Islands' EM I component, with debate over whether this represented an oceanic crustal component assimilated after magma genesis (Thirlwall et al., 1997) or a relic of the African sub-continental root present in the upper mantle (Gurenko et al., 2009a; Widom et al., 1999), with edge-driven convection proposed as a mixing mechanism to introduce this into the magmatic source (Geldmacher et al., 2005). In the younger, western islands, El Hierro provided evidence for the strongest DMM signature (Day et al., 2010), and this appeared to persist over the lifespan of the island. El Hierro was interpreted as the product of a mixed source

composed of 75% DMM to 25% young-HIMU, while the slightly older La Palma was interpreted as a mixture of 30% DMM to 70% young-HIMU (Gurenko et al., 2009b).

Debates over the source lithology of Canary Island magmas: pyroxenite or peridotite?

Sobolev et al. (2005) introduced a further variable into studies of the asthenospheric source of intra-plate magmas by proposing that, in olivine hosted melt inclusions in primitive magmatic rocks, elevated Ni contents could provide a record of asthenospheric mineralogy. They proposed that in melts from a peridotite source any variation in Ni contents should be buffered by ambient olivine. Therefore the observed variation in Ni contents determined in globally-sourced primitive melts was best explained by partial melting of asthenospheric "reaction pyroxenite" — this proposed mantle rock would form through the recrystallisation at depth of eclogite, which itself formed from the subduction and recrystallization of oceanic crust. Later work (Sobolev et al., 2007) developed a tool using relative proportions of Ni, Ca, Mn, Cr and Fe compositions in forsteritic olivine from which they determined mixing ratios of reaction pyroxenite and peridotite in a given magma's asthenospheric source.

In the Canary Islands, the shared origin through recycling of subducted oceanic crust proposed for both the new "reaction pyroxenite" source and the isotopic young-HIMU component led source-pyroxenite to be invoked in the mantle models for some purely isotopic studies (Day et al., 2009, 2010). However, studies emphasising olivine compositions of Gran Canaria lavas found pyroxenite/peridotite proportions derived from olivine compositions to only weakly co-vary with local radiogenic isotope variation (Gurenko et al., 2009a). This led them to invoke varying proportions of pyroxenite to peridotite in the isotopic end-members. Furthermore, the application of oxygen isotopic analyses and archipelago-wide studies to these problems has led to increasingly complex explanations (Day et al., 2012; Gurenko et al., 2009a, 2009b, 2011, 2012). It is likely that further work will provide fresh insights into these issues.

Discussion

The large and growing body of magmatic geochemical data, particularly the results of radiogenic isotope studies, has made the asthenosphere under the Canary Islands one of the most thoroughly characterised regions in the world. Its considerable complexity is well described by the global geochemical models (Zindler and Hart, 1986) that have been developed to interpret such variation. However, these end-member models are largely visualised in the abstract and it is common for our interpretation of this data to be independent of our understanding of the geology of individual Canary Islands. Specific islands are often treated as passive receivers of magma batches produced from these source-components. How these sub-lithospheric processes relate to the islands' geological expression has not often been addressed, and yet this asthenospheric source appears to form the root of each edifice's magma-supply system.

2.6 GIANT LANDSLIDES AND THE MAGMA SUPPLY SYSTEM

With strong evidence that the lifecycle of Canarian-type oceanic islands includes periodic giant landslides, the effects the accompanying rapid changes in edifice stress conditions have on the processes within the volcano's magma supply system have been inviting topics for further study. These studies have broadly focused on two approaches: 1) the development of numerical models of the effect of changing edifice conditions on underlying magma bodies, and 2) empirical studies of post-collapse eruptive sequences on oceanic island and island arc volcanoes.

The numerical studies, which mainly consist of 3D and 2D models of the effect of the load of a conical edifice on a spherical magma body at depth, have addressed three specific questions: what are the effects of changing edifice loading on 1) the controls on magma ascent (Pinel and Jaupart, 2000), 2) processes in the magma reservoir zone (Pinel and Jaupart, 2003, 2005), and 3) processes in the asthenospheric source (Smith, 2000).

On the simplest level, Pinel and Jaupart's (2000) work was based on reducing the buoyancy control on magma ascent beneath a planar surface to the following formula, and then adjusting this model's constraints based on different proposed edifice conditions (Figure 2-6):

$$\rho_{crit} = 2\frac{\Delta Po + \rho_c g h}{g(h_v(1+2v)+2h)}$$

Where ρ_{crit} is the critical density required for magma to ascend, *g* is the acceleration due to gravity, *h* is the depth of the magma body beneath the crustal surface, ΔPo is the magmatic overpressure of the magma body with respect to its surroundings, $\rho_c$is the density of the host lithology, for which the elastic medium is characterised by Poisson's ratio (*v),* and the height of the volcanic edifice (h_v). This equation and the accompanying diagram provide the main variables and mathematical model that underpins this, but equations derived from this are presented in considerably greater detail (Pinel and Jaupart, 2000, 2003, 2005) in this body of work.

Among the main implications of such mathematical models is that edifice destruction is always accompanied by sufficient pressure changes as to result in a decrease in reservoir pressure, a change that should increase the likelihood of magmatic ascent as well as reduce the limits controlling the eruption of dense magmas. The implications for the asthenospheric source are more ambiguous. However, little distinction is drawn in these models between island arc settings as distinct from oceanic islands, and this may present limitations on the model's applicability. The makeup of magma reservoir systems in these settings is likely to be very different and the scales of edifices involved differ between them by orders of magnitude.

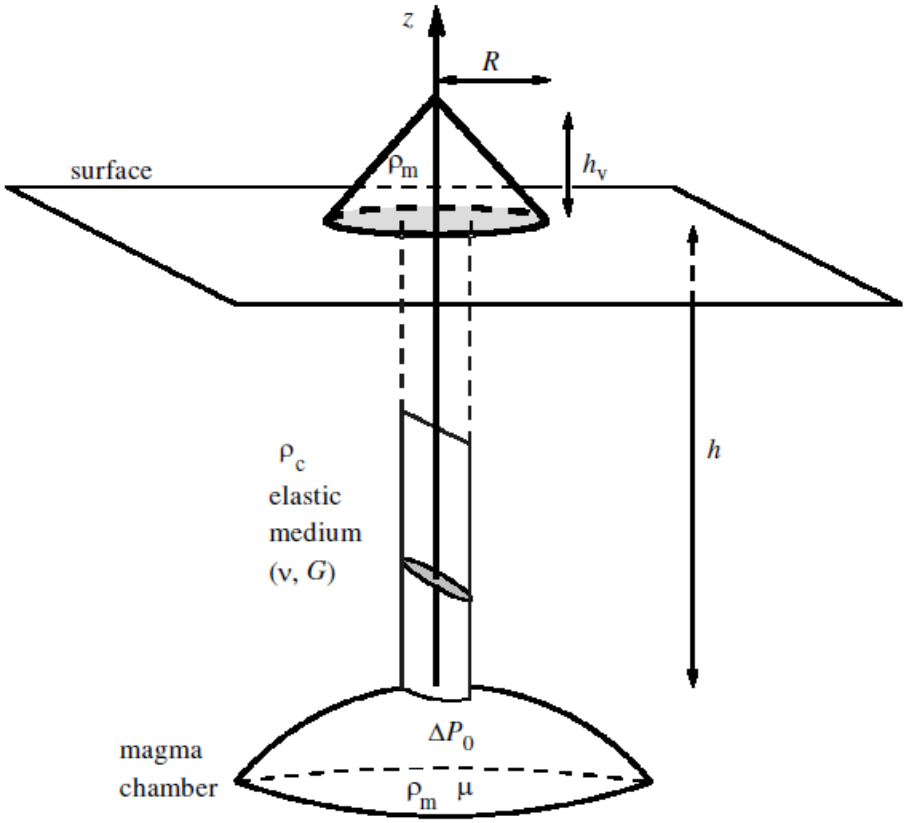

Figure 2-6 A diagram of the physical forces and variables used in Pinel and Jaupart's (2000) mathematical models of magma ascent controls, such models are commonly used (Pinel and Albino, 2013; Pinel and Jaupart, 2003, 2005) to determine the impact of changes in edifice conditions, such as those involved in volcanic collapses, on magmatic reservoirs. See text for explanation of main variables, with (G) indicating rigidity of the elastic medium.

Empirical studies on the Canary Islands of El Hierro (Manconi et al., 2009) and Tenerife (Longpré et al., 2009) have used cpx-melt thermobarometry to provide quantitative underpinnings to these numerical models. Building on previous thermobarometric studies (Klügel et al., 2005), the new numerical models indicate that the decompression effects of the most recent Canary Island flank collapses appear to penetrate to the depth determined for the main magma reservoir sill-network. Such depths estimates have been confirmed by analysing post-collapse flows from El Hierro's El Golfo sequence (Manconi et al., 2009).

These findings have been used to suggest that, after a lateral collapse, the stress changes are likely to disrupt otherwise steady-state processes in the magma supply system, leading to the eruption of dense magmas, volatile degassing and magma mixing (Manconi et al., 2009).

Observations of post-collapse sequences at the Bezymianny arc volcano (Turner et al., 2013) and Tenerife's *Teno Massif* (Longpré et al., 2009) appear consistent with this interpretation, showing evidence for the eruption of intensely mixed magmas and unusually porphyritic ankaramites, respectively.

Whether the influence of these processes extends into the zone of partial melting is a topic where work is less developed. Studies of Tahiti-Nui (Hildenbrand et al., 2004) have interpreted changes in Sr and Nd isotopic compositions of lavas within this oceanic island's collapse structures relative to its primary signature as evidence of a post-collapse change in the mantle source. However, this is a relatively radical claim for quite a small scale isotopic study, and this work would ideally be expanded to a more comprehensive suite of radiogenic isotope systems so it could be interpreted within end-member models. Should such mantle-source changes prove robust, this decompression-driven process would provide a parallel to the changes in Icelandic magmatism that occurred after glacial retreat reduced the island's lithostatic load at the end of the Pleistocene (Gee et al., 1998; Jull and McKenzie, 1996).

2.6 Discussion

Over the last 35 years studies of igneous processes in the Canary Islands have considerably deepened our understanding of volcanism in this oceanic island setting. They have identified key tectonic controls on regional igneous processes, described the structural controls acting on individual islands, determined the components of a lithospheric magma reservoir system, and characterised the compositional variability and heterogeneity in the asthenospheric-source of its magmas. The combined interpretation has mostly converged on a hot-spot tectonic model, with melt produced in an underlying, chemically heterogeneous, convecting plume and with the internal structure of each volcanic island providing a key control on how these magmas evolve and erupt.

Not all elements of these approaches are completely compatible. The tectonic studies have tended to invoke a static island-sized hot spot (Geldmacher et al., 2005), while the geochemical studies lead (Hoernle et al., 1995) towards a large regional-scale convecting mantle plume, within which individual hotspot tracks are minor, but long-lived, sub-elements. It is probably inevitable that, as these research fields have deepened, each sub-discipline's results, often on the same case studies, have been treated increasingly independently. This is particularly acute in the case of mantle geochemistry, where regional compositional variation is considerable but where this variation is rarely used to understand the geology of any given edifice. There is a growing potential for using the combination of field volcanology, igneous petrology, and mantle geochemistry to constrain an island's processes through integrated study.

The lateral collapse of a Canarian-type island appears an ideal candidate for an integrated approach. These dramatic events appear to form an essential part of the lifecycle of Canarian-type oceanic islands, and there is evidence (Longpré et al., 2009; Manconi et al., 2009; Pinel and Jaupart, 2005) that their effects should penetrate at least into a magma reservoir system believed to be in the upper lithospheric mantle. These periods of the island's activity are therefore among the most likely to present us with measurable variation on multiple scales. Furthermore, such collapses provide a major unconformity, simplifying the field relations and allowing the collection of large numbers of

different lava samples from flow-fields that are unambiguously separated by the event. This is a very useful feature when conducting geochemical studies that aim to resolve subtle asthenospheric variation.

Since the 1980's petrogenetic studies have often treated igneous systems in terms of the sequence of events: 1) first addressing the magma source and tectonic context, 2) then addressing the reservoir system and 3) briefly focusing on field volcanology. However, this sequence limits the potential contribution of field relations to understanding the overall system, since field relations can provide age relationships to any detailed geological study, and with them constrain the products of deeper processes. This thesis therefore presents a series of results chapters focusing on each sub-discipline in traditional geological order, with field relations described prior to petrological reservoir process and these described prior to mantle source processes. However, these chapters must be consistent within their sub-discipline, and are therefore treated as discrete papers that should stand on their own. Each results chapter therefore includes an introduction, a methods section, a results section, a discussion and a conclusion. This inevitably leads to a degree of repetition but also means that each chapter is intended to be readable independently. An outcome of this approach is that there is no methods section in this thesis, and each chapter approaches methodological issues in their introduction and discussion sections.

The final discussion of this thesis addresses how well this integrated approach has worked. This focuses on the combined interpretation of central La Palma and any discussing in detail any areas where the combined study leads us to interpret a stronger case than individual sub-studies would indicate on their own.

Chapter 3 : LITERATURE REVIEW – CASE STUDY

THE GEOLOGY OF CENTRAL LA PALMA AND THE ISLAND'S MAGMATIC RESERVOIR SYSTEM AND MELT SOURCE

3.1 INTRODUCTION

As the most historically active of the Canary Islands, and one of those still in its shield-building stage, La Palma has been the focus of extensive research into its geology, magma reservoir system and mantle source. In reviewing such literature this chapter adopts the same approach as the overall thesis, separately reviewing the island's literature by sub-discipline in geological order, from field relations descending to its mantle source.

Each sub-discipline's literature is reviewed at the scale at which studies tend to interpret their results: the geological section focuses purely on the sequences in the central region of the island, the petrological section addresses individual eruptions and the literature relating to all of La Palma's reservoir system, and the mantle geochemistry section focuses on regional signatures in the western Canary Islands. Within each sub-discipline this review aims to identify opportunities for new exploratory study in the period relating to the *Cumbre Nueva Collapse*.

3.2 THE GEOLOGY OF CENTRAL LA PALMA

La Palma's central region (Figure 3-1 and Figure 3-2) is a complex area where rocks are exposed from the duration of the island's volcanism including both the island's submarine Seamount Series and its sub-historical eruptions. This accessibility results from deep incisions cut into the island's northern *Taburiente* edifice in the *Caldera de Taburiente* and *Valle de Aridane* areas, and these areas are surrounded by major escarpments. This major embayment is believed to have resulted from the westward giant landslide of the *Cumbre Nueva Rift* of the *Taburiente* volcano (Carracedo et al., 1999b), and studies of these features have contributed to the model of Canarian-type oceanic island edifice evolution (Carracedo, 1994).

3.2.1 SEAMOUNT SERIES

La Palma's oldest exposed rocks are its Seamount Series (Carracedo et al., 2001). Exposed in the deep east-west *Barranco de las Angustias* canyon this unit was the focus of intensive work by Staudigel and Schmincke (1984), who assigned it a Pliocene age based on biostratigraphy. They described three main sub-units between the centre of *Caldera de Taburiente* and the island's coastal sedimentary sequences: 1) a core plutonic complex, 2) a swarm of thin intrusives (both dykes and sills) and 3) an upper volcanic series (Figure 3-3).

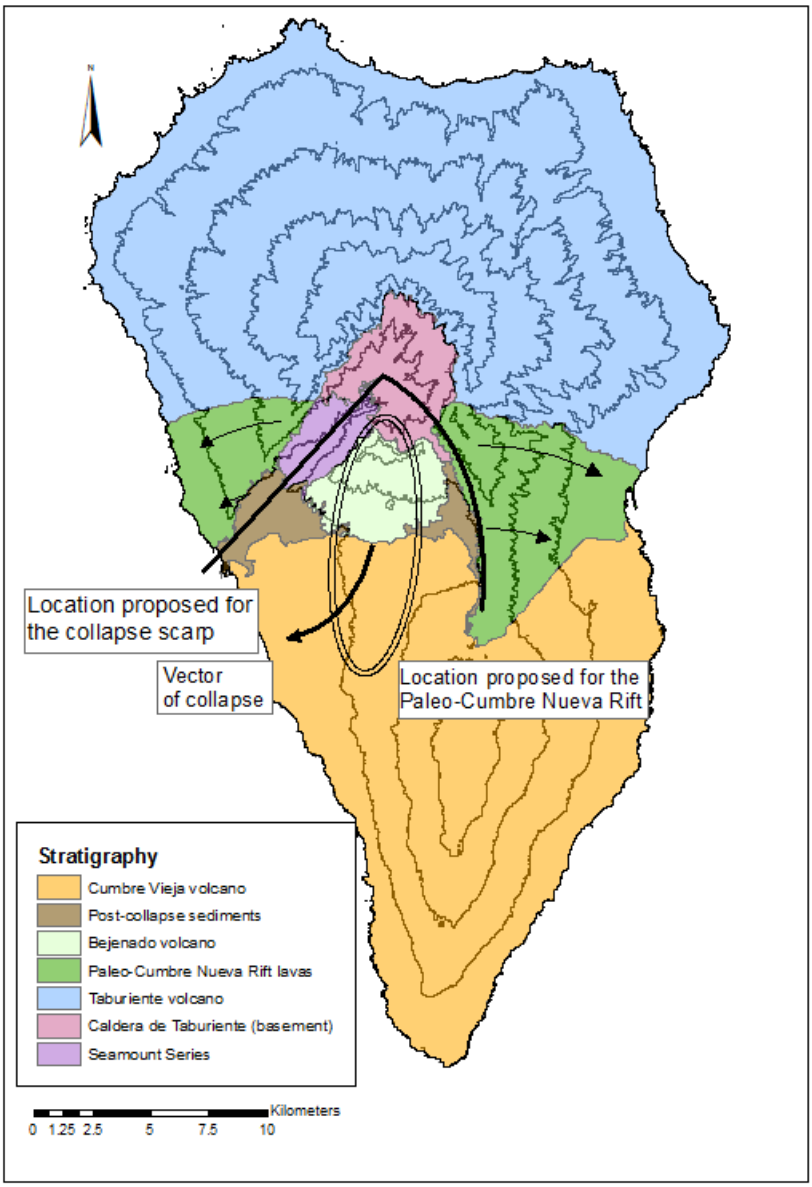

Figure 3-1 A simplified geological map of La Palma's main edifices and structural feature, 500m contours used to illustrate topography (based on maps in Carracedo et al., 1999a, Day et al., 1999, Navarro and Coello, 1994)

The volcanic series has been described as an east-west sequence of units emplaced under progressively shallower environments, with pillow lavas (interpreted as the product of deep water conditions) overlain by pillow breccias and hyaloclastites (emplaced in shallow water conditions at the terminal stages of submarine volcanism). Staudigel and Schmincke (1984) presented evidence for major uplift and rotation of this core sequence, with the extrusive sequences dipping 50° SW, and observed that the whole unit was exposed to approximately 1000 masl.

Petrology indicated the sequence was largely composed of alkali basalts, but with significant later recrystallization in the presence of hydrothermal fluids. Staudigel and Schmincke (1984) observed an

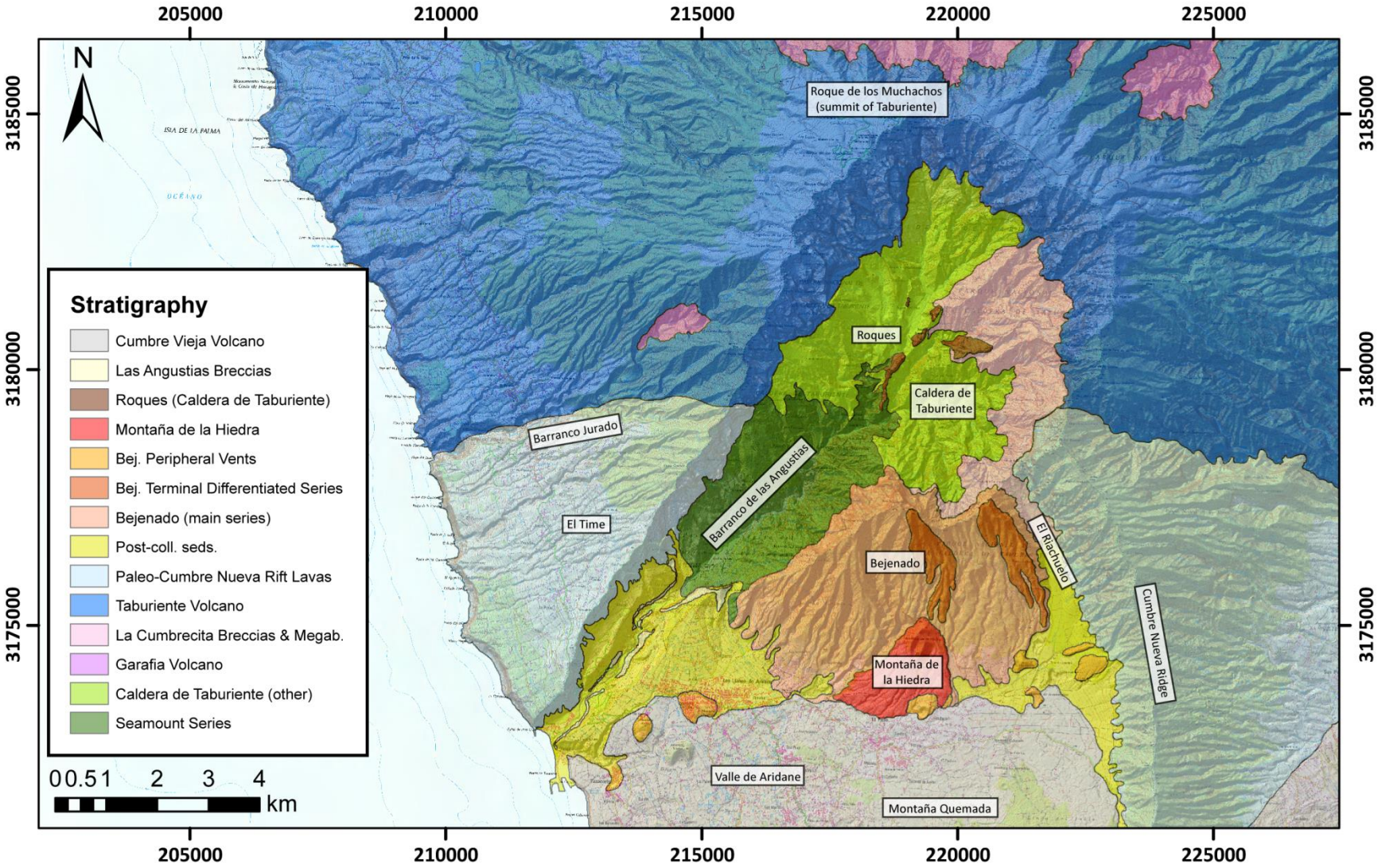

Figure 3-2 A geological map of central La Palma, assembled from the results of Carracedo et al. (2001), Colmenero et al. (2012), andNavarro and Coello. (1994).

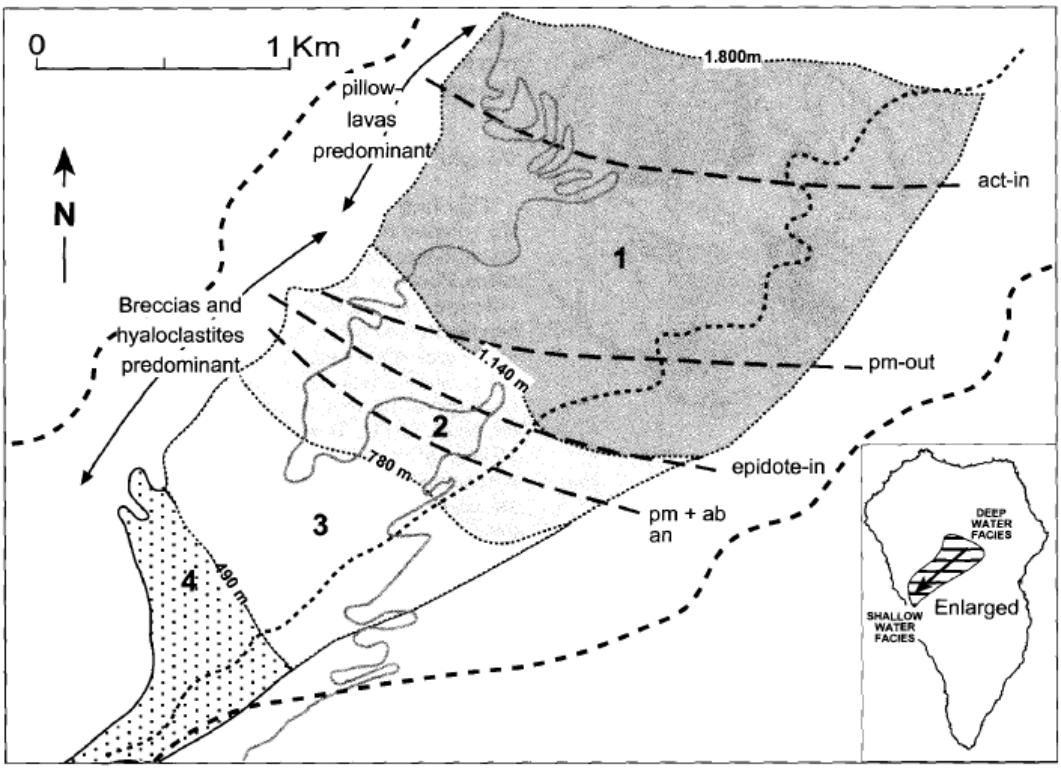

Figure 3-3 A map of the extrusive portion of the Seamount Series exposed in Barranco de las Angustias (Carracedo et al., 2001, adapted from Staudigel and Schmincke, 1984), units numbered 1-4 indicate lava and hyaloclastite sequences determined to have been emplaced at progressively decreasing water depths.

increasing metamorphic grade from a relatively minimal recrystallisation apparent in the shallow-marine sequences to full greenschist facies metamorphism towards the core plutonic units (Staudigel and Schmincke, 1984).

3.2.2 BRECCIAS AND INTRUSIONS IN *CALDERA DE TABURIENTE*

The *Caldera de Taburiente* basin is a spectacular geomorphological feature and as a result is La Palma's only national park. Since the 19th century it has been the focus of geological research (Lyell, 1855) with debate still ongoing over how it formed, and exposure within it of some of La Palma's oldest sub-aerial sequences. The terrain here is formidable and the geology is complex, with considerable thicknesses of massive breccias, young pyroclastic units, as well as major intrusive plutons and dyke swarms (Carracedo et al., 2001). There are no large outcrops of these units elsewhere on the island and all show varying degrees of alteration. With this complexity it is therefore understandable that different publications (Carracedo et al., 2001; Colmenero et al., 2012; Navarro and Coello, 1994; Roa, 2003) have proposed quite different interpretations for how they formed. This project is not focused on this period, and we will therefore treat these issues as unresolved.

Large gabbroic plutons and later alkaline gabbros dominate the centre of *Caldera de Taburiente,* and they are usually assigned to the same phase of activity as the extrusive Seamount Series (Carracedo et al., 2001). However, Carracedo and Paris (2001) have proposed that some of the latest plutonic rocks are the intrusive core to a vertical collapse caldera formed during one of early La Palma's major eruptions. These intrusives are onlapped by breccias, which have been described sedimentologically (Colmenero et al., 2012) as three distinct units: 1) *La Cumbrecita Breccias and Megabreccias*, 2) *El Pared de la Caldera Breccias and Conglomerates* and 3) *La Viña Breccias*. Colmenero et al. (2012) proposed that these units resulted from several giant landslides, described these units in detail and observed that they host very different populations of dykes and show distinct degrees of alteration. The key difference between the interpretations of the *Caldera de Taburiente* tends to be how many landslides are invoked to explain its features with Carracedo et al. (1999a) and Carracedo and Paris (2001) invoking one, Carracedo et al. (2001) invoking two, and Roa (2003) and Colmenero et al. (2012) invoking four.

A further key feature of the *Caldera de Taburiente* is the lack of exposure of the *Garafia* edifice (Carracedo et al., 2001). This minor volcano is believed to be La Palma's earliest subaerial shield-volcano and has often been identified in studies of the deep fluvial incisions and water mining tunnels (galleria) cut into *Taburiente* (Navarro and Coello, 1994). Its absence from the *Caldera de Taburiente* is surprising and Carracedo et al. (2001) invoked a SE-directed lateral collapse early in La Palma's growth to explain it.

3.2.3 *Taburiente* and *the Paleo-Cumbre Nueva Rift*

An overview of *Taburiente*

Taburiente is the largest of all La Palma's northern edifices and the island's summit (2423 masl – *Roque de los Muchachos*) is the remains of its peak. Its eruptive products cover the entire northern half of the island to a thickness of 1000m (Carracedo et al., 2001). Its oldest dated lavas indicate activity began here before 1.2 ± 0.02 Ma (Guillou et al., 2001). The coastline of this volcano forms a broad hexagon (Figure 3-1), and the regularity of this shape may be a result of the early stages of a Canarian-type triple-rift system (Carracedo, 1994). Three of the sides of the hexagon are perpendicular to the expected locations of rift zones (angled at 120°) but this geometry is less pronounced than vent distributions on El Hierro or Tenerife and the exact location of the three rifts on Taburiente remains open to interpretation (Carracedo et al., 2001; Carracedo and Troll, 2013).

Taburiente has been mapped using two magnetostratigraphic units (Carracedo et al., 2001), and as a result it is known that most of its extrusive sequences postdate the Brunhes-Matuyama magnetic reversal (Guillou et al., 2001). Brunhes-era lavas with normal polarities (oldest dated flows at 770 ± 11 ka) cover and extend beyond earlier Matuyama flows (Guillou et al., 2001). The Brunhes phase is notable for tightly distributed eruptive centres, with scoria cones largely confined to lines that

radiate from the island's summit to the corners of its hexagonal coast. Carracedo et al. (2001) used such features to propose this was representative of an early stage in the structural evolution of such oceanic islands.

The bulk of *Taburiente's* effusive products tend to be relatively primitive basanitic and alkali basalt lavas (Carracedo et al., 2001), with olivine pyroxene basalts and aphyric trachytes common across the north of the island. Carracedo et al. (2001) identified a suite of evolved flows in the lattermost stages of activity at this volcano (which they termed the Terminal Differentiated Series), with a progression from basanitic to increasingly evolved lavas also identified in their type-section at *Barranco Jurado*. The only identified phonolitic domes from this unit outcrop in *Taburiente's* summit area.

THE *PALEO-CUMBRE NUEVA RIFT* AND *EL TIME*

The thickest lava sequences from late volcanism at *Taburiente* are found to the south of the summit along the north-south trending *Cumbre Nueva Ridge*. This ridge's lavas overlie a relatively thin lava-succession of reverse-polarity, Matuyama flows — indicating that the focused eruptive phase at this rift began late in *Taburiente's* activity. *Taburiente* and the *Cumbre Nueva Ridge* are truncated by a major escarpment composed of three segments: 1) a N-S section parallel to the *Cumbre Nueva Ridge*, 2) an arcuate cliff around *Caldera de Taburiente*, 3) a NE-SW section at *Barranco de las Angustias*. The NE-SW section is the southern boundary of the minor *El Time* inland headland, the least eroded region of *Taburiente*.

Multiple papers (Carracedo et al., 1999a, 1999b; Day et al., 1999) have proposed that the *Cumbre Nueva Ridge* is the remains of a major polygenetic rift, the *Paleo-Cumbre Nueva Rift* (we adopt this name instead of the common "*Cumbre Nueva Rift*" to avoid confusion with the *Cumbre Nueva Ridge* and *Cumbre Nueva Collapse*). Studies have identified the two inland headlands as the remains of this rift, with the *Cumbre Nueva Ridge* formed from its eastern, downslope, flank (Figure 3-4), and *El Time* as a relic of its western flank, while the rift's axis and vent areas are believed to have been entirely removed in the SW directed *Cumbre Nueva Collapse*. The *El Time* area is bounded by *Barranco Jurado* to its north and the cliff sequences of *Barranco de las Angustias* to its south (Carracedo et al., 1999a).

The segmented nature of the main embayment headwall has led to debate over the geometry of the collapse. Ancochea et al. (1994) proposed that the landslide resulted from slip along several detachment surfaces, with the headwall of *Caldera de Taburiente* originating as a secondary, nested, collapse structure (see Figure 3-5). Alternatively, Carracedo et al. (1999b) invoked only one detachment surface and proposed that the rest of *Caldera de Taburiente* originated through erosion, discussed in more detail below.

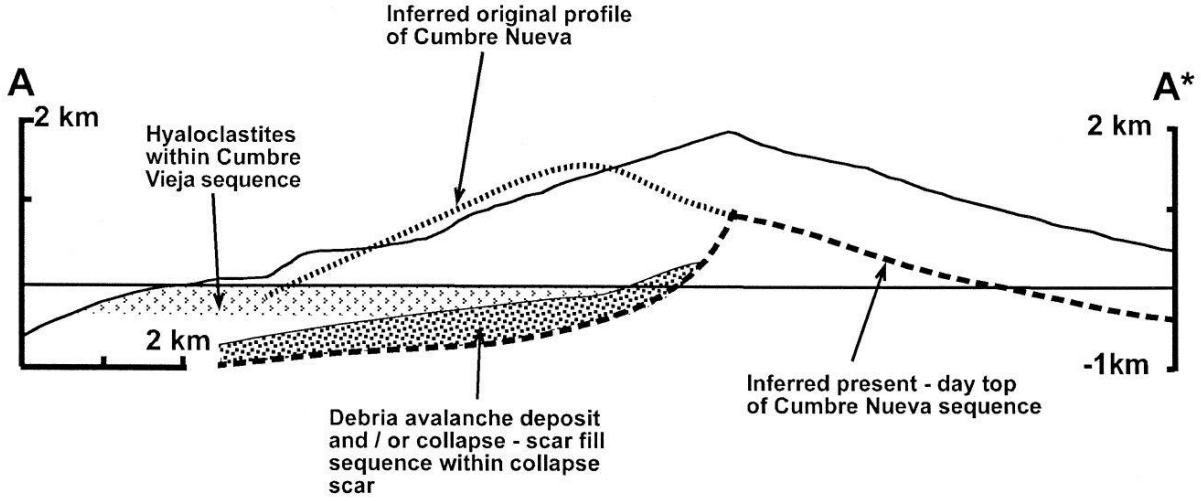

Figure 3-4 An inferred west-east topographic profile for the *Paleo-Cumbre Nueva Rift* prior to the *Cumbre Nueva Collapse* is illustrated by the dashed line, superimposed with the thicknesses of post-collapse deposits. The summit of volcano *Taburiente's* central cone is represented as a solid line to the rear of the profile of the *Cumbre Nueva Ridge* (from Day et al., 1999).

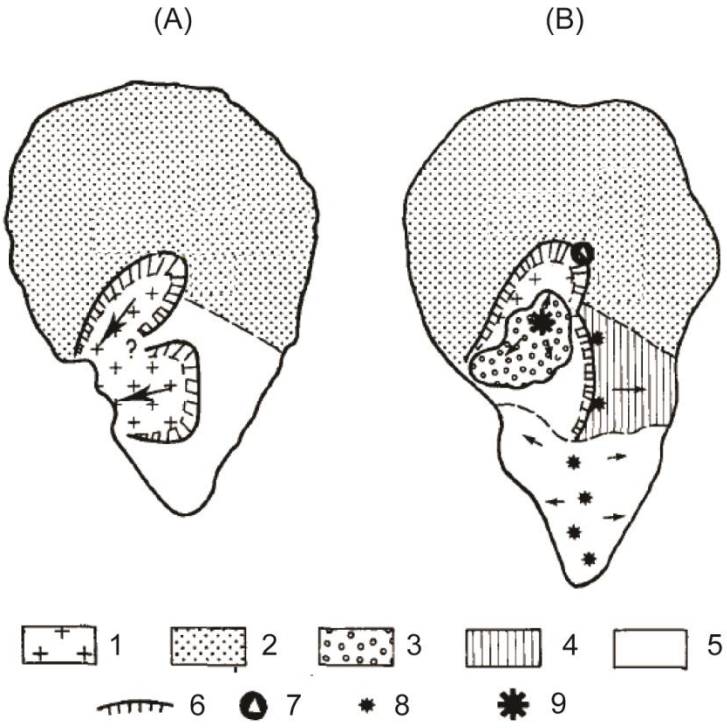

Figure 3-5 Volcano-structural model for the genesis of *Caldera de Taburiente* through a *Cumbre Nueva Collapse* that possessed two distinct detachment surfaces (adapted from Ancochea et al., 1994). The sequence involves: A) collapse of the Paleo-Cumbre Nueva Rift along two detachment surfaces, producing a pair of embayments, B) subsequent volcanism focused at the Bejenado volcano in the collapse structure. Diagram markers represent: 1=Garafia edifice; 2= Taburiente edifice; 3=Bejenado volcano; 4=Flow from Paleo-Cumbre Nueva rift; 5=Cumbre Vieja series; 6= Caldera rim; 7=centre of Taburiente edifice; 8=eruptive centres; 9= centre of Bejenado edifice.

In either scenario, the primary features of this *Paleo-Cumbre Nueva Rift* appear consistent with Carracedo's (1994) model for the evolution of Canarian-type oceanic islands. The *Paleo-Cumbre*

Nueva Rift would have been a major polygenetic rift fed by an underlying dyke swarm, with extensional stresses acting perpendicular to its axis (Day et al., 1999). Once this rift became a well-developed feature, later activity would have remained focused here as dyke injection and extensional stresses became more pronounced (Carracedo et al., 1999a). As the polygenetic ridge grew larger the final result of this focused volcanism would be flank failure.

3.2.4 *BEJENADO* AND THE ORIGIN OF *CALDERA DE TABURIENTE*

AN OVERVIEW OF POST-COLLAPSE CENTRAL LA PALMA

The large embayment cut into south-western *Taburiente* is dominated by three features: 1) *the Valle de Aridane*, 2) the *Caldera de Taburiente* basin, and 3) the *Bejenado* volcano. These features are closely inter-related, and so geological interpretations have usually attempted to explain all three at once (Ancochea et al., 1994; Carracedo et al., 1999a; Carracedo and Paris, 2001). The simplest to explain is the *Valle de Aridane* plain, where there is a wide consensus that this is the main basin resulting from the *Cumbre Nueva Collapse* (Ancochea et al., 1994; Carracedo et al., 2001; Navarro and Coello, 1994).

In the most north-easterly part of the *Valle de Aridane* are the *Bejenado* volcano and the *Caldera de Taburiente*. *Bejenado* is La Palma's third largest volcanic edifice (with a summit of 1844m), but in spite of this volcano's size, previous research into this part of La Palma has mostly focused on the *Caldera de Taburiente*, with *Bejenado* treated as a minor feature at the edge of the basin. This means that reviewing the literature for the post-collapse volcanism of *Bejenado* requires it to be treated largely in the context of its implications for models of the growth of *Caldera de Taburiente*.

Two broad mechanisms have been invoked to explain the origin of *Caldera de Taburiente*: 1) the volcano-structural model previously discussed in which a second detachment surface during the *Cumbre Nueva Collapse* produced a pair of nested basins, and 2) an erosive origin invoking an unusually aggressive fluvial system (Carracedo et al., 1999a; Carracedo and Paris, 2001; Lyell, 1855). A key tenet of recent erosive models has been that *Bejenado* grew soon after the *Cumbre Nueva Collapse* and then provided a obstacle to drainage in the newly formed collapse embayment (Carracedo et al., 1999a, 2001; Carracedo and Paris, 2001). This blockage resulted in an incision being channelled and focused between *Bejenado* (with erosion producing its northern cliffs) and the escarpment to its north (Figure 3-6). This model requires incision to have advanced rapidly, because radiometric age determinations of *Bejenado's* summit-region lavas (490 ±60 ka (Guillou et al., 2001)) allow for only a period of tens of thousands of years between the uppermost flows of the *Cumbre Nueva Ridge* and the end of primary activity at *Bejenado*.

PREVIOUS STUDIES OF *BEJENADO*

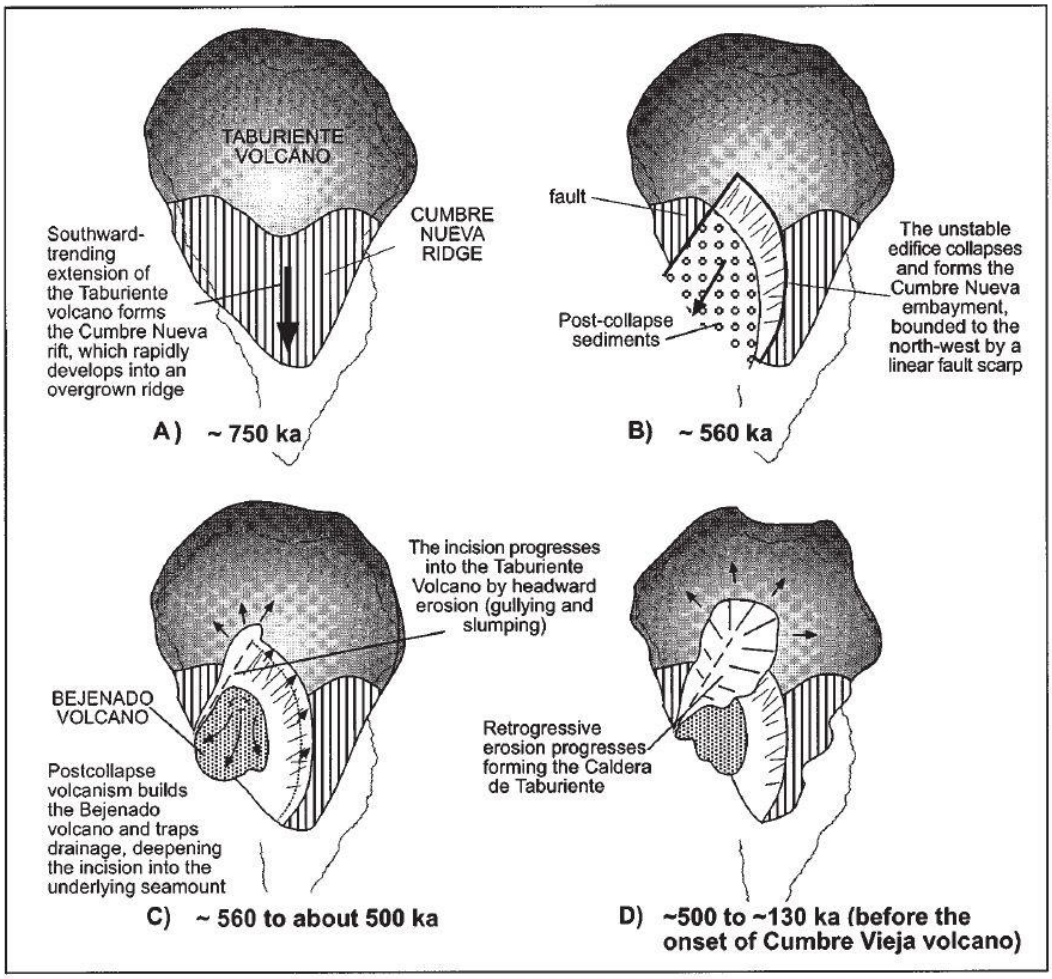

Figure 3-6 A schematic model of the growth of northern La Palma and of *Caldera de Taburiente* since the peak of activity at the *Taburiente* volcano (from Carracedo et al., 1999a). The sequence involves: A) *Taburiente's* volcanic focus migrated southward over time leading to the growth of the *Paleo-Cumbre Nueva Rift*; B) the *Paleo-Cumbre Nueva Rift* became increasingly unstable as it grew, eventually causing the *Cumbre Nueva Collapse*; C) post-collapse volcanism at *Bejenado* was nested within the collapse structure, while the early stages of *Caldera de Taburiente's* growth result from a trapped drainage system which drained to Bejenado's east; D) this erosional feature grew through retrogressive erosion that eventually bypassed the obstruction provided by Bejenado and began to drain directly to the *Caldera de Taburiente's* west.

Carracedo et al. (2001) presented the most complete description of *Bejenado's* geology, where the volcano was described as a rapidly constructed, steep sided, stratovolcano, formed from the continuation of *Taburiente's* volcanism immediately after the *Cumbre Nueva Collapse*. The volcano does not currently possess a northern flank, with erosion having incised a vertical cliff section to its north that provides *Caldera de Taburiente* with its southern enclosing headwall. Here, *Bejenado's* lower contact is exposed with 100m of sediments and debris avalanche deposits between its lowermost volcanic units and the underlying Seamount Series.

The volcano's stratigraphy has not been tightly constrained, with Carracedo et al. (2001) treating it as a single unit of various lavas, but with volcanic agglomerates identified at some of its lowermost exposures, and a separate late evolved series – a Terminal Differentiated Series similar to that described at *Taburiente*. The lava sequence is described as a sequence of progressively more evolved flows from early porphyritic basanites to mafic tephrites at its summit and lateral vents (the

Terminal Differentiated Series). *Bejenado* has been treated as a single petrological trend of progressively more evolved post-collapse lavas and this has been discussed as a possible parallel to the early construction of *Teide* on neighbouring Tenerife (Carracedo et al., 2007; Carracedo and Troll, 2013).

THE END OF VOLCANISM IN CENTRAL LA PALMA

Several small-volume, discrete, post-collapse volcaniclastic outcrops (the *Roques*) are present in the deepest central part of *Caldera de Taburiente* and these have been explained as resulting from late, major, eruptions (Carracedo and Paris, 2001; Roa, 2003) from *Bejenado*.

Roa (2003) interpreted *Bejenado* as the remains of a true, conical, stratocone that previously occupied the centre of *Caldera de Taburiente,* and he suggests this collapsed to the north as the result of a late, explosive eruption. In this model the *Roques* represent rotated blocks (toreva remnants) that were emplaced along slip planes. An alternative explanation was provided by Carracedo and Paris (2001) as part of their thorough model for how *Caldera de Taburiente* formed. They described a smaller *Bejenado* than proposed within Roa's model, with vents slightly to the north of its current crest, with its activity ending through a late explosive eruption. In their model these volcaniclastics were the product of a crater-forming eruption that provided the core bowl which later grew into *Caldera de Taburiente* through ongoing erosion. However, these *Roques* are found 900m beneath *Bejenado's* crest and therefore this mechanism requires a very large scale explosive eruption for an oceanic island volcano. It is notable that no pyroclastic deposits elsewhere on *La Palma* have been attributed to the late, major eruptions required by either of these two models.

The youngest eruptive units in the island's central region are believed to be a number of small adventive cones found across the north of the *Valle de Aridane* plain (Carracedo et al., 2001). Of these, the only vents that directly onlap *Bejenado* are the cluster of cones at *Montaña de la Hiedra* directly to the south of its summit.

3.2. 5 EL TIME SEDIMENTS

Since the *Cumbre Nueva Collapse*, the *Valle de Aridane* plain (particularly to *Bejenado's* southwest), has been progressively infilled by epiclastic sediments., referred to as the *El Time Sediments* unit (Carracedo et al., 2001; Colmenero et al., 2012). This thick unit (up to 300m) of poorly sorted conglomerates extends to the coast, and is best exposed in the vertical walls of the *Barranco de las Angustias* canyon. Carracedo et al. (2001) interpreted this sequence as the result of shallow marine fan delta deposition.

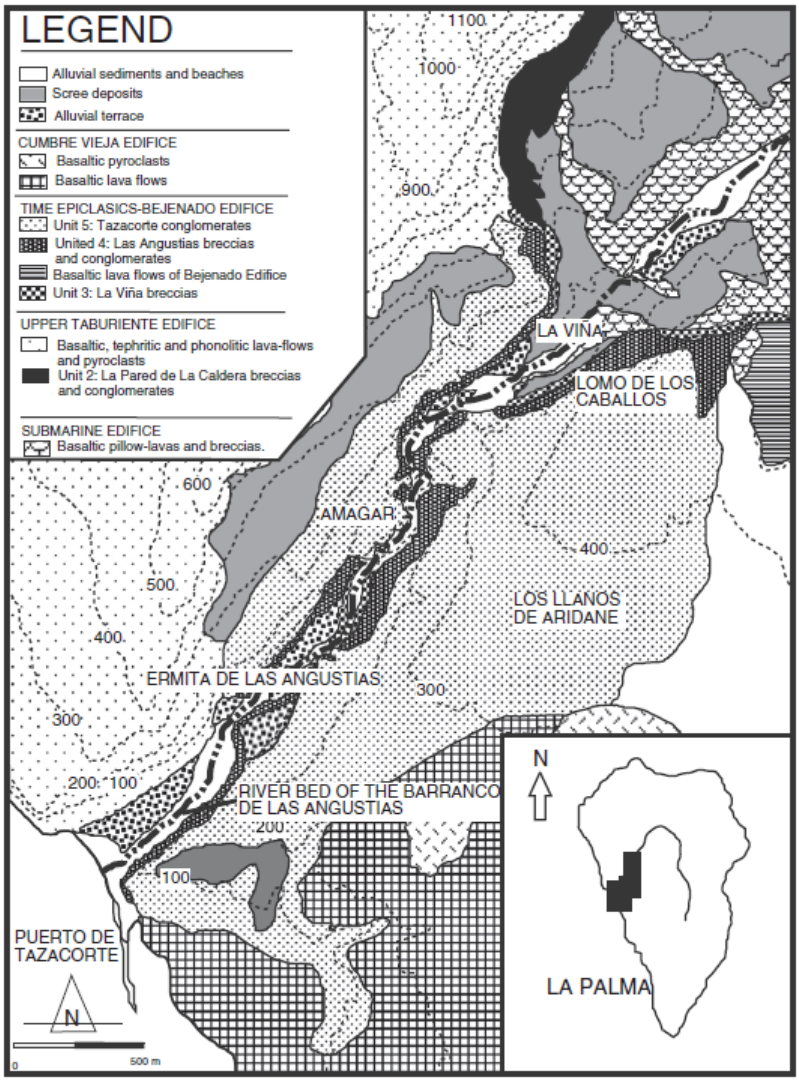

Figure 3-7 A map of the sediments of the *El Time* group in the lower stretch of *Barranco de las Angustias* (Colmenero et al., 2012) illustrating the extents of sedimentary sub-units. Units include *Las Angustias Breccias and Conglomerates* and the *Tazacorte Conglomerates*.

Colmenero et al. (2012) has produced the most complete study of these sediments (Figure 3-7), dividing them into two units separated by an unconformity: 1) the lower *Las Angustias Breccias and Conglomerates*, and 2) the upper *Tazacorte Conglomerates*. They described the lower *Las Angustias Breccias and Conglomerates* as being intercalated with lava flows from the *Bejenado* volcano, indicating that deposition of this unit began soon after the *Cumbre Nueva Collapse*. Colmenero et al. (2012) interpreted this unit as a series of superimposed, largely hyper-concentrated, debris flows of non-marine origin. They were described as mostly cohesive and showing evidence for material from the underlying beds being incorporated through erosion. The upper part of the group, the *Tazacorte Conglomerates*, was interpreted as valley-fill sequences of high energy stream-flow deposits.

Erosion, deposition and fluctuations in La Palma's sea-level

Despite the good exposures of complex coastal sediments in the *El Time* area, interpreting this sequence is made difficult by a major change in eustatic sea-level during the period of interest, as

well as conflicting evidence about how much regional uplift has taken place since: both the island and the sea level may have moved vertically over the period of these sediments' deposition. Marine isotopic stage 12 (between 500 ka and 440 ka (Colmenero et al., 2012)) was a global event which involved a sea-level drop of up to 150m with respect to current sea level, and this event occurred within measurement error of published dates for the end of activity at *Bejenado* (Guillou et al., 2001). Since there is a well-established link between eustatic falls in sea-level and increases in erosion rates, this change provides a convenient explanation for the dramatic incision of *Caldera de Taburiente* and the clastic material this would produce can provide a potential sediment source for these sequences.

However, pillow lavas from the Seamount Series outcrop in this area at an altitude of 1000m asl (Staudigel and Schmincke, 1984), and other rocks also assigned to the basement complex outcrop at 1300m asl (Hildenbrand et al., 2003). There is thus considerable evidence for regional uplift in central La Palma, but there is no documented evidence for a single thrust or a dateable uplift event. Hildenbrand et al. (2003) proposed instead a continuous uplift process that has acted across the whole island throughout its history. However, this is incompatible with the interpretations of Carracedo et al. (1999a), who have used the height of the island's current coastal cliff-sequences as a marker of palaeo-sea-level. Their interpretations of these cliffs require the island to have kept a stable profile throughout the recent phases of activity. If uplift has occurred, a possible mechanism has been provided by Klügel et al. (2005). In a petrological paper discussed in more detail below, they propose that the degree of magmatic evolution of La Palma's lavas requires significant cumulates to have formed with them, and use thermobarometry to suggest that these were small volume bodies emplaced in the upper lithospheric mantle. Such under-plating must be accompanied by an isostatic response, and would result in the island's uplift.

Coastal sediment and erosional sequences (particularly in *Caldera de Taburiente*) from this period of the island's geology must therefore be interpreted in the context of a potentially deforming, uplifting, edifice and synchronous eustatic sea-level changes (Colmenero et al., 2012).

3.2.6 Cumbre Vieja Rift

The *Cumbre Vieja* volcano is a major, active, polygenetic ridge that onlaps the *Cumbre Nueva Ridge* from the south. It last erupted in 1971. This edifice has been the subject of much recent research (Carracedo et al., 2001; Day et al., 1999; Guillou et al., 1998), which has described it in terms of Carracedo's (1994) model of Canarian-type volcanism. Its oldest dated flows (123 ± 3 ka) outcrop in cliff sequences in the southern *Valle de Aridane* (Guillou et al., 1998). Carracedo et al. (2001) interpret the apparent hiatus between the end of activity at *Bejenado* and this date as a sampling bias resulting from activity having moved to the south after post-collapse activity ended, with intervening eruptions subsequently buried by the growing *Cumbre Vieja*.

3.2.7 Geological discussion

La Palma's central region provides a well-preserved and well-exposed record of activity at an oceanic island volcano before and after a giant landslide. The pre-collapse *El Time* region and the post-collapse *Bejenado* volcano are areas with several attractive parallels. They are similar sized regions and in each case regional volcanism ended soon after the collapse-related sequences were emplaced, leaving an unusually complete record of the preceding period's lavas for sampling and study. Furthermore, the growth of the *Caldera de Taburiente* basin and later river erosion has led to well-exposed vertical sections through both these region's eruptive sequences.

There are a number of specific geological problems in La Palma's history that could be resolved through detailed study of these sequences. *Bejenado* is at present the least studied major edifice on the island, and is therefore an ideal opportunity for new fieldwork to determine a detailed eruptive stratigraphy and resolve its original morphology and duration of activity. The date of the *Cumbre Nueva Collapse* is currently an estimate ("about 560 ka" (Carracedo et al., 2001)) but the exposure and preservation in these two regions are ideal for focused geochronology within the context of new, more detailed, field relations. New geochronological data from this period should improve our age constraints for the *Cumbre Nueva Collapse* and the duration of activity at *Bejenado*.

Furthermore, addressing these issues may have implications for the origin of *Caldera de Taburiente*, a major issue about which there is little consensus in spite of a large body of literature extending over 200 years of research. It appears that study of *Bejenado* may provide insights into this, since there is broad agreement (Carracedo and Paris, 2001; Colmenero et al., 2012; Roa, 2003) that it played a key role the basin's early growth.

3.3 Petrological studies of La Palma's magma supply system

Studies of the petrology of La Palma's lavas, and through them the island's magma reservoir system, have significantly expanded in number and extent over the last 20 years. While the *Cumbre Vieja's* historic eruptions had long been an ongoing focus of petrological work (Johansen et al., 2005; Klügel et al., 2000; Praegel, 1986), the period since 2000 saw this expand to include rocks from the island's northern shield (Galipp et al., 2006; Nikogosian et al., 2002) and even local submarine edifices (Abratis et al., 2002).

3.3.1 Studies of the petrology of the *Cumbre Vieja's* historic eruptions

The 1585 eruption

Field studies of the 1585 eruption of the *Cumbre Vieja's* western flank indicate that this complex eruption included the emplacement of juvenile basanite and phonolite lavas, as well as the uplift and deformation into "spines" of a pre-historic phonolite dome (Carracedo et al., 2001). Johansen et al. (2005) sampled this flow-field and presented U-series disequilibrium data and whole rock characterisations of samples of basanitic, tephritic and phonolitic lava.

In terms of the magma supply system, these disequilibrium studies provided an indicator of the timescales required for magmatic differentiation in La Palma's reservoirs. The differentiation of the phonolite from basanites was determined through least squares disequilibria modelling to have potentially occured over relatively short timescales, with <15 ka indicated from from (^{230Th})/(^{232}Th), and 1550-1750 a indicated from (^{226}Ra)/(^{230}Th). However, since this project is known to have sampled the pre-historic phonolites (which are unlikely to be the product of a shared magma evolution process with the basanites) rather than the juvenile domes (where a shared origin is more likely), it is difficult to reconcile the results of disequilibria modelling with the eruption's field relations.

THE 1949 ERUPTION

The products of the 1949 eruption of the *Cumbre Vieja* are the most extensively studied lava flows on the island, having been addressed in terms of their relationship to local structural geology (Day et al., 1999), their extensive xenolith cargo (Klügel, 1998; Schmincke et al., 1998) and their compositional zonation (Klügel et al., 2000). The eruption carried a varied xenolith population (Hansteen et al., 1998; Klügel, 1998), including spinel peridotites, pyroxenite and hornblendite cumulates, and MORB gabbros from the Jurassic oceanic crust (Schmincke et al., 1998) indicating that entrainment of wall rocks was not restricted to one depth.

Study of the lava flow-field characterised it as three lava-units (Klügel et al., 2000): 1) a clinopyroxene kaersutite tephrite group, 2) a clinopyroxene olivine basanite group and 3) an amphibole clinopyroxene phono-tephrite group. This compositional complexity, combined with the detailed stratigraphy and historical accounts of this eruption (Klügel, 1999) allowed a comprehensive model of the ascent history and magmatic processes to be developed, and supplemented by whole-rock analysis, modelling of diffusion kinetics and least squares modelling of reservoir mass balance. They proposed a sequence of events involving three reservoirs over a period of 13 years, with shallow phonolitic reservoirs emplaced first, while basanitic and tephritic magmas evolved in deep reservoirs at 0.5-1.1 GPa, with these estimates obtained from early thermobarometric techniques. This remains the most comprehensive study of a single flow-field on any western Canary Island.

THE 1971 ERUPTION

The most recent subaerial eruption in the Canary Islands was located on the southern tip of La Palma close to the town of *Fuencaliente*. The resulting flow-field has been the focus of both a PhD thesis (Praegel, 1986), and a recent petrological project (Barker et al., 2015). Compared to the earlier studies of historic eruptions, the lavas are surprisingly compositionally uniform basanites (8-8.6 wt% MgO), but carried a population of kaersutite-rich cumulate xenoliths.

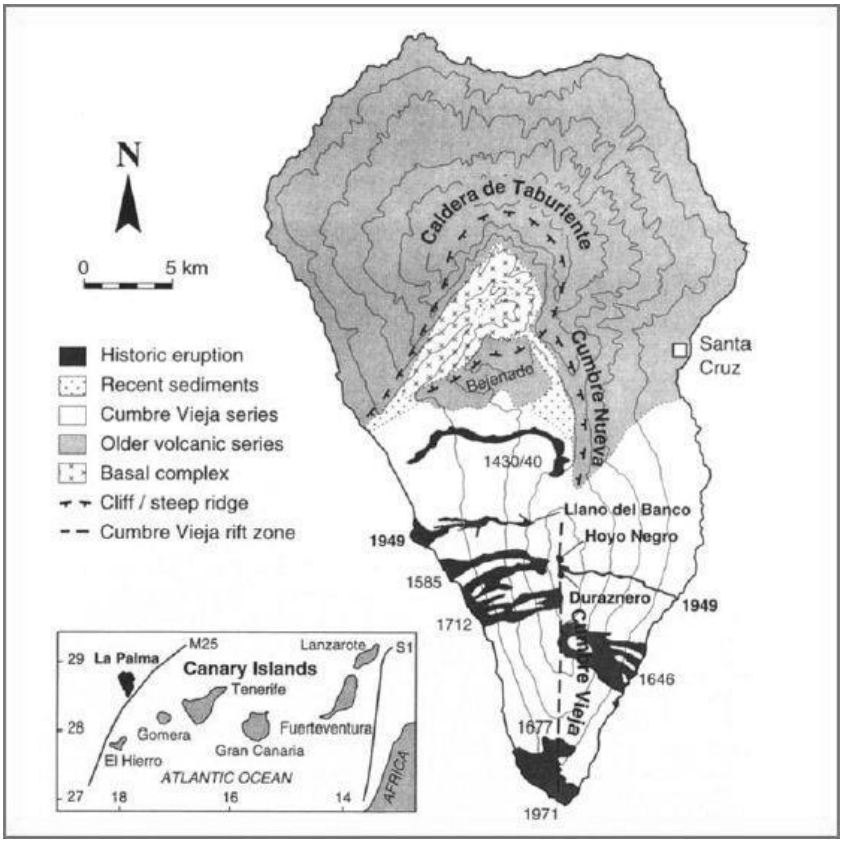

Figure 3-8 A map of the flow-fields of the seven eruptions of the *Cumbre Vieja* known to have taken place in the last 1000 years and their vent locations, from Klügel et al. (2000).

Detailed study of these cumulate xenoliths indicates that they are unlikely to be cognate with the 1971 lavas, with thermobarometry yielding formation pressures of 1.09 ± 0.28 GPa. Furthermore, the basanitic host magma yielded clinopyroxene-melt (cpx-melt) pressures of 0.6-1.2 GPa, putting this reservoir in the lithospheric mantle, and thus it appears to have entrained significant amounts of a deep, oceanic island plutonic complex.

3.3.2 Edifice-scale studies of La Palma's magma reservoir system

Such studies of historic eruption indicate that small-volume, compositionally heterogeneous, eruptions have been common on La Palma, and that their crystallisation has often been the product of reservoirs at lithospheric mantle depths. Wider studies of the remainder of the Cumbre Vieja (Klügel et al., 2005), followed by the island's older northern volcanoes (Galipp et al., 2006) then allowed a model to be developed of reservoir depths for the rest of La Palma's lavas.

Klügel et al. (2005) used cpx-melt thermobarometry of lavas from both the Cumbre Vieja and related submarine cones in combination with staged thermobarometry of xenolith fluid inclusions to determine the formation depths of La Palma's reservoirs. The results indicated a bimodal pressure population, with cpx-melt thermobarometry yielding pressures of 0.4-0.8 GPa in the lithospheric mantle, while fluid inclusions gave pressures of 0.2-0.4 GPa indicating they equilibrated in the oceanic crust. The authors interpreted this bimodality as indicating the presence of a primary

reservoir system where the depth of fractional crystallisation was being determined using the cpx-melt thermobarometer (Putirka et al., 1996), and a temporary magma stagnation stage during ascent determined from the more rapidly equilibrating fluid inclusion population (Figure 3-9). Furthermore, with such reservoirs forming and crystallising at depth, they implied that each eruption was accompanied by the underplating of a significant amount of material to the underside of the island, leading to isostatic uplift. Expanding this approach to samples from the island's older northern edifices (Galipp et al., 2006) showed that this two-stage thermobarometric model could be applied to much of the island's sub-aerial history. The main difference was that pressure determinations were repeatedly higher (1.2-0.6 GPa for cpx-melt and 0.5-0.35 GPa for fluid inclusion thermobarometry) in La Palma's earlier stages indicating a reservoir system that migrated to shallower depths over the course of the island's growth.

However, these studies have provided relatively few insights into what processes occurred within these reservoirs. Nikogosian et al. (2002) attempted to address this by studying magmatic inclusions in porphyritic alkaline lavas from La Palma's *Taburiente* edifice. Basanitic lavas in this area are dominated by olivine and clinopyroxene phenocrysts, and retain significant textural evidence for cotectic crystallisation of olivine, clinopyroxene and spinel. The authors identified the presence of relatively evolved, SiO_2-rich, melt inclusions hosted within these phenocrysts and, combined with thermobarometric data and phase-modelling, proposed that crystallisation of this mineral assemblage in a reservoir at 1.2 GPa would lead fractionation to produce melts that appeared primitive on a total alkali silica diagram but had progressively decreasing SiO_2 contents. Under these deep conditions alkaline, basanitic magmas need not be the product of relatively low degree partial melts. Furthermore this implied that the resulting deep reservoirs were likely to be full of olivine, clinopyroxene and spinel mushes.

Weis et al. (2015) addressed magmatic water content during crystallisation by taking basanitic samples from the Cumbre Vieja's historic eruptions and using FTIR spectroscopy and Mössbauer spectroscopy on clinopyroxene – a nominally anhydrous mineral with significant ionic H content, a component they proposed was linked to magma water-contents. Such data was then supported by plagioclase-liquid hygrometry which provided an independent magmatic H_2O measurement. The results were consistent across both techniques, with estimated parental magmatic water contents ranging from 0.84 ± 0.08 to 1.49 ± 0.51 wt% for Mössbauer spectroscopy, and 1.00 ± 0.35 to 1.3 ± 0.35 wt% for plagioclase-liquid hygrometry. This was consistent with the volatiles contents of the global type III OIB group described by Kovalenko et al. (2007). However, Weis et al. (2015) was predominantly written in terms of instrumental method development and did not focus on what these measurable water contents meant for the reservoir conditions in which these clinopyroxenes formed. Further application of these techniques would be needed to fully constrain magmatic H_2O variability in La Palma's reservoir system processes.

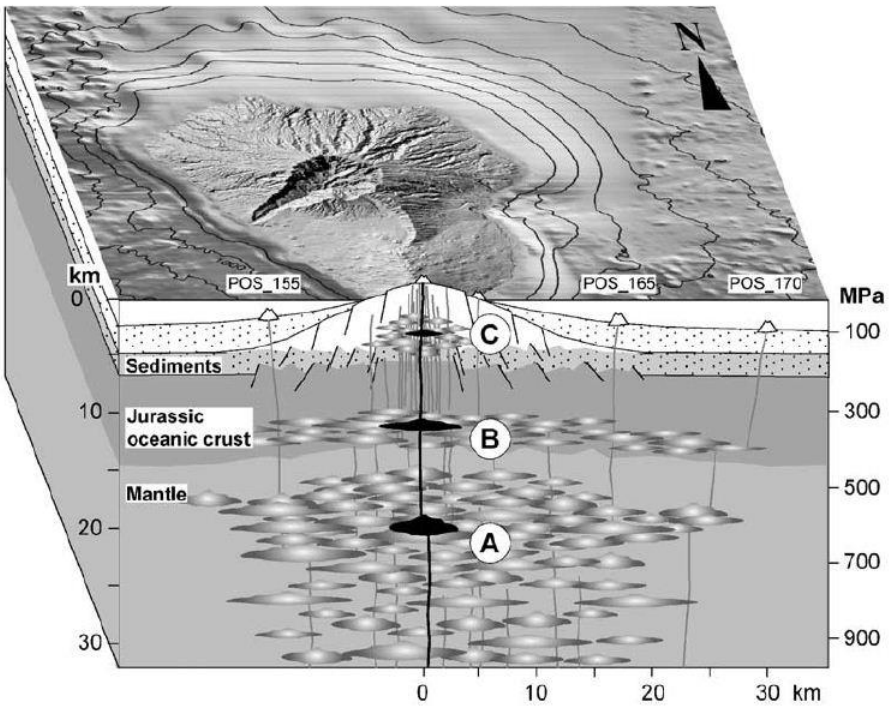

Figure 3-9 A model (Klügel et al., 2005) for the magma supply and reservoir system of La Palma based on cpx-melt and fluid inclusion thermobarometry, indicating three reservoir populations by depth. (A) is the main depth of fractional crystallisation, determined from cpx-melt thermobarometry, (B) is the secondary stagnation stage indicated by fluid inclusions, (C) is the shallow, edifice reservoirs of phonolitic plutons and temporary sub-volcanic feeder intrusions. All are visualised as small volume ephemeral sills.

3.3.3 PETROLOGICAL DISCUSSION

This growing and largely consistent body of work has established the presence of a deep, high-pressure, network of reservoirs in the lithospheric mantle and its contribution towards the differentiation of La Palma's magmas. In these deep reservoirs, basanitic magmas are believed to crystallise a clinopyroxene, olivine and spinel group assemblage that provides a major control on erupted composition. More evolved reservoirs appear to lead to the production of amphibole, clinopyroxene and feldspathoid cumulates. Reservoirs at shallower depth appear to be more ephemeral and less significant in terms of magmatic evolution.

Focused studies of individual eruptions have provided the most detailed petrological insights into what occurs within this reservoir system, indicating that La Palma's lavas are often compositionally heterogeneous and are best treated as complex flow-fields of multiple lava-units. The products of separate eruptions, even those separated by as short an interval as between La Palma's 1949 and 1971 eruptions, can have considerably different petrological characteristics as a result of their different evolutionary pathways in ephemeral, small volume, reservoirs. The mineralogy and textures of the resulting magmatic products provide a means of simplifying interpretations of field relations and magmatic processes on La Palma, since the products of individual eruptions and their

component magma-batches are likely to be petrologically distinctive when studied in detail, a result of their complex multi-stage evolutionary history.

3.4 The whole rock geochemistry and mantle source of La Palma's lavas

The total database of whole-rock elemental and isotopic analyses of lava flows from the western Canary Islands is now sufficiently extensive to allow each island to be characterised. In particular, the number of combined Sr, Nd and Pb isotope analyses, the key isotope systems in mantle component models (Hofmann, 2014; White, 2015; Zindler and Hart, 1986), have expanded through focused studies of individual edifices (Abratis et al., 2002; Day et al., 2010; Praegel and Holm, 2006) as well as studies of other isotopes that include such data for context (e.g. Os and Hf, Geldmacher et al., 2010; Widom et al., 1999).

Among petrological techniques whole rock analyses are unusually suitable for combining and comparing the results between laboratories, since a well-prepared, powdered, lava sample is widely treated as representative of lavas at the locality from which it was collected. Robust radiogenic isotope data, combined with precise provenance information (ideally GPS co-ordinates of localities), together provide an ideal basis for meta-analysis. In the following section we present a combined study of published whole rock analyses from samples taken at La Palma's main edifices, with a subsequent review of the aims and interpretations that were provided in studies that produced this data.

3.4.1 A meta-analysis of Sr, Nd and Pb isotope data from La Palma and the western Canary Islands

Sr, Nd and Pb whole rock isotope data from La Palma's main volcanic edifices (Abratis et al., 2002; Day et al., 2010; Elliott, 1991; Galipp et al., 2006; Geldmacher et al., 2010; Gurenko et al., 2006; Praegel and Holm, 2006; Turner et al., 2015) are presented in Figure 3-10 and Figure 3-11. All La Palma data points used[2] possess sufficient provenance information to robustly identify their source volcanic edificies. These are accompanied by data-fields of analyses from the neighbouring islands of Tenerife (Abratis et al., 2002; Geldmacher et al., 2010; Simonsen et al., 2000; Wiesmaier et al., 2011), La Gomera (Gurenko et al., 2006) and El Hierro (Day et al., 2010; Gurenko et al., 2009b).

All four islands have overlapping data-ranges that have been described (Day et al., 2010; Gurenko et al., 2006) as the product of mixtures of HIMU and DMM mantle components, but while La Palma, Tenerife and La Gomera all have abundant radiogenic Sr and Pb and proportionately less radiogenic

[2] Data-selection: Among data from La Palma the unusually large uncertainties on Nd data from the University of Copenhagen TIMS laboratory (Praegel and Holm., 2006) form a major obvious feature, while uncertainties on their Pb data were not reported. However, the average isotope compositions reported are typical of their source edifices and this merits their inclusion. From other islands only data with clear provenance co-ordinates (typically post-1995 for Tenerife) was used, while data from Ovchinnikova et al. (1995) was not used since the considerable scatter on their La Palma Sr data appeared to indicate issues with leaching prior to analysis.

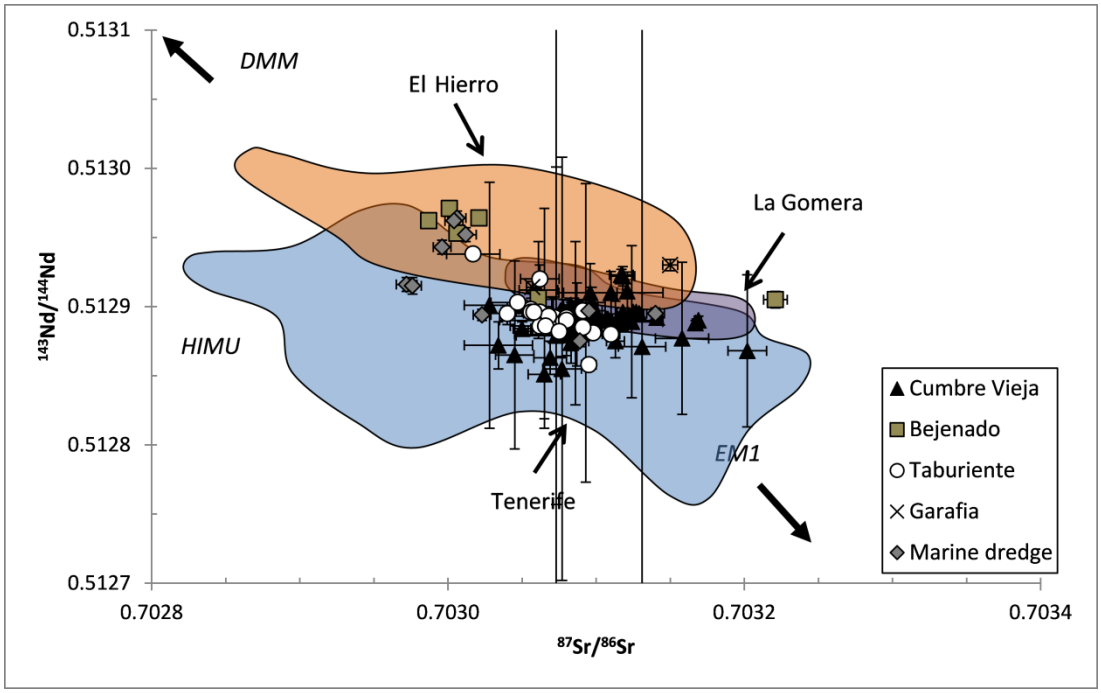

Figure 3-10 Post-1995 Sr and Nd isotope analyses of lava samples from La Palma's individual volcanic edifices interpreted in terms of relevant mantle components, all uncertainties are 2σ. Coloured fields indicate data from previous studies of western Canary Island lava flows where GPS co-ordinates are available (post-1995, data sourced from publications cited in the text).

Nd, they contrast with El Hierro where the DMM component appears stronger. Tenerife has the largest data-loop, with more than twice the range in $^{87}Sr/^{86}Sr$ of La Gomera, and this is likely to result from the difference in quantity of data available from these islands, with the scarcity of data from La Gomera contrasting with the large number of studies from Tenerife.

In terms of $^{206}Pb/^{204}Pb$ versus $^{207}Pb/^{204}Pb$ these lavas typically plot beneath the Northern Hemisphere Reference Line (NHRL), identifying them as the product of the young-HIMU variant of the HIMU mantle component (Thirlwall, 1997). Notably, the widely discussed EM1 signature (Gurenko et al., 2009a; Hoernle and Schmincke, 1993; Thirlwall et al., 1997) characteristic of the eastern Canary Islands has only been identified in lavas from Tenerife's *Anaga* massif (Simonsen et al., 2000), and is absent from the more westerly islands.

Taburiente and the *Cumbre Vieja,* La Palma's two largest edifices, each have large numbers of analyses that have broadly overlapping ranges in spite of being the product of data from four laboratories. There is no discrimination apparent in the Sr and Nd isotope composition of each volcano's lavas and only a subtle difference in radiogenic Pb content distinguishes the lavas from *Taburiente*.

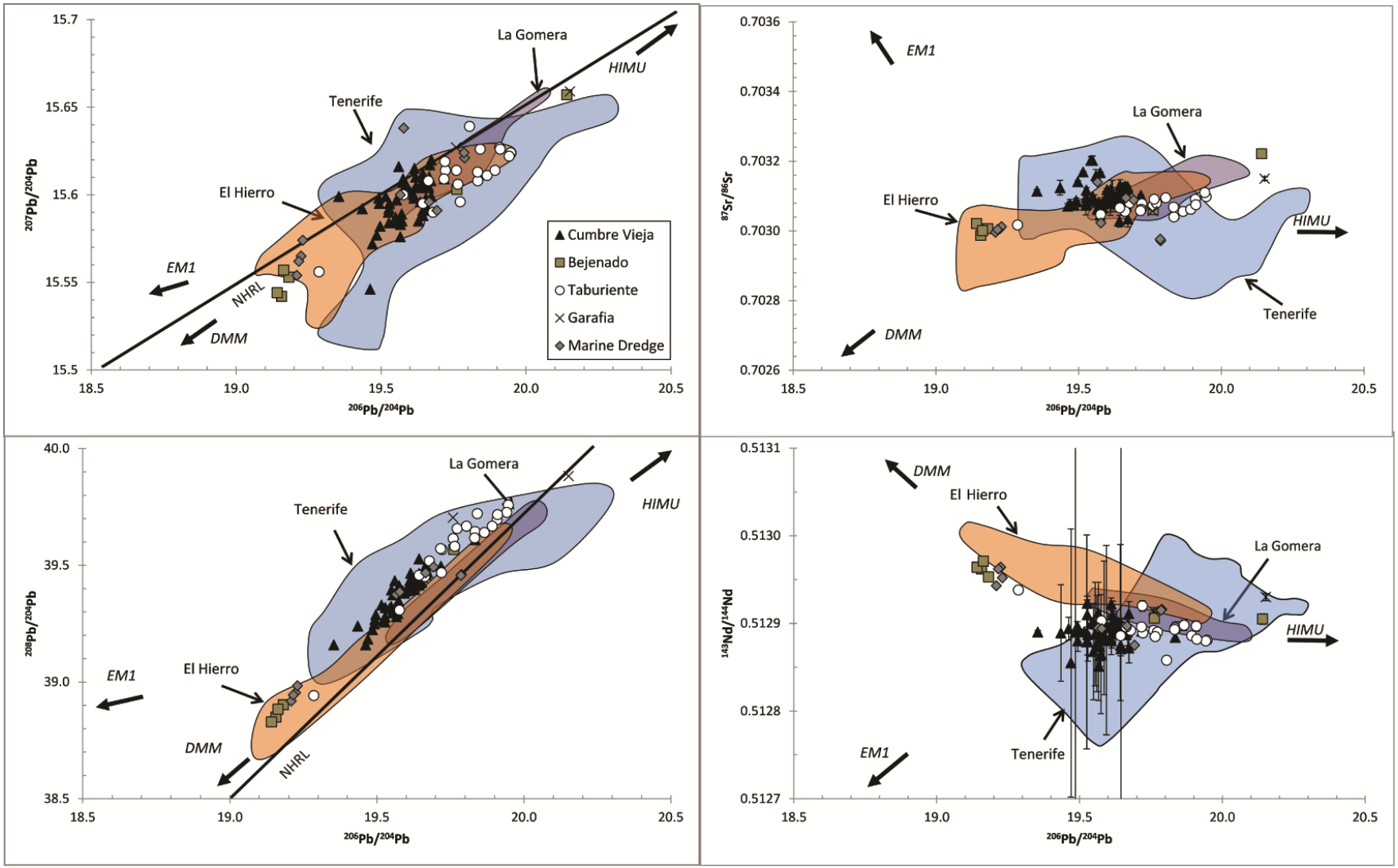

Figure 3-11 Pb, Sr and Nd isotope systematics of lava samples from La Palma's individual volcanic edifices interpreted in terms of relevant mantle components., all uncertainties are 2σ except Pb data from the University of Copenhagen. Coloured fields indicate data from previous studies of western Canary Island lava flows where GPS co-ordinates are available (post-1995, data sourced from publications cited in the text).

Lava samples from La Palma's minor edifices yield the widest isotopic variation. Our meta-analysis includes analyses of six samples from *Bejenado* (Day et al., 2010; Galipp, 2005) but these have widely different $^{206}Pb/^{204}Pb$ compositions (ranging from 19.157 ± 0.02 to 20.141 ± 0.01). A cluster of four samples from this edifice together have the strongest DMM signature identified on La Palma, with isotopic compositions more characteristic of El Hierro than the rest of the island.

This variability is also observed in a suite of dredge samples from a submarine ridge to the south of the *Cumbre Vieja* (Abratis et al., 2002), where the majority of samples show similar compositions to those of lavas from *Taburiente* and the *Cumbre Vieja*, but a cluster of four samples are extremely similar to *Bejenado*. Only one sample from *Taburiente's Cumbre Nueva Ridge* shows similarly DMM-dominated isotope signatures to the clusters from dredge samples and *Bejenado*.

The submarine dredge samples are difficult to place within La Palma's stratigraphy, since this ridge could be the product of an unknown number of eruptions from any period of the island's growth, but *Bejenado* is much better constrained as a post-collapse volcano. The unusually large range in isotopic compositions of lavas from this volcano, and the cluster of four samples which exhibit an unusually strong DMM component, indicate that there may be unusual processes contributing to the mantle source signature of erupted lavas in the period after the *Cumbre Nueva Collapse*.

3.4.2 Interpretations of La Palma's whole rock geochemistry and mantle source

In combination these studies provide a comprehensive overview of the origin of La Palma lavas in terms of mantle components. However, each individual study chose their samples for specific reasons, proposed their own interpretation of what their isotopic data meant, and analysed their rocks for other properties (incompatible elements, mineral chemistry, stable isotopes). In the section that follows we review the interpretations of whole-rock data starting from the base of the volcanic system, addressing mantle components, through source mineralogy and into assimilation processes during transport.

Recycled lithospheric material in the western Canary Islands mantle source

The study of Marcantonio et al. (1995) was significant as one of the first to investigate Os isotopes in HIMU lavas. Taking samples from across La Palma's subaerial history, this study identified hyperbolic mixing arrays on $^{187}Os/^{186}Os$ vs $^{206}Pb/^{204}Pb$ diagrams with lavas with the strongest HIMU signature exhibiting the most radiogenic Os isotope signature. Since elevated radiogenic Os is believed to be among the best isotopic indicators of the presence of recycled lithospheric material in primitive magmas, this correlation was used to support the concept of the HIMU component originating through recycling of oceanic crust. This approach was then expanded to a larger lava sample (Widom et al., 1999), demonstrating that this trend was representative of lavas from across the region of the Canary Islands and Madeira.

Such isotopic indicators of a recycled component in basalts were increasingly being interpreted in terms of the source lithology of the melts, particularly after Sobolev et al. (2007) developed a tool for determining source proportions of pyroxenite and peridotite based on EPMA analyses of olivine phenocrysts. Day et al. (2009) addressed this by sampling a stratigraphically comprehensive suite of lavas from La Palma and El Hierro and applying a combination of Os isotopes of whole rock samples and $\delta^{18}O$ determinations of phenocrysts, a second indicator of the presence of lithospheric material. The resulting data formed two linear arrays, distinct for each island, which they interpreted as the product of a mixed pyroxenite/peridotite with differences between La Palma and El Hierro in the nature of the recycled oceanic crust component (recycled pillow lavas would be different from recycled gabbro). Gurenko et al. (2009b) similarly took samples from the western Canary Islands, but derived their pyroxenite and peridotite contents on the basis of Pb isotopes and the Sobolev et al. (2007) olivine EPMA approach. They identified the pyroxenite signature as associated with the "DMM" component that was strongest among samples from El Hierro, indicating this could not be the simple, peridotitic, depleted MORB source sampled at oceanic ridges and that this was also the product of recycled material.

Day et al. (2010) expanded their previous study to include an extensive suite of isotopic systems (Sr-Nd-Pb) as well as analyses of highly siderophile element concentrations (HSE). The resulting strong correlations between different radiogenic isotope systems (Os-Pb-Sr-Nd) were independent of the $\delta^{18}O$ groups previously proposed and difficult to reconcile with the heterogeneity described in the earlier study. The results indicated that La Palma and El Hierro yielded distinct mantle-component signatures originating from their positions on a shared array, and that both provided evidence of subduction recycling. However over a succession of later papers (Day et al., 2012; Gurenko et al., 2011, 2012) the positions presented by these two research groups became increasingly incompatible. Nonetheless, both agreed that the young-HIMU component was the product of recycled material, and also that the DMM component appeared to contain recycled pyroxenite and therefore was only "DMM-like".

HYDROUS MINERALS IN THE CANARY ISLANDS' MANTLE SOURCE

Detailed studies of incompatible element abundances in lavas from the *Cumbre Vieja* and all of La Palma led several studies (Galipp, 2005; Praegel and Holm, 2006) to propose there was a hydrous mineral present in the Canary Island mantle source. On mantle-normalised incompatible element profiles La Palma lavas are relatively depleted in K, which along with Ti has relatively constant concentrations independent of variation in highly incompatible elements such as La. The authors of both studies assumed that variations in La concentrations in primitive lavas provided a proxy for degree of partial melting, and therefore the relative stability of K and Ti concentrations indicated that these two elements were being buffered by a mineral in the melt source.

Based on abundances of Nb, Ba and Rb in La Palma lavas, and the relative compatibility of these elements in hydrous minerals, Galipp (2005) proposed phlogopite and amphibole as the most likely buffering minerals, with the caveat that amphibole was the better candidate. Praegel and Holm (2006) adopted a similar approach, modelling batch-melting for various parent lithologies, and similarly determined that amphibole was more likely. However, a later study (Turner et al., 2015) used comparable data to interpret the source lithology as a garnet lherzolite with residual phlogopite content, and therefore the exact nature of this hydrous mineral remains open to interpretation.

LITHOSPHERIC ASSIMILATION DURING MAGMA TRANSPORT

Working on a stratigraphically comprehensive suite of primitive La Palma lava samples, Galipp (2005) identified Nb/U ratios extending well beyond the normal range of 47 ± 10 determined for OIB basalts (Hofmann, 1988), particularly for the older *Taburiente* lavas which ranged up to Nb/U of 88. Furthermore, since this study had already proposed that amphibole was present in La Palma's melt source, they determined this should be buffering the concentrations of these amphibole-compatible elements. They therefore suggested that this variation was best explained through bulk assimilation of variable volumes of an amphibole-rich lithology during magma transport, modelling several possible scenarios and settling on a contribution of 20% assimilated amphibole to the melt.

Day et al. (2010) were relatively sceptical about the role of assimilated material in the evolution of La Palma lavas, successively dismissing several potential "crustal contamination" sources such as oceanic crust, pelagic sediment and peridotitic xenoliths based on how each would be expected to contribute to the variation within their study's large isotopic dataset (Pb-Sr-Nd-Os-O) for its sample suite. Nonetheless, Turner et al. (2015) recognised that if the material were produced at an earlier stage of the island's growth it would not necessarily provide any isotopic contrast with normal oceanic island processes, but could strongly influence trace element chemistry (they interpreted a strong role for assimilation in terms of Nb/U, Ce/Pb and Th/U). They proposed that *Cumbre Vieja* lavas were best modelled with a significant contribution by partial melting of oceanic island syenite into the magma.

Barker et al. (2015) was the first study to identify such an assimilated component in terms of an eruption's cargo, identifying a significant population of mafic cumulate xenoliths and partially resorbed amphibole xenocrysts in the lavas of the *Cumbre Vieja's* 1971 eruption. On the basis of thermobarometry, they proposed that this eruption's magma assimilated a leucogabbro mineral assemblage in the lithospheric mantle. This appears to provide petrological confirmation of the whole-rock assimilation trend.

The origin of DMM-like samples from La Palma's minor edifices

Abratis et al. (2002) identified their four most DMM-like dredge samples as a subgroup of alkali basalts, in contrast to the basanite and "high Zr/Nb" subgroups of the remaining dredge samples. They commented on the unusually high V/Ti (0.018 ± 0.002) and Fe/Ti (5.41 ± 1.20) ratios of these samples, but since the number of isotopic analyses from the remainder of the island was relatively limited at the time of publication, the exotic nature of these samples was not so apparent. Galipp (2005) did not discuss the petrology of their four most DMM-like *Bejenado* samples in detail, these had been collected opportunistically and were as a result not well constrained stratigraphically. The author interpreted them as the product of a process relating to the *Cumbre Nueva Collapse* and discussed them in the context of their wider study of the island. In both cases these samples originated from edifices with limited stratigraphy and so their isotopic variation has largely been treated in terms of mantle components and whole-rock processes rather than individual eruptive units.

3.4.3 Whole rock geochemistry discussion

The lava data from La Palma's separate edifices appears to characterise the island as transitional between the more HIMU dominated compositions of Tenerife and the more DMM-like compositions of El Hierro, with sufficient variation present to reward more detailed study if the considerable scatter between samples from each edifice can be overcome. Within this, the unusually depleted compositions identified on *Bejenado* (and also from dredge samples) provide an attractive research opportunity, since that edifice's isotopic variability could be addressed with new samples with detailed field constraints.

However, while petrological studies are typically rooted in the field relations of individual eruptions, whole-rock data tends to be best interpreted in terms of mantle components. It is unclear how to reconcile the pyroxenite/peridotite debates of mantle component studies with the presence of amphibole in a lherzholite source as discussed in magma transport studies, since these lithological models appear mutually exclusive. This is without including a contribution caused by amphibole assimilation during the later stages of the transport process. One possibility may be through treating trace elements as varying independently of isotopic variation, a convenient explanation for whole-rock variation in transport studies. Nonetheless, given the instrumentation required for acquiring new high precision radiogenic isotope data, it is unreasonable to expect studies of the reservoir

system to incorporate them into their studies, but otherwise it is difficult to unite the transport-based view of the reservoir system with the whole rock models of mantle geochemistry.

3.5 Discussion

There is potential in central La Palma for a new study to be conducted that integrates field evidence, igneous petrology and mantle geochemistry. The *Cumbre Nueva Collapse* was the key event that led to this region's subsequent complexity and spectacular exposure, and a detailed study of this area is likely to provide insights into how such a collapse affects oceanic island processes. It is a region with a number of unstudied geological features and unresolved field relationship issues while the radiogenic isotope variation observed from this area's small number of analyses is considerable.

However, because of the extensive previous body of literature and extreme geological complexity, such a study must be opportunistic rather than comprehensive. It is unrealistic to attempt to study the Seamount Series, *El Time*, *Bejenado* and the *Caldera de Taburiente* in the course of one PhD project, particularly since a number of these features (the Seamount Series and *Caldera de Taburiente's* sedimentology) have been the focus of previous work and are largely understood. Furthermore, each sub-discipline has subtly different requirements, with field studies valuing exposure and access, petrological studies benefiting from porphyritic eruptions with multiple lava-units, while mantle geochemistry studies ideally address moderate to large numbers of eruptive units suitable for sampling.

The relatively unstudied post-collapse *Bejenado* volcano is an opportunity both for field and geochronological research as well as mantle-source geochemistry. Study of its field relations has the potential to determine the sequence and age relations of eruptions on a post-collapse volcano, while the extreme isotopic variation observed in previous opportunistic studies could be understood with more detailed sampling and study. *El Time* provides an attractive contrast to this edifice, a relic sequence from before the *Cumbre Nueva Collapse* composed of lava flows erupted under less dynamic conditions than *Bejenado*. We propose that a systematic comparison of suites of lava samples from *El Time* and *Bejenado* may provide insights into the origin of *Bejenado's* anomalously depleted samples, and therefore whether these result from the effects of a giant landslide affecting mantle source signatures.

In the results sections that follow, we present three opportunistic studies into this region's geology and rock samples that we hope are together greater than the sum of their parts: 1) a field relations and geochronology study aimed to improve our understanding of the *Cumbre Nueva Collapse* and *Bejenado*, 2) a petrological study of a major flow-field identified in the previous chapter aimed to determine reservoir system processes after a lateral collapse, 3) a whole rock geochemistry and petrological study of the lava samples from both *El Time* and *Bejenado* aimed to determine the deep

magma supply system processes after the collapse and decrypt the depleted *Bejenado* isotope signature.

Chapter 4 : GEOCHRONOLOGY AND FIELD EVIDENCE

THE GEOCHRONOLOGY OF THE PERIOD OF LA PALMA'S *CUMBRE NUEVA COLLAPSE*, AND THE GEOLOGY OF THE EASTERN SECTOR OF THE *BEJENADO* VOLCANO

ABSTRACT

La Palma's last giant landslide ended activity on its *Paleo-Cumbre Nueva Rift* and resulted in an 11 km diameter collapse embayment with 750m-scale cliffs. Our study investigated the magmatic products erupted both before and after this collapse. We present $^{40}Ar/^{39}Ar$ dates of key lava flows as well as a new stratigraphy for the post-collapse *Bejenado* volcano's eastern flank. *Bejenado's* eruptive products are spectacularly well exposed, since volcanism in the region ended after its last eruptions.

New age determinations constrain the date of the *Cumbre Nueva Collapse* (between 529±13 ka and 530 ±21 ka), as well as indicating it ended a period of rapid, but not atypical, re-surfacing of the island's *Paleo-Cumbre Nueva Rift*. Post-collapse activity at *Bejenado* was very brief (from 529 ±13 ka to 496 ±16 ka). Field studies of *Bejenado's* eastern sector have described five volcano-stratigraphic units: 1) a relatively inaccessible *Bejenado Lower Series*, 2) the Los Rodeos Evolved and Volcaniclastic Phase: a laterally extensive volcaniclastic sequence with both an evolved composition and evidence of phreatomagmatic fragmentation, 3) the Bejenado Effusive Phase: a mainly primitive, compositionally and morphologically complex lava flow-field, 4) the Terminal Sheet Phase: a series of evolved, but compositionally complex, lava sheets, 5) *Montaña de la Hiedra,* a late cluster of tephri-phonolitic vents.

Re-constructing the volcanic history from these units indicates that La Palma's post-collapse volcanism took place in a new within-collapse environment where intense magma-mixing and interactions with local hydrology complicated the initial stages of volcanism. The brief phase of volcanism at *Bejenado* provides one of the best parallels to the early volcanism at Tenerife's *Teide*, and the differences between the resulting volcanoes leads us to suggest that these early post-collapse stages provided a significant control over the eventual morphology of the island.

4.1 INTRODUCTION

Our understanding of the major volcanic edifices of the Canary Islands has advanced over recent decades concurrently with improvements in geochronological studies (Carracedo et al., 2001, 2007, Guillou et al., 1998, 2001; Thirlwall et al., 2000). Radiometric ages can provide geological mapping projects and their resulting relative age relationships with an absolute chronology and as their precision has improved this has led to newer, higher-resolution, field studies. Unfortunately, there are technical limitations controlling whether young lavas can be dated in radiometric studies, since precise age determination is dependent on the time-integrated enrichment of radiogenic daughter isotopes. In the young, western, Canary Islands this has presented a challenge. Radiocarbon dating

of charcoal has provided one solution, taking samples from vegetation incorporated into volcanic sequences, and this has allowed young and sub-historic eruptions to be dated, but suitable samples (e.g. the remains of a tree trunk incorporated in a pyroclastic deposit) are very difficult to find and their appropriate use requires particularly strong field evidence (Carracedo et al., 2013). Fortunately, progress in unspiked K/Ar dating and $^{40}Ar/^{39}Ar$ dating of lavas has permitted their application to progressively younger volcanoes (Guillou et al., 1998; Thirlwall et al., 2000), including La Palma's *Taburiente* (Guillou et al., 2001) and *Cumbre Vieja* (Guillou et al., 1998) as well as Tenerife's *Teide* (Carracedo et al., 2007).

On La Palma, geological research on the eruptive products from the period of its most recent giant landslide illustrates these issues. Estimated to have occurred at "about 560 ka" (Carracedo et al., 2001), the *Cumbre Nueva Collapse* followed a period of spatially focused volcanism (Carracedo et al., 1999a; Navarro and Coello, 1994). The focused nature of La Palma's volcanism across this period, and the major unconformity resulting from the collapse, offer a good potential for high stratigraphic resolution geological study. Previous attempts to produce a stratigraphy from this period supported by geochronological data (Carracedo et al., 2001; Guillou et al., 2001) have yielded two key results: 1) the pre-collapse rift activity involved a late, rapid, growth phase bracketed to between 621 ± 9 ka and 566 ± 8 ka, 2) the post-collapse *Bejenado* volcano was dated to between 537 ± 8 ka and 490 ± 60 ka, indicating it was also the product of rapid growth. The number of key events in this period and its apparent brevity, along with limitations on dating lavas of this age range, present a significant technical challenge to field and geochronological study.

To address this problem this project presents a combination of: 1) 14 new lava-flow dates of stratigraphically well-constrained flow lobes, obtained by $^{40}Ar/^{39}Ar$ step-heating, from across the period of La Palma's *Cumbre Nueva Collapse*, 2) the results of a reconnaissance geological mapping study of post-collapse *Bejenado's* eastern flank.

4.2 GEOLOGICAL BACKGROUND

The seven islands of the Canary Islands chain generally decrease in age from east to west, and as a result each island provides insights into subtly distinct stages of the evolution of Canarian-type oceanic islands (Carracedo et al., 1998; Carracedo, 1999). La Palma and neighbouring El Hierro are situated at the westernmost tip of the chain and are both currently in their early shield stage. On La Palma this leads to a rapidly growing volcanic shield composed largely of relatively primitive lavas. La Palma has had six well-documented eruptions since the beginning of Spanish habitation in 1493 CE, making this the most volcanically active Canary Island in historic times.

La Palma is dominated by two main volcanic edifices, the older *Taburiente* shield volcano in the north, and the younger *Cumbre Vieja* polygenetic ridge to the south (Figure 4-1). In the central region of the island these edifices are separated by a major unconformity, the product of a giant

landslide known as the *Cumbre Nueva Collapse.* This collapse structure provides both access to some of the island's oldest rocks, the intrusions of the island's interior, and cliff sections through pre-collapse lava sequences. This area is also the site of the *Caldera de Taburiente*, a spectacular basin that has long been the focus of geological research (Carracedo and Paris, 2001; Colmenero et al., 2012; Lyell, 1855). This central region therefore provides the most complete access to La Palma's varied lithologies of anywhere on the island. A comprehensive review of its geology is provided[3].

It has been proposed that, towards the end of activity at *Taburiente*, volcanism became focused at its southern region (Carracedo et al., 1999a; Navarro and Coello, 1994), forming a feature referred to here as the *Paleo-Cumbre Nueva Rift*. Activity from this surfaced its area with some of *Taburiente's* youngest eruptive products. Nonetheless, there is no single stratigraphic marker of when this focused activity began and therefore it was likely to be the result of a gradual southward progression of volcanism (Carracedo et al., 1999a). The collapse removed the entire crest and the majority of the western flank of the *Paleo-Cumbre Nueva Rift*, but numerous authors (Carracedo et al., 1999b; Day et al., 1999; Navarro and Coello, 1994) have interpreted *Taburiente's El Time* region as a relic of its north-western flank.

The collapse embayment and subsequent incision have also provided access to some of the oldest units on the island and these provide the geological basement in this region. In the *Barranco de las Angustias* canyon, these exposures include the submarine extrusives of La Palma's Seamount Series (Staudigel and Schmincke, 1984), while to the east in the *Caldera de Taburiente* basin there is a complex formation of intrusives and breccias. The focus of post-collapse volcanism, the *Bejenado* volcano, onlaps these features and dominates the interior of the collapse structure. Previous studies of *Bejenado* have provided us with a relatively minimal stratigraphy: Navarro and Coello (1994) used changes in lava textures across the volcano to distinguish aa and pahoehoe morphology units, while Carracedo et al. (2001) used a change in magmatic composition towards the top of the sequence to distinguish a Terminal Differentiated Series from an underlying main *Bejenado* unit, while also identifying previously undocumented exposures of pyroclastic sub-units.

The *El Time* region and the *Bejenado* post-collapse volcano provide the most complete, and least altered, exposures of the phases immediately prior to and following the *Cumbre Nueva Collapse*.

[3] 3.2 The geology of central La Palma. pp. 40-52.

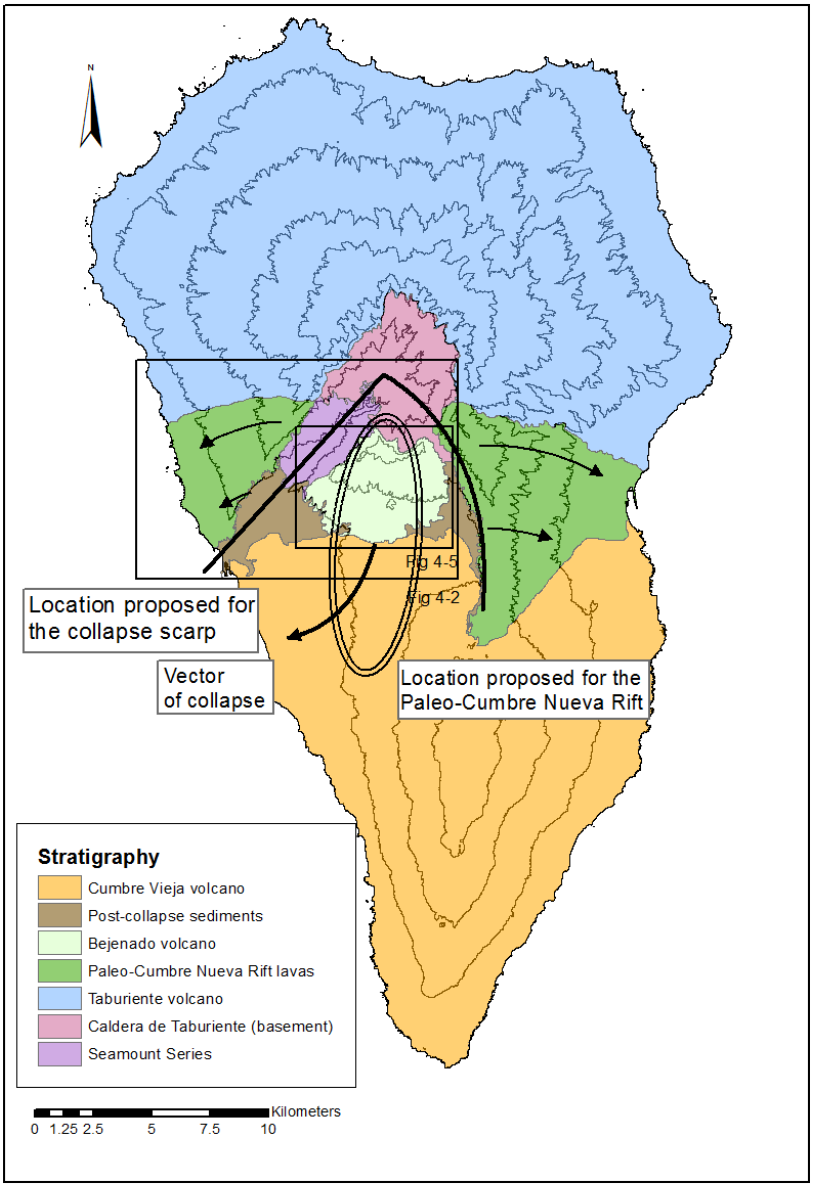

Figure 4-1 A simplified map of the primary stratigraphic units of La Palma including inferred locations of its major structural features (based on maps in Carracedo et al., 1999a, Day et al., 1999, Navarro and Coello, 1994). Topography is illustrated with 500m contours.

4.3 Methods

4.3.1 Geochronology

Samples were collected in the field on grounds of freshness, and initial preparation involved petrographic screening prior to crushing. 600mg of groundmass separates (250µm – 500µm fraction), representing two 300mg aliquots, were prepared by iterative cycles of jaw-crushing followed by sieving, with procedures optimised to maximize the yield of this size fraction. Alteration-free groundmass separates were then purified by a combination of leaching in dilute HNO_3,

magnetic separation and meticulous hand-picking under a binocular microscope. Hand picking focused on the removal of remaining phenocrysts and grains with evidence of alteration.

Preparation and analysis followed the protocols established at the Argon Isotope Facility (AIF) at SUERC in East Kilbride[4]. Samples and neutron flux monitors were placed in copper foil packets and stacked in quartz tubes. The relative positions of the packets were precisely measured for later reconstruction of neutron flux gradients. The sample package was irradiated for 2.0 hours in the Oregon State University reactor, Cd-shielded facility. Alder Creek sanidine (1.2056 ± 0.0019 (1σ) Ma, Renne et al. (2011)) was used to monitor ^{39}Ar production and establish neutron flux values (J) for the samples.

Gas was extracted from samples via step-heating using a mid-infrared (10.6 μm) CO_2 laser, with samples housed in a doubly-pumped ZnS-window laser cell. Individual sample grains were loaded into a copper planchette containing 1.0x1.0 cm square wells. Liberated argon was then purified of active gases (e.g., CO_2, H_2O, H_2, N_2, CH_4) using three Zr-Al getters; one at 16°C and two at 400°C. Data were collected on a GVi instruments ARGUS V multi-collector mass spectrometer using a variable sensitivity faraday collector array in static collection (non-peak hopping) mode (Mark et al., 2009; Sparks et al., 2008). Time-intensity data were regressed to t_0 with second-order polynomial fits to the data. Mass discrimination was monitored by comparison to running-average values of an air standard. The average total system blank, measured between each sample run, was 2×10^{-15} mol ^{40}Ar, 9×10^{-17} mol ^{39}Ar, 3×10^{-17} mol ^{36}Ar.

All data are blank, interference and mass discrimination corrected using the Massspec software package (authored by Al Deino, BGC). Plateau acceptance criteria were that the plateau consists of at least three contiguous steps and the scatter between the ages of the steps is low, i.e., MSWD close to 1, and the fraction of ^{39}Ar released for these steps is ≥50%. Isochrons were calculated using only the plateau steps to confirm that the composition of the trapped component. A plateau age was accepted if it was concordant at the 2σ level with the isochron age, had a trapped component indistinguishable from air (298.56±0.31, 1σ) at the 2σ level and met the other criteria listed above.

4.3.2 FIELDWORK

Reconnaissance geological mapping was conducted on 1: 10 000 fieldslips using a green-line exposure mapping methodology, following recent guidelines (Coe, 2010; Lisle et al., 2011) for the traditional methods. Contacts were finalised from LIDAR topographic data sourced from Spain's Instituto Geográfico Nacional after the excursion.

The last few decades have seen significant progress in reconstructing the emplacement processes of effusive and pyroclastic eruptions through interpretation of lava morphology (Hon et al., 1994;

[4] The remainder of this analytical methodology section was written by Dan Barfod of the AIF (SUERC), who was responsible for these stages of the analysis.

Kilburn, 2000; Self et al., 1998; Thordarson and Self, 1998) and pyroclastic sedimentology (Branney and Kokelaar, 2002). This project's observations are presented using this nomenclature.

Observations and interpretations are presented separately, and discussed in terms of individual stratigraphic units. The summary of each stratigraphic unit includes separate field descriptions and interpretation sections.

4.4 Results – part 1 : geochronology and sample sourcing

A map of sampling localities for dated lava flows is provided (Figure 4-2), with resulting dates and how they constrain regional stratigraphy (Table 4-1, Figure 4-3). Step-heating plateau and sampling co-ordinates from all these samples are included[5]. In almost all cases plateau ages passed the verification criteria, the only exception being LP14SG02 discussed below, and therefore plateau ages provide the most precise estimate of emplacement date. The resulting 2σ uncertainties all range from 1.9%-4.9% of the mean sample date.

Dated samples were mostly of basanitic to tephritic composition, with the LP13SG16 phono-tephrite sample possessing the most evolved composition. However the strongly porphyritic ankaramites present in both the pre-collapse and post-collapse suites presented a risk of argon inheritance, and these samples were therefore subject to the most rigorous preparation procedures.

4.4.1 Pre-collapse sequences

Large scale field observations and sample sourcing

El Time is best described as a raised, inland, headland that ends with the deep canyon of *Barranco Jurado* to its north and the cliffs of *Barranco de las Angustias* to its south. Previous studies have suggested that these cliff sequences are located very close to the original plane of the *Cumbre Nueva Collapse* (Carracedo et al., 1999b).

El Time is *Taburiente's* least eroded region (Figure 4-2), with the result that it is moderately densely cultivated and inhabited, and this unfortunately reduces the potential resolution of fieldwork in this area. Where exposed, lavas flows tend to possess aa morphology, but evidence for any of their vents is absent. The topography of surface flows can often be followed up-flow until their truncation to the east by the *Barranco de las Angustias* cliffs.

[5] Appendix C: Supporting analytical data. pp.207-pp.247.

Samples	Volcano-stratigraphic Unit	Lava composition	Plateau age (ka)
Bejenado (post-collapse)			
LP14SG07	Montaña de la Hiedra	Tephrite	496 ± 16
LP13SG16	Phono-tephrite (TSP)	Phono-tephrite	500 ± 14
LP12SG02	Amphibole Tephrite (TSP)	Tephrite	527 ± 15
LP14SG09	Plagioclase Basalt (BEP)	Plagioclase Basalt	497 ± 17
LP13SG29	Glomerocrystic Ankaramite (BEP)	Ankaramite	528 ± 23
LP13SG30	Xenolithic Pyroxene Tephrite (LREVP)	Tephrite	522 ± 16
LP14SG02	Xenolithic Pyroxene Tephrite (LREVP)	Tephrite	628 ± 48
LP12SG87	West Bejenado Surface Flow	Basalt	529 ± 12
LP13SG38	Bejenado Basal Ankaramite	Ankaramite	530 ± 21
El Time (pre-collapse)			
LP12SG14	Surface Flow	Basanite	529 ± 13
LP12SG10	Surface Flow	Basanite	550 ± 20
LP12SG15	Base Barranco de los Gomeros	Basalt	610 ± 30
LP13SG06	Barranco Jurado - marker ankaramite	Ankaramite	585 ± 11
LP13SG05	Barranco Jurado - lowest sampled flow	Basanite	600 ± 15

Table 4-1 $^{40}Ar/^{39}Ar$ age determinations from samples of effusive eruptions in La Palma's central region presented in stratigraphic order. Stratigraphic units on Bejenado: LREVP — Los Rodeos Evolved and Volcaniclastic Phase, BEP — Bejenado Effusive Phase, TSP — Terminal Sheet Phase.

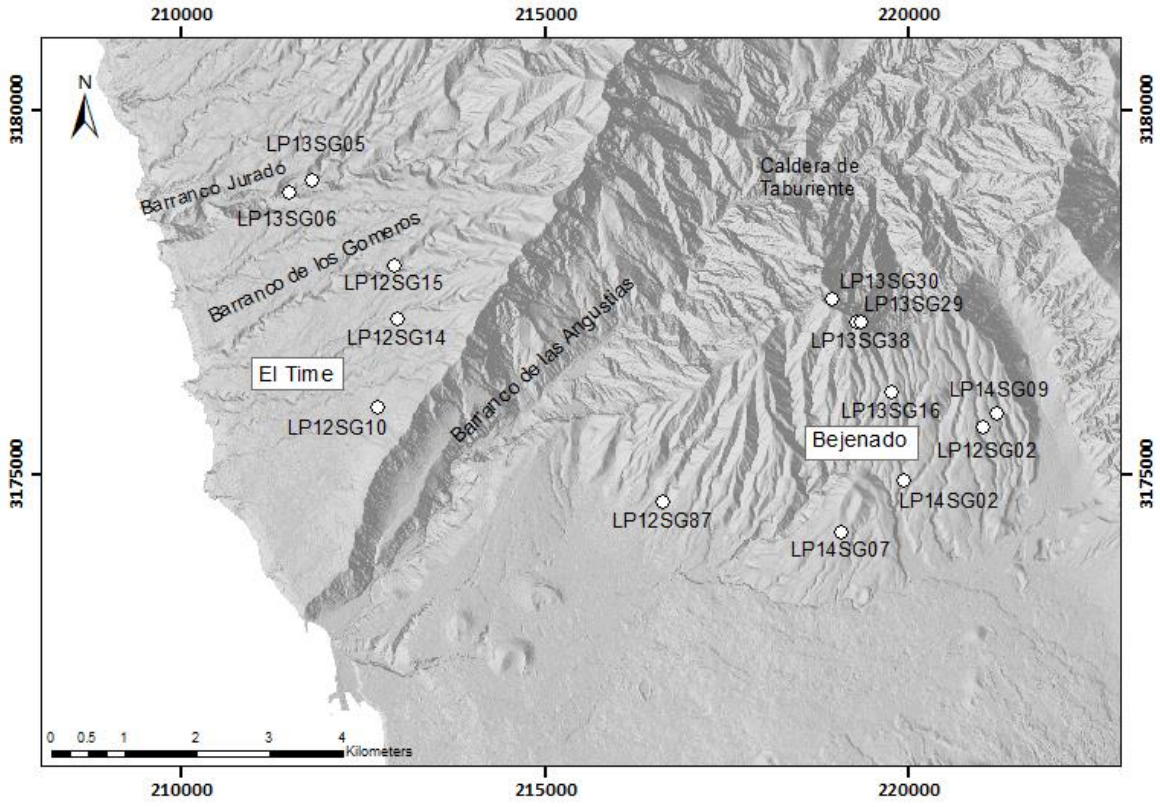

Figure 4-2 A map of the localities of lavas sampled for $^{40}Ar/^{39}Ar$ dating.

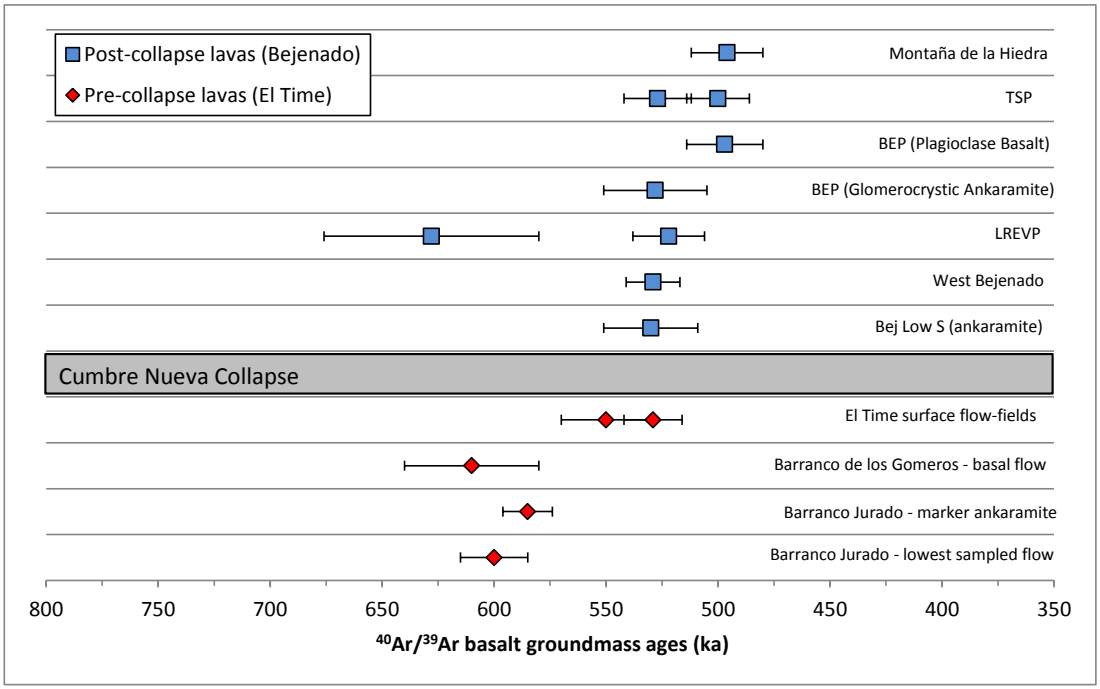

Figure 4-3 Summary of $^{40}Ar/^{39}Ar$ age determinations from collapse related lava-flows in the region of Central La Palma. Vertical units indicate relative age relationships between horizons and known stratigraphic units in eruptive sequences. Where multiple samples have been assigned to the same vertical unit this indicates they have equal significance in a stratigraphically indistinguishable horizon.

The limited erosion of the *El Time* lavas probably resulted from a combination of 1) late re-surfacing of the area when *Taburiente's* volcanism was focused at the *Paleo-Cumbre Nueva Rift*, and 2) post-collapse drainage upslope having been restricted by the cliff that bounds *El Time* to the east. It seems likely the truncated aa flows were the products of focused volcanism in the axial region of the *Paleo-Cumbre Nueva Rift*. Thus, the cliff at *Barranco de las Angustias* has both preserved the lavas of this region from erosion, and provided unambiguous evidence that these flows are the product of pre-collapse volcanism. This is important since in previous studies any young dates from *Taburiente's* lava flows have been explained as the product of residual post-collapse volcanism (Carracedo et al., 2001; Guillou et al., 2001), but in this area all lavas must predate the collapse.

A suite of rock samples from *El Time* was collected from surface flows in roadcuts (where exposures are commonly <5m wide), from deeper river incisions (termed barrancos), and from the deep *Barranco Jurado* where a further suite with approximate age relations was taken from the canyon's central *Camino Real de la Costa* trail. The results of detailed geochemical study of lavas from the entire *El Time* suite are presented[6]. A sub-sample of this suite was taken for dating, aiming to provide dates from the oldest accessible flows in fluvial incisions as well as using surface flows to date some of the youngest eruptions in the region.

GEOCHRONOLOGY

[6] 6.4 Results, part 1: comparison of lavas from Pre-Collapse *El Time* and Post-Collapse *Bejenado*. pp.144-158.

The date obtained from our stratigraphically lowermost sample (LP13SG05) of 600 ± 15 ka provides an age limit for our suite of samples from the pre-collapse period. The short interval until eruption of an up-sequence flow in *Barranco Jurado* (LP13SG06, 585 ± 11 ka), chosen because it is easily identified from its ankaramitic mineralogy and large euhedral phenocrysts, suggests rapid re-surfacing in the area in the period prior to collapse. This is supported by the date of the lowermost flow sampled from *Barranco de los Gomeros* (LP12SG15) which yields an age of 610 ± 30 ka and is overlain by two subsequent flow fields.

This activity continued until the eruption of the LP12SG14 and LP12SG10 lavas flows, each exposed on the upper surface of the *El Time* flank, which are likely to be among the *Paleo-Cumbre Nueva Rift's* youngest extant eruptive products. These both yield dates younger than the previous estimate ("about 560ka", Carracedo et al., 2001) for the date of the *Cumbre Nueva Collapse* and the 529 ± 13 ka date for LP12SG14 provides our best upper-limit for estimating the date of this event.

4.4.2 Post-collapse Sequences

Large scale field observations and sample sourcing

The summit of *Bejenado* (1844m) is the highest point within the collapse embayment. This edifice gradually rises to the north of the *Valle de Aridane* plain until its crest meets the southern-most of the *Caldera de Taburiente* basin's kilometre-scale cliffs (Figure 4-4). These cliffs provide excellent exposure of the internal stratigraphy of *Bejenado*, as well as access to the underlying collapse-structure and its related breccia sequences.

Bejenado's steeply dipping southern flank is the primary remnant of La Palma's post-collapse volcanism, and these units are truncated by the *El Riachuelo* canyon to the east and onlapped by the young *Cumbre Vieja* volcano to the south. *Bejenado* has been repeatedly referred to as a stratovolcano (Carracedo et al., 2001; Roa, 2003), however this description is misleading since no flows have been identified dipping north, east or west.

There is a marked distinction on *Bejenado's* southern flank between its eastern and western halves. To the west it is deeply incised by north-south trending canyons, while to its east the flank is better preserved with a less developed drainage network. As a result, access routes and paths are far more extensive on the eastern half than in the poorly accessible west. Only this eastern region has been addressed by this project's fieldwork.

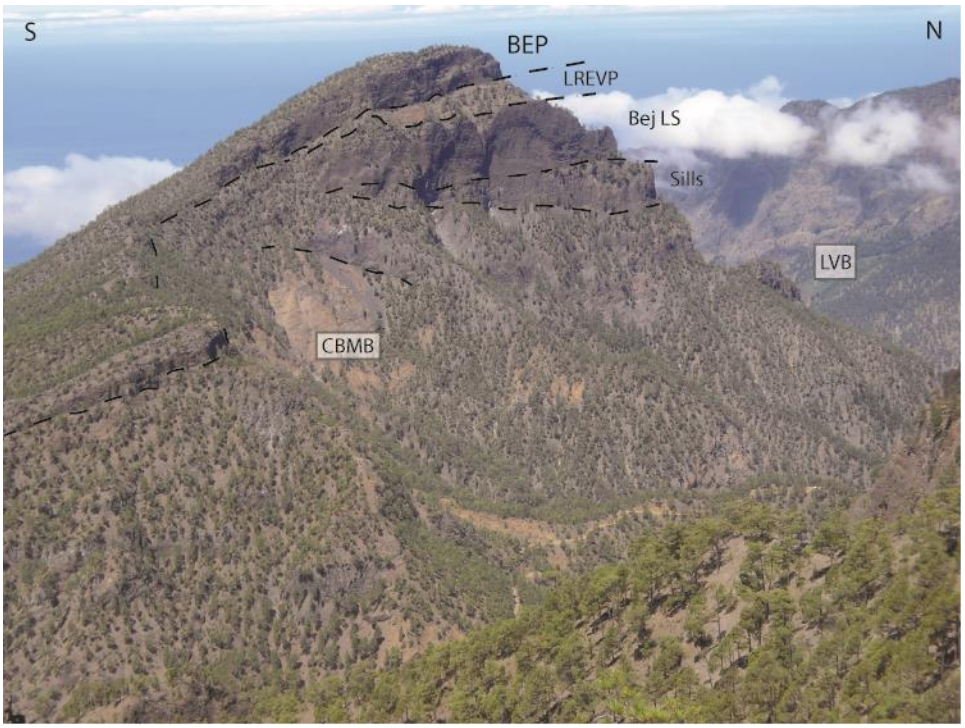

Figure 4-4 A view of the northern cliff section through *Bejenado*, viewed from the crest of the *Cumbre Nueva Ridge*, the lowermost cliff-section step at the right of the image is 600m beneath *Bejenado's* summit. The main stratigraphic units visible in this section are: Bejenado Effusive Phase (BEP), Los Rodeos Evolved and Volcaniclastic Phase (LREVP), Basal Sills, La Viña Breccias (LVB), La Cumbrecita Breccias and Megabreccias (CBMB). The Bejenado Lower Series of apparently ankaramitic lavas (Bej LS) has not been separately mapped as a result of inaccessibility. Photograph by Conny Spelbrink.

GEOCHRONOLOGY

With the exception of LP14SG02, all samples from the lower part of *Bejenado's* stratigraphy yield dates consistently between 530 ± 21 and 522 ± 16 ka. LP14SG02 yields an age inconsistent with its stratigraphic location, and the high intercept of its isochron indicates the presence of inherited argon, leading us to disregard this sample from further interpretation. The known presence of xenolithic material in this lava flow provides a convenient explanation for the origin of this inherited component.

Further up the *Bejenado* sequence multiple samples yield younger ages, with a sample (LP14SG07) from a late parasitic cone (*Montaña de la Hiedra*) yielding an upper-bracket for the lattermost eruptions of this volcanic phase at 496 ± 16 ka. Prior to this terminal eruption, lava flows on *Bejenado's* primary edifice yield dates as young as 497 ± 17 ka.

4.5 RESULTS – PART 2 : THE GEOLOGY OF THE EASTERN SECTOR OF *BEJENADO*

The reconnaissance geological map of *Bejenado's* eastern flank and cross section are presented in Figure 4-5 and Figure 4-6. East *Bejenado* is composed of a series of laterally extensive, roughly planar, volcanic units. *Bejenado's* uppermost flows are all truncated at the volcano's crest indicating

they originated at vent complexes that must have existed to the north. This area is now the interior of *Caldera de Taburiente,* a region of cliffs and formidable terrain.

Bejenedo's earliest sequences overlie epiclastic, collapse-related, breccias that onlap the collapse structure. The collapse's footwall consists of La Palma's core complex of the Seamount Series and some of the intrusive complexes common in the interior of *Caldera de Taburiente.* Viewed from the north, *Bejenado's* extrusive sequences appear remarkably thin, comprising only the uppermost part (<300m thick) of the kilometre-high basin walls (Figure 4-4).

Across *Bejenado's* eastern sector, lava-flows mostly dip parallel to topography but individual eruptive units are laterally and vertically variable in petrology and morphology. This variation makes it difficult to correlate lava-units between different localities, a problem exacerbated by the scarcity of paleosols. It has not been possible to divide the volcano's stratigraphy into unconformity-bound units. This project has therefore combined these into stratigraphic "phases" where there is strong evidence that one or more than one petrological sub-unit were unambiguously erupted together despite variations in lithology.

4.5.1 Regional Basement: La Cumbrecita Breccias and Megabreccias

The regional basement in the area of study is provided by the "La Cumbrecita Breccias and Megabreccias" unit previously characterised by Colmenero et al. (2012). Large outcrops of this unit extend into *Caldera de Taburiente* and *El Riachuelo* from the *La Cumbrecita* saddle.

This unit is a highly friable, pervasively altered, polymict breccia with a strong yellow colour throughout. Its angular clasts are exclusively of igneous origin and include grey dolerites and vesicular olivine basalts.

The dyke content of this breccia is high (<50% by volume), and increases towards the westernmost limit of the mapped area. The primary dyke population comprises finely crystalline, equigranular dolerites although leucocratic, cream-grey dykes are also present. Dykes are typically non-planar, trend NNW-SSE, and are relatively thin (10-30cm thicknesses). These dykes strongly resemble the doleritic clasts present within the host unit.

A detailed interpretation of this unit is presented[7]. In brief: this unit appears to be a collapse breccia from the early stages of La Palma's subaerial growth prior to the formation of *Taburiente*.

[7] 4.6.1 Unit-by-unit interpretation of the eastern sector of *Bejenado*. p.89.

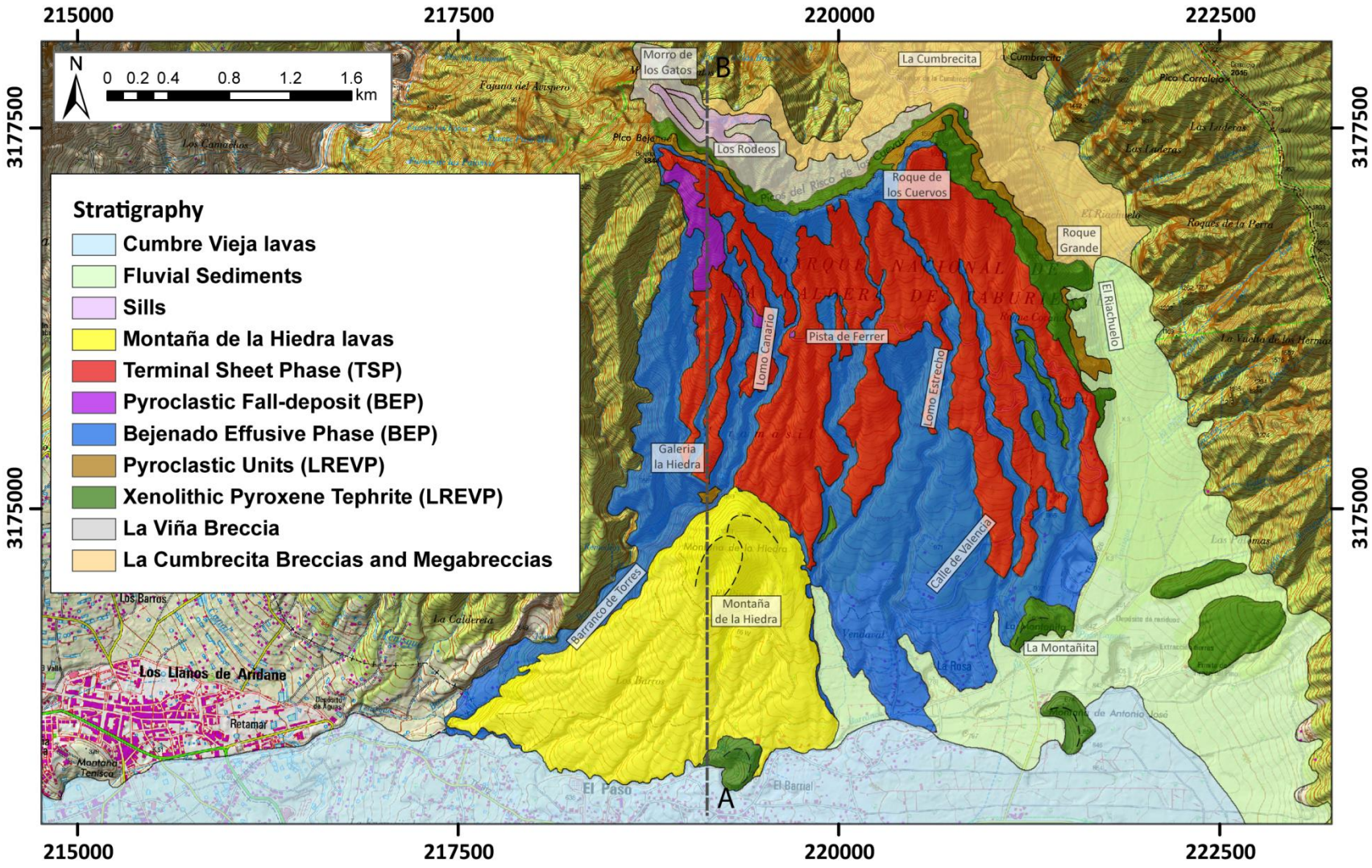

Figure 4-5 Reconnaissance geological map of Eastern flank of Bejenado volcano, contacts derived from field slips and remote mapping using LIDAR –derived topographic data. Lateral and Peripheral Vents of Bejenado have been inferred to be of the Xenolithic Pyroxene Tephrite unit, the dashed line A-B is the line of section in Figure 4-5.

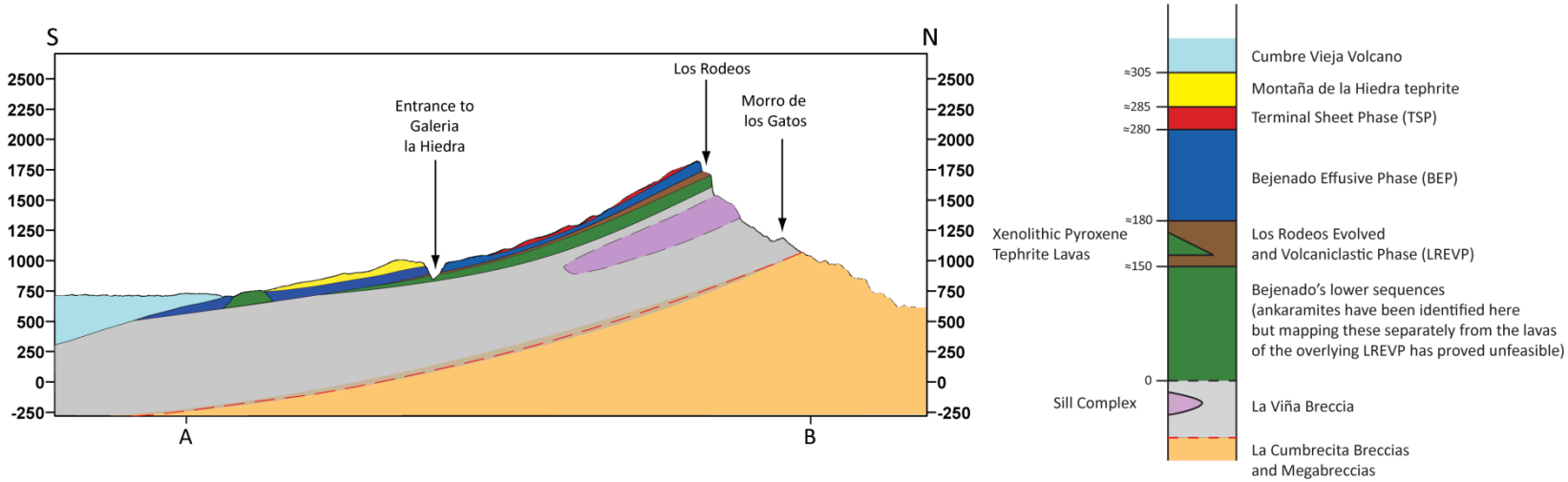

Figure 4-6 Approximate geological section and stratigraphic column of the Bejenado volcano and related units. The line of section extends further north and south than the extent of the map in Figure 4-4 in order to show Bejenado's relationship to Caldera de Taburiente and how it is onlapped by the Cumbre Vieja volcano.

Figure 4-7 Field photograph showing a representative outcrop of the La Viña Breccias unit: a polymict, matrix-supported, breccia commonly host to thin, planar, intrusions (both dykes and sills), taken near *Morro de los Gatos* mirador (vertical field of view = 4m).

4.5.2. *Sub-Bejenado* breccia: La Viña Breccias

The most extensive outcrops of this unit in the study area (<200m thickness) are found at the base of *Bejenado's* northern cliff section at the *Morro de los Gatos* mirador. This unit was previously characterised by Colmenero et al. (2012). It becomes progressively thinner to the east of this locality.

This is a matrix-supported, poorly sorted, polymict breccia (Figure 4-7). Its clasts (<30cm diameter) are subangular, with clast populations including coarsely crystalline gabbro, porphyritic amphibole tephrite, equigranular dolerite, ankaramite and loose scoria. Its matrix is a poorly consolidated pink to cream mud with single loose mafic crystals occasionally present. The majority of the sequence is massive, although individual lenses (≈1m thick) with planar bedding are present.

Detailed interpretation of this unit is presented[8]. In brief: this unit is believed to be the re-worked brecciated products resulting from the *Cumbre Nueva Collapse*.

4.5.3 *Bejenado: Bejenado Lower Series*

Formidable terrain difficulties have prevented the detailed description of *Bejenado's* lowermost extrusive sequences. These outcrop midway up the headwall of *Caldera de Taburiente's* southern cliff, where the presence of a marked step in the middle of the lower part of this section (Figure 4-4)

[8] 4.6.1 Unit-by-unit interpretation of the eastern sector of *Bejenado*. pp.89-90.

may indicate the lower series is composed of two separate eruptive units. Access through this section to the crest of *Bejenado* (via unstable scree-slopes) is only possible with close National Park assistance, and as a result unit-by-unit descriptions have not been obtained; and their exposure on a near-vertical section has prevented them being mapped separately from the lava-units of the LREVP. Where studied, highly oxidised scoriaceous beds were observed at the lowermost outcrops in this sequence, where they were overlain by intensely porphyritic ankaramites.

Detailed interpretation of this unit is presented[9]. In brief: this unit or units are believed to be the earliest lava flows of *Bejenado*, erupted in the period after the *Cumbre Nueva Collapse*.

4.5.4 *Bejenado*: *Los Rodeos Evolved and Volcaniclastic Phase* (LREVP)

The most complete exposure of this *Los Rodeos Evolved and Volcaniclastic Phase* (LREVP) unit occurs in the *Los Rodeos* path section (≈75m thick) towards the top of *Bejenado's* northern cliff sequence. This unit has not previously been described or identified as a single feature. However, because access to this area is hazardous and feasible only with National Park assistance, an alternative type-section has been chosen where *Pista de Ferrer* meets the western rim of the *El Riachuelo* canyon. Representative images of key features are included (Figure 4-8).

The LREVP unit is composed of two intercalated units: 1) a series of tephritic lava flows (the Xenolithic Pyroxene Tephrite unit), and 2) volcaniclastic deposits of both lapilli tuff and scoria (the Volcaniclastic Unit). The sub-units characteristically occur together, although their relative sequence varies across the field, and intercalation is visible at both type-sections (Figure 4-8A).

LREVP Lava-unit: Xenolithic Pyroxene Tephrite

The Xenolithic Pyroxene Tephrite lavas (<15m thick) consist of sequences of pairs of massive lava lobes and rubble (≈5m combined thickness) indicating they were emplaced as aa morphology lava flows (Figure 4-8B). These lavas are dark blue to purple, pervasively altered, and are poorly vesiculated. The lava contains abundant phenocrysts of prismatic clinopyroxene as well as sparse blue-grey sodalite-group feldspathoids. Mafic xenoliths hosted in the lava (<5% by volume) provide the characteristic feature of this sub-unit and they are largely of cumulate hornblendite origin (Figure 4-8C). Detailed petrographic descriptions of samples from this unit are included[10].

An agglutinate texture is visible in this lava unit at a number of localities, with lobes at both *Los Rodeos* and the *Roque Grande* cliff (≈50m high) consistent with ejecta re-welding after their explosive eruption.

[9] 4.6.1 Unit-by-unit interpretation of the eastern sector of *Bejenado*. p.90.
[10] Appendix D: Supplementary petrology — petrography of sample groups from *Bejenado* used in Chapter 6. pp.251-253.

Figure 4-8 Field photographs representative of morphological variation observed in the LREVP unit. A. Field relations at the most complete LREVP succession at *Los Rodeos*. In the foreground, oxidised scoria (OS) grades into a grey Laminar Lapilli Tuff (LLT) phreatomagmatic unit, In background the contact between these units is host to a lava flow of Xenolithic Pyroxene Tephrite (XPT) composition (trees provide approximate 8m scale). B. Succession of intercalated lava lobes and rubble in the Xenolithic Pyroxene Tephrite unit indicating their emplacement as aa lava flows, easternmost *Pista de Ferrer* (rucksack for scale). C. Xenoliths of cumulate hornblendite hosted in a lobe of Xenolithic Pyroxene Tephrite lava, *Los Rodeos* (knife for scale). D. Beds of oxidised scoria and spatter with minor horizons of yellow palagonitised tuff, *Los Rodeos* (National Park ranger for scale). E. Beds from the phreatomagmatic horizon near the top of the LREVP unit, showing fine grey laminar lapilli tuffs and palagonitised yellow tuffs, *Pista de Ferrer/El Riachuelo* canyon rim (vertical field of view 5m). F. Beds also from the phreatomagmatic horizon showing finely laminated ash and lithic lapilli, pencil for scale (El Riachuelo canyon rim).

LREVP MORPHOLOGY: VOLCANICLASTIC PHASE

The LREVP's volcaniclastic deposits are variable laterally and in thickness (<25m thick at *Los Rodeos*). They include two distinct members: 1) massive to poorly stratified beds of oxidised lapilli, scoria, bombs and spatter, 2) planar-bedded, palagonitised, ash and lapilli tuff sequences and lithic breccias.

The red, oxidised scoria and lapilli sequences (<20m thick) have the most laterally restricted individual beds and exposures and dominate the lower part of the *Los Rodeos* section. They are poorly consolidated and weakly stratified to massive beds of scoria (1-5m thick). They are commonly intercalated with similarly thick layers of more consolidated, yellow, palagonitised material (Figure 4-8D), indicating variable abundance of water during their eruptions. At the core of these scoria layers are spatter-dominated lenses (<50% by volume) of breadcrust bombs and spindle bombs, surrounded by beds of finer scoria that dip away from the spatter, indicating that these sequences formed as a number of distinct cones. Two such eruptive centres have been identified at *Los Rodeos* and a further centre near *La Cumbrecita*, and combined with the agglutinate textured lavas strongly indicates this eruption was focused at a number of dispersed vents.

The planar-bedded lapilli tuffs are much more laterally extensive, having been identified across an area of 12 km² to the south (at the mouth of *Galeria la Hiedra*) and east (along the western rim of *El Riachuelo*). These sequences vary from yellow to grey-brown, indicative of changing palagonite content across the unit (Figure 4-8E). Individual planar-beds show variable concentrations of lithic lapilli with fine ash often forming discrete laminations (<1cm thick, Figure 4-8F). Cross-stratification between laminar beds has been identified along the section exposed at *El Riachuelo* (Figure 4-8E), indicating this was the product of an erosive phreatomagmatic explosion. How this unit relates to the overlying sequences is ambiguous: in the near-summit *Los Rodeos* sequences a finely laminated grey-ash horizon is found at the top of the LREVP unit (Figure 4-10A), where it has a mostly undisturbed contact with the lavas of the overlying Bejenado Effusive Phase unit indicating a conformable relationship, but in the *El Riachuelo* section the sequence is capped by a tephritic lava flow.

Detailed interpretation of this unit is presented[11]. In brief: this complex unit is believed to be the product of an eruption of intermediate magma at multiple strombolian vents that interacted with the island's hydrology resulting in phreatomagmatism.

4.5.5 *Bejenado*: Bejenado Effusive Phase (BEP)

The Bejenado Effusive Phase (BEP) lava flow-field (≈100m thick at *Los Rodeos*) is the largest volume unit of the post-collapse period. It has not previously been identified or described as a unit. It is a laterally extensive (>3.5km wide) embankment composed of numerous individual lava lobes, with the unit thinning towards its eastern edge (<30m thick). The flow-field's flow morphology and magmatic composition are highly complex. Representative images of all morphological units are shown in Figure 4-10.

[11] 4.6.1 Unit-by-unit interpretation of the eastern sector of *Bejenado*. p.90

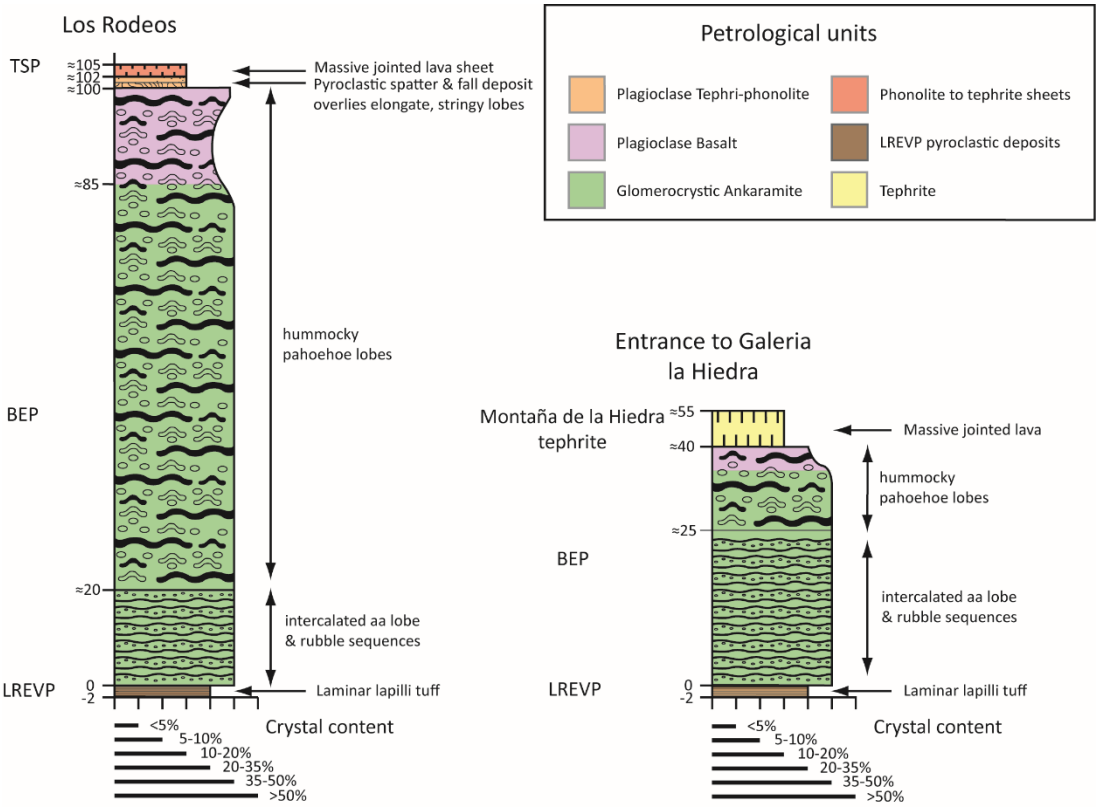

Figure 4-9 Approximate, schematic, logs of the BEP flow-field's morphological and petrological sequences as identified in vertical sections. The thick, sub-summit, Los Rodeos cliff is likely to provide the flow-field's most vent-proximal section, while at *Galeria la Hiedra* located 2.25km to its south the cliffs provide the most complete vent-distal section.

This complexity has permitted the flow-field to be divided into distinct morphological members, and within these to characterise petrological lava-units. A representative horizontal road-section through much of the flow-field can be found at the *Calle de Valencia* car park.

The flow-field's characteristic progression in lava morphology can be seen at this locality, but also at less accessible cliff sequences (Figure 4-9): 1) in the lowermost units intercalated sequences of lava lobes and rubble indicate that they were emplaced as aa lava flows, 2) up-section this changes into a major sequence of numerous small bell-shaped lava lobes (≈1m long but variable) indicating emplacement as pahoehoe. A further two morphological units are visible at more laterally restricted localities towards the centre of the flow-field: 3) towards the top of the sequence lava flows become increasingly sheet-like and laminar, 4) the lavas are capped by a bomb, spatter and pyroclastic fall deposit sequence composed of the same lava unit as the uppermost flows.

BEP Morphology: aa lobe and rubble sequence

The pairs of lava lobes and rubble clast beds (<10cm diameter) at the base of the sequence are laterally extensive and can be individually traced across outcrops. However, across the flow-field there is variation in both the total thickness of the aa lava formation and the individual thicknesses of the lobe and rubble pairs. At *Los Rodeos*, a locality that is likely to be close to the vent, there are

Figure 4-10 Field photographs of representative morphological variation across the BEP unit. A. Intercalated pairs of lava lobes and rubble (with combined thicknesses of <50cm) at the base of the BEP sequence, above the contact with laminar LREVP phreatomagmatic unit (LLT), at *Los Rodeos* (National Park Ranger for Scale). B. Intercalated pairs of lava lobes and rubble (with combined thickness of >6m) indicating emplacement occurred as flows of aa lava, *Calle de Valencia* car park (rucksack for scale). C. Lava lobes of hummocky pahoehoe morphology with ropey surface textures common, *Pista de Ferrer* (hammer for scale). D. A lava tube in a pahoehoe flowfield shows a roof lobe with vesicle populations indicating a P-type lobe that formed through inflation, *Lomo Estrecho/Pista de Ferrer* (rucksack for scale). E. The transition between Plagioclase Basalt composition pahoehoe lobes (Paho-L) and the elongate, stringy, poorly vesiculated sheet lobes of Plagioclase Tephri-phonolite (PTS), *Lomo de tamarahoya/Pista de Ferrer* (rucksack for scale). F. Locality where Plagioclase Basalt pahoehoe transitions into Plagioclase Tephri-phonolite sheets and is followed by a change of eruption style to bomb and spatter horizons (B+S) of same mineralogy, overlain by pyroclastic fall deposits (PFD), *Lomo Canario/Pista de Ferrer* (rucksack for scale).

only small successions of aa flows (≈10m thick) before the change to pahoehoe hummocks. Here, lava lobe and rubble pairs are particularly thin (<0.5m thick, Figure 4-10A). Conversely, on the lower flanks at the entrance to *Galeria la Hiedra,* the aa-type lobe and rubble pair succession is much larger (≈25m thick), while at the similarly downslope *Calle de Valencia* locality individual lobe and

rubble pairs can be extensive (≈6m thick), with large, massive, individual lobes (<3.5m thick, Figure 4-10B).

BEP Morphology: Pahoehoe sequence

The overlying pahoehoe sequence is much larger (forming >60% of most vertical series) and is formed of numerous small volume lava lobes without interstitial material. The change between these units is best observed at *Galeria la Hiedra*, where aa lobes become increasingly sheet-like with progressively less interstitial rubble before developing into full pahoehoe, which is often ropey textured with lava tubes in their interior.

Pahoehoe lobes possess the characteristic hummocky morphology (Figure 4-10C) identified at Hawaii's *Kilauea* (Self et al., 1998), and fit the P-type and S-type morphological categories described from this volcano (Self et al., 1998; Thordarson and Self, 1998). These categories provide evidence for variable degrees of lobe inflation during emplacement. Bell-shaped hummocks (≈2.5m basal-diameter) with large elongated vesicles and relatively dense cores are interpreted as P-lobes and they are believed to indicate lobe inflation. Such P-lobes are often found in the roof of lava tubes (Figure 4-10D). Globular lobes are smaller (<25cm diameter) with more evenly vesiculated, spongy, cores and these are interpreted as S-lobes that resulted from lava emplaced without inflation. On the lower parts of *Bejenado's* flank the lava-tube network is most extensive, with the interior of tubes accessible (>25m depth).

BEP Morphology: sheet-like, laminar lava lobes and BEP pyroclastic fall deposits

In an upper sequence best exposed at *Lomo Canario,* but also in a laterally restricted area towards the summit, lavas with poorly developed pahoehoe morphology (<2m thick) overlie the more typical hummocks found beneath. Here, the lava lobes are elongated, stringy and poorly vesiculated (Figure 4-10E). This thin unit is overlain by a poorly consolidated pyroclastic member composed of two beds (Figure 4-10F) that has been mapped as a separate unit (BEP Pyroclastic fall-deposit). The lower bed comprises bomb-sized spatter with bombs of identical lava to the underlying poorly vesiculated lobes, and the upper is a pyroclastic fall deposit of brown scoriaceous lapilli.

Lava-units of the Bejenado Effusive Phase

Three petrologically distinct lava-units can be identified in this flow-field, and although they are vertically stratified it has been unfeasible to trace their contacts laterally because of complexities in their emplacement discussed below. These lavas are: 1) the Glomerocrystic Ankaramite, 2) the Plagioclase Basalt, 3) the Plagioclase Tephri-phonolite. Samples from these lava-units have been the focus of detailed petrological study and description[12].

The Glomerocrystic Ankaramite lava-unit is the BEP's largest volume petrological unit, forming the lower part (≈85% thickness) of vertical sections (Figure 4-9). It is a strongly porphyritic (crystals

[12] Chapter 5: Petrology. pp.98-138

comprise ≈40% of its cross-sectional area), highly vesiculated, metallic blue olivine, clinopyroxene basanite. It is xenolithic with dunitic aggregates (<2.5cm diameter) common as well as occasional larger xenoliths of gabbro or cumulate hornblendite.

The Plagioclase Basalt lava-unit is present towards the top of the pahoehoe morphological unit, and is the first change in lava composition. The Plagioclase Basalt is a highly vesiculated, plagioclase-phyric, lava with abundant euhedral feldspar laths (<5mm diameter) in a vitreous, purple-blue, groundmass that when altered has a distinctive yellow crust. The thickest (≈15m) sequences of this unit are found south of *Bejenado's* summit. At individual sections the change between this lava and the underlying Glomerocrystic Ankaramite occurs as discrete steps between compositionally distinct pahoehoe lobes near the top of the pahoehoe morphological unit. However, lavas with compositions intermediate between these steps have been identified at localities across the flow-field indicating a full range of compositions were erupted. To distinguish the two lavas the Plagioclase Basalt is defined as rocks with more plagioclase laths visible (>50% crystal content) than the mafic glomerocrysts of the Glomerocrystic Ankaramite.

The uppermost lava-unit is the Plagioclase Tephri-phonolite. This is a poorly vesiculated, vitreous, plagioclase-phyric, lava with a grey groundmass, with strongly flow-aligned plagioclase crystals. The appearance of this lava accompanies the morphological change from pahoehoe lobes to poorly-vesiculated (Figure 4-9), stringy sheet lobes, and this lava-unit is present in the uppermost pyroclastic beds.

A detailed interpretation of this unit is presented[13]. In brief: the spectacular BEP flow-field is the product of an effusive eruption where magma mixing and the maturing of the flow-field's lava transport system resulted in considerable morphological complexity.

4.5.6 *BEJENADO:* TERMINAL SHEET PHASE (TSP)

The uppermost unit of the main *Bejenado* edifice is the Terminal Sheet Phase (TSP) which consists of thin, laterally extensive, lava sheets with variable composition. TSP units typically outcrop on the top of the minor plateaux common on *Bejenado's* eastern flank. These are locally termed "lomo" (translated as "whaleback") and these features are cut by shallow north-south trending barrancos. Previous workers (Carracedo et al., 2001) have identified this unit as *Bejenado's* Terminal Differentiated Series.

[13] 4.6.1 Unit-by-unit interpretation of the eastern sector of *Bejenado*. p.91.

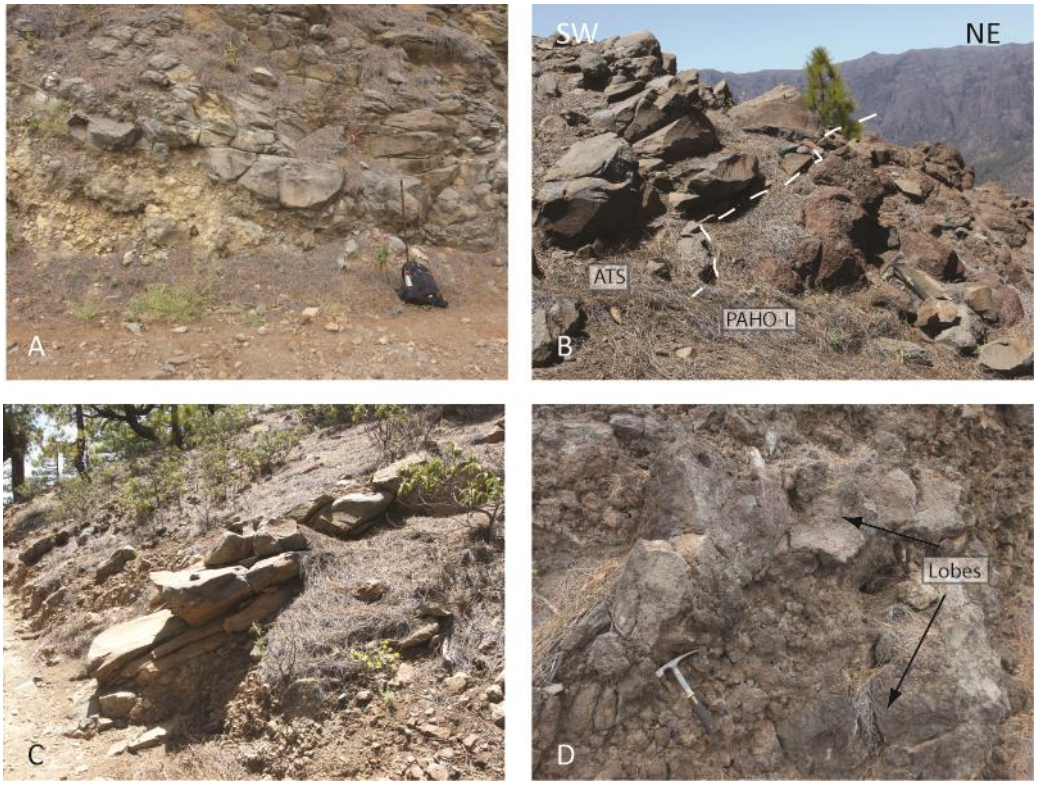

Figure 4-11 Field photographs of representative morphological variation across the TSP unit. A. Intercalated pairs of Amphibole Tephrite lava lobe sheets and rubble, where flow-parallel plates indicate laminar shearing during emplacement, taken at *Lomo Estrecho/Pista de Ferrer* (rucksack for scale). B. The contact between Amphibole Tephrite lava sheets (ATS) and the pahoehoe lobes of Plagioclase Basalt (Paho-L) beneath, taken at the crest of *Bejenado* east of *El Rodeo* (hammer for scale). C. The contact between a Phono-tephrite lava sheet and the underlying BEP pyroclastic fall deposit, southeast of *Pico Bejenado* (hammer for scale). D. A succession of Amphibole-Olivine Tephrite lava lobes and rubble indicating lava was emplaced as aa flows, *Roque de los Cuervos* (hammer for scale).

Three related lava-units can be identified within the TSP: 1) an Amphibole Tephrite, 2) a Clinopyroxene Phono-tephrite (TSP Phono-tephrite), and 3) an Amphibole-Olivine Tephrite. Representative photographs of the morphology of these units are included (Figure 4-11), as well as detailed petrographic descriptions[14].

The most laterally extensive lava-unit is the Amphibole Tephrite, and a characteristic section can be seen along *Pista de Ferrer* at *Lomo Estrecho.* The lateral extent of this unit is very similar to the BEP flow-field beneath (Figure 4-11B), although it also directly overlies LREVP lava flows to the east. This poorly vesiculated, porphyritic tephrite is typically grey-blue but weathers to a pale yellow. It consists of a single lava lobe and rubble pair (<3.5m thick, Figure 4-11A), with the lobe composed of a number of flow-parallel plates. It is xenolith-rich with cumulate hornblendites commonly observed.

The TSP Phono-tephrite outcrops in a small area to the south of the summit, centred on *Lomo Canario*. This also outcrops as a single rubble and lava sheet pair (≈1m thick but variable), largely

[14]Appendix D: Supplementary petrology — petrography of sample groups from *Bejenado* used in Chapter 6.pp.253-255

found above the BEP unit's late pyroclastic fall deposits (Figure 4-11C). It is a poorly vesiculated, pale grey, lava with small prismatic clinopyroxenes and feldspathoids commonly hosted in a microcrystalline groundmass.

The Amphibole-Olivine Tephrite outcrops at *Roque de los Cuervos,* the minor eastern summit of *Bejenado*. It forms three aa pairs of lava lobe and rubble (<0.75m thick, Figure 4-11D) above a conformable contact with the Amphibole Tephrite. It is a highly porphyritic (>30% cross sectional area crystals), strongly vesiculated, metallic grey lava. It is rich in mafic minerals containing a surprising abundance of both acicular amphibole and unaltered olivine phenocrysts rendering its mineralogically between basanitic and intermediate.

Detailed interpretation of this unit is presented[15]. In brief: this late eruption exhibited dramatic magma-mixing during the emplacement of a laterally extensive but volumetrically small cap of late evolved lavas.

4.5.8 *Bejenado*: *Montaña de la Hiedra*

Montaña de la Hiedra consists of a cluster of two monogenetic scoria cones and their associated, small volume lava flows (<2km² resurfaced area); it onlaps the southernmost part of *Bejenado's* flank. A third vent located at the southern tip of *Montaña de la Hiedra* is the product of an earlier eruption and not part of this unit.

The lavas at both vents are poorly vesiculated, poorly phyric, finely crystalline, pale grey tephrites. They contain prismatic clinopyroxenes (≈1mm long but variable) and traces of sodalite-group feldspathoids. Lavas in this flow-field tend to form large, planar, lava sheets without rubble layers.

A detailed interpretation of this minor unit is presented[16].

4.5.8 Intrusions

Two suites of intrusions have been identified that post-date the *Cumbre Nueva Collapse,* with both best exposed in *Bejenado's* northern cliff section. The more significant of these is a major sill complex intruded between beds of the *La Viña Breccia* at the base of *Bejenado*. The largest sill of this unit (>100m thick) is a heavily jointed, porphyritic, olivine gabbro intruded close to the collapse surface, and is found separating the post-collapse *La Viña Breccias* from the pre-collapse *La Cumbrecita Breccias and Megabreccias*. There is limited access to this sill-complex in the area of study.

A dispersed swarm of minor dykes and sills (widths and thicknesses typically <1m) with compositions similar to those of *Bejenado's* eruptive units are intruded into the shallow sections near *Bejenado's*

[15] 4.6.1 Unit-by-unit interpretation of the eastern sector of *Bejenado*. pp.91-92.
[16] 4.6.1 Unit-by-unit interpretation of the eastern sector of *Bejenado*. p.92.

crest, but can also be identified in deeper barrancos on the flank. These intrusions occur as far south as *Barranco de Torres*, where they are common.

The similar composition of these intrusions to the main eruptive units suggests these are likely to be sub-volcanic units emplaced beneath *Bejenado's* surface in a chaotic feeder and ponding system. The origin of the deeper sill complex is likely to be more complicated, and may be associated with the gabbroic intrusions common in the interior of *Caldera de Taburiente*.

4.6 Interpretation

The superb exposure of La Palma's post-collapse volcanism results from the preservation of the southern flank of *Bejenado* and the sections into its earliest eruptive units provided by *Caldera de Taburiente*. Detailed observations taken from these units permits an interpretative model to be developed for the post-collapse period and anchored with radiometric dates to an absolute chronology. In the following section the features of each unit are separately interpreted, followed by a synthesis for the whole *Bejenado* edifice.

4.6.1 Unit-by-unit interpretation of the eastern sector of *Bejenado*

Regional basement - La Cumbrecita Breccias and Megabreccias

Colmenero et al. (2012) interpreted this breccia as the product of La Palma's earliest subaerial collapse (≈1.2 Ma) affecting the *Garafia* volcano, preceding the growth of *Taburiente.* This places this breccia unit in the island's interior during the growth of the *Paleo-Cumbre Nueva Rift,* re-exposed only after that edifice's collapse.

As a volcanic edifice collapse breccia, its doleritic clasts are likely to result from the disaggregation of *Garafia's* feeder dyke system. Such feeder systems are superbly illustrated by the main dyke swarm hosted within this unit, which is likely to have fed the *Paleo-Cumbre Nueva Rift* considered to have been focused in this area (Carracedo et al., 1999b). Thus the rift's axis is likely to have been above the dense part of the dyke swarm observed towards the western limit of the mapping area.

Sub-Bejenado Breccia: La Viña Breccias

The absence from this breccia of the NNE-SSW dyke swarm identified in the underlying units indicates this unit was deposited after the end of activity at the *Paleo-Cumbre Nueva Rift,* making it likely that this breccia is the earliest sedimentary deposit preserved from the period after the *Cumbre Nueva Collapse*. Because of this, the lowermost contact of this unit must be either the detachment surface of the collapse or the product of erosion of this surface.

However, the significant matrix concentration and slight rounding of clasts within the unit are both indicative of sedimentary re-working, implying a hiatus between the *Cumbre Nueva Collapse* and initial eruptions at *Bejenado*. Colmenero et al. (2012) has characterised this breccia as a series of

cohesive debris flows, formed through re-mobilisation of primary collapse-related landslide deposits (which have not been observed).

Bejenado Lower Series

Due to access difficulties, very little is known about the earliest eruptive units on *Bejenado*. Furthermore, this unit's ankaramite mineralogy is concerning, since it strongly resembles the Glomerocrystic Ankaramite of the Bejenado Effusive Phase, to which it could potentially have a complex magmatic relationship. This problem is exacerbated by the poor field-relations for this *Bejenado Lower Series*. Nonetheless, the presence of scoria means it is unlikely to be part of this later unit's sub-volcanic system.

The best prospect for understanding this period may potentially be found in the deeper incisions on western *Bejenado*, where the extensive BEP lava sequence that overlies these units appears to be absent. However, without further fieldwork we cannot provide detailed insights into this early phase of post-collapse activity.

Los Rodeos Evolved and Volcaniclastic Phase

The complex LREVP sequences appear to have been the product of an eruption of intermediate, xenolith-rich, magma where a combination of hydromagmatism and multiple strombolian vents led to considerable lateral variation in the resulting deposits.

It is likely that the major focus of this eruption was a summit vent complex at or near the *Los Rodeos* locality (1750m), where the volcaniclastic sequences are thickest. The oxidised scoria beds identified here are consistent with air-fall deposits from a strombolian eruption, capped by the laminar lapilli beds produced in a late phreatomagmatic episode.

A number of small volume monogenetic cones have been identified across the northern *Valle de Aridane* plain and assigned to *Bejenado*-phase volcanism (Carracedo et al., 2001). These include cones at *La Montañita* and at the south of *Montaña de la Hiedra,* and in both cases their large-scale field relations indicate they preceded *Bejenado's* late eruptions. Since there is strong evidence that the LREVP unit was the product of a number of dispersed vents, it seems reasonable to assign some if not all of these cones to this eruptive phase.

Laminar lapilli tuffs deposited in the major phreatomagmatic episode can be identified across *Bejenado's* eastern sector. The cross-stratification of these planar-bedded ash and lithic lapilli layers indicates their deposits were produced by an erosive, low particle concentration pyroclastic density current (Branney and Kokelaar, 2002). Similar deposits on neighbouring *Tenerife* have been described by Clarke et al. (2009) as transitional, where they propose this indicates phreatomagmatic activity with relatively minimal water contents. Such an eruption would require a non-marine water source. A possible parallel to this eruption is provided by the 1949 eruption on the *Cumbre Vieja* (at

altitudes of 1880m), where phreatomagmatic sequences have been attributed to groundwater-magma interaction (Klügel, 1999).

BEJENADO EFFUSIVE PHASE

The BEP is the product of a major post-collapse effusive episode which re-surfaced an area of the collapse structure with significant volumes of lava. Its unusual degree of morphological and compositional variation as well as its impressive exposure makes this a potentially rewarding case study on which to investigate the controls on lava morphology (which include slope during emplacement, and rheology, crustal strength, advance and cooling rates of the lava) but this is largely beyond the scope of this project. Nonetheless, some basic observations and interpretations are possible.

Firstly, *Bejenado's* southern flank appears to be a surprisingly steep slope (29° across the 1 km of slope to the south of the summit) for a flow-field that transitions between early aa morphology lava flows to later pahoehoe. Pahoehoe requires the formation of stable lava flow crusts after the lava emerges from the vent and these must remain intact as the flow advances — should this crust tear as a result of too-rapid advance, this leads to aa flow production and this change is irreversible for individual flows (Kilburn, 2000). A critical value has been established (Solana et al., 2004) between the sine of the angle of slope and the lava advance rate in a pahoehoe field beyond which the flow will be emplaced as aa. Thus despite the considerable slope, the change in morphology over the course of the eruption indicates that lava advance rate and crustal strength were finely balanced at the beginning of the BEP sequence, and that the advance rate of the flow-field decreased as the eruption continued.

Secondly, this flow-field demonstrates that the relationship between changes in lava composition and changes in morphology are situation specific. The emergence of the Plagioclase Basalt lava-unit – that followed the Glomerocrystic Ankaramite lava-unit – appears to have had no influence on flow-field morphology, which continued to consist of hummocky pahoehoe lobes. This contrasts with the later appearance of the Plagioclase Tephri-phonolite lava-unit which was accompanied by a morphological change to more sheet-like lobes, overlain after a thin succession by fall deposits. This evolved lava-unit therefore appears to have caused this phase to become explosive, with fragmentation likely to have resulted from degassing of this magma's greater volatile content. There is considerable potential in this flow-field to investigate models of how varying lava rheology controls lava-flow form (Kilburn, 2000), and we observe that the aa and pahoehoe flow-field is mainly composed of an intensely crystal-rich, dense, ankaramitic lava indicating that this dense, exotic, lava-unit must have had a relatively low viscosity during its eruption.

TERMINAL SHEET PHASE

The evolved cap provided by TSP lavas indicates activity on *Bejenado's* main edifice ended with another compositionally varied eruptive episode, this time comprised of more evolved lava-units.

The extent of the TSP lavas closely corresponds to that of the underlying BEP flow-field, to which it appears to have been related. The two eruptions re-surfaced similar areas and are likely to be the product of similarly located vents.

The largest and most laterally extensive unit, the Amphibole Tephrite, appears to have been sufficiently evolved as to have been shearing laterally during emplacement, leading to its structure as sequences of flow-parallel plates. The emplacement of this thin lava-unit was followed by the emergence of more primitive (Amphibole-Olivine Tephrite) and evolved (The TSP Phono-tephrite) lava-units from two distinct volcanic centres. Notably, the higher vesicle content and clear rubble and lobe aa layers of the Amphibole-Olivine tephrite indicate it was the product of lower viscocity flows than the other lava-units.

The TSP lava sheets are poorly-vesiculated, laterally extensive and probably relatively impermeable, and this is likely to be responsible for the local "whaleback" topography. In the period since activity ended at *Bejenado* the development of local drainage will have been resisted by these units, and they will have protected the original topography. However, where channel formation has cut through this thin layer, the underlying rubble and BEP hummocks are likely to have incised more rapidly, leading to barrancos between such "lomos".

Montaña de la Hiedra

The *Montaña de la Hiedra* vents are the youngest identified eruptive centres in this central region of the island, indicating that after this activity was focused at the new *Cumbre Vieja* ridge. They were the product of the eruption of similar lavas from two distinct cones produced in one eruption. The presence of scoria from the southern cone onlapping the lavas in the core of the northern vent provides evidence that activity continued at the southern vent after the end of activity at the northern cone.

4.6.2 A model for the evolution of central La Palma and growth of *Bejenado*

We present a qualitative model for the evolution of central La Palma, intended to provide the simplest explanation consistent with the features identified at *Bejenado* and *El Time* (Figure 4-12). This model has been strongly influenced by recent models for the growth of *Caldera de Taburiente* (Carracedo and Paris, 2001; Colmenero et al., 2012).

Stage A) the collapse ended a period of focused activity at the Paleo-Cumbre Nueva Rift that resurfaced the *El Time* area with young lavas and led to progressively greater flank instability. Stage B) following the collapse, the landslide deposits underwent sedimentary re-working during a brief eruptive hiatus, after which effusive volcanism began with emplacement of lava-flows. Stage C) subsequent multi-vent volcanism began to consolidate into a single *Bejenado* edifice, while explosive

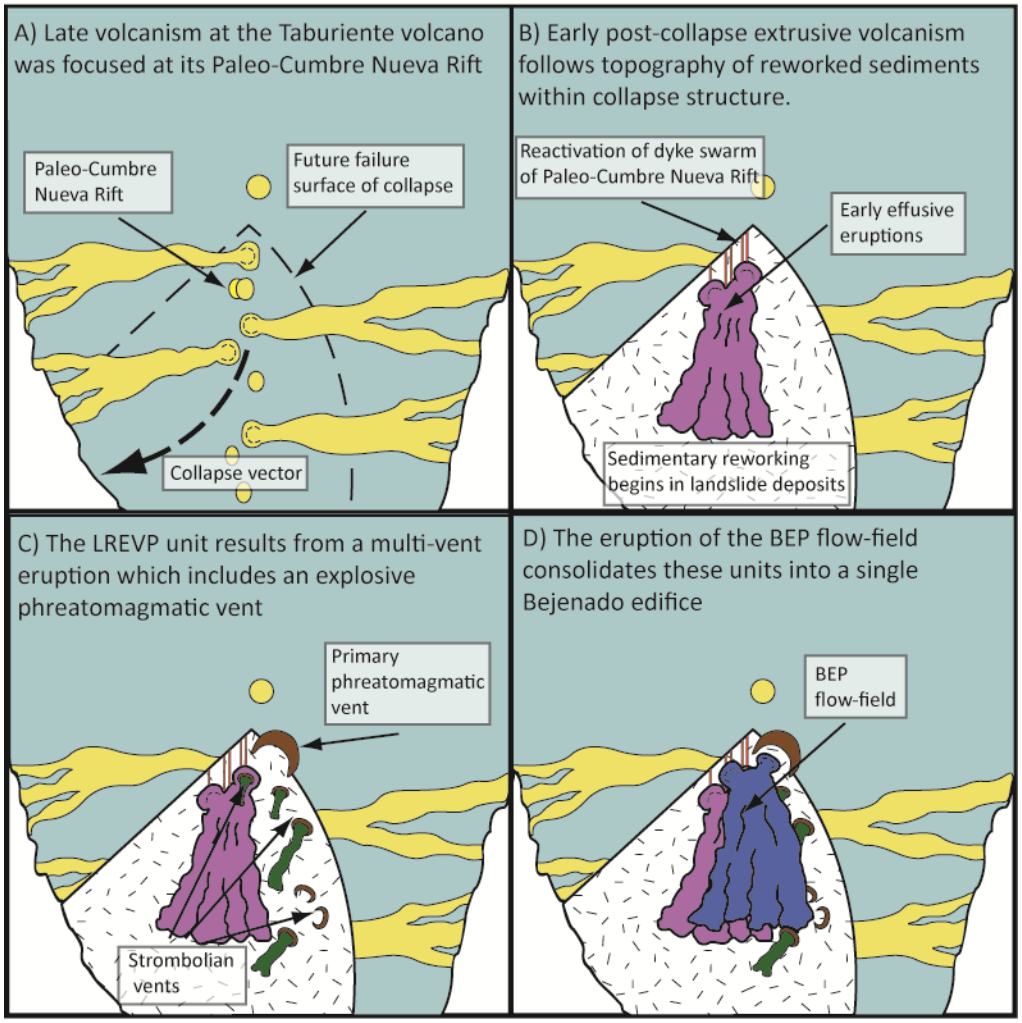

Figure 4-12 A schematic model for the evolution of central La Palma in the period of the *Cumbre Nueva Collapse*. The geometry of the collapse structure, and main sequence of events, have been taken from Carracedo et al. (1999b), while the primary phreatomagmatic crater in C) may have provided the initial space that grew into *Caldera de Taburiente*.

eruptions and phreatomagmatism led to the beginning of crater formation that would become *Caldera de Taburiente*. Stage D) the major, long-term, effusive eruption of the BEP flow-field led to a defined *Bejenado* volcano. After this the evolved, volumetrically small TSP and *Montaña de la Hiedra* eruptions produce the last units on this edifice before volcanism migrated permanently to the *Cumbre Vieja* to the south.

4.6.3 Interpreting radiometric dates from stratigraphically sourced lavas

Radiometric dating has allowed us to put this eruptive stratigraphy within an absolute chronology. It allows us to refine the date for the *Cumbre Nueva Collapse,* estimate the duration of activity at *Bejenado* and provide some insights into the rate at which lavas re-surfaced the Paleo-Cumbre Nueva Rift. We provide a new bracket for the *Cumbre Nueva Collapse* at ≈530 ka, with ages of 529 ± 13 ka for the youngest dated pre-collapse eruption, and 530 ± 21 ka for the earliest post-collapse eruption. This estimate is further supported by the suite of dates from both younger and older flows with known stratigraphic relations to these bracketing lava flows. Such dates are largely consistent

with the stratigraphic sequence. The post-collapse phase of volcanism at *Bejenado* appears to have been brief, with a date derived from the stratigraphically youngest eruptive unit on this edifice (496 ± 16 ka) providing a bracket for the end of activity here.

All lava flows we have studied have yielded dates between 610 ± 30 ka and 496 ± 16 ka, indicating that the period when volcanism was focused in the current centre of the island was relatively brief. The ≈70 ka period prior to the *Cumbre Nueva Collapse* was responsible for the emplacement of significant vertical successions of petrologically distinct flow-fields in the *El Time* area and this leads us to suggest that this inland headland was constructed in a brief period prior to the collapse. A very approximate re-surfacing rate for this area by the Paleo-Cumbre Nueva Rift, of one vertically superimposed flow every 20 ka, can be estimated from these sequences. Thus rates over this period appear similar to those observed in recent activity at comparable segments of the *Cumbre Vieja* to the south (Carracedo et al., 2001), along which the "platform-forming series" of flow-fields of <20 ka form an extensive cap of lavas above the earlier phases of the rift's activity. The relative youth of our oldest dates suggests that the *El Time* inland headland was constructed in a brief period prior to the collapse.

Dates from the *Bejenado* edifice indicate this also was the product of brief, focused volcanism but because the variation in age estimates from stratigraphically young and old flows is of a similar magnitude to individual analytical uncertainties, it is difficult to determine quite how brief this activity was (Figure 4-3). Due to the small number of distinct eruptive units identified at *Bejenado*, it is reasonable to suggest that they could all have been erupted extremely rapidly (possibly continuously) in a period soon after the collapse, but this is inconsistent with the youngest dates from the Plagioclase Basalt, the Terminal Sheet Phase and *Montaña de la Hiedra* which together form a cluster around ≈500ka.

4.7 Discussion

Our estimate for the age of the collapse is a refinement of the ≈560 ka estimate provided in previous studies (Carracedo et al., 2001; Guillou et al., 1998, 2001). Differences between their and our estimates are likely to result from previous studies sampling the significantly more altered flows from the crest of the *Cumbre Nueva Ridge* to provide the pre-collapse bracket, while their post-collapse bracketing date of 537 ± 8ka is consistent with, but at the upper limit of, analytical uncertainty for our dates for early flows from *Bejenado*. These previous studies also presented six younger age determinations from the wider *Taburiente* edifice and interpreted them as the product of post-collapse volcanism, while our younger estimate puts these in the pre-collapse phase. On the basis of our estimate, only two of their 32 age determinations from *Taburiente* would be the product of residual post-collapse volcanism, indicating that volcanism on *Taburiente* almost completely ended with the collapse.

Bejenado provides a superb case study on which to investigate post-collapse oceanic island volcanism. If compared to other post-collapse edifices, such as *Teide* on Tenerife or *Pico de Fogo* in the Cape Verde islands, the brevity of volcanism at *Bejenado* has led to significantly better access to the earliest phases of activity, with units exposed that would otherwise be buried by the products of subsequent eruptions. However, while these comparable volcanoes are both stratovolcanoes this description has been misleadingly applied to *Bejenado* (Carracedo et al., 2001; Roa, 2003), where the eruptive units are largely planar and show no evidence of together having formed a central volcanic cone. *Bejenado's* small number of eruptive units largely follow the steep gradient of post-collapse topography and it is likely that volcanism ended before a central stratocone could develop.

Bejenado's volcanic units were emplaced onto a sequence of post-collapse breccias (*La Viña Breccias*) within a part of the collapse structure underlain by a dense dyke swarm, and together these characteristics provide our best insights into the environment at the time volcanism began after the collapse (Figure 4-12B). In light of our dating results, the characteristics of the *La Viña Breccias* unit appear surprising. These sediments have been characterised as cohesive debris flow deposits (Colmenero et al., 2012) resulting from the reworking of earlier landslide sediments, an interpretation that appears to require a significant hiatus between the *Cumbre Nueva Collapse* and *Bejenado´s* earliest eruptions. Such an initial pause before the rapid, subsequent, growth of *Bejenado* is not unreasonable, but is surprising given the scale and complexity of the subsequent eruptive units, which appears to be more consistent with emplacement in a dynamic environment such as the immediate post-collapse phase.

The dyke swarms visible in *Barranco de la Angustias* and *Caldera de Taburiente* appear most dense beneath *Bejenado's* earliest effusive units and thickest successions, a feature that is unlikely to be a coincidence. Multiple dyke populations are visible here, with many dykes inferred to result from a feeder system for *Taburiente*, including the *Paleo-Cumbre Nueva Rift* (Carracedo et al., 2001). We suggest the core of this swarm provides the best indicator of the exact location of this rift. The presence of a swarm of planar dykes are likely to have restricted magma migration in the pre-collapse phase, leading to a focus of vents above it, and *Bejenado's* location suggests that this restriction continued after the collapse when new pulses of magma were injected into this shallow magma supply system.

The small number of newly identified eruptive units at *Bejenado* provides an absolute constraint on the nature of post-collapse volcanism, although what these units mean for reservoir system and eruptive processes is open to interpretation. Previous petrological studies of volcanism on La Palma and particularly at the *Cumbre Vieja* (Carracedo et al., 2001; Klügel et al., 2005) have indicated that individual eruptive units are the product of infrequent and intermittent eruptions that have involved discrete, petrologically distinctive, magma batches or mixtures of multiple batches. Such magma

batches are believed to result from the emptying of reservoirs that form a network of ephemeral, small-volume sills in the lithospheric mantle (Klügel et al., 2005). In such a petrological framework the small number of eruptive units and compositional lava-units identified at *Bejenado* would indicate this edifice was the result of a small number of discrete eruptions. An alternative interpretation for this volcano's features would be if its larger volume units were the product of prolonged phases of high-frequency volcanism, of a type more similar to that observed at Italy's Mount Etna than at the *Cumbre Vieja*. At Mount Etna the presence of less-ephemeral reservoirs, refilled at intervals with fresh pulses of magma, appears to lead to phases of episodic but essentially continuous volcanic activity that last for several decades and can result in numerous eruptions with shared petrological characteristics, where such phases are characterised as "eruptive cycles" (Allard et al., 2006; Guest and Murray, 1979). While the authors of the present study cannot identify any recent or historic examples of such cyclic volcanism in the Canary Islands, in the unusual conditions after a lateral collapse this style of activity may become more likely, since depressurisation may result in elevated rates of melt production. The two contrasting interpretations of individual petrological units for processes in the reservoir system (discrete processes occurring over a short period, versus continuous processes occurring over a longer period) are central to how we interpret the results presented in the following chapters, and will be discussed throughout the remainder of this thesis.

Within *Bejenado* only the presence of the early *Los Rodeos Evolved and Volcaniclastic Phase* unit provides evidence of major explosive eruptions (Figure 4-12C). Previous models for the growth of *Caldera de Taburiente* (Carracedo and Paris, 2001; Colmenero et al., 2012; Roa, 2003) have involved explosive eruptions from late in *Bejenado's* activity*,* often suggesting these provided a core crater or feature that later eroded outwards to form *Caldera de Taburiente*. If the core crater they propose existed, it must have been produced earlier in *Bejenado's* activity by the LREVP eruption, and must not have been infilled by later effusive eruptions.

This LREVP unit appears to result in part from high altitude phreatomagmatic activity early in the post-collapse phase when there was not a well-developed *Bejenado* volcano. Previous authors have suggested that such pyroclastic sequences are characteristic of Canarian-type islands' post-collapse phase (Longpré et al., 2009) and this feature would therefore require a general explanation. In this case, the eruption would have occurred within a period of major change in the island's groundwater and fluvial systems, since the interior of the collapse structure and its debris deposits must have provided an entirely new sedimentary environment. Investigating how the island's hydrology would respond to a new collapse structure is beyond the scope of this project. However, we tentatively suggest the new topographically lower embayment may have resulted in the island's groundwater being channelled into the area that then became the focus of volcanism. Other pyroclastic sequences from post-collapse phase La Palma have been found in *Barranco de las Angustias* and

Caldera de Taburiente (Carracedo et al., 2001), and further study of these may provide insights into their relationship to the main LREVP unit.

The effusive eruptions of eastern *Bejenado* (BEP and TSP) are spectacular examples of post-collapse magma-mixing and lava emplacement, and the identification of the BEP flow-field is the most significant unexpected outcome of this study. This major unit exhibits morphological variation, highly porphyritic lavas ideal for petrological study, and variability in magma composition addressed in detail in the following chapter. Its study provides insights into both magma reservoir processes and the emplacement of complex lava flow-fields on an oceanic island. This unit appears to have consolidated the early, discrete, effusive lavas and the multiple vents of the LREVP unit into a single *Bejenado* edifice.

4.8 CONCLUSIONS

Our field and geochronological studies of central La Palma indicate that the period of the *Cumbre Nueva Collapse* was an exceptionally dynamic phase for central La Palma. The *El Time* headland and the *Bejenado* volcano provide a window on the ≈110 ka period before and after this giant landslide.

1) We provide a new age estimate for the *Cumbre Nueva Collapse* of ≈530ka, based on $^{40}Ar/^{39}Ar$ dating of stratigraphically sourced lava flows.
2) We present a reconnaissance map and detailed stratigraphy for the eastern sector of *Bejenado*, accompanied by the first systematic description of this volcano's eruptive units.
3) On the grounds of reconnaissance mapping and unit-by-unit descriptions, *Bejenado* is composed of ≈5-7 eruptive units. Combined with new $^{40}Ar/^{39}Ar$ age determinations indicating *Bejenado's* activity ended after 496 ±16 ka, this means *Bejenado* may have been emplaced rapidly after the collapse.
4) We present the first identification and description of the major Bejenado Effusive Phase and the *Los Rodeos Evolved and Volcaniclastic Phase* eruptive units. The BEP is a major, morphologically complex, flow-field composed of multiple lava-units. The pyroclastic LREVP is a complex, tephritic, eruptive unit with multiple strombolian vents and a major associated laminar phreatomagmatic deposit.

Chapter 5 : PETROLOGY

THE PETROLOGY OF THE BEJENADO EFFUSIVE PHASE LAVA FLOW-FIELD – MAGMA RESERVOIR PROCESSES AFTER A LATERAL COLLAPSE

ABSTRACT

The Bejenado Effusive Phase lava flow-field is the largest volume eruptive unit from the period after La Palma's *Cumbre Nueva Collapse*. It is comprised of three lava-units, these are: 1) the Glomerocrystic Ankaramite lava-unit, a highly porphyritic basanite containing abundant clinopyroxene and olivine aggregates, 2) the Plagioclase Basalt, a porphyritic tephrite containing a large abundance of plagioclase laths, 3) the Plagioclase Tephri-phonolite, an evolved lava-unit showing strong evidence of magma mixing.

Detailed descriptions of lava-unit textures allow us to reconstruct a likely sequence of events in the magma reservoir system during their crystallisation. We place a particular focus on glomerocrysts which we regard as fragments of reservoir material. These textural models are supplemented with microanalysis of characteristic mineral populations, whole rock variation trends and clinopyroxene-melt thermobarometry.

The resulting reconstructions indicate that this flow-field was the product of three main events in the reservoir system: 1) the disruption of an olivine-diopside lithology, 2) a feldspar-dominated crystallisation phase in the lithospheric mantle under super-saturated conditions, and 3) the late mixing into this feldspar-phyric magma-batch of a phonolitic magma that was residing in the oceanic crust. The post-collapse phase was one of unusually dynamic conditions in the magma reservoir system when depressurisation permitted volatile degassing and magma-mixing.

5.1 INTRODUCTION

The magma plumbing system of an intraplate oceanic island provides the filter that regulates how the processes in the underlying region of melt production affect the zone of eruptions (Cashman and Sparks, 2013). Fortunately, there are numerous sources of evidence — both using remote techniques and directly from physical samples — with which to study the processes within this system. Traditionally, the petrology of lava flows has provided a record of reservoir processes, held in petrographic textures, element partitioning, and in major element variations across a suite of lavas. More recently, seismic monitoring has begun to produce increasingly accurate three dimensional reconstructions (Paulatto et al., 2012) of active magma reservoir systems in a variety of volcanic settings. The application of thermobarometic techniques to lavas and phenocrysts (Hansteen and Klügel, 2008; Putirka et al., 1996; Putirka, 2008) has provided a quantitative means of anchoring petrological observations to the depths and temperature at which they formed. Systematic thermobarometric studies of lavas from several Canarian-type islands (Galipp et al.,

2006; Klügel et al., 1997, 2000, 2005) have provided depth constraints for their main magmatic reservoir systems, which have been interpreted as networks of small volume sills in the lithospheric mantle (Klügel et al., 2005). This model has been tested against seismic data in recent eruptions (Longpré et al., 2014) and is becoming increasingly robust.

The post-collapse Bejenado Effusive Phase (BEP) lava flow-field provides an opportunity to apply the petrological approach to reconstructing magma supply processes. This well exposed flow-field was emplaced soon after the giant landslide of the crest and western flank of the *Paleo-Cumbre Nueva Rift* (Carracedo et al., 2001) and can be divided into compositionally distinct, stratified, lava-units. The stratigraphy results from the presence of several magma batches, together forming a flow-field that is unusually rich in petrological information: porphyritic lavas inherently provide more textural information than less crystal-rich units, while the presence of multiple lava-units provides petrological contrasts that should allow groups of mineral populations to be characterised. This petrological information derives from a key period in La Palma's evolution. Studies on El Hierro (Manconi et al., 2009) and Tenerife (Longpré et al., 2008, 2009) have shown that post-collapse volcanic activity often produces lavas of unusually complex petrology, with highly porphyritic ankaramites and volcaniclastic units present. These features are shared by the *Bejenado* edifice. The BEP flow-field's high quality exposure and petrological complexity mean that its study may provide insights into how the magma supply system responds to substantial changes in the island's edifice.

This chapter presents petrological results from 16 lava samples from across the BEP flow-field, studied using a combination of petrographic observations, mineral chemistry and whole rock elemental compositions. Detailed petrography provides a framework for interpreting magma reservoir processes which can be quantitatively underpinned by geochemical analysis.

5.2 Field relations of the Bejenado Effusive Phase flow-field

The *Bejenado* volcano is the primary volcanic feature in the embayment produced by the *Cumbre Nueva Collapse* that ended activity at the island's *Paleo-Cumbre Nueva Rift*. Within *Bejenado*, the Bejenado Effusive Phase (BEP) flow-field is the largest (≈100m thick at the core of the sequence) and most extensive (>3.5km wide) single eruptive unit[17]. It was not the product of immediate post-collapse volcanism, but overlies the products of at least two other eruptive phases (the *Los Rodeos Evolved and Volcaniclastic Phase* and the *Bejenado Lower Series*). It is well-exposed across the eastern sector of the volcano's southern flank.

[17] 4.5 Results – part 2 : the geology of the eastern sector of *Bejenado*. pp.82-86.

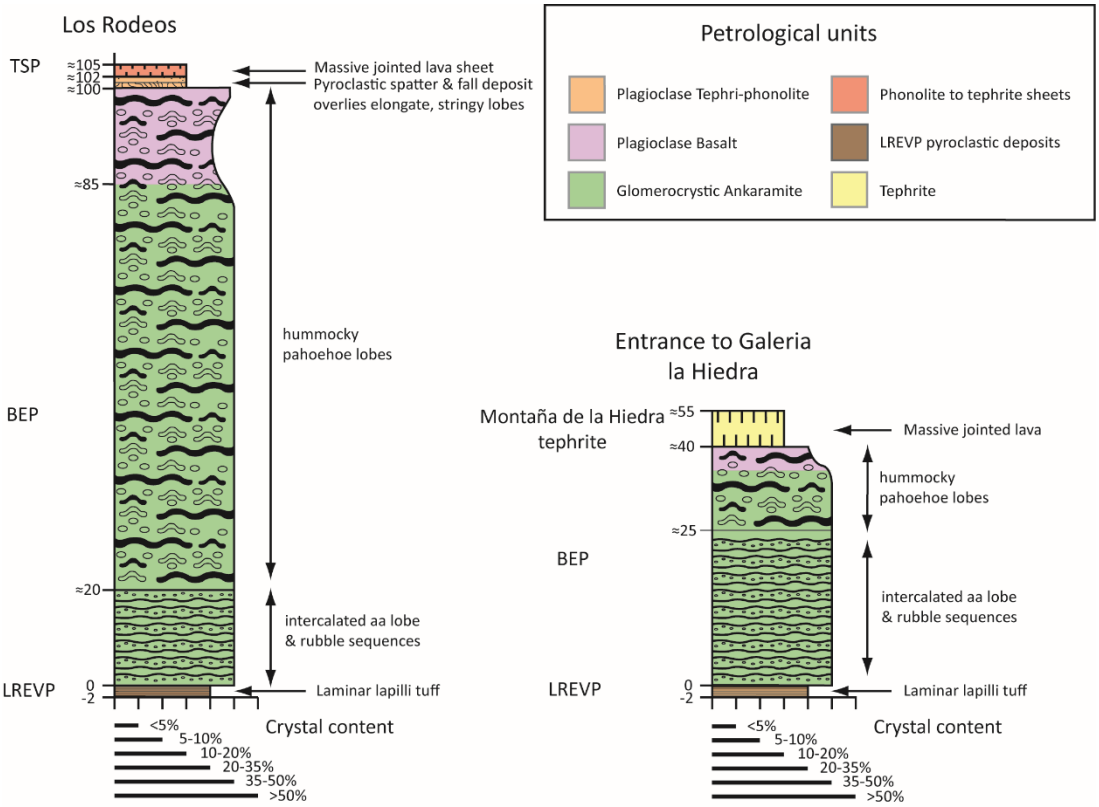

Figure 5-1 Approximate, schematic, logs of the morphological and petrological variation across the Bejenado Effusive Phase lava flow-field at localities inferred to be vent proximal (Los Rodeos) and distal (Entrance to Galeria la Hiedra).

It is morphologically complex (Figure 5-1) and progresses from a succession of numerous aa flows at the base into a hummocky pahoehoe sequence that forms most of the unit. In the uppermost flows this pahoehoe morphology is poorly developed, with stringy, poorly-vesiculated sheet lobes directly underlying a layer composed of bomb, spatter and pyroclastic fall deposits of similar composition lava. This pyroclastic unit indicates there was a late change in the eruption from predominantly effusive activity to a more explosive style.

There are three petrologically distinct lava-units within this flow-field: 1) the Glomerocrystic Ankaramite (dated at 528 ±23 ka), 2) the Plagioclase Basalt (dated at 497 ±17 ka), 3) the Plagioclase Tephri-phonolite. These are found in a vertical, stratified, sequence at numerous localities, indicating they were likely to have been erupted sequentially.

The Glomerocrystic Ankaramite is the largest volume lava-unit, forming the lower part (≈85% thickness) of vertical sections. This unit forms the entirety of the lower aa morphology units, and the majority of the hummocky pahoehoe flow-field. It is an intensely porphyritic (rich in olivine and clinopyroxene crystals), highly vesiculated, metallic blue lava. It is overlain by the Plagioclase Basalt, a highly vesiculated plagioclase-phyric lava with a vitreous, purple-blue groundmass. This lava-unit is the most plagioclase-phyric lava so far identified on northern La Palma (Galipp et al., 2006), indicating it was the product of unusual crystallisation conditions. The Plagioclase Tephri-phonolite is the thinnest (<2.5m thick) and least extensive of the lava-units. It forms stringy, poorly vesiculated

sheet lobes overlain by a bomb and pyroclastic fall-deposit of identical mineralogy and lithological characteristics. It is a plagioclase-phyric lava with a grey groundmass, and its spatter horizon is composed of highly vitreous bombs.

5.3 METHODS

5.3.1 SAMPLE SOURCING

Samples were collected from lava lobes across the BEP flow-field. The extensive outcrops of this unit meant unaltered samples could be taken without concern for systematic sampling bias. The result is 6 samples taken from key stratigraphically-constrained parts of the sequence, as well as 10 opportunistically collected samples (Table 5-1 and Figure 5-2). The stratified samples were taken from 3 localities: 1) *Los Rodeos,* 2) *Calle de Valencia* and 3) *Lomo Canario*. All samples were prepared as polished thin sections and whole-rock powders.

LP13SG29 was collected from *Los Rodeos*, which is the most northerly and highest altitude locality of the BEP with the thickest sequences of lava lobes. Since the flow-field's main vent complex must have been located at a topographic high, it is likely that these are among the most vent-proximal lavas, and the lowermost lobe in this succession is a strong candidate for the earliest unit in the flow-field.

LP14SG08 and LP14SG09 were sampled from the *Calle de Valencia* car park, where a representative section through the BEP unit's morphological and compositional sequence is exposed. Here, the change in lava petrology from Glomerocrystic Ankaramite to Plagioclase Basalt occurs between two layers of morphologically unremarkable pahoehoe lobes. Samples were taken from the lobes above and below this contact to provide a late Glomerocrystic Ankaramite sample and an early Plagioclase Basalt sample.

LP14SG04, LP14SG05 and LP14SG06 were sampled from the intersection of the *Pista de Ferrer* road section and the *Lomo Canario* whaleback. This section exposes the uppermost petrological sequence (<10 m wide, <5 m thick) from pahoehoe lobes of Plagioclase Basalt composition through Plagioclase Tephri-phonolite sheet lobes and into the Plagioclase Tephri-phonolite spatter member. Samples from here cover the late phase Plagioclase Basalt lava unit as well as the effusive and explosive sub-divisions of the Plagioclase Tephri-phonolite lava-unit.

Sample	Petrological Unit	Stratigraphic significance	Lava morphology	Locality
LP14SG04	Plagioclase Tephri-phonolite	BEP pyroclastic fall deposit	Bomb	*Lomo Canario*
LP14SG05	Plagioclase Tephri-phonolite	Lowermost lobe of petrological unit	Platey sheet-lobe	*Lomo Canario*
LP14SG06	Plagioclase Basalt	Uppermost lobe of petrological unit	Pahoehoe lobe	*Lomo Canario*
LP14SG09	Plagioclase Basalt	Lowermost lobe of petrological unit	Pahoehoe lobe	*Calle de Valencia*
LP14SG08	Glomerocrystic Ankaramite	Uppermost lobe of petrological unit	Pahoehoe lobe	*Calle de Valencia*
LP13SG29	Glomerocrystic Ankaramite	Lowermost lobe of BEP flow-field	aa lobe	*Los Rodeos*

Table 5-1 Locality and origin information for the key stratigraphically constrained BEP lava samples, presented in stratigraphic order with oldest at the base of the table

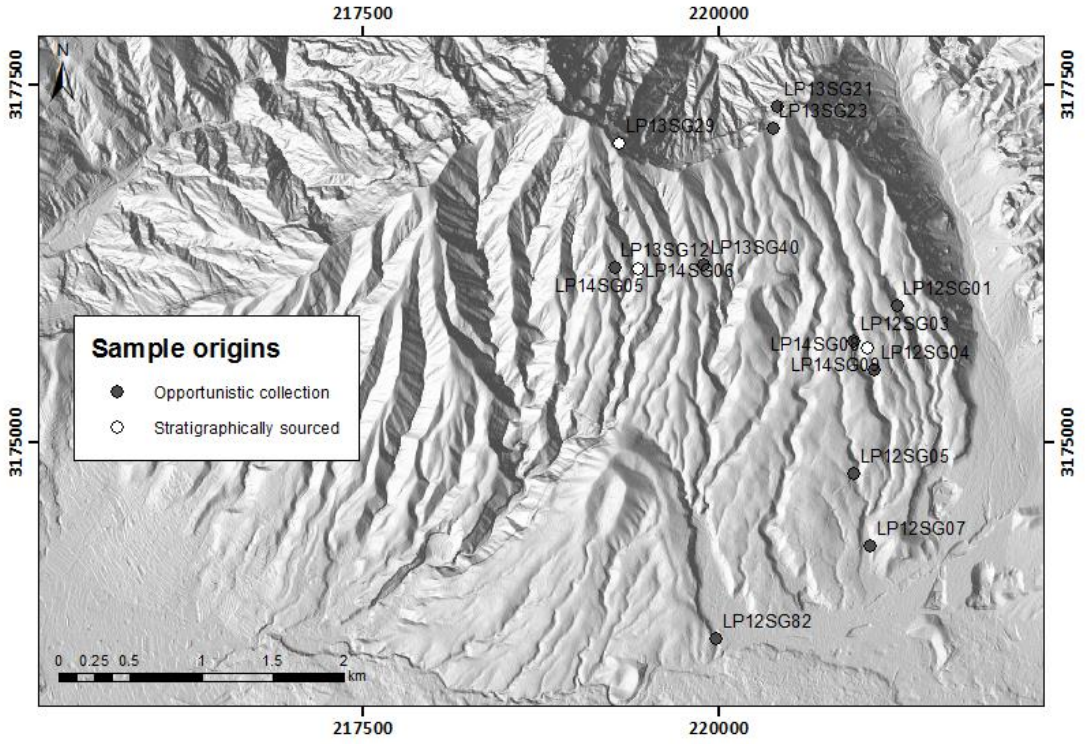

Figure 5-2 Shaded topographic map (topographic data sourced from Instituto Geographico Nacionale) of sampling localities for BEP lava samples used in this study.

The 10 opportunistic samples were taken from path and road sections across the BEP flow-field and mostly originate from the voluminous Glomerocrystic Ankaramite, although they include one sample of Plagioclase Basalt (LP13SG12).

5.3.2 Analytical procedures

MINERAL CHEMISTRY

Major element analyses of characteristic minerals were obtained using a JEOL 8100 Superprobe at Birkbeck, University of London using an Oxford Instruments Aztec (EDS) detector with an accelerating voltage of 15 kV, current of 1 μA and a beam diameter of 1 μm. Analyses were calibrated against standards of natural silicates, oxides and Specpure metals, using a ZAF correction procedure. Repeated analyses of basaltic reference standard BCR-2 were performed at the end of analytical sessions to determine precision, accuracy and instrumental drift[18].

The strategy for analysing sub-populations of minerals was determined on the basis of previous observations from petrographic and electron backscatter imaging. Analyses were ideally performed in triplicate and focused on mineral cores where no compositional zonation was apparent. Where xenocrystic cores or sector-zoning was visible, representative populations of each mineral sub-population were analysed.

WHOLE-ROCK MAJOR AND TRACE ELEMENTS

The major and trace element compositions of lava samples were determined by X-ray fluorescence spectrometry (XRF) using the Philips PW1480 XRF located at Royal Holloway, University of London using the techniques summarised in Thirlwall et al. (2000). Samples were split and sawed to remove any traces of alteration (weathering crusts, areas where the olivines showed greater than average iddingsite formation and zones with infilled voids) prior to jaw-crushing. Crushates were then coned and quartered before powdering in a tungsten carbide ring and puck mill. Bulk rock powders were roasted to 1100°C to determine loss on ignition (LOI) before fusion in platinum-gold crucibles, then prepared as fused glass discs for major element analyses. Trace elements were analysed on pressed powder pellets with matrix corrections calculated from the major element composition. All data are presented on a volatile-free basis with total Fe as Fe_2O_3.

CLINOPYROXENE-MELT BAROMETRY

All new analyses were performed at the Department of Geosciences, University of Bremen[19]. Major element analyses of clinopyroxenes were performed on the facility's Cameca SX-100. The instrument performed analyses with a focused beam operating with a 15 kV acceleration voltage and a 15 nA beam current, with quantification provided using the built-in PAP correction procedure. Analytical precision and accuracy were monitored by comparison to natural mineral standards. In all cases, the compositions of clinopyroxene rims were determined as the average of 4-20 microprobe analyses each taken 5-10 μm from the rim of individual euhedral phenocrysts.

Compositions of sample groundmasses were obtained by LA-ICP-MS using a NewWave UP193ss connected to a Thermo Element2. Analytical conditions included an irradiance of ca. 1 $GWcm^{-2}$, spot

[18] Appendix B: Analytical methods and history. p.202.
[19] The remainder of this section was written by Andreas Klügel of the University of Bremen.

size 75 µm, laser pulse rate 5 Hz, plasma power 1200 W, He (~0.8 l·min^{-1}) as sample gas, and subsequent addition of Argon (~0.8 l·min^{-1}) as make-up gas.

Sample ablation was performed through line scans of up to 1 mm length at 5 µm/s scan speed. The isotopes ^{23}Na, ^{24}Mg, ^{27}Al, ^{28}Si, ^{31}P, ^{39}K, ^{44}Ca, ^{48}Ti, ^{55}Mn and ^{56}Fe were analysed at high resolution with a total dwell time of 25 ms per isotope. Blanks measurements were collected for 30s prior to ablation. After every 4-7 samples the USGS glass BCR2-G was analysed as external calibration standard using the values of Jochum et al. (2005). Data was quantified using the Cetac GeoPro™ software with ^{44}Ca used as internal standard, with concentrations subsequently normalized to 100 wt.% oxides.

Data quality was assessed by analyses of reference materials BHVO2G, StHs6/80-G and ATHO-G (Jochum et al., 2005; 2006) over the same analytical runs as the samples. For most elements, except for phosphorus, external precision of analytical results was better than 5%, and the results for phosphorous were due to the anticipated presence of minor apatite grains.

5.4 Petrology of BEP lava samples: results

In terms of the categories provided by the TAS diagram, all BEP samples (Table 5-2) lie along the strongly alkaline evolution trend (Figure 5-3), with compositions extending from the basanite/tephrite field to the tephri-phonolite field. They show a restricted range of SiO_2 contents (42.3 - 52.0 wt%) falling into 3 clusters. Basanitic samples from the Glomerocrystic Ankaramite unit show the greatest range in alkali abundances (2.94 wt% to 4.01 wt% Na_2O, 0.96 wt% to 1.67 wt% K_2O), while samples from the Plagioclase Basalt and Plagioclase Tephri-phonolite lava units cluster separately at the upper boundary of the tephrite/basanite field and centre of the Tephri-phonolite field, respectively.

5.4.1 Petrography of BEP lava-units

The textures apparent in the samples from lithological lava-units are sufficiently uniform to allow them to be characterised as a group. Nonetheless, there is variation within each sample group and examination of those of known stratigraphic context indicates that the variation is progressive through each lava-unit. The following section presents gross textural characterisations of each unit, followed by description of the key features that vary within them.

Sample ID	LP12SG01	LP12SG03	LP12SG04	LP12SG05	LP12SG07	LP12SG82
Unit	Glom Ank	Glom Ank	Glom Ank	Glom Ank	Glom Ank	Glom Ank
SiO_2	43.30	42.50	43.25	42.30	42.63	42.80
Al_2O_3	12.85	11.42	12.68	11.31	11.37	14.17
Fe_2O_3T	13.44	13.53	13.48	13.62	13.52	13.74
MgO	10.45	12.95	10.33	13.08	13.12	8.61
CaO	11.27	10.74	10.99	10.87	10.88	9.17
Na_2O	2.94	3.10	3.41	2.71	3.05	4.02
K_2O	0.96	1.26	1.36	1.17	1.04	1.67
TiO_2	3.44	3.14	3.37	3.12	3.12	3.49
MnO	0.19	0.18	0.18	0.18	0.18	0.19
P_2O_5	0.59	0.56	0.59	0.54	0.55	0.73
Total	99.97	99.97	100.19	99.47	100.04	100.01
LOI (%)	0.30	-0.27	-0.39	-0.04	-0.06	-0.51
Ni	233	382	237	379	373	189
Cr	437	640	451	625	622	260
V	312	298	305	294	300	291
Sc	23	23	21	23	23	13
Cu	95	108	96	107	115	127
Zn	102	104	104	102	103	112
As						
S	18	27	40	43	16	45
Ga	21.0	18.8	20.9	19.1	18.8	22.6
Pb	3.0	1.9	2.3	2.4	2.6	3.1
Sr	847.9	689.5	763.3	730.9	720.0	916.4
Rb	23.2	27.4	30.5	25.9	27.9	37.3
Ba	511.4	438.7	483.3	452.0	442.4	603.9
Zr	254.5	224.5	250.8	225.0	225.6	277.2
Nb	81.7	69.4	81.0	69.5	69.2	101.1
Ta	4.6	4.2	4.2	4.1	3.3	5.3
Mo	1.4	1.8	1.7	1.7	1.7	2.0
Th	3.8	3.6	3.7	3.6	3.7	4.9
U	0.7	1.2	0.8	0.8	0.5	0.8
Y	24.5	21.6	24.0	22.0	21.6	25.0
La	44.2	38.5	43.1	39.8	39.0	50.3
Ce	85.0	79.7	82.8	78.5	80.6	100.3
Nd	45.4	39.9	42.9	39.8	40.8	48.3
Sm	8.4	9.2	7.3	7.7	7.7	10.1
Yb	1.9	1.6	1.5	1.4	2.1	1.9
Hf	7					
Cs			1			

Table 5-2 Major element (wt %) and trace element (ppm) compositions of samples from BEP lava-units, determined by XRF. Replicate samples and reference material analyses are presented in Appendix C. Lava units: Glom Ank = Glomerocrystic Ankaramite, Plag Bas = Plagioclase Basalt, Plag Teph-pho = Plagioclase Tephri-phonolite.

Sample ID	LP13SG21	LP13SG23	LP13SG29	LP13SG40	LP14SG08	LP14SG06
Unit	Glom Ank	Glom Ank	Glom Ank	Glom Ank	Glom Ank	Plag Bas
SiO_2	43.11	42.65	42.97	43.15	43.28	46.63
Al_2O_3	12.48	12.49	12.24	12.91	12.70	18.04
Fe_2O_3T	13.31	13.33	13.46	13.47	13.45	10.37
MgO	10.39	10.40	11.02	10.01	10.36	3.57
CaO	11.22	11.02	10.98	11.32	11.30	8.12
Na_2O	3.14	2.83	2.85	2.80	3.03	5.51
K_2O	1.31	1.27	1.30	1.27	1.28	2.64
TiO_2	3.35	3.33	3.29	3.43	3.32	3.18
MnO	0.18	0.18	0.18	0.18	0.18	0.18
P_2O_5	0.58	0.58	0.56	0.57	0.55	0.95
Total	99.60	98.63	99.39	99.65	99.99	99.79
LOI (%)	-0.44	-0.08	0.11	0.04	1.10	0.24
Ni	231	239	263	207	237	18
Cr	452	468	502	397	470	6
V	288	297	296	303	308	170
Sc	23	22	24	23	25	7
Cu	124	116	110	120	116	65
Zn	97	104	104	105	106	103
As		1	1			1
S	19	43	62	37	20	149
Ga	20.2	20.5	19.9	20.7	20.4	24.6
Pb	2.2	2.0	2.2	2.3	2.1	3.7
Sr	748.9	771.3	705.0	811.0	818.9	1217.7
Rb	28.8	27.5	28.4	28.2	27.2	60.1
Ba	491.3	514.6	464.6	496.1	485.7	794.3
Zr	249.9	248.4	242.5	255.8	246.4	391.7
Nb	78.7	81.3	79.0	82.9	81.2	138.1
Ta	4.4	4.9	4.3	4.5	4.7	7.2
Mo	1.6	1.8	1.8	1.2	1.5	2.6
Th	4.0	3.9	3.8	3.7	3.7	7.5
U	1.2	1.5	1.1	0.7	1.0	2.4
Y	23.7	23.5	22.8	24.0	24.8	29.9
La	39.9	41.6	40.3	43.8	45.9	68.2
Ce	83.4	80.8	77.3	85.3	77.4	131.0
Nd	41.7	40.4	39.0	43.3	42.2	58.5
Sm	9.5	6.5	8.7	8.7	9.4	11.4
Yb	3.2	3.6	3.8	2.6	2.5	1.7
Hf	5	5	5	5	6	4
Cs	1		1	1	1	1

Table 5-2 (continued) Major element (wt %) and trace element (ppm) compositions of samples from BEP lava-units, determined by XRF.

Sample ID Unit	LP14SG09 Plag Bas	LP13SG12 Plag Bas	LP14SG04 Plag Teph-pho	LP14SG05 Plag Teph-pho
SiO_2	46.60	47.02	51.55	53.22
Al_2O_3	18.03	18.31	20.22	20.77
Fe_2O_3T	10.06	9.99	6.76	5.26
MgO	3.52	3.32	1.68	1.09
CaO	7.93	7.78	5.28	4.22
Na_2O	5.55	5.35	7.60	7.87
K_2O	2.67	2.76	3.65	4.05
TiO_2	3.11	3.13	1.81	1.41
MnO	0.17	0.17	0.17	0.16
P_2O_5	0.97	0.98	0.49	0.28
Total	99.26	99.42	99.86	99.00
LOI (%)	0.10	0.66	0.11	-0.01
Ni	16	11	8	5
Cr	4	2	16	3
V	164	160	82	55
Sc	7	7	1	1
Cu	66	47	10	7
Zn	106	109	107	99
As	1	1	1	2
S	226	277	119	112
Ga	24.0	24.4	25.4	26.2
Pb	3.6	4.3	6.4	8.0
Sr	1200.2	1283.2	1152.4	1597.7
Rb	59.8	64.6	94.1	113.5
Ba	803.8	786.5	855.1	971.4
Zr	392.9	412.3	507.5	547.6
Nb	140.8	145.4	157.7	161.0
Ta	7.5	7.8	8.3	8.3
Mo	2.0	3.2	5.9	4.1
Th	7.5	7.6	10.4	12.1
U	2.0	2.4	3.6	3.7
Y	29.5	30.4	24.7	22.1
La	68.9	67.2	72.5	71.2
Ce	132.6	131.1	133.0	125.1
Nd	59.3	58.9	50.9	42.8
Sm	12.9	11.4	9.6	8.4
Yb	2.3	2.1	2.7	2.3
Hf	4	5	5	6
Cs	1		1	2

Table 5-2 (continued) Major element (wt %) and trace element (ppm) compositions of samples from BEP lava-units, determined by XRF.

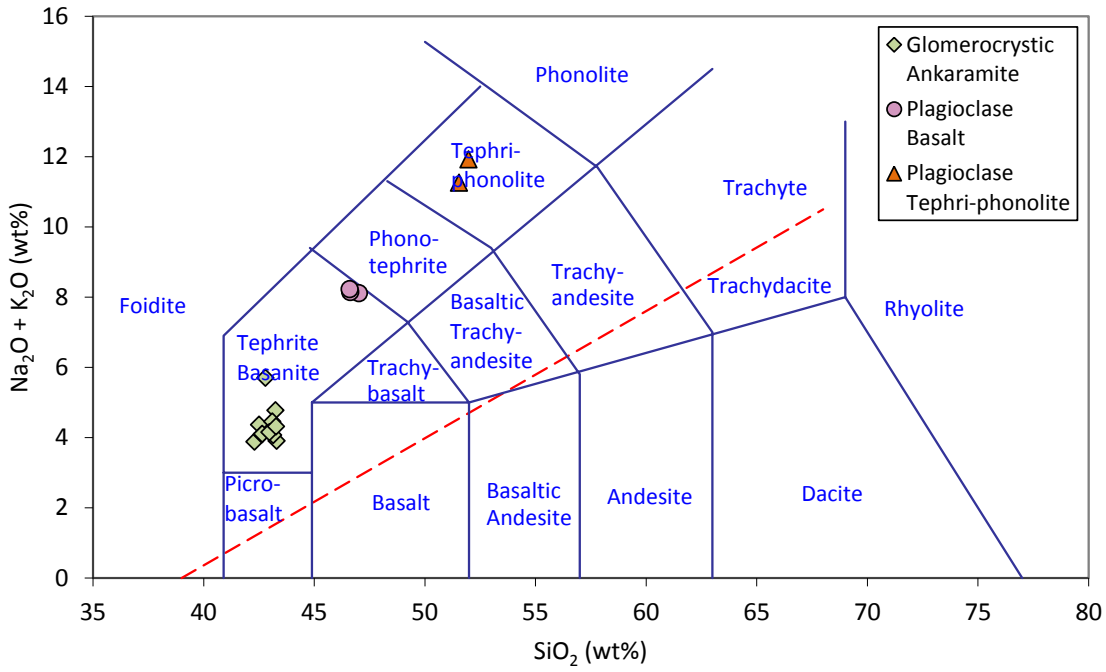

Figure 5-3 A TAS classification diagram of the whole rock compositions of 16 samples of BEP flow-field lavas. The TAS diagram is in the style of Le Bas et al. (1986), lavas present from all three lava-units.

GLOMEROCRYSTIC ANKARAMITE

All samples of the Glomerocrystic Ankaramite lava unit are glomeroporphyritic basanites with abundant (≈40% cross-sectional area) aggregates of olivine and clinopyroxene in a plagioclase-bearing groundmass. There is considerable variation within this unit; images of representative textural features are shown (Figure 5-4).

The characteristic features of this unit are the glomerocryst aggregates, which are composed of clinopyroxene and olivine with traces of titanomagnetite. These aggregates are holocrystalline, and crystal interfaces in their interior tend to be subhedral to anhedral (Figure 5-4A). The average size of aggregates (0.9-4.0 mm) varies through the suite, reflecting both variation in the number of crystals per aggregate and the average crystal size. The relative abundance of clinopyroxene to olivine in aggregates varies within the unit. Clinopyroxene is generally more common but dunite glomerocrysts (<6 mm diameter, Figure 5-4A) indicate variability in the dominant crystal cargo.

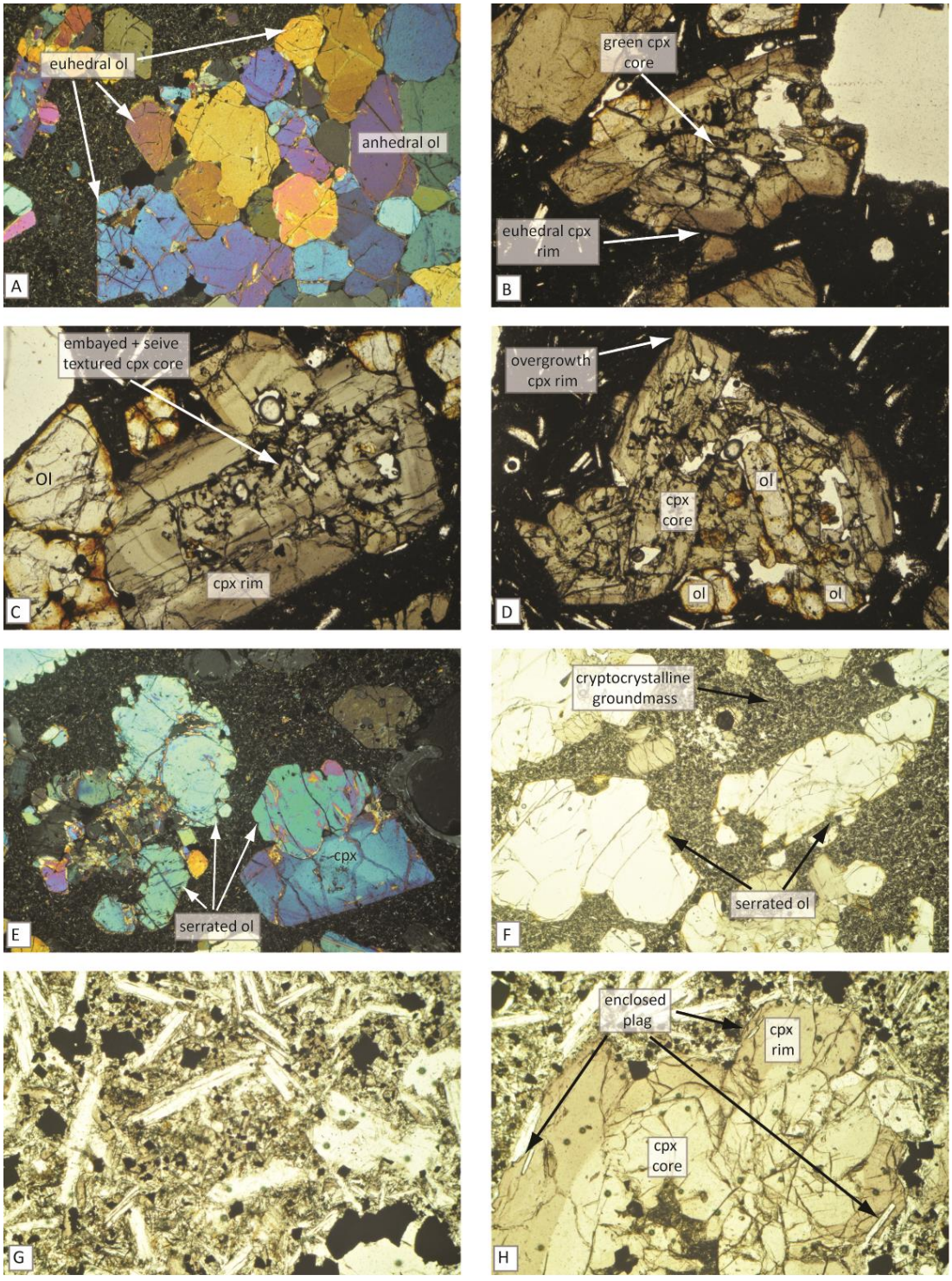

Figure 5-4 Photomicrographs of textural variation in the Glomerocrystic Ankaramite lava-unit. A. Dunitic glomerocryst hosted in a cryptocrystalline groundmass, in the interior of the aggregate olivines have anhedral crystal faces, but are euhedral on the aggregate's outer surface (XPL, FOV = 4.4mm). B. Characteristic clinopyroxene-dominated glomerocryst, the core is diopsidic, fractured and sieve-textured while the rim is well preserved, titanian augite and euhedral (PPL, FOV = 4.4mm). C. Clinopyroxene-olivine glomerocryst, the glomerocryst's diopsidic core is embayed with anhedral internal crystal, the titanian augite rim is euhedral (PPL, FOV = 4.4mm). D. Characteristic clinopyroxene-olivine glomerocryst (PPL, FOV = 4.4mm). E. Olivine-clinopyroxene glomerocrysts with olivines showing serrated rims indicating a period of embayment followed by regrowth (XPL, FOV =4.4mm). F. Olivine crystals also showing serrated rims (PPL, FOV = 4.4mm). G. Plagioclase-phyric crystalline groundmass with microcrystals of spinel and augite (PPL, FOV = 2.2mm). H. Clinopyroxene glomerocryst in plagioclase-phyric groundmass, with similar sized plagioclase crystals enclosed in augitic rim (PPL, FOV = 2.2mm). FOV = field of view, PPL = plane polarised light, XPL = cross-polarised light, cpx = clinopyroxene, ol = olivine, plag = plagioclase.

Clinopyroxene crystals are often strongly zoned, allowing a characteristic texture to be identified in clinopyroxene-rich aggregates. Entire aggregates (containing up to 40 crystals) are zoned and can be divided into two mineral sub-populations, found in aggregate cores and rims. In aggregate cores, clinopyroxenes are colourless to pale green (diopside) and these tend to be heavily fractured and sieve-textured with anhedral crystal faces. The outermost zones of the aggregate core show signs of embayment (Figure 5-4B-D). In aggregate rims, clinopyroxenes are pale brown/pink titanian augites which are better preserved with less fracturing. They exhibit concentric normal zonation and well-developed euhedral crystal faces. These rims commonly contain euhedral titanomagnetite crystals. Zonation is less distinct in olivine-dominated aggregates (particularly where minor alteration to iddingsite has occurred) but evidence for multiple phases of crystal growth is provided by outer rim crystal faces, which are serrated, indicating crystal growth was followed by a period of resorption (Figure 5-4E-F). In all aggregates the cores appear to be a xenocrystic crystal cargo, while aggregate rims appear to be co-magmatic with the host magma.

The groundmass varies from cryptocrystalline and near-opaque (Figure 5-4F) to crystalline. Throughout the unit euhedral plagioclase laths (<1.5mm long) with few twins are the primary groundmass mineral. These are commonly seriate textured, with accessory spinel and augitic clinopyroxene in the most crystalline samples (Figure 5-4G). In these samples plagioclase laths of similar size to the primary population are visible enclosed within titanian augite aggregate rims (Figure 5-4H), indicating the formation of rims and plagioclase crystallisation were contemporaneous.

Groundmass crystal content varies stratigraphically, with the lowermost sample (LP13SG29) exhibiting fewer and smaller plagioclase crystals than the uppermost samples (LP14SG08). This increase in plagioclase content is accompanied by a broad increase in aggregate size, with large aggregates noticeably more common at the top of the sequence but with no obvious change in aggregate mineralogy or composition.

Plagioclase Basalt

Samples of Plagioclase Basalt are seriate-textured plagioclase, titanian augite tephrites with vitreous groundmasses. Titanomagnetite, olivine and apatite are common accessory minerals in this unit. Glomerocrysts similar to those in the Glomerocrystic Ankaramite are present. Images of representative textural features are shown in Figure 5-5.

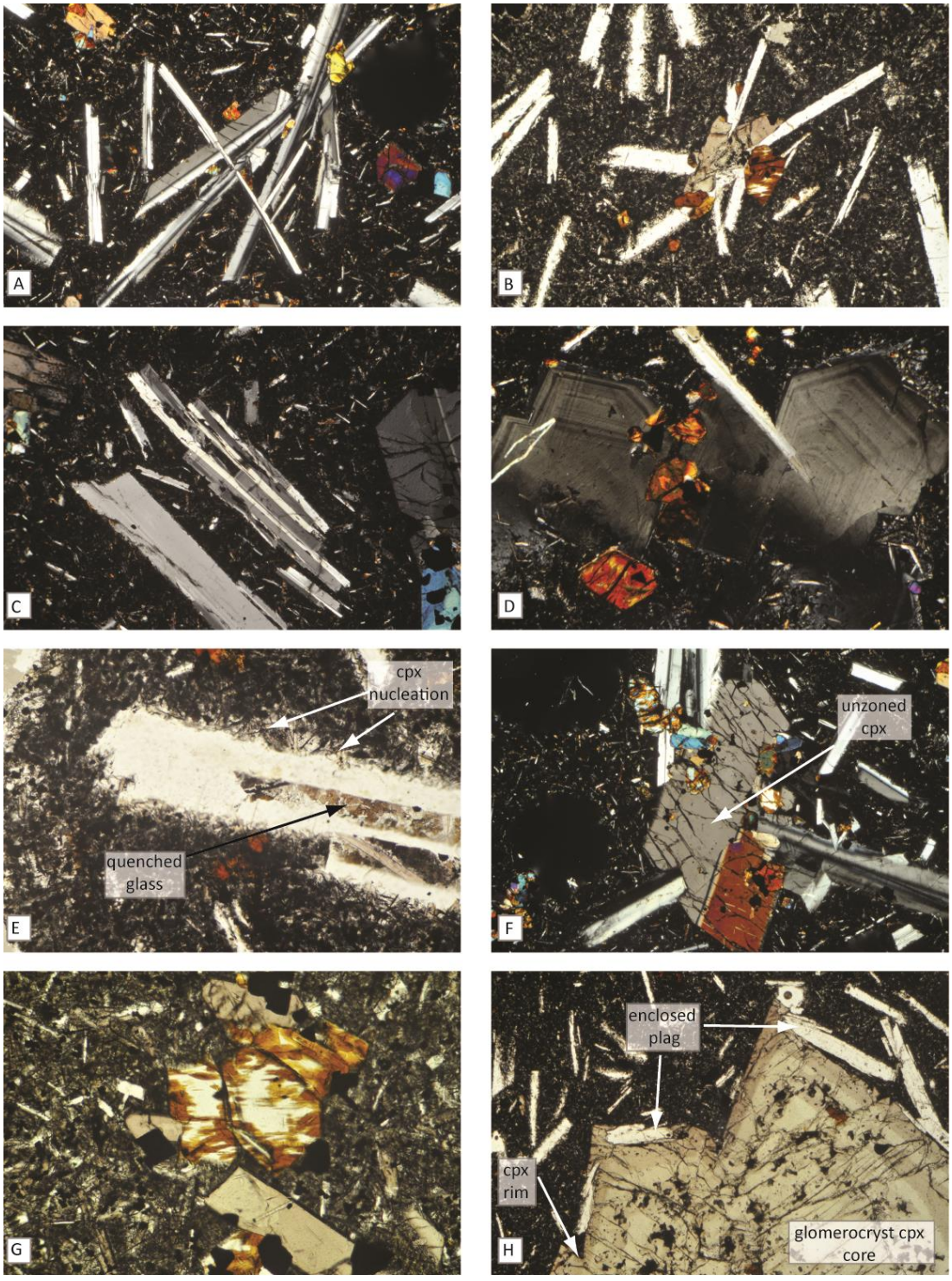

Figure 5-5 Photomicrographs showing textural variation in the Plagioclase Basalt lava-unit. A. Plagioclase glomerocryst with crystals showing a branching, variolitic, texture (XPL, FOV = 4.4mm). B. Plagioclase-clinopyroxene glomerocryst with plagioclases showing a radiate texture from core clinopyroxene (XPL, FOV = 2.2mm). C. Plagioclase glomerocryst showing a trachytoid texture (XPL, FOV = 2.2mm). D. Oscillatory zoned plagioclase showing fine bands (XPL, FOV = 2.2mm). E. Plagioclase phenocryst with quenched glass in core and rims showing nucleation of augite microcrystals (PPL, FOV = 1.1mm). F. Plagioclase-clinopyroxene glomerocryst with un-zoned clinopyroxene (XPL, FOV = 4.4mm). G. Olivine glomerocryst with streaks and blebs of iddingsite (PPL, FOV = 1.1mm). H. Glomerocrystic Ankaramite-type green-core clinopyroxene glomerocryst with phenocryst plagioclase enclosed in its augitic rim (PPL, FOV = 4.4mm). FOV = field of view, XPL = crossed polarised light, PPL = plane polarised light, cpx = clinopyroxene, ol = olivine, plag = plagioclase.

Plagioclase crystals often occur in non-holocrystalline aggregates, with textures indicative of variolitic (Figure 5-5A), radiate (Figure 5-5B) and trachytoid (Figure 5-5C) plagioclase growth. Aggregates also commonly contain titanian augite, olivine and titanomagnetite. Interstitial spaces between crystals are filled with magmatic glass, indicating that they result from disaggregation of a network of crystals. Plagioclase crystals are predominately single laths with few twins (<4 average) and fine oscillatory zoning (Figure 5-5D). Plagioclase crystal faces are often obscured by intergrowth with clinopyroxene microcrystals, leading to a serrated appearance, while the interior of crystals often contains melt inclusions (Figure 5-5E). Radiate textures in plagioclase (typically surrounding clinopyroxene crystals) and serrated plagioclase crystals are both indicators of nucleation, indicating the magma was out of chemical equilibrium in terms of both plagioclase and clinopyroxene.

Clinopyroxenes in this unit show little zonation (Figure 5-5F) while olivines are heavily iddingsitised (Figure 5-5G). The groundmass in all samples is near-opaque and vitreous, with occasional microcrystals of plagioclase and titanomagnetite.

The uppermost sample (LP14SG06) shows the highest crystal content (≈33% cross-sectional area), the largest plagioclase crystals (<6mm) and has the most heavily iddingsitised olivines. In this sample clinopyroxene-olivine aggregates similar to those in the Glomerocrystic Ankaramite have been identified (Figure 5-5H), with the characteristic sieve-textured diopside cores and euhedral titanian augite rims. The augite rims in this sample enclose large plagioclase crystals indicating a co-magmatic, contemporaneous origin for these two minerals.

Plagioclase Tephri-phonolite

Samples from the Plagioclase Tephri-phonolite lava unit are plagioclase, hornblende, tephri-phonolites with a strong trachytic alignment of plagioclase laths accompanied by dark and light schlieren bands in the groundmass. Images of representative textural features are given (Figure 5-6).

The unit contains abundant plagioclase laths but while large laths (<5mm) of the type seen in the Plagioclase Basalt are present (Figure 5-6A), the average plagioclase crystal in this unit is much smaller (<0.5mm) and tends to show simple twinning. The strong trachytic alignment leads to the appearance of sub-parallel crystals hosted within a hyalopilitic groundmass (Figure 5-6B), alignment direction primarily varies where banding follows the outline of larger mafic phenocrysts.

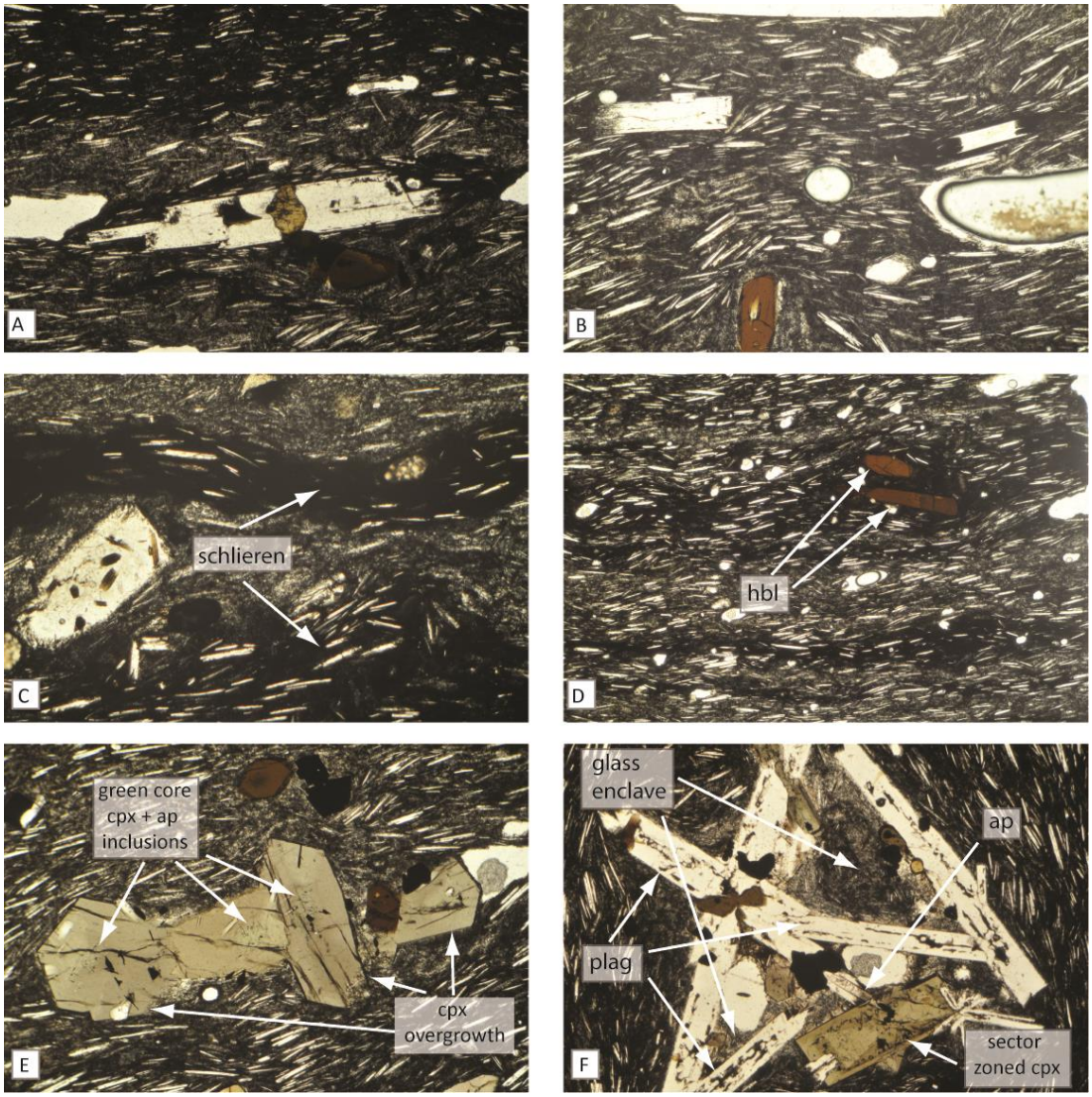

Figure 5-6 Photomicrographs representative of textural variation within the Plagioclase Tephri-phonolite lava-unit, all viewed in PPL. A. Plagioclase phenocryst in dark schlieren bands (FOV = 4.4mm). B. Undulating trachytic texture in groundmass plagioclases (FOV = 2.2mm). C. Dark and pale schlieren bands in cryptocrystalline groundmass (FOV= 4.4mm). D. Hornblende crystals distort schlieren and trachytic banding in groundmass (FOV = 4.4mm). E. Glomerocryst of clinopyroxene crystals with green diopside cores encasing apatite microcrystals, jointly enclosed in augitic rims (FOV = 2.2mm). F. Evolved glomerocryst containing plagioclase, sector zoned clinopyroxene, hornblende and apatite (FOV = 4.4mm). FOV = field fo view, cpx = clinopyroxene, hbl = hornblende, plag = plagioclase, ap = apatite.

However, plagioclase abundance is variable between two populations (dark and pale) of undulating, sub-horizontal schlieren bands that run parallel to the trachytic texture (Figure 5-6C-D). The darker bands (<3mm thick) are poorly-phyric with less feldspar and are near opaque, where the pale bands (<5mm thick) are cryptocrystalline to vitreous and host the primary plagioclase population.

Accessory phenocrysts are amphibole, clinopyroxene and apatite. Kaerustitic amphibole phenocrysts are euhedral and well preserved with only minor oxidation of rims (Figure 5-6C). Clinopyroxene phenocrysts are typically prismatic and often have small, green ferroan-diopside cores overgrown by thick augitic rims, with acicular micro-crystals of apatite commonly hosted within the cores (Figure 5-6E).

Glomerocrysts are less common in this unit than those underlying it, but a single network of large plagioclase laths contains sector-zoned augite, apatite and anhedral hornblende, shown in Figure 5-6F. Cavities within such aggregates are infilled with the characteristic groundmass of the unit. This indicates that, as in the Plagioclase Basalt, these glomerocrysts did not originate from a holocrystalline source.

The mineralogy and textures of samples of the lava lobe (LP14SG05) and pyroclastic bomb (LP14SG06) are broadly similar. In both samples the bands of schlieren and feldspar are aligned, although this orientation is more weakly developed in the bomb. The pyroclastic sample is notably less feldspar-phyric and has a more opaque, vitreous groundmass.

5.4.2 Mineral chemistry

The complete results of microanalysis are presented[20]. Representative analyses (chosen for median compositions in terms of mg#, An (Mol%) or oxide wt% of characteristic components) of each mineral sub-population are presented in Table 5-3 and Table 5-4.

Clinopyroxene

All analyses of clinopyroxenes from the BEP flow-field form a cluster in the upper left part of the clinopyroxene quadrilateral and are diopsides, titanian augites and ferroan-diopsides (Figure 5-7). There is considerable variation in clinopyroxene composition both within and between units (Figure 5-8). The most primitive diopsidic compositions are exhibited by the high mg# (0.81-0.76) xenocrystic cores of the Glomerocrystic Ankaramite aggregates. These possess a narrow compositional range, with low contents of TiO_2 (1.8-2.8 wt%), Al_2O_3 (6.3-7.7 wt%) and FeO (5.8-7.0 wt%). The rims of these aggregates, along with the pyroxenes of the Plagioclase Basalt, are more variable in composition. They are titanian augites with higher TiO_2 (2.8-4.9 wt%), Al_2O_3 (5.3-10.1 wt%) and FeO (6.6-7.7%) and these all increase with decreasing mg# (0.72-0.79). This is most apparent in the linear relationships of mg# to TiO_2 and Al_2O_3 across this group (Figure 5-8B-C). The clinopyroxenes of the Plagioclase Tephri-phonolite are compositionally distinct with two sub-populations, their xenocrystic ferroan-diopside cores possess the lowest mg# (0.56-0.68) and highest Na_2O contents (1.0-1.3 wt%) of all pyroxenes, while the rim population are sector-zoned and possess intermediate compositions between these xenocrysts and the primary population of titanian augites found across the flow-field.

[20] Appendix C: Supporting analytical data. p.207

Pyroxenes

Stratigraphic unit	Glom Ank	Glom Ank	Plag Bas	Plag Bas	Plag Teph-pho	Plag Teph-pho
Sample	LP13SG29	LP14SG08	LP14SG09	LP14SG09	LP14SG04	LP14SG04
Mineral ID	CPX_5	CPX_4	CPX_3	CPX_2	CPX_1	CPX_3
Mineral Population	Aggregate Core	Overgrowth Rim	Core	Rim	Xeno-Core	Rim (S-Zone)
SiO_2	47.8	44.0	47.9	45.1	47.8	45.8
TiO_2	1.8	3.7	3.1	4.4	2.4	3.2
Al_2O_3	7.0	8.9	6.2	8.3	5.0	7.8
FeO	6.2	7.3	6.7	7.1	11.5	9.2
MnO	0.1	0.1	0.2	0.2	0.4	0.3
Cr_2O_3	0.4	0.1	0.1	0.0	0.1	0.0
MgO	13.7	11.6	13.2	11.8	9.8	11.1
CaO	21.8	22.0	22.7	22.7	22.6	22.8
Na_2O	0.6	0.6	0.7	0.6	1.0	0.9
K_2O	0.0	0.0	0.0	0.0	0.0	0.0
Total	99.6	98.3	100.6	100.1	100.5	101.0
mg #	0.80	0.74	0.78	0.75	0.60	0.68

Table 5-3 Elemental compositions of typical pyroxene minerals within each BEP stratigraphic sub-unit. Examples chosen for median, representative chemistry in terms of mg# and CaO wt%. All presented concentrations were determined in oxide wt% with oxygen determined by stoichiometry - all Fe is determined as FeO.

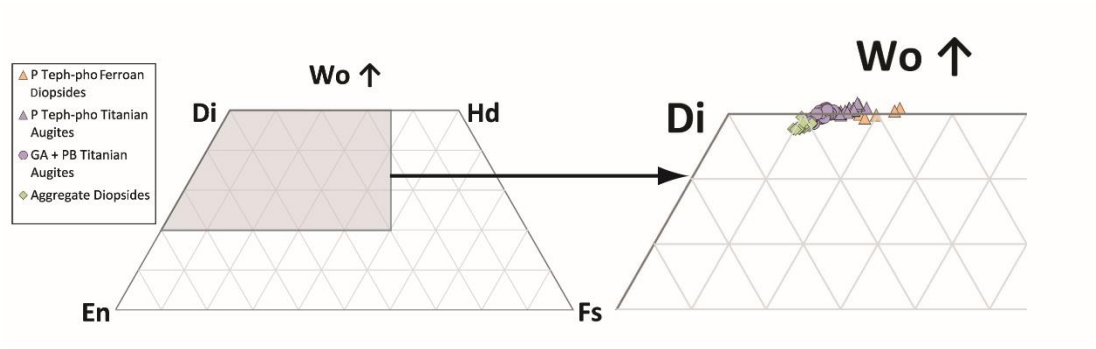

Figure 5-7 Mineral categorisation quadrilateral for BEP pyroxenes. Pyroxene end-members: Di = diopside, Hd = hedenbergite, En = enstatite, Fs = ferrosilite, Wo = wollastonite. BEP units: Aggregate = aggregate cores in Glomerocrystic Ankaramite, GA = Glomerocrystic Ankaramite, PB = Plagioclase Basalt, P Teph-pho = Plagioclase Tephri-phonolite.

These transitional pyroxenes share the high Na_2O (0.9-1.2 wt%) of the ferroan-diopsides, but also possess the elevated TiO_2 (3.3-4.17 wt%) and Al_2O_3 (6.4-9.3 wt%) contents more characteristic of the titanian augites. Across the units of the BEP, there is a negative linear correlation of mg# to Na_2O content in cpx (Figure 5-8C), although the xenocrystic Glomerocrystic Ankaramite aggregate cores have slightly elevated Na_2O relative to this trend.

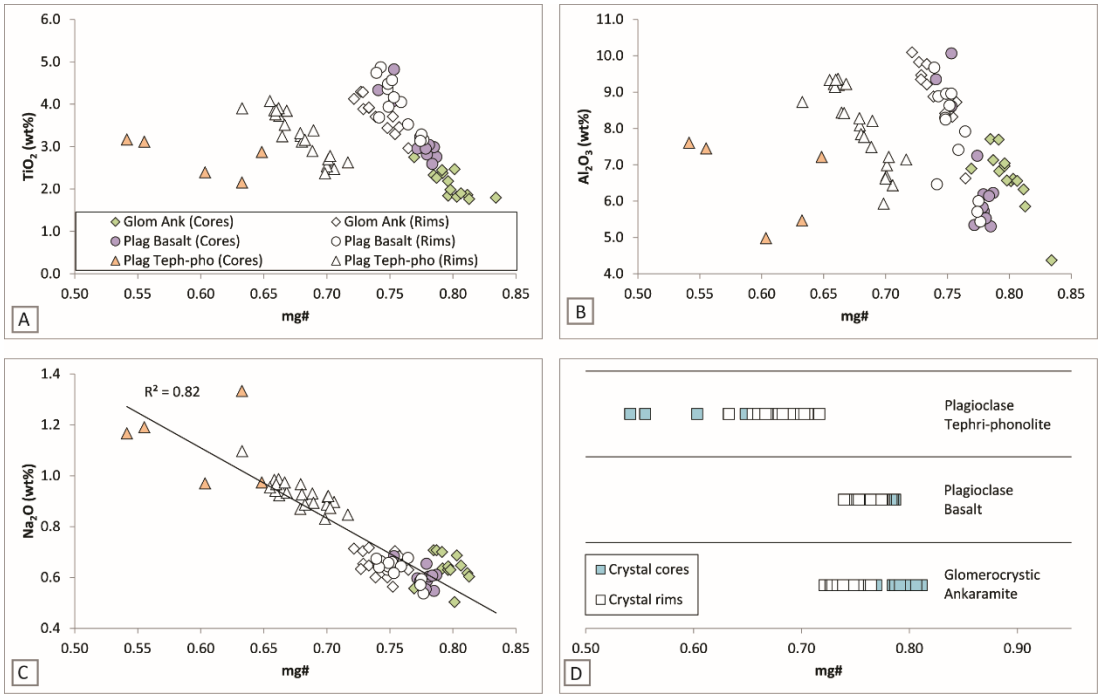

Figure 5-8 Bivariate plots of pyroxene mg# against concentrations of key compatible elements and stratigraphic unit. Panel D shows core rim variation in pyroxene mg# by stratigraphic unit. Units: Glom Ank = Glomerocrystic Ankaramite, Plag Basalt = Plagioclase Basalt, Plag Teph-pho = Plagioclase Tephri-phonolite.

FELDSPAR

Feldspar is the primary groundmass mineral in the lava-units of the BEP flow-field, with plagioclases common throughout the sequence. These feldspars all lie on a continuum that becomes progressively more albitic and CaO-depleted (13.5 to 6.7 wt%) up-sequence (Figure 5-9A), but each lava-unit possesses its own discrete compositional range (Figure 5-9B). In the voluminous Glomerocrystic Ankaramite the compositional variation of feldspars is relatively restricted, with low concentrations of Na_2O (3.7-4.2 wt%) and K_2O (0.3 - 0.4 wt%), high FeO (0.5 - 0.7 wt%) and traces of TiO_2 (<0.3 wt%). The range is similarly restricted in the overlying Plagioclase Basalt, although these are richer in Na_2O (4.4 - 4.6 wt%) and K_2O (0.3 - 0.5 wt%) with lower FeO contents (0.2 - 0.4 wt%). There is considerably greater variation in the high Na_2O (4.7-7.3 wt%) and K_2O (0.4 - 0.9 wt%) Plagioclase Tephri-Phonolite unit, which has the largest range in FeO (0.2 - 0.5 wt%).

OLIVINE

Olivine is only present in the lower two lava-units, the Glomerocrystic Ankaramite and the Plagioclase Basalt, and towards the top of the Plagioclase Basalt this mineral is pervasively iddingsitised. The xenocrystic cores of the Glomerocrystic Ankaramite aggregates possess the most forsteritic compositions (mg# 0.79-0.82), with low CaO (0.3-0.5 wt%) and MnO contents

Feldspars

Stratigraphic Unit	Glom Ank	Plag Basalt	Plag Teph-pho
Sample	LP14SG08	LP14SG09	LP14SG04
Mineral ID	Plag_4	Plag_8	Plag_6
SiO_2	52.4	53.1	56.1
TiO_2	0.2	-	-
Al_2O_3	30.7	29.5	28.7
FeO	0.5	0.3	0.4
CaO	13.5	12.0	10.5
Na_2O	3.9	4.5	5.4
K_2O	0.3	0.4	0.4
Total	101.45	99.97	101.65
An (Mol%)	65.9	59.7	51.6

Olivines

Stratigraphic Unit	Glom Ank	Glom Ank	Plag Basalt
Samples	LP14SG08_	LP14SG08_	LP14SG09_
Mineral ID	OL_1 Aggregate	OL_5 Overgrowth	OL_8
Analysis Label	Core	Rim	Core
SiO_2	40.6	39.2	39.4
FeO	17.1	21.3	24.9
MnO	0.3	0.4	0.5
MgO	42.1	38.2	36.4
CaO	0.5	0.4	0.5
NiO	0.1	0.1	0.0
Total	100.55	99.68	101.77
mg #	0.81	0.76	0.72

Spinel Group Minerals

Stratigraphic Unit	Glom Ank	Plag Basalt	Plag Teph-pho
Sample	LP13SG29	LP14SG06	LP14SG05
Mineral ID	Spin_3	Spin_1	Spin_7
TiO_2	18.6	24.6	16.2
Al_2O_3	9.6	5.8	4.3
Cr_2O_3	1.3	0.1	0.1
FeO	60.7	59.7	70.2
MnO	0.4	0.6	1.1
MgO	7.7	6.1	3.6
Total	98.26	96.88	95.43

Amphiboles

Stratigraphic Unit	Plag Teph-pho
Sample	LP14SG04
Mineral ID	Amp_5
SiO_2	40.1
TiO2	6.3
Al_2O_3	14.1
FeO	12.9
MnO	0.3
MgO	11.4
CaO	12.2
Na_2O	2.7
K_2O	1.2
Total	101.08

Table 5-4 Compositions of typical main minerals within each lava-units of the BEP flow-field. Examples were chosen for median compositions in terms of mg#, An (Mol %) and oxide wt% of characteristic components. All presented concentrations were determined in oxide wt% with O_2 derived by stoichiometry - all Fe is calculated as FeO.

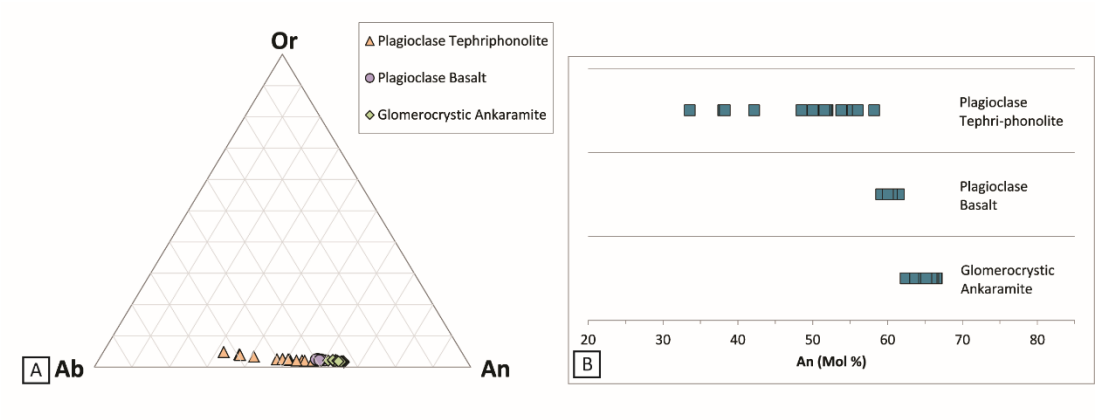

Figure 5-9 A) Mineral categorisation ternary for BEP plagioclase feldspars. Feldspar end-members: Ab = albite, An = anorthosite, Or = orthoclase. B) Plagioclase end-member composition by stratigraphic unit, all analyses from crystal cores.

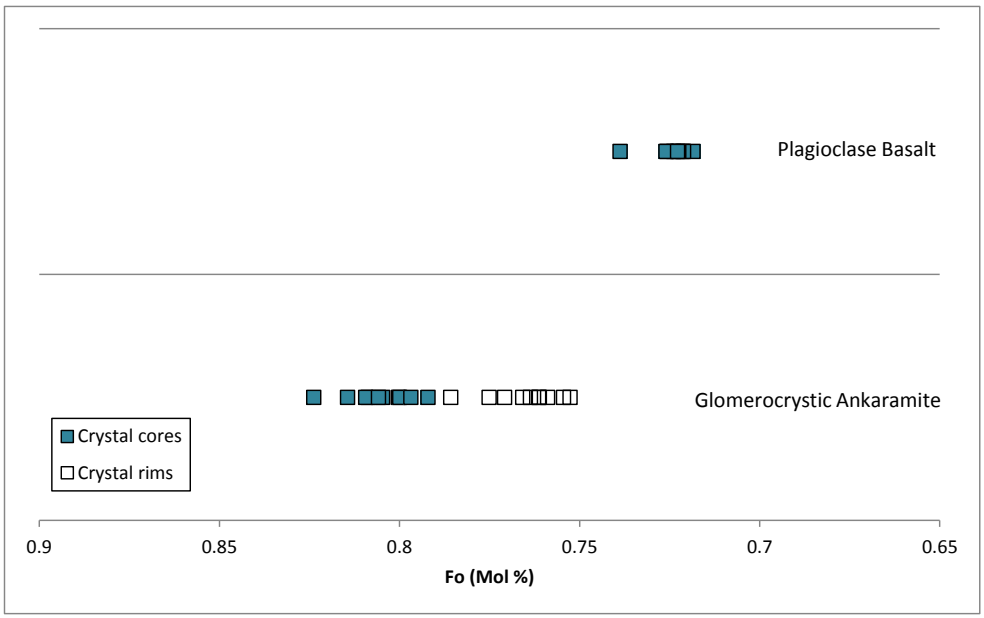

Figure 5-10 End-member composition of BEP olivines, olivines are absent in the Plagioclase Tephri-phonolite unit and heavily iddingsitised in the upper part of the Plagioclase Basalt.

(0.3-0.4 wt%), and these are enclosed in lower mg# (0.8), more fayalitic, overgrowth rims (Figure 5-10). Within the Plagioclase Basalt the olivines form a distinct population, with lower mg# (0.7) and higher MnO (0.4-0.6 wt%) contents.

SPINEL GROUP MINERALS

Titanomagnetite is abundant in all lava-units across the flow-field and shows considerable compositional variation both within and between lava-units. Titanomagnetites in the Glomerocrystic Ankaramite are the most compositionally complex, possessing high Al_2O_3 (7.2 – 10.6 wt%), MgO (3.9 -8.1 wt%) and Cr_2O_3 (0.4-6.0 wt%) with chromium concentrations varying markedly between individual crystals. The Plagioclase Basalt is host to high TiO_2 titanomagnetites (19.9 - 25.5

wt%) where there is a corresponding reduction in Cr_2O_3 (< 0.2 wt%) and Al_2O_3 (5.5 - 7.6 wt%). In the Plagioclase Tephri-phonolite magnetites exhibit their highest FeO contents (67.0 – 73.5 wt%), with an accompanying high concentration of MnO (0.8 – 1.7 wt%).

AMPHIBOLE

Amphibole is only present in the uppermost Plagioclase Tephri-phonolite lava-unit, where TiO_2-rich (6.0 - 6.9 wt%) hornblende (kaersutite) is common.

5.4.3 WHOLE-ROCK MAJOR AND TRACE ELEMENT VARIATION

Samples from the Glomerocrystic Ankaramite exhibit (Table 5-2) the most compositional variability (Figure 5-11, Figure 5-12) of the three lava-units. Three sub-groups with different MgO contents can be identified: high (13.12 - 12.95 wt%), medium (11.02 - 10.33 wt%) and low (8.61 wt%). Collectively, these sub-groups form tight linear variation trends, particularly in terms of Al_2O_3, TiO_2, Sr, Zr and Y contents, with the lowest MgO sample (LP12SG82) showing slightly anomalous compositions in terms of K_2O (1.67 wt%) and P_2O_5 contents (0.73 wt%), which are relatively high, and CaO (4.02 wt%) content which is relatively low.

In general, the trends across the Glomerocrystic Ankaramite samples do not intersect the cluster of analyses produced by the Plagioclase Basalt samples. The Plagioclase Basalt is relatively depleted in TiO_2 (3.11 - 3.18 wt%) and Fe_2O_3T (3.32 - 3.57 wt%) contents, and comparatively enriched in K_2O (2.64 - 2.76 wt%) and Zr (392-412 ppm). This could collectively result from the Plagioclase Basalt having undergone greater fractionation of either titanomagnetite or titanian augite.

The two samples of the Plagioclase Tephri-phonolite commonly form linear trends with the Plagioclase Basalt cluster (particularly in terms of TiO_2, Fe_2O_3, CaO, K_2O, P_2O_5, Zr and Y). The low P_2O_5 (0.28-0.49 wt%), Y (22-25 pmm) and TiO_2 (1.41-1.81 wt%) and Fe_2O_3T (5.26-6.76 wt%) contents of Plagioclase Tephri-phonolite lavas suggest this evolved magma batch has undergone considerably more titanomagnetite and apatite crystallisation than the earlier erupted units.

5.4.4 CLINOPYROXENE-MELT THERMOBAROMETRY

A BRIEF REVIEW OF THE PRINCIPLES OF CLINOPYROXENE-MELT THERMOBAROMETRY

The development of increasingly robust thermobarometers based on analysis of both pyroxene crystals and melt (Masotta et al., 2013; Putirka et al., 1996, 2003) has allowed the routine determination of magmatic crystallisation conditions. Such thermobarometers use the considerable pressure and temperature dependency of the pyroxene jadeite ($NaAlSi_2O_6$) when in solution with diopside-hedenbergite ($Ca(Mg,Fe)Si_2O_6$) to estimate both the pressure and the temperature of mineral formation. This dependency is a result of the small partial molar volume of jadeite in basaltic liquids relative to the large partial molar volumes of the oxides of Na and Al. This leads to semi-theoretical thermobarometers based on pre-existing thermodynamic models but which are then

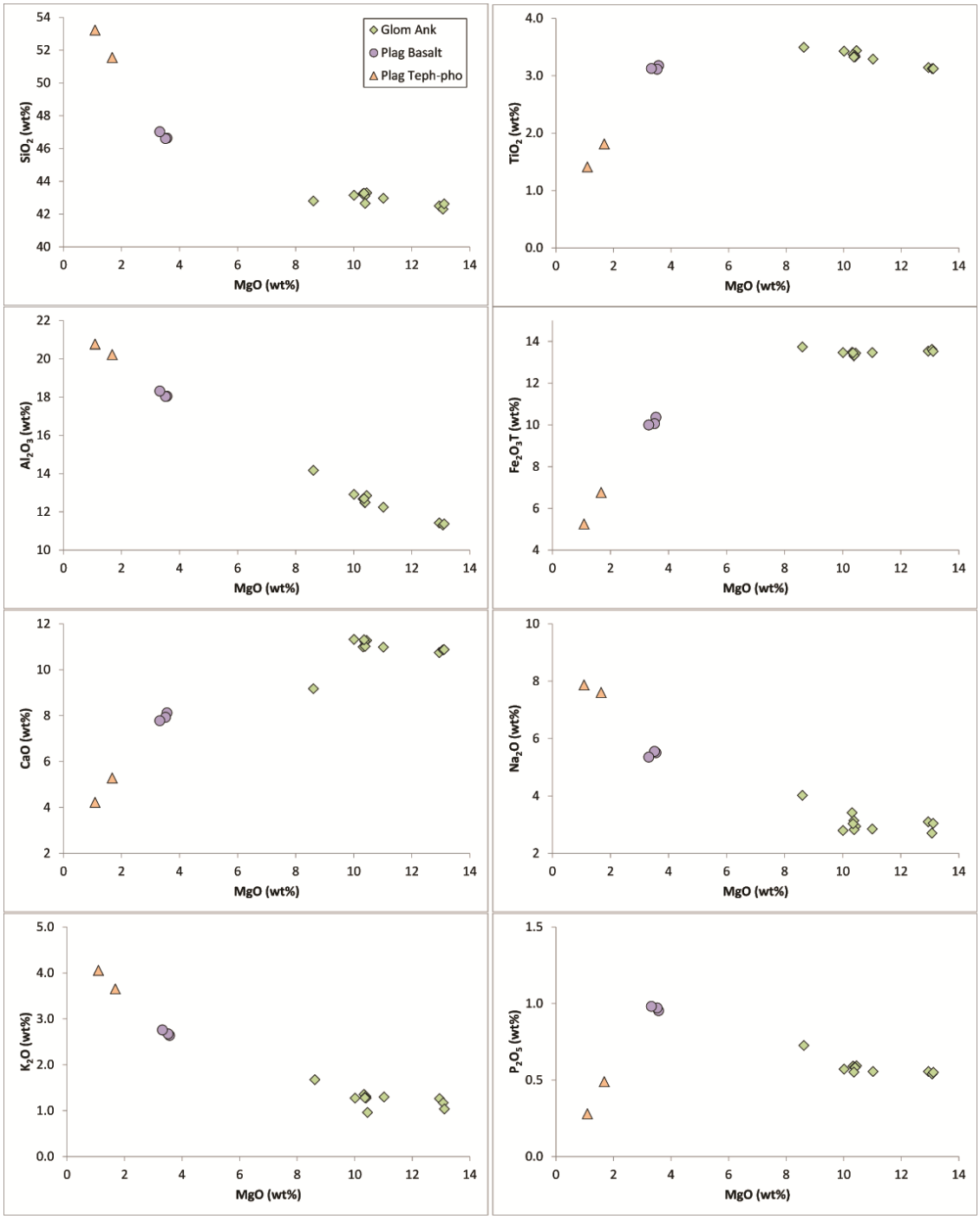

Figure 5-11 Major element MgO-variation diagrams for samples from the BEP flow-field, data grouped by lava unit. The legend is shown in the SiO_2 panel.

adjusted for different geological scenarios with empirical parameters each derived from a focused experimental calibration study.

The robust application of such thermobarometers is acutely dependent on: 1) assuming equilibrium between mineral and melt, 2) the determination of a representative melt composition, 3) the petrological interpretation of the pyroxene population. To demonstrate that crystallisation was under equilibrium conditions the measured clinopyroxene compositions are compared with

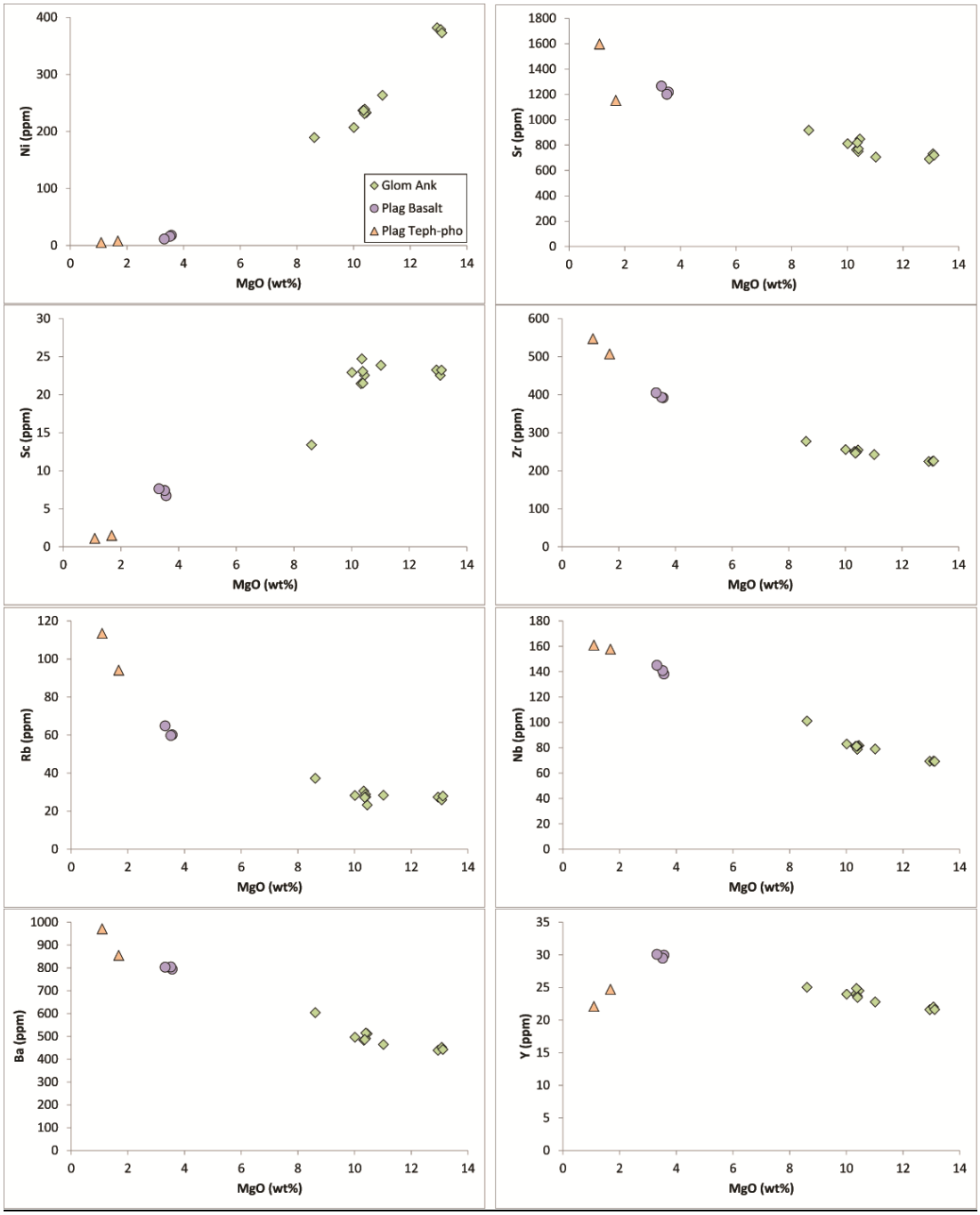

Figure 5-12 Trace element MgO-variation diagrams for samples from the BEP flow-field, data grouped by lava unit. The legend is shown in the Ni panel.

those predicted from the composition of the melt by theory, while whole rock compositions have commonly been used as melt proxies. Using whole rock compositions assumes that the samples are relatively homogeneous and are representative of the wider host magma during crystallisation.

CLINOPYROXENE-MELT THERMOBAROMETRY ON BEP SAMPLES

In the case of the majority of BEP samples, difficulties in determining the melt composition (a result of the high xenocryst contents and often microlitic groundmasses) have mostly prevented us from producing

new thermobarometric determinations. However, a previous study (Galipp et al., 2006) of lavas from across northern La Palma which utilised the Putirka et al. (2003) thermobarometric calibration for mafic and hydrous lavas included a number of determinations from *Bejenado* and after reviewing the samples, their provenance and the results we believe they can be integrated with our petrological observations to fix our interpretations to the pressures at which these processes occurred. That study presented five primitive lava samples from *Bejenado* and these all originated from the distinctive lower units of the BEP flow-field.

We therefore re-present the results of Galipp et al. (2006) in terms of the BEP's newly described petrological units (Figure 5-13 A-C)[21] as well as presenting new results from analysis of clinopyroxenes and interstitial glass from the Plagioclase Tephri-phonolite lava-unit (LP14SG04 and LP14SG05) and comparing them both with published cpx-melt thermobarometry data from the rest of the island. In the course of field collection for Galipp et al. (2006) an emphasis was placed on samples where interstitial glass was present with the aim of providing the most robust melt compositions possible. Where such glass was absent groundmass separates were prepared, finely ground and fused on an Ir-filament before quenching to glass. Minor discrepancies between the pressure determinations presented here and in the original publication result from our removal of P_2O_5 from analytical results before the thermobarometric calibration (Putirka et al., 2003) was applied: P_2O_5 was not present in the original calibration, but was included in the study by Galipp et al. (2006) resulting in a pressure overestimation of 0.03-0.05 GPa for the *Bejenado* samples. The new data from the evolved alkaline samples were collected to allow newer calibrations to be used (Masotta et al., 2013) that overcome the known limitations of the Putirka et al. (2003) calibration when it is applied to phonolitic melts. Barometric determinations are associated with standard errors of estimate derived from the fit of each calibration's regression, with ± 0.17 GPa for Putirka et al. (2003) and ±0.115 GPa for Masotta et al. (2013). All analyses passed an equilibrium filter based on comparing the observed mg# of a clinopyroxene crystal with that estimated from the Fe/Mg of the melt after applying the empirically derived formala of Duke (1976):

$$\log\left(\frac{Fe_{tot}}{Mg}\right)_{cpx} = -0.564 + 0.755 * \log\left(\frac{Fe_{tot}}{Mg}\right)_{liq}$$

Since all pressures are determined from analyses of clinopyroxene rims, we can associate the pressure determinations with the growth of individual mineral populations. In the Glomerocrystic Ankaramite and Plagioclase Basalt all pressures are derived from the crystal rims of the main titanian augite mineral population. Those from the Glomerocrystic Ankaramite pyroxenes yielded relatively variable pressures (0.54-0.73 GPa) which were generally greater than those from the Plagioclase Basalt (0.46-0.57 GPa). This was supported by the one sample (KLP106) with a texture that appeared transitional between these groups, this yielded pressure estimates of 0.60-0.65 GPa.

[21] Appendix C: Supporting analytical data. p.207

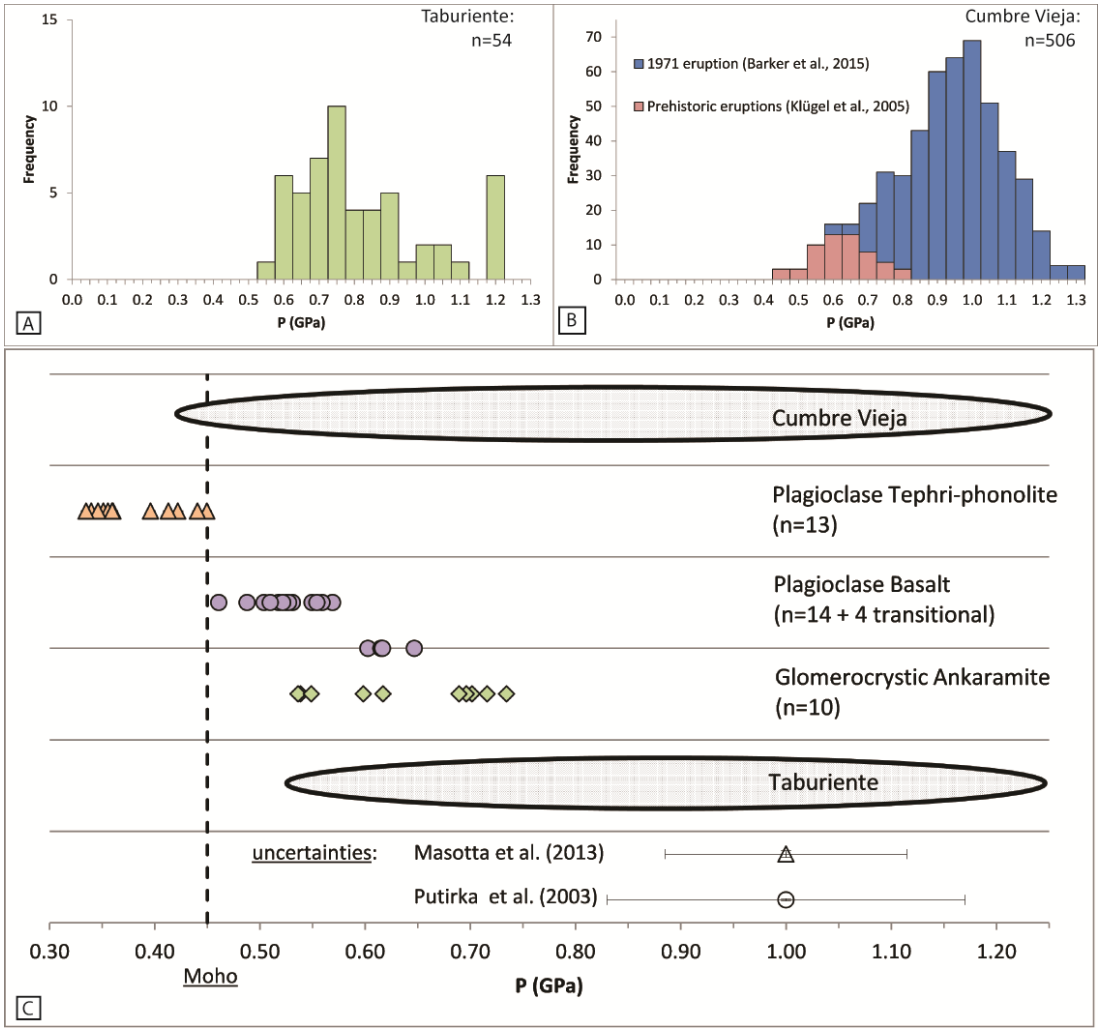

Figure 5-13 Pressure determinations for La Palma samples using clinopyroxene-melt thermobarometry. A) Histogram of literature-sourced pressures determined from individual pyroxenes from samples from Taburiente (data from Galipp et al., 2006). B) Histogram of literature-sourced pressures determined from individual pyroxeness from samples from the Cumbre Vieja (data from Klügel et al., 2005 & Barker et al., 2015). C) Pressure determinations from Bejenado samples recently identified as originating from BEP lava-units, arranged in stratigraphic order and compared with data-loops from Taburiente and the Cumbre Vieja. Plagioclase Tephri-phonolite data points are the product of work in the course of this study, while Plagioclase Basalt and Glomerocrystic Ankaramite data points were produced in the course of Galipp et al., 2006. Each data point represents an average of 5-20 analyses of rim compositions from individual pyroxene phenocrysts. Pressures determinations from the evolved Plagioclase Tephri-phonolite were obtained using the Masotta et al. (2013) calibration; those from the more primitive units were obtained using the Putirka et al. (2003) calibration, standard errors of estimate of these calibrations are shown.

In the Plagioclase Tephri-phonolite pressures were determined from the crystal rims of this lava-units lower mg# titanian augite population. The samples yielded the shallowest pressures (0.35-0.44 GPa) consistent with crystallisation in the crust.

5.5 Interpretation

The textures of the three lava-units of the BEP flow-field record the crystallisation processes that contributed to their formation. Fragments of reservoir material are seen in the abundant glomerocrysts, and these allow the millimetre-scale physical processes occurring during

crystallisation to be reconstructed, while the trends identified from whole rock and mineral chemistry provides insights into reservoir-scale mass balance and element partitioning.

However, these lava-units are the product of several magmas successively emplaced over the course of one flow-field's growth, and combining the information from their petrology requires them to be interpreted within a model of how this eruptive stratigraphy developed. There are three feasible explanations: 1) the progressive eruption or tapping of a strongly zoned magma body, 2) a suite of magma batches produced in different reservoirs that mingled during ascent, or 3) the distinct products of ongoing crystallisation within a single reservoir. Scenario one is least likely, since the evidence of cycles of resorption and recrystallization (Figure 5-4E and Figure 5-6E) as well as magma mixing (Figure 5-6C) is difficult to explain through magma heterogeneity, but scenarios 2 and 3 both appear consistent with certain features of the flow-field, and must both be carefully considered.

Within a lava-unit's crystal cargo, age relationships are provided by a textural stratigraphy derived from superposition between mineral zones. The next sections sequentially address each lava-unit with the aim of using these relationships to reconstruct the processes responsible for its textural features. Interpreting the relative sequence of reservoir processes that contributed to the BEP flow-field requires field and textural stratigraphies to be combined. In the following section, the key mineralogical and textural markers from each unit are identified and synthesised to propose temporal and spatial relationships between the reservoir processes. Within this framework, a unified textural model can be presented explaining the flow-field's complete stratigraphy in terms of reservoir processes.

5.5.1 Interpreting textures of individual BEP lava-units

Glomerocrystic Ankaramite

The characteristic abundant olivine clinopyroxene glomerocrysts provide detailed textural information that record the earliest crystallisation processes in the reservoir system. A model for the formation of these glomerocrysts is presented in Figure 5-14.

Figure 5-14A illustrates the earliest identified event, when a primitive magma reservoir was gradually crystallising an olivine-diopside lithology at depth. The remains of this lithology are preserved in aggregate cores. The glomerocryst relics are holocrystalline with anhedral internal crystal faces, indicating space-restriction in the reservoir during the later stages of its crystallisation. The magmatic body was mineralogically zoned, as evidenced by the varying abundance of olivine-dominated aggregates, indicating there were heterogeneities, probably bands or layers, containing varying proportions of olivine and clinopyroxene. The lack of any interstitial glass suggests that little residual melt was present late in the formation of this lithology. Figure 5-14B illustrates the

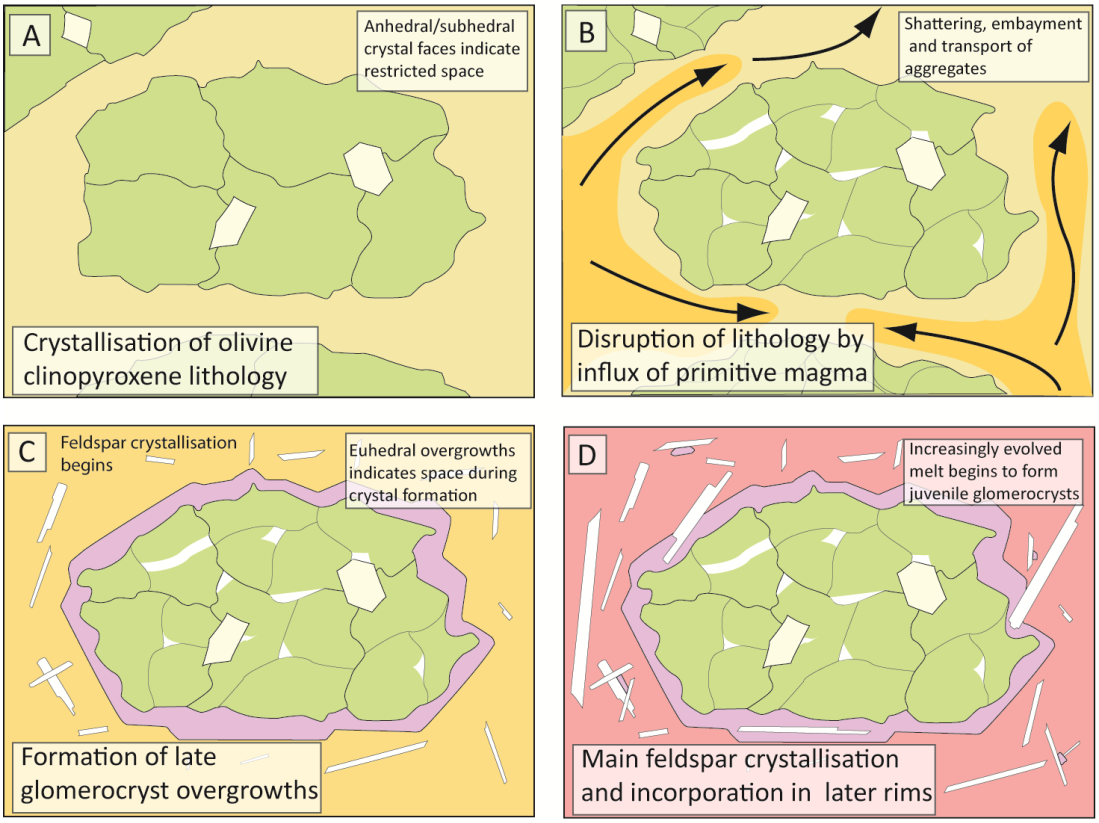

Figure 5-14 Process model for the origin of the olivine-diopside glomerocrysts characteristic of the Glomerocrystic Ankaramite. Panels A-C indicate processes that took place during the formation of all aggregates, while panel D indicates processes identified in the uppermost lobes of the Glomerocrystic Ankaramite and the sparse aggregates in the Plagioclase Basalt, where feldspar is common and is incorporated into aggregate rims.

disruption of the olivine-diopside lithology when a second influx of primitive magma disaggregated it into millimetre-scale fragments. This pulse of magma had a significant physical impact on the aggregates: 1) the sieve-texturing of pyroxenes indicates that it raised local temperatures leading to minor partial melting, 2) the embayment of pyroxenes and olivines indicates that it resorbed their outer crystal faces, and 3) the heavy fracturing of pyroxenes indicates that it shattered them through either thermal or mechanical processes.

The magma pulse then transported these fragments into a new environment where crystallisation recommenced. Figure 5-14C Illustrates the late overgrowth stage when the better-preserved titanian augite rims enclosed whole aggregates, and serrated surfaces formed on olivines. Both olivines and pyroxenes from this phase tend to be euhedral, indicating there was no space restriction during their growth. Figure 5-14D illustrates the incorporation of feldspar phenocrysts into the rims of pyroxenes in the upper, more feldspar-rich, part of the BEP flow-field and links the crystallisation of feldspar in the host magma to this late overgrowth stage.

Since the Glomerocrystic Ankaramite is the most voluminous unit in the BEP flow-field, and it is commonly composed of ≈40% aggregate material, this indicates that considerable volumes of this lithology were disrupted and transported to the surface during this event. In the lower parts of the

lava-unit, the host magma was relatively crystal-poor, indicating minimal crystallisation before its migration to the edifice.

Plagioclase Basalt

The glomerocrysts of the Plagioclase Basalt are also rich in textural information. In this case the main glomerocryst population is not holocrystalline, and the abundance of interlocking plagioclase laths with interstitial magmatic glass, often supporting pyroxene and olivine crystals, indicates that these crystallised as a chaotic network of plagioclase laths that together formed a crystal mush.

Towards the top of the unit, these plagioclase-network glomerocrysts show evidence for nucleation crystallisation textures, both of pyroxenes and plagioclases, indicating they formed through rapid crystallisation of a mineral super-saturated magma. Nucleation textures are commonly radiate, with pyroxene surfaces often providing the nucleation site for plagioclase crystals (Figure 5-5B,D,F). The radiate geometry indicates pyroxene crystals were suspended within the magma, as opposed to growing inwards from outer chamber surfaces. However, this nucleation of plagioclase crystals onto clinopyroxene is mirrored by needles of clinopyroxene growing on the surface of plagioclase crystals, giving a serrated appearance (Figure 5-5E). The presence of individual glomerocrysts showing both of these nucleation textures indicates super-saturated crystallisation of both minerals occurred concurrently (Figure 5-5B). This indicates crystallisation under dynamic reservoir conditions, although the mechanism responsible for super-saturation is unclear. Neither pyroxenes nor plagioclase crystals are either heavily zoned or multiply twinned, indicating that crystallisation did not proceed through a number of increasingly evolved stages.

While there are branching plagioclase glomerocrysts, radiate textures predominate over variolitic or trachytoid ones and indicates that, in spite of the abundance of crystals, the networks were still forming on a relatively small scale within the magmatic reservoir.

Plagioclase tephri-phonolite

This lava-unit yields the most evolved samples identified on *Bejenado*. However, the evidence of magma mixing and low crystal content means the textures in this unit provide more insights into melt-migration and mingling processes than reservoir crystallisation.

Interlocking networks of plagioclase crystals have been identified in the glomerocryst population of this lava-unit (Figure 5-6F), indicating disruption of another non-holocrystalline, but crystal-rich, magma. However, these are associated with a more evolved phenocryst suite than is found in underlying units: plagioclase, low mg# titanian augites, hornblende, titanomagnetite and apatite. Magma mixing may be responsible for the large range of feldspar compositions in this unit, which show greater variation in An content than either of the earlier units. This variation in composition is accompanied by a bimodal feldspar size distribution, indicating conditions were less favourable to the formation of large plagioclase crystals than in the Plagioclase Basalt.

The low mg# ferroan diopside cores within the unit's pyroxenes provide a crystallisation signature of the evolved magma that contributed one of the mixing members and crystallised earlier than other mineral populations. However, the only textural evidence retained from this melt is the abundance of microcrystals of apatite enclosed within cores (Figure 5-6E). These ferroan diopsides are enclosed in titanian augite rims with low mg#, forming reverse zoned pyroxene crystals. This population of low mg# titanian augites is similar to both the Plagioclase Basalt's titanian augites, and also the ferroan diopsides they enclose, indicating a complex relationship between the Plagioclase Tephri-phonolite and the Plagioclase Basalt units.

5.5.2 Relationships between lava-units

Temporal and spatial relationships between the processes responsible for lava-unit textures.

Feldspars in the BEP flow-field provide the best potential proxy for the reservoir system's temporal evolution. From base to top of the sequence all feldspars follow an uninterrupted trend of increasing albite content. Furthermore, their textural characteristics appear to be progressive, starting as sparse, simple-twinned, laths at the base of the Glomerocrystic Ankaramite. From here, they become increasingly large, abundant and interconnected towards the top of the Plagioclase Basalt, until they separate into two bimodal populations in the Plagioclase Tephri-phonolite. If their changing characteristics can be interpreted as the product of a progressive process, then plagioclase morphology and composition provides a blunt but robust indicator of temporal evolution from the earliest to latest stage reservoir processes.

The other stratigraphic marker in petrographic textures is provided by the titanian augite pyroxene population, characteristic of the two lower lava-units. This marks in mineral zones the stage of pyroxene crystallisation that followed after the magma pulse disrupted the Glomerocrystic Ankaramite's olivine-diopside lithology and therefore provides a signature of the host magma of the early BEP sequence. Fortunately, throughout the BEP succession, feldspars are either intergrown with, or form glomerocrysts with, the pyroxene population and this allows these separate stratigraphic and temporal markers to be coupled together.

In the Glomerocrystic Ankaramite, this titanian augite stage was responsible for the late-overgrowth rims on olivine-diopside aggregates, where the incorporation of small, early, feldspars allowed this titanian augite crystallisation to be identified as concurrent with the early stages in the feldspar evolution trend. Titanian augite also provides the only pyroxene population in the Plagioclase Basalt, providing evidence that this lava-unit was the product of crystallisation of the same magma batch responsible for disrupting the olivine-diopside lithology.

This interpretation of the Plagioclase Basalt is further supported by the presence of residual aggregates of disrupted olivine-diopside lithology within the unit. These aggregates show two key

features: 1) their late overgrowth rims incorporate large feldspar crystals characteristic of the Plagioclase Basalt population (Figure 5-5H), and 2) these rims are of similar thickness to those from the Glomerocrystic Ankaramite glomerocrysts, indicating they have not been the product of an extended period of crystallisation. The simplest explanation for these features is that residual olivine-diopside material continued to be disaggregated from the environment while the feldspar population was evolving. The combination of the shared titanian augite population, common evolving feldspar population, as well as the common reservoir wall-rock material implied by the aggregates, provides strong grounds to argue that the Plagioclase Basalt and Glomerocrystic Ankaramite are closely related. We propose that the Plagioclase Basalt was produced by late crystallisation in the same reservoirs as the Glomerocrystic Ankaramite.

The Plagioclase Tephri-phonolite shows the most evidence for magma mixing, and so components within this unit may be the products of a separate series of events that cannot be correlated with, but are likely to precede, those following disruption of the olivine-diopside lithology. Identifying these pre-mixing magmas texturally, the low mg# ferroan diopside cores in its pyroxenes provide the best signature of its evolved end-member, while the large plagioclase population derives in part from the other endmember, which on this evidence is likely to be the Plagioclase Basalt. The best evidence of the sequence of crystallisation is provided by the presence in glomerocrysts (Figure 5-6F) of low mg# ferroan diopside core pyroxenes enclosed in rims with low mg# titanian augite composition relative to the pyroxenes of the Plagioclase Basalt. This indicates the glomerocryst and phenocryst population of this unit formed after the Plagioclase Basalt magma began interacting with the more evolved melt. The schlieren banding within this unit indicates mixing was incomplete at the time of emplacement, and thus the phenocryst population appears to have formed in a relatively brief period between initial interaction of the two magma batches, but before their emplacement on the edifice.

In each lava-unit it is possible to identify progressive trends that indicate changes over time in the reservoir-system. However, it is unclear how this temporal progression in reservoir conditions should be related to the sequence of the lavas. Without the use of an ascent-rate determination technique this must be assumed. The simplest explanation would be that the primitive, earliest erupted, magma batches were tapped before the more evolved units had crystallised, since they would be unlikely to co-exist in a shared reservoir as the melt became more evolved. This interpretation fits well with the nucleation textures in the Plagioclase Basalt, which indicates rapid crystallisation in a dynamic environment. Furthermore, an interpretation involving continuous tapping has the benefit of providing space for crystallisation of new products in an environment where space restrictions previously occurred. Thus it is reasonable to consider that the duration of crystallisation after disruption of the olivine-diopside lithology is comparable to the duration of emplacement of the lava sequence.

5.5.3 A TEXTURAL MODEL FOR THE EVOLUTION OF THE BEP FLOW-FIELD'S RESERVOIR SYSTEM

A schematic model for the textural and mineralogical evolution of the BEP flow-field's lava-units is presented in Figure 5-15. Since this model is derived from millimetre-scale features, its shape is not intended to realistically reflect either magmatic volumes or chamber geometry. Stages involved in this model are: 1) initial crystallisation of an olivine-diopside lithology, 2) disruption of this magmatic unit by a pulse of primitive magma and the beginning of magma transport to the edifice, 3) progressive crystallisation caused this reservoir to become more evolved and richer in feldspar, 4) a more evolved magma interacted with this migrating magma towards the end of its tapping, resulting in a texturally complex, mingled, magma that provided the last material to be erupted.

INTERPRETING RESERVOIR-SCALE PROCESSES THROUGH GEOCHEMICAL CONSTRAINTS

Whole rock MgO variation trends across a lava suite give a combined perspective on the relationships between evolving magmas against which we can test these textural models. The chemical trends exhibited by BEP samples (Figure 5-11, Figure 5-12) are typical for La Palma, indicating staged crystallisation of the mineral suites characteristic of the island ((Carracedo et al., 2001; Praegel and Holm, 2006). However, while whole-rock variation diagrams commonly compare samples from different lava flows from the same edifice or region, the BEP sample suite is the result of taking multiple samples from a single flow-field. A nuanced interpretation is therefore needed with an emphasis on discrete magma batches mixing together rather than purely on variable degrees of fractional crystallisation of a similar parent melt. Furthermore, while three lava-units have been identified in the field, textural evidence within them shows there is considerable evidence for magma-mixing within and between them, particularly in the xenocrysts of the Glomerocrystic Ankaramite and the schlieren of the Plagioclase Tephri-phonolite. Thus the lava-units should not be treated as end-members of these magma batches, but rather as mixtures of these components and any heterogeneity within them.

The most primitive lava-unit in the suite, the high MgO Glomerocryst Ankaramite, provides the starting point for interpreting variation trends, together with the earliest crystals in our textural stratigraphy. However, these samples contain a large proportion of disrupted aggregate material, so the linear variations in this lava-unit could result from: 1) variation in the proportions of host magma to xenocryst content in individual samples, 2) mineralogical variation within olivine-diopside lithology material between olivine, diopside and titanomagnetite, and 3) variability, such as degree of evolution, in the host magma across the unit. The abundance of olivine indicates that accumulation is likely to contribute to within-unit MgO variation.

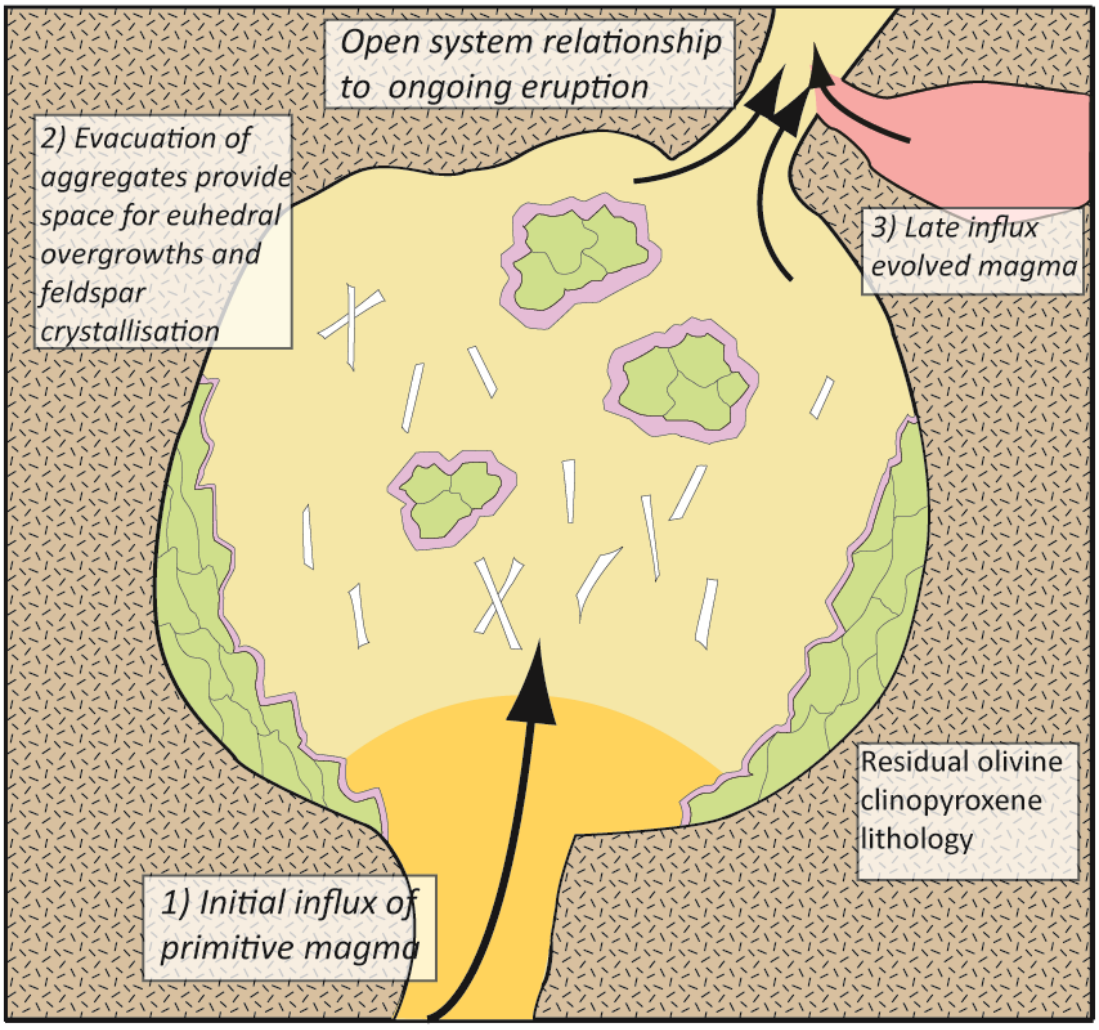

Figure 5-15 A textural process model for the spatial relationships between reservoirs and sequence of events involved in the petrological evolution of BEP flow-field lava units.

Our textural model proposes that the Plagioclase Basalt is the evolved product of fractionating the host magma of the Glomerocrystic Ankaramite, and this should be reflected in chemical variation trends. Yet this is difficult to reconcile with the gap in MgO compositions (8.61-3.57 wt%) between Glomerocrystic Ankaramite and Plagioclase Basalt samples, and the accompanying non-linear trends in TiO_2, Fe_2O_3, K_2O and Zr. Nonetheless, examining the groundmass of the lowest MgO sample (LP12SG82) in the Glomerocrystic Ankaramite unit, often anomalous on variation trends (e.g. CaO, P_2O_5 Sc and Ni), shows transitional textural features between Glomerocrystic Ankaramite and Plagioclase Basalt, including larger plagioclase crystals and a more crystalline groundmass. This is consistent with our textural model. It seems reasonable to suggest that a combination of fractionating the host magma, and overprinting of MgO contents in Glomerocrystic Ankaramite samples by mineral accumulation, may be responsible for the linear trends and the MgO gap. However, the relatively linear negative trends in Sr contents (Figure 5-12) across all lava-units are surprising, since feldspar crystallisation would be expected to remove this element as MgO

decreases. This is likely to indicate that there has been only limited removal of plagioclase crystals from the magma.

Between the late Plagioclase Tephri-phonolite and the Plagioclase Basalt the strong linear trends in most chemical variation diagrams (Figure 5-11, Figure 5-12) are consistent with the Plagioclase Tephri-phonolite being the product of mixing a more evolved magma with the compositionally homogeneous Plagioclase Basalt. This strongly supports the relationships interpreted from petrographic textures.

5.5.4 Estimating the pressures of reservoir processes through thermobarometry

Thermobarometry can potentially provide a means of fixing this reconstruction of reservoir processesl and the textural sequence of events to the pressures and depths at which crystallisation occurred. In the Glomerocrystic Ankaramite and the Plagioclase Basalt, these pressure determinations are derived from analysis of the titanian augite pyroxene population, the mineral population that formed both the late overgrowth rims of the olivine-diopside aggregates and the nucleation-surface pyroxenes of the Plagioclase Basalt.

The range of pressures from these titanian augites (0.46-0.73 GPa) is notable, with suprisingly little overlap between determinations from the shared clinopyroxene population of the Plagioclase Basalt samples and those of the Glomerocrystic Ankaramite. This is in spite of the considerable compositional and textural evidence that these are a single mineral population. This range appears to indicate that this shared mineral population (and its resulting textures) may have crystallised across a vertically extensive zone in a shared part of the lithospheric mantle. This raises issues of how best to visualise the geometry and scale of these processes since this range is hard to reconcile with the assumed sill geometry of (Klügel et al., 2005). However all estimates from these lower two lava-units lie within a range comparable to the standard error of estimate of the Putirka et al. (2003) calibration, so this variation should not be overinterpreted. In combination, it seems reasonable to ascribe the Plagioclase Basalt and Glomerocrystic Ankaramite to a common reservoir process in a shared part of the upper lithospheric mantle.

Pressure estimates from the Plagioclase Tephri-phonolite are the result of analysing the low mg# titanian augite population whose crystallisation marks the period post-dating the mixing of the two magma batches. Pressure determinations from these pyroxenes provide shallower, crustal, depth estimates. As the product of the Masotta et al. (2013) thermobarometer there may be problems with directly comparing these determinations with those from the lower more mafic units. Nonetheless, the lower pressure is unsurprising on the basis of our textural evidence which indicates this lava-unit was the product of late mixing processes with a shallower magma body. It appears that the mantle-sourced, Plagioclase Basalt and Glomerocrystic Ankaramite magma interacted with this phonolitic reservoir as it passed the Moho, likely crystallising this population in-situ.

Unfortunately, since these samples are not the same as those used to describe our textural sequence it is difficult to fully constrain the depths at which each glomerocryst population formed, and with it resolve subtleties such as the pressures at which plagioclase crystals began to be incorporated into clinopyroxene rims. A more systematic future study of samples from across the flow-field may allow a full reconstruction of the vertical extent of the reservoir system process that led to the BEP sequence.

5.6 Discussion

The Bejenado Effusive Phase flow-field and particularly its crystal cargo provides a remarkably detailed record of processes in the island's magma reservoir and transport system after a lateral collapse. The relationships between lava-units and thermobarometry, whole rock trends and petrographic textures allow us to provisionally reconstruct the reservoir processes and put them in a sequence of events occurring in the island's established reservoir structure.

Many features of this flow-field are shared with the products of individual Canary Island eruptions. Studies of the *Cumbre Vieja's* six historic eruptions (Barker et al., 2015; Johansen et al., 2005; Klügel et al., 2000) have indicated that flow-fields with multiple lava-units are common on La Palma. The 1949 eruption (Klügel et al., 2000) provides the clearest parallels, with five proposed magma batches contributing to its three lava-units (basanite, tephrite and phono-tephrite). It also included green-core pyroxenes in its basanite lava-unit, and abundant groundmass plagioclase in its phono-tephrite lava-unit. However, it does not share the unusual phenocryst plagioclase content, evolved tephri-phonolites, nor the intensely porphyritic nature of the BEP flow-field, and was not associated with a lateral collapse. Contrasted with these petrological studies, The BEP flow-field appears to provide an extreme example of the types of reservoir processes that have been observed in the products of individual eruptions.

If this flow-field was not emplaced in the course of such a single eruption, the alternative would be for it to have been the product of an eruptive cycle of the type described on volcanoes such as Mount Etna (Allard et al., 2006; Guest and Murray, 1979) where the characteristic volcanism is regular but episodic with small eruptives volumes. In such a cycle, continuous processes in the magma reservoir system, fed by high magma-supply rates, would result in intermittent, higher-frequency, eruptions than have been historically observed on La Palma. In such a scenario the shared petrological characteristics of the products of the BEP's multiple eruptions would result from each originating through the tapping of a shared reservoir. Such a cycle model would also mostly fit the interpretations presented in the previous section, but would allow the observed magmatic processes to have occurred over a longer duration.

The morphology of the flow-field does not constrain the relative likelihood of a single eruption, or eruptive cycle model, since the extremely numerous small-volume pahoehoe lobes that form the

main body of the flow-field could easily have been emplaced either intermittently or continuously. $^{40}Ar/^{39}Ar$ geochronology from the base (528 ± 23 ka) and upper part (497 ± 17 ka) of the flow field yield a duration of ≈ 30ka for the emplacement of this unit. However, this period is similar to the total uncertainty on each date, and may reflect our inability to resolve shorter duration events with current instrumental precision. The greatest petrological constraint on the relative likelihood of these two models is provided by the evolution of the feldspar population from the base of the sequence, since the progressive nature of these changes is difficult to reconcile with a repeatedly-refilled reservoir under conditions of high magma-supply rates.

The structure of the magma storage system of the western Canary Islands, where the observed petrological record originated, has been the focus of considerable research largely using thermobarometry (Galipp et al., 2006; Klügel et al., 2005, 2015; Longpré et al., 2014). Our cpx-melt thermobarometric determinations are derived in part from these previous studies, so it is unsurprising that their results are in agreement with this body of work. The reservoir system in which the BEP magmas evolved is broadly consistent with the model presented for La Palma by Klügel et al. (2005), in which the main fractionation stage occurs beneath the Moho in the lithospheric mantle. Pressure determinations from our more evolved magma batches are consistent with that model's "stagnation stage" (Galipp et al., 2006) lower-crustal reservoirs, previously only identified from fluid inclusion thermobarometry. Prior to disruption, the main Glomerocrystic Ankaramite magma appears to have been the product of a static, gradually-crystallising olivine, clinopyroxene reservoir. This has remarkable parallels to the deep cotectic reservoirs described in Nikogosian et al. (2002) who described them as a major stage in the evolution of basanites on La Palma's northern shield, and alkaline oceanic island settings in general.

However, it is difficult to reconcile the spread of 0.26 GPa (equivalent to ≈8.5 km depth), from analyses of the Glomerocrystic Ankaramite and Plagioclase Basalt with these lava-units originating in a shared environment. Textural evidence leads us to assume they originated in a single reservoir, where the regional wall-rock is an olivine-diopside lithology, but the spread of pressure estimates mean this would have to be vertically extensive. Since this study uses pressure determinations from three petrologically distinct lava-units contributing to the same eruption, we have the potential to provide an exceptionally detailed reservoir model for the processes that contributed to this flow-field, but this would be best supported by determinations from our stratigraphically well-constrained samples. Without this it is difficult to fully reconcile the spread of pressures with the textural sequence of events. We propose that further thermobarometric study may potentially fully resolve this issue and provide a robust model for the BEP reservoir system.

While the individual characteristics of the BEP flow-field's lava-units each merit comparison to the products of wider processes observed on La Palma, the flow-field is nonetheless among the most

exotic lava-sequences identified on the island, and it seems reasonable to ascribe this to the collapse. Physical modelling (Pinel and Jaupart, 2005) and finite element modelling (Manconi et al., 2009) of sector collapse scenarios has suggested that the decompression effects that result are likely to affect magmas stored at the 10-25km depth range estimated for the oceanic island magma reservoir system, resulting in magma mixing, melt mobilisation and degassing. Therefore, even if the processes taking place at depth in this eruption are not unique, then their rate, magnitude and combination may be.

Such a dynamic, post-collapse, interpretation of the reservoir system processes inferred from our petrological observations is supported by two key features of the flow-field: 1) the significant crystallisation of feldspar in the Plagioclase Basalt, a rare phenocryst phase on northern La Palma (Galipp et al., 2006), and 2) the mobilisation of a dense, crystal-rich, magma in the Glomerocrystic Ankaramite. Both of these observations are more readily explained in the context of reservoirs where volatiles are being exsolved from the magma and where dynamic mixing processes are taking place.

The shared feldspar population of the Plagioclase Basalt and Glomerocrystic Ankaramite magma batches crystallised beneath the MOHO, and such unusually deep crystallisation is more easily explained in the context of a magma batch that had undergone significant volatile loss. Experimental petrology indicates that feldspar crystallisation in basaltic magmas is primarily controlled by temperature, pressure and magmatic pH_2O, with studies indicating (Johannes, 1989) that feldspar crystallisation should begin at considerably higher temperatures (≈ 300°C) in an anhydrous magma than in one with water contents of 0.5 GPa H_2O. In the case of the Plagioclase Basalt gradual cooling is unlikely, since the observed nucleation textures indicate it crystallised under super-saturated conditions. Pressure determinations for the titanian augite mineral population (which forms glomerocrysts with plagioclase laths) yield lithospheric mantle depths (0.46-0.73 GPa). On La Palma such conditions are typically expected to lead to clinopyroxene and olivine dominated fractionation (Nikogosian et al., 2002), not plagioclase crystallisation. A reduction in magmatic pH_2O at depth is therefore the simplest change in conditions that can explain the presence of plagioclase in the crystal rims of pyroxene-dominated glomerocrysts.

The more evolved, heavily studied, post-collapse magmatism of Mount St. Helens has significant parallels to the Plagioclase Basalt. Studies of this system indicate that decompression-driven crystallisation provides the best explanation for zoned feldspars in its post-collapse eruptive products (Blundy et al., 2006; Blundy and Cashman, 2005). H_20 saturated experimental studies on the Mount St. Helens' rhyodacites provide the strongest textural parallels (Riker et al., 2015) to the features we have identified in the Plagioclase Basalt lava-unit. Among these single-step decompression experiments (a scenario consistent with post-collapse unloading of the edifice) are

surprisingly similar, particularly in the case where 50 MPa was unloaded from the charge over the course of a 24 hour experiment. The resulting samples exhibit radiating aggregates of tabular plagioclase laths similar to those in the Plagioclase Basalt.

Further analytical study of magmatic water contents, ideally focusing on stratigraphically well-constrained samples, would help address this issue and would ideally include ion microprobe analyses of melt inclusions and plagioclase crystals or FTIR analyses of pyroxene crystals to directly determine the magmatic volatile variation across the sequence. Such data cannot be obtained for this thesis.

If we accept the possible presence of a volatile vapour phase at these depths, the resulting bubbles within the magma would aid in providing an explanation of how the dense Glomerocrystic Ankaramite magma-batch became mobilised, since that unit's high contents of dense, rigid clinopyroxene-olivine glomerocrysts would otherwise be expected to resist eruption. The rheological properties and mobility of crystal mushes has been the focus of considerable modelling (Mader et al., 2013; Truby et al., 2015) as well as investigating potential mobilisation mechanisms for crystal-rich magmas (Burgisser and Bergantz, 2011; Huber et al., 2010). While these studies have usually addressed evolved, granitic magmas stored at shallow depth, they provide the best framework for understanding crystal mushes in oceanic island settings. Burgisser and Bergantz (2011) propose that the injection of a sill of high temperature, low viscosity melt beneath a crystal-rich magma body results in a process they term "unzipping": 1) the sill heats the crystal-rich magma body, 2) the resulting partial melting weakens crystal frameworks, and 3) convective mixing at the contact disaggregates crystalline material, mixing it into the more primitive magma body. This "unzipping" process would provide a convenient explanation for the sieve texturing, embayment and size of the Glomerocrystic Ankaramite's aggregates. Huber et al. (2010) take this process further, proposing that with high volatile fluxes (degassing of the primitive magma) bubble formation and circulation will accelerate the breakup of the overlying crystal-rich body.

The role of bubbles in mobilising such magmas is supported by models of the rheological properties of magmas, which are modelled in terms of the number of physical phases (melt, crystals and bubbles) acting under conditions of Newtonian strain. Computationally demanding three phase models (Truby et al., 2015) that include all of these components indicate that the addition of bubbles to a system containing melt and crystals will always reduce this three-phase melt suspension's viscocity and therefore that bubble formation provides a potential mechanism for the mobilisation of an otherwise flow-resistant magma.

Combining these rheological models and the volatile chemistry literature provides an attractive explanation for many of the characteristic petrological features of BEP samples. It is therefore

tempting to consider the flow-field to be the product of a dynamic reservoir system process where degassing, nucleation and wall-rock disagreggation are all rapidly occurring and ongoing.

Overall, the alternative case study showing the strongest parallels to the BEP flow-field is found at Tenerife's early post-collapse *Teno* massif, where plagioclase basalts overlie ankaramities (Longpré et al., 2008, 2009). Comparable characteristics observed there are: 1) clinopyroxene crystals mantled by TiO_2-rich dark outer rims, 2) intergrowth of these rims with plagioclase and apatite, 3) chemical evidence of disequilibrium crystallisation, where measured mg# was not consistent with predicted mg# (Putirka, 1999). These studies similarly invoke crystallisation induced by post-collapse decompression where rapid magma ascent would be accompanied by degassing and magmatic supersaturation. Further studies on El Hierro (Manconi et al., 2009) have also identified dense, crystal-rich magmas, basaltic phreatomagmatic sequences, and plagioclase basalts as characteristic features of post-collapse Canarian-type volcanism, also concurring with this result. However, these case studies have not yielded the detailed stratigraphic and petrographic information of the BEP, which so far represents the best record of processes in the magmatic reservoir system after a Canary Island lateral collapse.

5.7 Conclusions

Interpretation of the petrographic record provided by stratigraphically-sourced, porphyritic lava samples in a multiple lava-unit flow-field has led us to develop a detailed model of the chain of events in the reservoir system. This is supported by fingerprinting mineral populations through EPMA techniques and whole rock trends, largely without expensive instrumentation. The resulting model is of a complex, dynamic reservoir environment after the collapse, where magma-mixing, super-saturation and degassing lead to complex crystallisation conditions. In such an approach, textural description of glomerocrysts provide a potential "Rosetta Stone" that can join the results of analyses of different minerals together as the product of shared processes.

Our studies of the Bejenado Effusive Phase flow-field provide material for a uniquely detailed interpretation of reservoir processes after the collapse of a Canary Island rift system. These indicate:

1) The BEP flow-field was the product of at least three magma-batches that mixed in a reservoir system located between the lithospheric mantle and the oceanic crust in the period when this system was disrupted after the *Cumbre Nueva Collapse*.
2) The Glomerocrystic Ankaramite lava-unit, a highly porphyritic, large volume, lava-unit located at the base of the BEP sequence, is likely to be the result of a pulse of primitive magma that disrupted a pre-existing olivine-diopside lithology located in the lithospheric mantle.
3) The Plagioclase Basalt lava-unit, a porhyritic and unusually feldspar-phyric lava-unit,

appears to be the result of super-saturated crystallisation of this primitive magma under dynamic conditions.

4) The Plagioclase Tephri-phonolite lava-unit, an evolved unit with strong petrographic evidence of mixing between multiple magma-batches, may have resulted from mixing these two early magma-batches with a more evolved, phonolitic, crustal reservoir during its ascent.
5) Magmatic degassing may have been involved in these processes. This would help explain both the mobilisation and disruption of the olivine-diopside lithiology, as well as the super-saturation of plagioclase and clinopyroxene. If this occurred it is also likely to have resulted from post-collapse decompression.

Chapter 6 : MAGMATIC GEOCHEMISTRY

THE GEOCHEMISTRY OF THE MAGMATIC PRODUCTS LINKED TO THE *CUMBRE NUEVA COLLAPSE* – A COMPARISON OF REGIONAL-SCALE AND EDIFICE-SCALE COMPOSITIONAL AND PETROLOGICAL VARIATION IN LAVA FLOWS.

ABSTRACT

Lava flows samples from the *El Time* inland headland (17 samples) and the post-collapse *Bejenado* volcano (23 samples) were collected for a comparative study of the period bracketing La Palma's *Cumbre Nueva Collapse*. They have been studied in terms of petrographic groups, major and trace element whole rock geochemistry and Sr, Nd and Pb radiogenic isotope compositions to describe La Palma's source and the gross characteristics of its magma supply processes.

Almost all the lava samples can be described in terms of four petrographic groups: 1) basanites and primitive lavas, 2) porphyritic ankaramites, 3) amphibole tephrites and 4) phono-tephrites and evolved foidites. Major and trace element MgO-variation diagrams indicate that all samples lie on shared curvilinear arrays, often with points of inflection at ≈6 wt% MgO, consistent with staged fractionation of the phenocryst mineral observed in these groups. Radiogenic isotope data indicates that their mantle source signatures lie on arrays between young-HIMU and DMM-like mantle components, consistent with all magmas resulting from combinations of these end-members.

Studying *Bejenado* samples in the context of stratigraphic units and age sequences indicates geologically significant groups can be descrimininated with the data forming arrays between several local compositional sub-components: 1) DMM-like basanites with low incompatible element contents, 2) young-HIMU phono-tephrites with high incompatible element contents, 3) a pair of stratigraphic units with young-HIMU isotopic signatures and primitive compositions. The differences between these components in absolute element abundances suggests that they are distinct magma batches. The basanites have the strongest DMM-like signature of any samples so far analysed from La Palma, and their presence at the beginning of the post-collapse phase is likely to be a direct result of the collapse affecting processes at depth. *Bejenado* appears to be the product of a period of unusually dynamic processes in the resulting from disruption and decompression of the magma supply system and its contents after the *Cumbre Nueva Collapse*.

6.1 INTRODUCTION

Each eruptive unit on an oceanic island holds a record in its whole-rock elemental and isotopic composition of the magmatic processes and events that contributed to it. The most fundamental of these chemical records is the radiogenic isotope composition (particularly for the systems Sr, Nd and Pb, (Zindler and Hart, 1986)), since it should be largely invariant during partial melting and fractional crystallisation of an individual magma batch. This should provide a fingerprint of the mantle source rock from which the magma batch partially melted. After partial melting, relative abundances of

incompatible trace elements should also be largely invariant (Sun and McDonough, 1989), while major and minor element variation across a suite of rocks records the effects of the combined impact of reservoir system processes in inferred fractional crystallisation trends. However, these quantitative geochemical techniques provide greatest insights when discriminating differences between groups of genetically distinct lava samples, and are less meaningful when applied to individual whole rock samples. Selecting the most meaningful scale on which to sample eruptive products on an oceanic island is therefore essential to the success of a study.

Studies of lava samples taken from several of the Canary Islands have often discriminated clear groupings of samples (Day et al., 2010; Geldmacher et al., 2010; Gurenko et al., 2006), with radiogenic isotope studies providing insights into the spatial heterogeneity of the region's asthenospheric source. The magma source beneath the western Canary Islands has been characterised as a mixture of the "young HIMU" component (high time integrated $\mu = {}^{238}U/{}^{204}Pb$) and the region's most depleted "DMM-like" component, (similar to Depleted MORB Mantle, Day et al., 2010; Gurenko et al., 2009). A previous study of La Palma (Galipp, 2005) has shown that its last major flank collapse (the *Cumbre Nueva Collapse*) was accompanied by unusually extreme variability in the isotope signatures of its lavas. This study also identified a degree of scatter between samples from each of the island's individual edifices that was greater than the study's analytical error and masked any fine temporal variation in the magma source signature.

The *Cumbre Nueva Collapse* was among the most structurally significant events in the evolution of La Palma, and therefore its association with a marked anomaly in isotopic signature may indicate a causal relationship between the collapse and processes in the magma source. The nature of this relationship is geologically significant, since while the effect of such collapses on these islands' reservoir system processes has been increasingly well established (Longpré et al., 2008, 2009; Manconi et al., 2009), the impact of collapses on processes in the magma source is still relatively speculative (Hildenbrand et al., 2004). Accessible sequences from the pre-*Cumbre Nueva Collapse* phase in the *El Time* area, and the discrete, well-exposed, *Bejenado* volcano from the post-collapse phase offer the opportunity for high stratigraphic-resolution sampling of the lavas from this period of the island's evolution.

This chapter presents whole rock analyses of 17 lava samples from *El Time* and 23 lava samples from *Bejenado*. In interpreting the data it is important to present the results at the most meaningful scale. For approaches such as radiogenic isotope graphs or bivariate plots of trace element ratios, a uniform sampling resolution is preferred to avoid artefacts in group discrimination (for example, artificial groups resulting from plotting multiple samples from one eruption against the products of several eruptions). Such issues are less important when presenting elemental variation diagrams since these provide only a gross characterisation of regional fractional crystallisation trends. Our suite of lava samples from central La Palma therefore provides an opportunity to use a previously

observed change in radiogenic isotope signature to determine the best scale at which to study the variability in the island's asthenospheric source signature. Are changes in source signature the product of long-lived mantle heterogeneities (best studied by comparing numerous separately erupted flow-fields), or are they the product of individual magma batches that undergo magma-mixing during transport (best studied through high resolution sampling of individual eruptions)?

To address this issue our results are presented twice. First, a regional scale interpretation compares all pre-collapse and post-collapse lavas. This is followed by an edifice-scale presentation of the *Bejenado* data to determine if this volcano's isotopic variability is best studied at the scale of individual stratigraphic units.

6.2 GEOLOGICAL BACKGROUND

La Palma is dominated by two large edifices, the older *Taburiente* shield volcano in the north and the younger *Cumbre Vieja* ridge to the south[22]. A major unconformity (Figure 6-1) separates these two edifices, a result of the *Cumbre Nueva Collapse* of Taburiente's *Paleo-Cumbre Nueva Rift* (Carracedo et al., 1999a; Navarro and Coello, 1994). The only remains of this rift zone's western half are in the *El Time* region, a raised inland headland extending south from *Taburiente* that is bounded to the north by *Barranco Jurado,* and to the south-east by the cliffs of the collapse embayment.

Caldera de Taburiente, a dramatic basin usually attributed to erosion, occupies the north of the embayment (Carracedo et al., 1999a; Lyell, 1855) and is still the subject of debate over its origin. This central part of La Palma provides the most complete exposures of the island's subaerial stratigraphy including Seamount Series (Staudigel and Schmincke, 1984), a number of large and laterally extensive breccia units (Colmenero et al., 2012) as well as major intrusive suites, largely dykes and sills, of the island's sub-volcanic system. Onlapping these units is the southward-dipping *Bejenado* volcano which is the main eruptive feature from immediately after the *Cumbre Nueva Collapse.*

The *El Time* and *Bejenado* edifices provide the most complete and least altered exposures of eruptive units from before and after the giant landslide. *El Time* is the least eroded region of *Taburiente* and lavas exposed here tend to be aa morphology flows that dip westwards away from the collapse structure. Detailed information about the field relations and geochronology of this area is presented[23]. Vents are absent here, indicating that these flows were the product of focused volcanism further up-slope in the *Paleo-Cumbre Nueva Rift's* axial region, and therefore must pre-date the collapse.

[22] 3.2 The geology of central La Palma. pp.39-51.
[23] 4.4 Results – part 1 : geochronology and sample sourcing.pp.70-73.

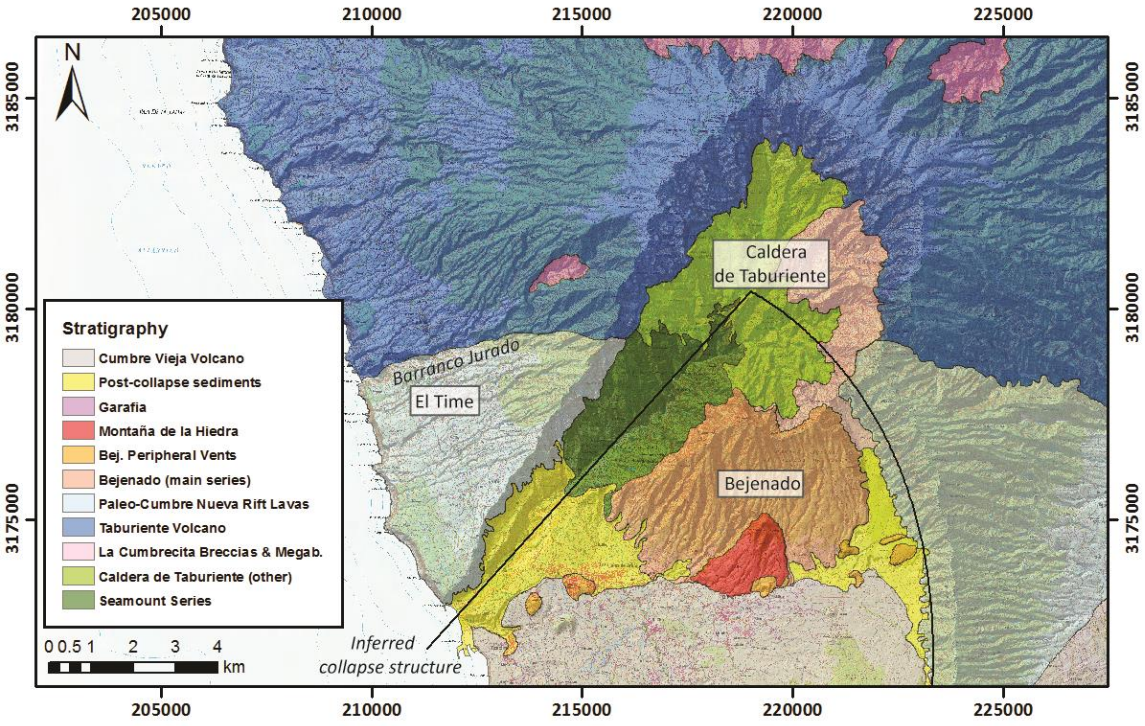

Figure 6-1 A composite geological map of Central La Palma, assembled from Carracedo et al. (2001), Colmenero et al. (2012), and Navarro and Coello (1994).

The summit of *Bejenado* (1844m) is the highest point in the collapse embayment, where this small volcano's flank dips southwards away from the *Caldera de Taburiente* and towards its contact with the young *Cumbre Vieja* volcano. Prior to this study little was known about the eruptive stratigraphy of *Bejenado,* but it is now known[24] to be mainly composed of a small number of laterally extensive lava flow-fields, with the products of a phreatomagmatic eruption of evolved magma in the middle of the sequence. Its present form is the result of a complex erosional history, with its summit truncated by *Caldera de Taburiente* to the north, allowing access to its lowermost sequences. Furthermore, there is a marked distinction between its heavily eroded western sector and its better preserved eastern sector about which much more is known.

6.3 Methods

6.3.1 Sample sourcing

New analyses from 40 lava samples are presented in this chapter, with a map of origin localities provided (Figure 6-2), while data from previously presented BEP samples[25] are also included in graphs.

[24] 4.5 Results – part 2 : the geology of the eastern sector of *Bejenado*. pp.75-89.
[25] 5.4 Petrology of BEP lava samples: results. pp.104-132.

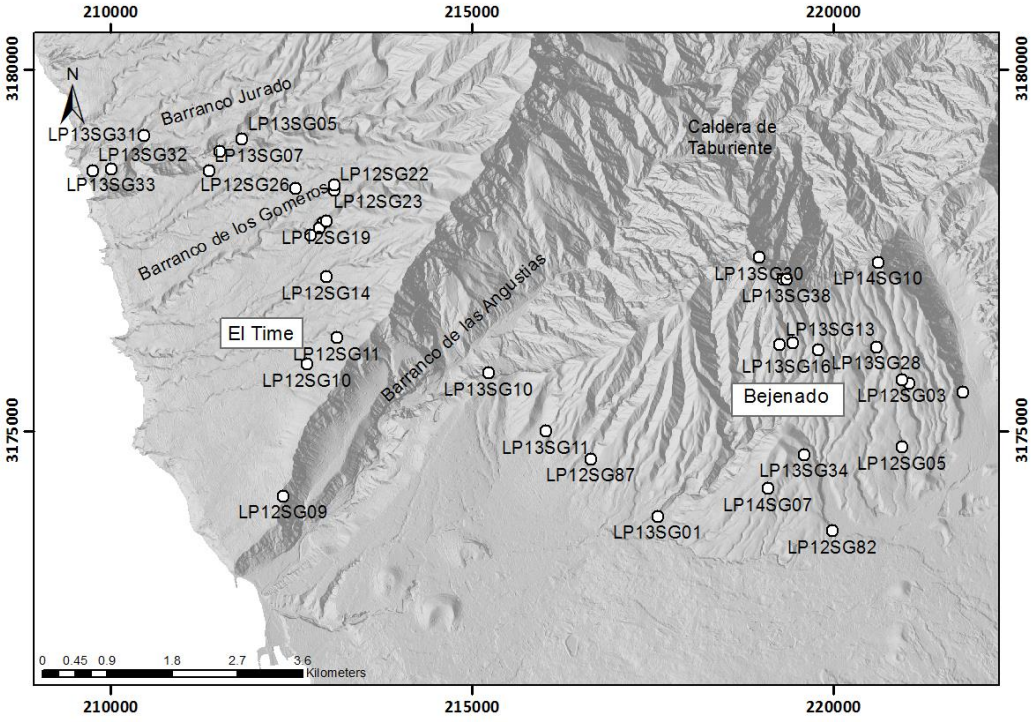

Figure 6-2 Shaded topographic map (topgraphic data sourced from Instituto Geographico Nacionale) of sampling localities for analysed lavas.

This is a sub-set of a larger suite (72 samples) collected over the course of the project that, where analyses are absent, largely consists of samples from the same lava flows; results of analysing these apparent duplicates are presented and sourcing information provided[26]. Collection criteria in the field was freshness within outcrops, and all samples were initially petrographically screened prior to whole-rock powder preparation. In selecting the best samples from the larger suite, preference was given to those with lower degrees of alteration (lower LOI wt%) and better determined field-relations.

In the *El Time* area unaltered lavas were collected from a combination of surface flows exposed in road sections and from within river sections (termed barrancos) such as the deep *Barranco Jurado*. Each sample presented from this region is believed to sample a distinct eruptive unit. Surface flows provide samples of lavas from the immediate pre-collapse phase (from 585 ±11 ka to 529 ±13 ka), while lavas taken within barrancos extend earlier into the late phase of activity at *Taburiente* (from 610 ±14 ka).

Post-collapse samples were largely collected from *Bejenado's* eastern flank where five volcano-stratigraphic units have been described[27]: 1) *Bejenado Lower Series* (Basal Ankaramite), 2) the *Los Rodeos Evolved and Vocaniclastic Phase* (LREVP), 3) the Bejenado Effusive Phase (BEP), 4) The

[26]Appendix C: Supporting analytical data.p.207. p.194, Appendix A: Sample index and sourcing information. p.198

[27] 4.5 Results – part 2 : the geology of the eastern sector of *Bejenado*. pp.75-89.

Terminal Sheet Phase (TSP) and 5) the *Montaña de la Hiedra* cone-cluster. These stratigraphic units often consist of multiple lava-units and have been sampled with a focus on petrological variation. A further opportunistic collection of samples was taken from the periphery of the deeply incised and inaccessible western flank of *Bejenado*.

6.3.2 Analytical procedures

Whole-Rock Major and Trace Elements

The major and trace element compositions of lava samples were determined by X-ray fluorescence spectrometry (XRF) using the Philips PW1480 XRF located at Royal Holloway, University of London using the techniques summarised in Thirlwall et al. (2000).

Samples were initially split and sawed to remove any traces of alteration (weathering crusts, areas where the olivines showed greater than average iddingsite-formation and zones with infilled voids) prior to jaw-crushing. Crushates were then coned and quartered before powdering in a tungsten carbide ring and puck mill. Bulk rock powders were roasted to 1100°C to determine loss on ignition (LOI) before fusion in platinum-gold crucibles, then prepared as fused glass discs for major element analyses. Trace elements were analysed on pressed powder pellets with matrix corrections calculated from the major element composition. All data are presented on a volatile-free basis with total Fe as Fe_2O_3T.

Whole-Rock Sr-Nd-Pb radiogenic Isotopes

All isotope analyses were conducted at the NERC Isotope Geosciences Laboratory, British Geological Survey, Keyworth. Sr and Nd compositions were determined on a Thermo Scientific Triton mass spectrometer, Pb compositions were determined on the Nu Instruments Nu Plasma, MC-ICP-MS.

For all isotopic determinations[28], ≈250mg of powdered sample were precisely weighed into Savillex beakers and leached on a hotplate in 6M HCl (60°C, for >0.5 hours) prior to dissolution using HF-HNO_3, and subsequently converted to chloride or nitrate form as appropriate. Sr and Pb were separated in a staged procedure using SR-SPEC ion exchange columns following the methods of Deniel and Pin (2001). Nd was separated using a primary cation exchange column (Eichrom AG-50) followed by a LN-SPEC column. Procedural blanks for Sr, Nd and Pb across the time of analysis were < 100pg.

Sr fractions were loaded onto outgassed single Re filaments using a TaO activator solution, and analysed in multi-dynamic mode. Data have been normalised to $^{86}Sr/^{88}Sr$ = 0.1194. Fifty-five measurements of the SRM987 Sr standard run across the time of sample analysis gave a value of 0.710254 ± 0.000006 (1-sigma).

[28] The remainder of this section was adapted from an established laboratory methods section written by Ian Millar of the NERC Isotope Geosciences Laboratory, who ran all Sr, Nd and Pb fractions.

Nd fractions were loaded onto one side of an outgassed double Re filament assembly using dilute HCl, and analysed in multi-dynamic mode. Data are normalised to $^{146}Nd/^{144}Nd = 0.7219$. Across the period of analysis, 20 analyses of the JND-i standard gave a value of 0.512098 ± 0.000011 (1-sigma). All other standard and sample data are quoted relative to a value of 0.512115 for this standard.

Prior to Pb isotope analysis each sample was spiked with a thallium solution, which was added to allow for the correction of instrument-induced mass bias. Samples were then introduced into the instrument via an ESI 50µl/min PFA micro-concentric nebuliser attached to a de-solvating unit, (Nu Instruments DSN 100). For each sample, five ratios were simultaneously measured ($^{206}Pb/^{204}Pb$, $^{207}Pb/^{204}Pb$, $^{208}Pb/^{204}Pb$, $^{207}Pb/^{206}Pb$ and $^{208}Pb/^{206}Pb$). Each individual acquisition consisted of 75 sets of ratios, collected at 5-second integrations, following a 60 second de-focused baseline.

The precision and accuracy of the method was assessed through repeat analysis of an NBS 981 Pb reference solution (also spiked with thallium). The average values obtained for each of the measured NBS 981 ratios were then compared to the known values for this reference material (Thirlwall, 2002). All sample data were subsequently normalised, according to the relative daily deviation of the measured reference value from the true, with the aim of cancelling out the slight daily variations in instrumental accuracy, allowing the direct comparison of the data obtained during different analytical sessions. Internal uncertainties (the reproducibility of the measured ratio) were propagated relative to the external uncertainty.

6.4 Results, part 1: comparison of lavas from Pre-Collapse *El Time* and Post-Collapse *Bejenado*

On the TAS classification diagram (Figure 6-3), samples from collapse-related lava flows in central La Palma mostly lie on the strongly alkaline evolution trend between basanitic and tephri-phonolitic compositions. The exceptions are six low-SiO_2 foidites and a single alkali basalt. The majority of samples from both the *El Time* and *Bejenado* suites lie in the basanite/tephrite field, with the *El Time* collection including a tight cluster of low-alkali basanites, while the *Bejenado* samples exhibit considerably greater compositional scatter. The two tephri-phonolites originate from *Bejenado*, as well as three of the four phono-tephrites, indicating that the post-collapse phase was characterised by lavas with greater variability in magmatic differentiation.

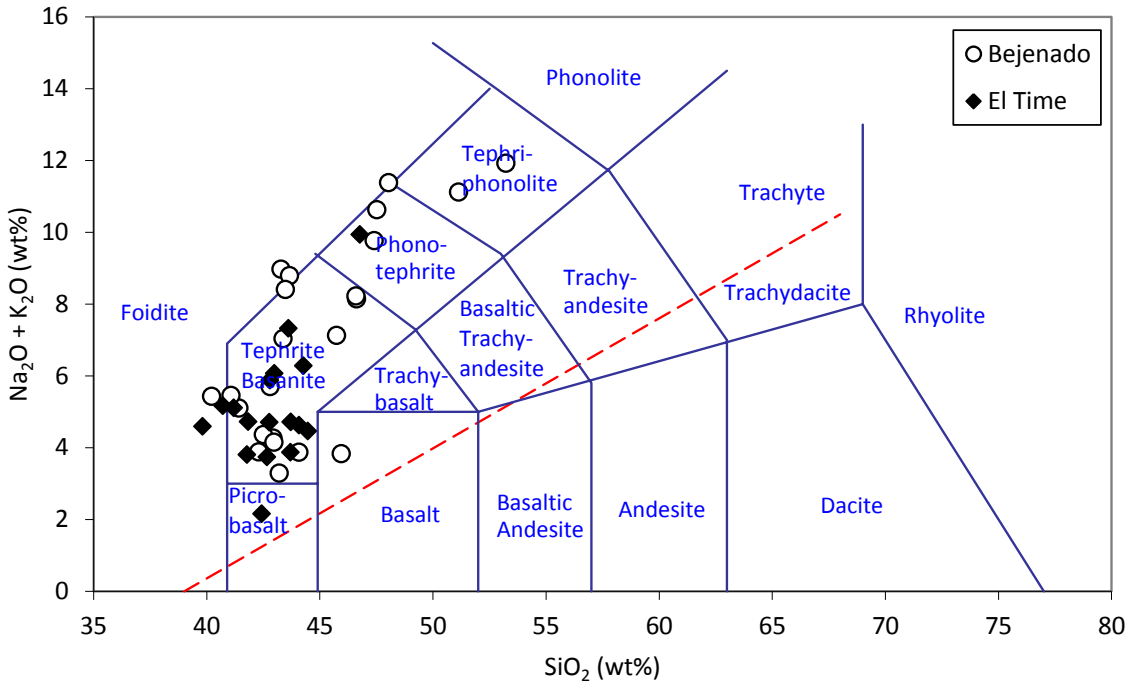

Figure 6-3 A TAS compositional classification diagram of *El Time* and *Bejenado* lava flows samples presented in this chapter as well as selected BEP lavas. The TAS diagram is in the style of Le Bas et al. (1986).

The majority of lava samples from both sub-regions form shared petrological groups (Table 6-1) with characteristic textures and mineralogies. These groups do not always correspond to the TAS diagram categories. The only samples that do not fit within these groups are from the upper units of the Bejenado Effusive Phase (BEP) where the unusual plagioclase-dominated crystallisation has led to different petrological characteristics. These samples have been described separately[29] but included in the graphs of the subsequent sections.

Among the primitive lavas, the considerable variation in crystal content has allowed them to be characterised as two sub-groups (Figure 6-4): 1) less crystal-rich "basanites and primitive lavas" and 2) highly porphyritic "ankaramites". Such primitive lavas can be distinguished from more evolved samples by the presence of olivine and the absence of kaersutitic amphibole. Amphibole is first observed in intermediate lavas: 3) "amphibole tephrites" where it is rarely seen to be in equilibrium with olivine. Finally, 4) the "phono-tephrites and evolved foidites" group of evolved lavas can be distinguished by their considerable abundances of phenocryst feldspathoids. Throughout all units, there is extensive petrographic evidence for magma-mixing.

6.4.1 Petrographic contrasts between *El Time* and *Bejenado* lavas

[29] 5.4.1 Petrography of BEP lava-units. pp.110-112.

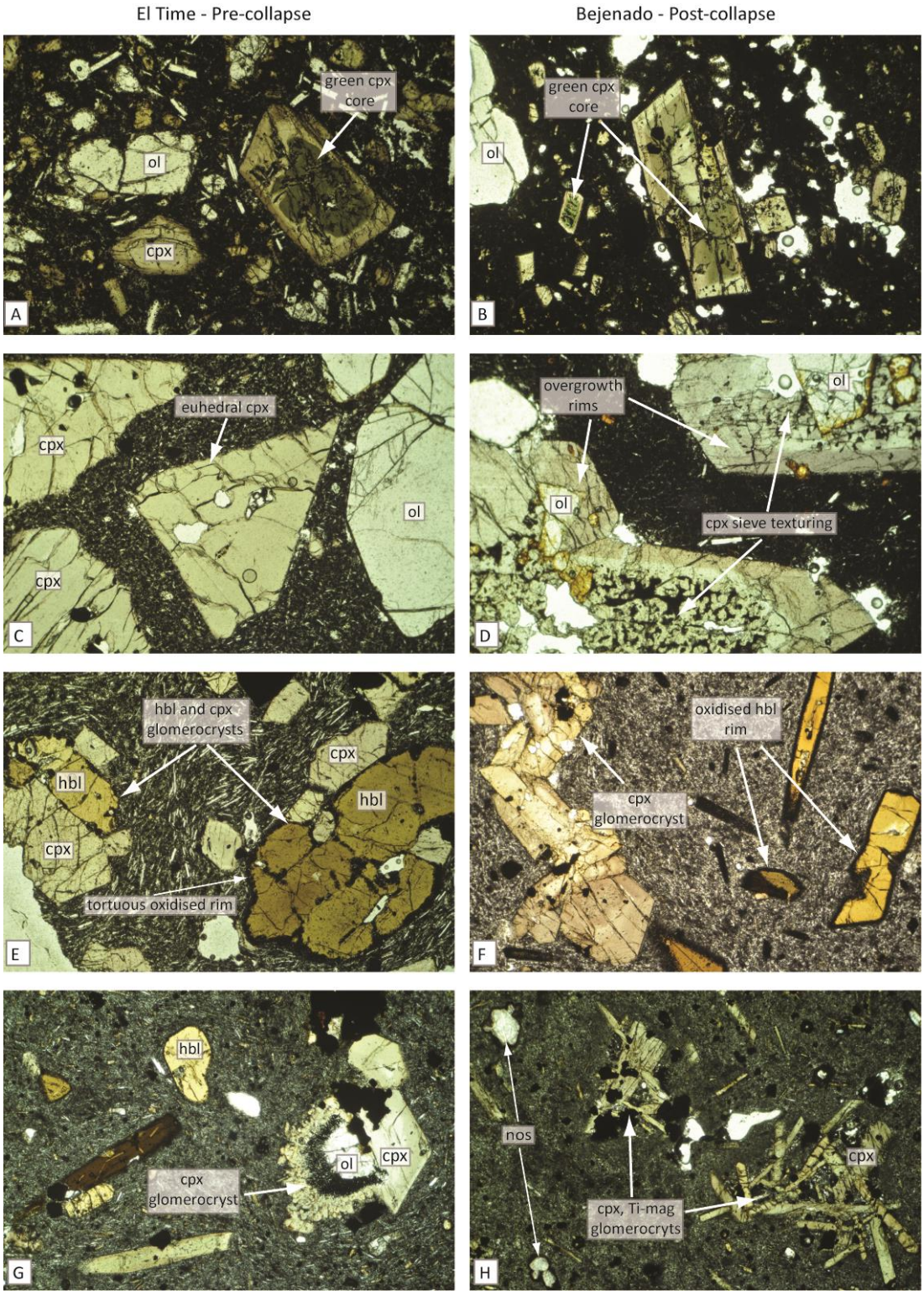

Figure 6-4 Representative micrographs of lava groups from central La Palma, all viewed in PPL. A. LP12SG11, basanite with ol and green core cpx (FOV = 4.4mm). B. LP13SG01, basanite with ol and green core cpx (FOV = 4.4mm) C. LP13SG06, ankaramite with few glomerocrysts in a microlitic groundmass (FOV = 4.4mm). D. LP13SG38, glomeroporphyritic ankaramites have tabular cpx enclosed in overgrowth rims (FOV = 4.4mm). E. LP12SG26, amphibole tephrite with holocrystalline glomerocrysts, amphibole exhibit tortuous, oxidised rims (FOV = 4.4mm). F. LP13SG28, an amphibole tephrite with non-holocrystalline glomerocrysts. G. LP12SG22, an amphibole rich phono-tephrite, glomerocryst enclosing ol in its interior (FOV = 4.4mm). H. LP13SG13, phono-tephrite with non-holocrystalline glomerocrysts of tabular cpx (FOV = 4.4mm). PPL = plane polarised light, FOV = field of view, cpx = clinopyroxene, ol = olivine, hbl = kaersutitic amphibole, nos= nosean, Ti-mag = Titanomagnetite.

Basanites and primitive lavas

At both *El Time* and *Bejenado* the most common primitive lavas are dominated by clinopyroxene and olivine with varying abundances of titanomagnetite in a microlitic groundmass with sparse plagioclase. Clinopyroxene is usually observed as single, texturally complex, phenocrysts although glomerocrysts are also present. Euhedral augite rims often enclose sieve-textured or reverse-zoned green cores (Figure 6-4A, Figure 6-4B), indicating they are the product of multi-stage crystallisation. Olivine crystals are common and of varying preservation. In samples from *El Time* crystal contents vary between poorly-phyric lavas with crystalline groundmasses dominated by plagioclase and clinopyroxene, and porphyritic lavas which are more similar to those of the ankaramite group.

Ankaramites

Aankaramites contain up to 50% phenocrysts; they are primitive clinopyroxene, olivine basanites or picro-basalts containing minor titanomagnetite and groundmass plagioclase. *El Time* ankaramites largely contain single crystals, with euhedral or fragmentary clinopyroxene and olivine phenocrysts (Figure 6-4C). In contrast *Bejenado* has largely glomeroporphyritic ankaramites (Figure 6-4D) where holocrystalline aggregates are very common. In *El Time* and *Bejenado* ankaramites, groundmasses are often rich in plagioclase and titanomagnetite, with one *El Time* sample (LP12SG09) exhibiting large (<4mm) groundmass plagioclase laths.

Amphibole Tephrites

The intermediate samples form the most homogeneous petrographic group, with clinopyroxene, kaersutitic amphibole, titanomagnetite tephrites common at both *El Time* and *Bejenado* with groundmasses that vary between microlitic and plagioclase-rich. Both regions tephrites commonly contain glomerocrysts, such as the holocrystalline fragments rich in clinopyroxene and amphibole observed at *El Time* (Figure 6-4E). Clinopyroxene crystals often host accessory acicular apatite. Kaersutitic amphibole crystals are often poorly preserved, with round phenocrysts with tortuous rims enclosed in iron oxide microcrystals. At *El Time* groundmasses tend to be more plagioclase-rich, leading to trachytic textures.

Phono-tephrites and evolved foidites

Amphibole content allows us to distinguish LP12SG22, the most evolved sample in the *El Time* suite which is an amphibole, clinopyroxene phono-tephrite, from *Bejenado's* more evolved lavas where amphibole is largely absent. At *Bejenado* the more evolved lavas are dominated by clinopyroxene and titanomagnetite. However, both regions' phono-tephrite lavas are characterised by the presence of feldspathoids, which are usually zoned sodalite group minerals with blue hauyne rims enclosing nosean cores. There is further evidence of magma-mixing at *El Time*, with heavily embayed olivine present in the core of a holocrystalline glomerocryst (Figure 6-4G), while at *Bejenado* non-holocrystalline clots are commonly formed of minerals indistinguishable from the phenocryst population (Figure 6-4H).

EL Time Suite

Sample ID	LP13SG05	LP13SG06	LP13SG07	LP13SG31	LP13SG32	LP13SG33
Region	Barr. Jur.	Barr. Jur.	Barr. Jur.	Barr. Jur.	Barr. Jur.	Barr. Jur.
Unit	Bas & Prim	Ank.	Amph Teph	Amph Teph	Bas & Prim	Amph Teph
SiO_2	39.82	42.43	42.78	43.71	42.66	44.27
Al_2O_3	12.36	8.45	15.24	14.84	12.71	15.97
Fe_2O_3T	14.97	14.42	12.94	13.95	14.33	12.87
MgO	9.73	15.36	5.88	6.41	9.30	4.85
CaO	12.07	12.74	10.47	10.64	11.59	10.18
Na_2O	3.12	1.61	4.29	3.90	2.64	4.45
K_2O	1.47	0.55	1.59	0.82	1.10	1.83
TiO_2	4.18	2.70	3.90	4.14	3.78	3.55
MnO	0.20	0.17	0.20	0.19	0.19	0.19
P_2O_5	1.01	0.26	0.88	0.76	0.56	0.77
Total	99.64	99.16	98.88	99.87	99.41	99.47
LOI (%)	-0.01	-0.30	0.50	0.30	0.26	-0.20
Ni	174	384	30	66	163	21
Cr	368	944	49	75	354	5
V	386	347	292	336	350	300
Sc	27	45	17	23	30	16
Cu	122	154	50	100	157	30
Zn	115	85	110	106	101	106
As	1	1	1		1	1
S	333	66	170	89	127	59
Ga	20.7	14.5	22.1	22.0	19.7	22.7
Pb	2.4	0.5	4.2	3.0	1.7	4.0
Sr	838.5	326.8	980.8	941.0	662.2	947.4
Rb	31.0	11.6	33.5	7.1	24.0	41.6
Ba	471.8	180.0	542.4	517.0	317.5	549.7
Zr	277.4	136.4	333.1	308.1	250.2	325.1
Nb	77.9	24.3	85.9	71.4	49.4	81.7
Ta	4.4	1.0	5.0	3.6	2.0	3.9
Mo	2.4	0.9	2.4	1.8	1.4	2.4
Th	4.3	1.8	5.5	5.3	3.3	5.9
U	1.5	0.7	1.4	1.3	1.3	1.6
Y	28.4	16.9	34.3	31.4	26.8	32.1
La	52.3	20.6	59.4	61.7	40.1	59.7
Ce	106.3	42.4	124.4	126.4	83.8	125.1
Nd	56.4	22.8	60.7	61.4	45.0	56.2
Sm	10.6	5.0	10.7	10.9	10.6	11.5
Yb	3.2	4.0	3.1	3.7	3.1	3.1
Hf	5	3	6	6	6	5
Cs			2	1	3	1

Table 6-1 Major element (wt %) and trace element (ppm) compositions of samples from Central La Palma lava-suites, determined by XRF. Barr. Jur. = Barranco Jurado, Bas & Prim = Basanites and primitive lavas, Ank = Ankaramites, Amph Teph = Amphibole Tephrites.

EL Time Suite

Sample ID	LP12SG15	LP12SG16	LP12SG19	LP12SG09	LP12SG10	LP12SG11
Region	Barr. Gom.	Barr Gom.	Barr Gom.	Surf. Flow	Surf. Flow	Surf. Flow
Unit	Bas & Prim	Amph Teph	Ank.	Amph Teph	Bas & Prim	Bas & Prim
SiO_2	44.07	43.61	44.47	40.71	42.77	41.78
Al_2O_3	14.45	16.06	14.51	14.17	13.93	12.14
Fe_2O_3T	14.09	11.93	13.18	15.04	14.10	14.58
MgO	6.53	4.70	7.62	6.85	7.70	10.64
CaO	10.90	10.29	10.85	11.91	11.48	11.92
Na_2O	3.43	4.90	3.30	3.67	3.47	2.86
K_2O	1.20	2.42	1.17	1.50	1.23	0.94
TiO_2	3.78	3.68	3.54	4.38	3.84	3.58
MnO	0.19	0.22	0.19	0.20	0.18	0.18
P_2O_5	0.80	0.92	0.69	0.93	0.67	0.63
Total	99.94	99.42	100.07	100.00	99.91	99.77
LOI (%)	-0.39	0.11	0.31	0.04	-0.24	-0.29
Ni	79	13	87	41	131	258
Cr	116	7	191	29	200	379
V	322	275	312	370	361	356
Sc	25	12	25	23	29	31
Cu	85	39	43	74	136	156
Zn	114	126	103	114	109	103
As		1				1
S	70	586	110	598	139	37
Ga	22.6	23.3	20.9	21.2	21.6	19.0
Pb	3.0	5.8	3.3	3.6	3.3	2.8
Sr	811.4	1213.8	863.3	868.7	781.5	711.6
Rb	24.6	56.5	23.5	28.4	23.6	16.8
Ba	404.2	726.5	460.6	584.7	432.0	350.8
Zr	261.0	418.0	302.0	287.6	253.1	209.9
Nb	60.9	127.2	73.9	64.6	60.2	49.3
Ta	3.6	7.2	4.1	4.4	3.2	3.1
Mo	1.6	3.9	1.8	1.5	1.8	1.5
Th	3.9	7.9	4.9	4.3	4.0	3.3
U	0.8	1.8	0.7	0.7	0.5	0.5
Y	31.0	37.4	29.9	31.3	27.4	25.0
La	50.4	85.9	56.3	51.6	45.7	43.9
Ce	100.2	169.9	111.0	105.8	93.8	89.1
Nd	53.0	76.6	54.9	57.0	47.7	45.5
Sm	11.0	12.5	10.5	12.3	11.7	9.7
Yb	2.3	2.7	2.9	2.5	2.3	1.9
Hf	7	9	7	7	7	6
Cs	1	2		1	1	1

Table 6-1 (continued) Major element (wt %) and trace element (ppm) compositions of samples from central La Palma lava-suites, determined by XRF. Surf. Flow = Surface Flow Barr. Gom = Barranco de los Gomeros, Ank = Ankaramite, Amph Teph = Amphibole Tephrite, Bas & Prim = Basanites and Primitive Lavas

EL Time Suite

Sample ID	LP12SG14	LP12SG18	LP12SG22	LP12SG23	LP12SG26
Region	Surf. Flow	Surf. Flow	Surf. Flow	Surf. Flow	Surf. Flow
Unit	Bas & Prim	Bas & Prim	Pho-Teph	Ank.	Amph Teph
SiO_2	43.70	41.19	46.77	41.83	42.99
Al_2O_3	13.32	13.60	17.67	12.55	15.60
Fe_2O_3T	14.31	14.85	9.21	14.65	13.62
MgO	8.15	6.36	3.08	9.35	5.58
CaO	11.32	12.93	7.83	11.42	10.82
Na_2O	2.99	3.61	6.61	3.27	4.30
K_2O	0.88	1.50	3.32	1.45	1.77
TiO_2	3.39	4.26	2.80	3.95	3.96
MnO	0.19	0.20	0.20	0.19	0.21
P_2O_5	0.65	0.78	0.86	0.73	1.01
Total	99.36	99.91	99.25	99.96	100.47
LOI (%)	-0.47	0.33	0.37	-0.11	0.37
Ni	136	67	10	129	26
Cr	227	32	9	258	17
V	329	434	223	356	313
Sc	27	23	5	28	16
Cu	74	142	19	45	43
Zn	111	119	117	107	121
As			1		
S	78	263	812	116	436
Ga	20.9	23.3	26.6	20.7	21.9
Pb	2.6	3.6	8.1	3.8	4.3
Sr	753.8	937.4	1427.2	851.7	1011.2
Rb	17.0	37.1	85.9	32.2	37.3
Ba	344.8	634.8	953.9	480.7	568.8
Zr	216.6	280.4	523.4	346.5	346.7
Nb	51.3	87.4	160.9	77.5	84.2
Ta	2.9	5.6	9.4	4.3	4.8
Mo	1.8	2.9	3.4	1.8	2.1
Th	4.0	5.7	12.7	4.7	5.4
U	0.5	1.2	3.1	1.0	0.7
Y	28.3	29.1	36.4	28.7	34.0
La	52.4	57.2	95.3	55.8	62.7
Ce	102.3	110.6	171.8	117.2	124.8
Nd	49.8	58.4	73.5	56.5	65.6
Sm	9.3	11.1	12.6	10.3	12.0
Yb	1.9	2.3	2.7	2.4	2.5
Hf	6	6	10	7	7
Cs	2		2	1	1

Table 6-1 (continued) Major element (wt %) and trace element (ppm) compositions of samples from central La Palma lava- suites, determined by XRF, Surf. Flow = Surface Flow , Ank = Ankaramite, Amph Teph = Amphibole Tephrite, Bas & Prim = Basanites and Primitive Lavas

Bejenado Suite

Sample ID	LP13SG38	LP12SG87	LP13SG01	LP13SG10	LP13SG11	LP13SG26
Eruptive Unit	Bej L. Ser	West Bej	West Bej	West Bej	West Bej	LREVP-XPT
Petro-Unit	Basal Ank.	Bas & Prim	Bas & Prim	Bas & Prim	Bas & Prim	Amph Teph
SiO_2	43.20	45.95	41.08	40.22	44.08	41.43
Al_2O_3	11.23	13.71	13.41	13.63	13.02	14.89
Fe_2O_3T	13.84	13.97	14.21	14.87	14.22	14.34
MgO	12.37	7.62	7.83	7.22	9.10	5.98
CaO	11.26	10.25	11.54	11.99	10.65	11.68
Na_2O	2.45	2.96	4.48	3.62	2.87	4.13
K_2O	0.84	0.87	0.97	1.81	1.00	0.97
TiO_2	2.85	3.19	4.37	4.08	3.42	4.11
MnO	0.18	0.18	0.19	0.22	0.18	0.22
P_2O_5	0.48	0.51	0.76	1.03	0.58	0.95
Total	99.20	99.83	99.53	99.39	99.60	99.32
LOI (%)	-0.31	-0.47	0.50	0.56	-0.11	0.41
Ni	313	171	104	71	203	30
Cr	501	216	116	98	287	34
V	298	295	385	379	310	338
Sc	26	26	23	23	28	20
Cu	105	73	230	85	133	56
Zn	108	106	103	123	107	118
As	1			1	1	
S	19	9	292	489	90	118
Ga	18.9	20.6	21.3	20.8	19.5	21.4
Pb	1.6	1.9	4.2	3.5	1.8	4.2
Sr	653.7	581.9	960.4	968.9	640.5	1058.8
Rb	19.8	15.3	31.7	40.3	18.9	69.3
Ba	388.0	287.6	667.8	569.2	340.5	608.9
Zr	178.7	184.3	323.5	328.3	210.5	340.2
Nb	52.6	39.4	85.9	101.4	47.3	91.3
Ta	2.6	1.4	4.1	5.9	1.9	5.3
Mo	1.7	0.9	2.1	2.2	1.6	1.7
Th	3.2	2.4	5.8	6.3	3.4	5.8
U	0.7	0.6	0.7	1.4	1.3	1.4
Y	22.0	27.8	31.1	33.6	27.8	34.8
La	36.7	33.8	69.9	74.3	42.5	69.8
Ce	71.3	71.2	129.3	142.0	80.8	136.3
Nd	35.8	39.0	64.1	66.9	44.0	66.3
Sm	7.2	6.3	13.5	12.5	9.5	11.6
Yb	3.2	2.5	2.5	2.0	4.0	2.1
Hf	4		8	6	4	7
Cs	1	1	1			1

Table 6-1 (continued) Major element (wt %) and trace element (ppm) compositions of samples from central La Palma lava-suites, determined by XRF. Bej L. Ser = Bejenado Lower Series, TSP = Terminal Sheet Phase, Basal Ank = Basal Ankaramite, Amph Teph = Amphibole Tephrite, Bas & Prim = Basanites and Primitive Lavas

Bejenado Suite

Sample ID	LP13SG30	LP12SG02	LP13SG28	LP13SG13	LP13SG16	LP14SG10
Region	LREVP-XPT	TSP	TSP	TSP	TSP	TSP
Unit	Amph Teph	Amph Teph	Amph Teph	Pho-Teph	Pho-Teph	Amph Teph
SiO_2	43.47	43.38	47.40	48.05	47.52	45.74
Al_2O_3	15.63	15.20	18.24	18.03	17.73	16.04
Fe_2O_3T	11.49	12.19	8.77	8.33	9.14	10.91
MgO	3.97	5.25	3.30	2.21	2.66	6.01
CaO	10.18	10.46	7.43	6.70	7.24	9.00
Na_2O	5.55	5.04	6.60	7.80	7.20	4.75
K_2O	2.85	2.00	3.16	3.58	3.43	2.38
TiO_2	3.60	3.62	2.66	2.55	2.76	2.93
MnO	0.25	0.21	0.18	0.21	0.22	0.18
P_2O_5	1.00	1.13	0.74	0.59	0.72	0.83
Total	98.92	99.30	99.20	99.00	99.43	99.44
LOI (%)	0.31	1.11	0.61	0.49	0.50	0.56
Ni	17	38	23	7	9	75
Cr	19	30	25	4	6	135
V	266	302	210	171	185	226
Sc	11	12	7	3	5	14
Cu	41	61	35	20	35	52
Zn	135	114	103	129	131	104
As	1		1	1	1	1
S	795	201	390	1186	353	399
Ga	26.7	26.0	27.9	31.3	32.4	23.3
Pb	7.2	7.1	8.0	10.7	10.7	4.3
Sr	1463.6	1342.9	1441.5	1602.7	1605.5	1041.1
Rb	83.7	31.7	82.2	109.6	106.4	72.3
Ba	927.1	735.4	917.1	993.9	1032.0	679.9
Zr	647.1	668.6	635.1	884.2	882.1	412.9
Nb	167.0	152.7	182.9	214.3	206.6	118.3
Ta	11.0	9.3	10.7	12.4	11.4	6.7
Mo	3.8	2.6	2.6	3.5	2.5	2.8
Th	9.5	9.7	12.4	13.3	13.0	7.3
U	2.4	2.4	3.3	3.4	3.0	2.2
Y	43.8	35.5	31.4	37.4	37.5	27.2
La	102.4	89.2	89.0	106.2	105.6	64.5
Ce	204.8	169.7	161.4	196.4	194.8	121.9
Nd	92.0	77.3	64.2	80.4	79.2	54.6
Sm	15.3	13.3	10.6	11.7	12.6	10.3
Yb	3.1	3.3	2.6	2.4	3.3	1.5
Hf	11		10	11	14	5
Cs	2	1	2	1	1	1

Table 6-1 (continued) Major element (wt %) and trace element (ppm) compositions of samples from central La Palma lava-suites, determined by XRF. LREVP = Los Rodeos Evolved and Volcaniclastic Phase, TSP = Terminal Sheet Phase, Pho-Teph = Phono-Tephrite, Amph Teph = Amphibole Tephrite,

Bejenado Suite

Sample ID	LP13SG34	LP14SG07
Region	Mon L Hie	Mon L Hie
Unit	Foidite	Foidite
SiO_2	43.28	43.66
Al_2O_3	14.80	15.17
Fe_2O_3T	12.23	12.44
MgO	3.86	4.06
CaO	9.80	10.00
Na_2O	6.19	5.99
K_2O	2.78	2.80
TiO_2	3.57	3.67
MnO	0.26	0.27
P_2O_5	1.23	1.28
Total	98.86	100.27
LOI (%)	0.60	0.11
Ni	11	11
Cr	12	10
V	230	245
Sc	9	10
Cu	35	37
Zn	149	147
As	1	1
S	462	593
Ga	29.4	29.9
Pb	7.9	8.2
Sr	1631.0	1585.9
Rb	81.8	81.6
Ba	904.8	954.3
Zr	839.8	837.4
Nb	200.7	201.3
Ta	13.2	12.6
Mo	2.8	2.4
Th	10.6	10.7
U	2.4	2.5
Y	43.6	43.0
La	107.9	109.8
Ce	217.4	213.3
Nd	101.7	99.9
Sm	17.1	17.8
Yb	3.0	1.9
Hf	14	9
Cs	1	3

Table 6-1 (continued) Major element (wt %) and trace element (ppm) compositions of samples from central La Palma lava-suites, determined by XRF. Mon L Hie = Montaña de la Hiedra, Ank = Ankaramite, Amph Teph = Amphibole Tephrite, Bas & Prim = Basanites and Primitive Lavas

6.4.3 WHOLE-ROCK ELEMENTAL COMPOSITIONS

On MgO variation diagrams the whole rock data from both pre-collapse and post-collapse lavas form coherent, shared geochemical arrays (Figure 6-5, Figure 6-6). The range of compositions is more restricted among *El Time* lavas. Despite abundant olivine and clinopyroxene phenocrysts, ankaramites from *El Time* generally have lower MgO (<10 wt%) than those from *Bejenado*, with the exception being an intensely phenocryst-rich sample (LP13SG06, 15.36 wt% MgO). Furthermore, at *El Time* highly evolved rocks are scarce (none has <3 wt% MgO). In contrast, *Bejenado* lavas are more compositionally diverse, with a wide continuous compositional range (1.09-13.12 wt% MgO).

Major element MgO-trends are broadly linear and negative for Al_2O_3 and Na_2O, indicating progressive enrichment of these oxides as La Palma's magmas evolved. This is mirrored in trace element trends of Sr, Zr, Nb and Ba, although a number of *Bejenado* samples (all from the phenocryst-poor phono-tephrites and foidites of the TSP and *Montaña de la Hiedra*) are anomalously rich in Zr (635-884 ppm) and Nb (160-214 ppm) and lie off the main trend of all other analyses. For several major elements (SiO_2, CaO, K_2O, Fe_2O_3T), there is little variation in concentration at higher MgO contents (≈6-15.36 wt% MgO) with points of inflection at ≈6 wt% MgO leading to positive (SiO_2, K_2O) or negative (Fe_2O_3T, CaO) trends. Data for Ni and Rb possess positive and negative curvilinear trends, respectively, both with inflection points at ≈6 wt% MgO. Further points of inflection are identified in P_2O_5 and Y trends at ≈4 wt% MgO.

The relative abundances of incompatible trace elements in lavas from *El Time* and *Bejenado* are consistent with previous whole studies of La Palma (Figure 6-7, Day et al., 2010; Galipp, 2005), which categorised La Palma having a young-HIMU OIB source (Simonsen et al., 2000; Thirlwall, 1997). Our samples have relatively steep mantle-normalised incompatible element profiles, with generally high U, Nb, Ta and La contents and negative anomalies in K, Pb and Y.

Pairs of incompatible elements potentially provide a subtle means of discriminating groups of lava samples (Hofmann, 2014; McDonough and Sun, 1995). Ratios of elements with similar bulk partition coefficients (D) are used to distinguish small differences in the melt source rocks, while ratios of elements with greater differences in D are likely to provide insights into differences in the degree of partial melting. We present bivariate diagrams (Figure 6-8) of elemental ratios that together cover the traditional, petrogenetically significant, groups of incompatible elements (Large Ion Lithophile Elements, High Field Strength Elements and Rare Earth Elements). In terms of Ba/Nb (a LILE/HFSE pair we propose provides one of the best potential means of discriminating source lithology), *Bejenado* lavas show a wide distribution of values (4.5 – 7.8), while *El Time* samples form a tighter cluster (5.8 – 7.4). Generally, incompatible element ratios yield poor discrimination between suites of pre-collapse and post-collapse samples, with *El Time* samples typically lying within the greater ranges of *Bejenado* samples. Nb/U (Figure 6-8A) and Ba/Rb (Figure 6-8B) both show large ranges (37-134 and 9-20 respectively) that extend beyond the canonical OIB values:

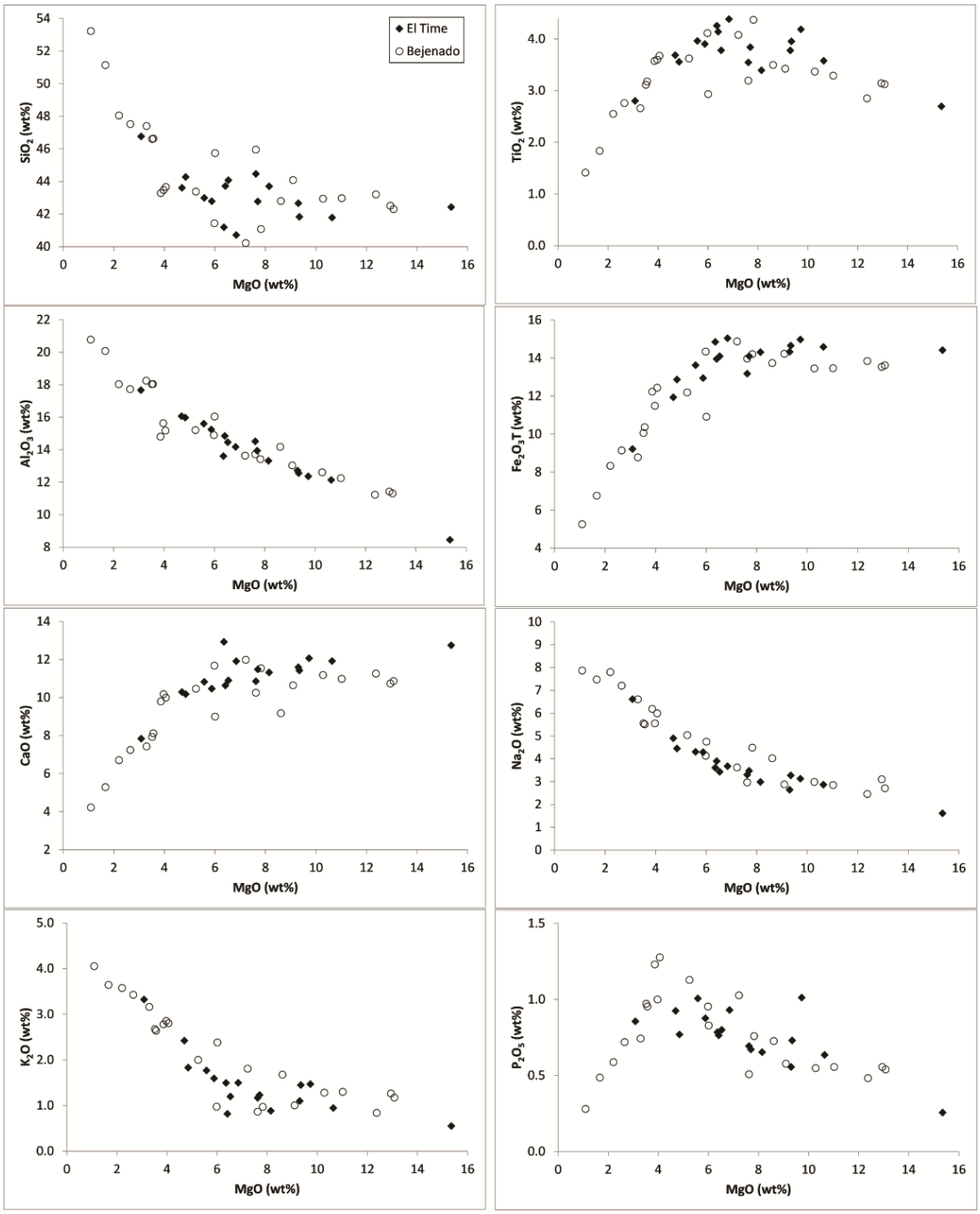

Figure 6-5 Major element MgO-variation diagrams for samples from central La Palma including BEP samples, data grouped by sub-region. The legend is shown in the SiO2 panel.

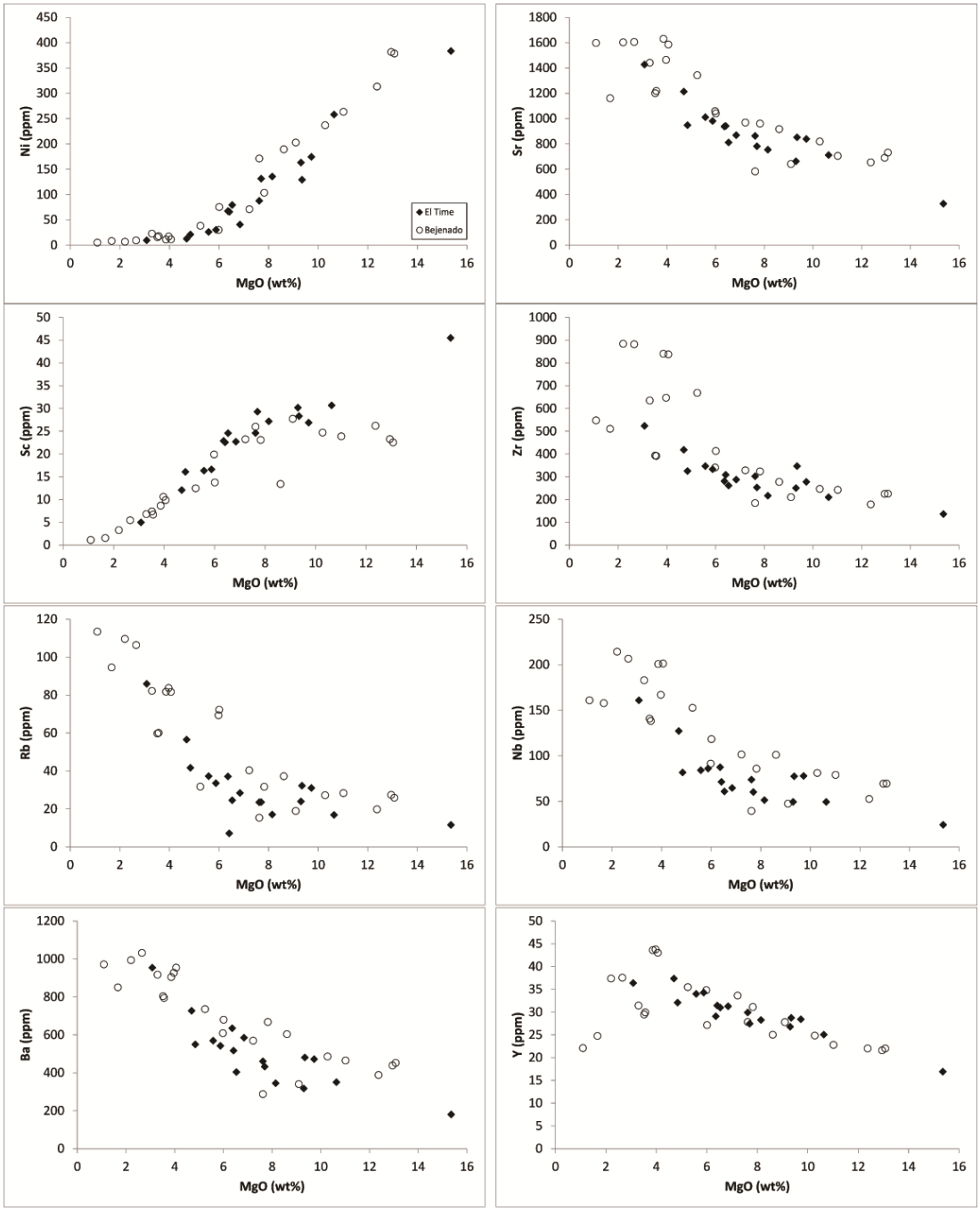

Figure 6-6 Trace element MgO-variation diagrams for samples from central La Palma including BEP samples, data grouped by sub-region. The legend is shown in the Ni panel.

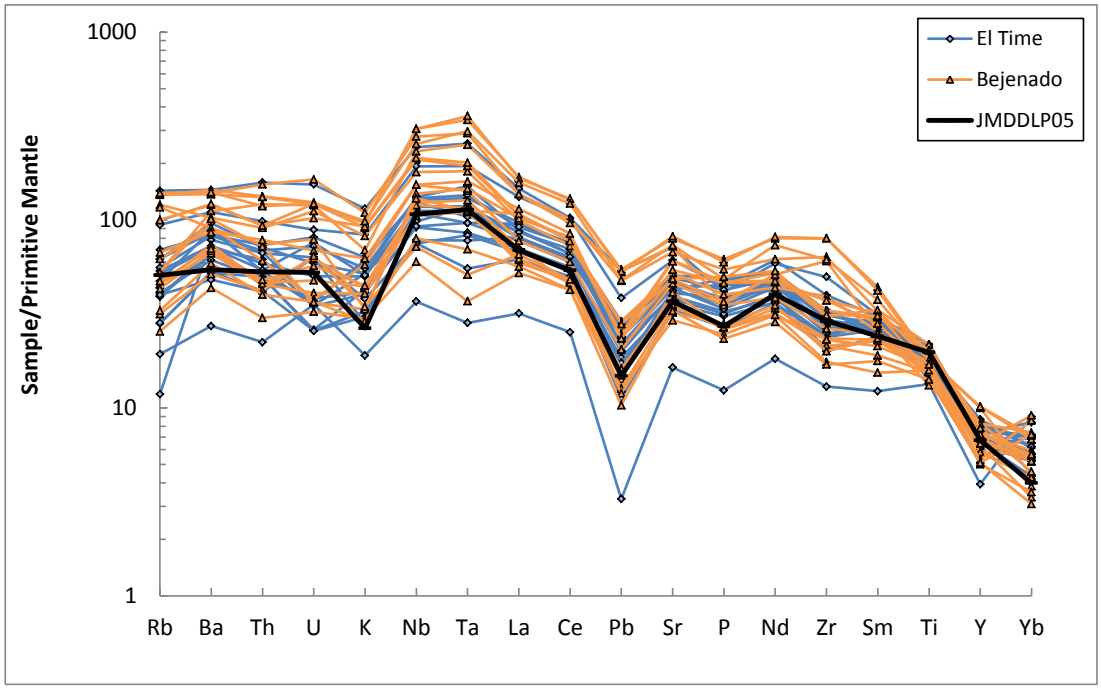

Figure 6-7 Multi-element primitive mantle-normalised diagram (McDonough & Sun, 1995) of samples of primitive lavas (>3 wt% MgO) from pre-collapse (*El Time*) and post-collapse (*Bejenado*) La Palma. JMDDLP05 is included as a comparative sample from pre-collapse *Taburiente* (Day et al., 2010).

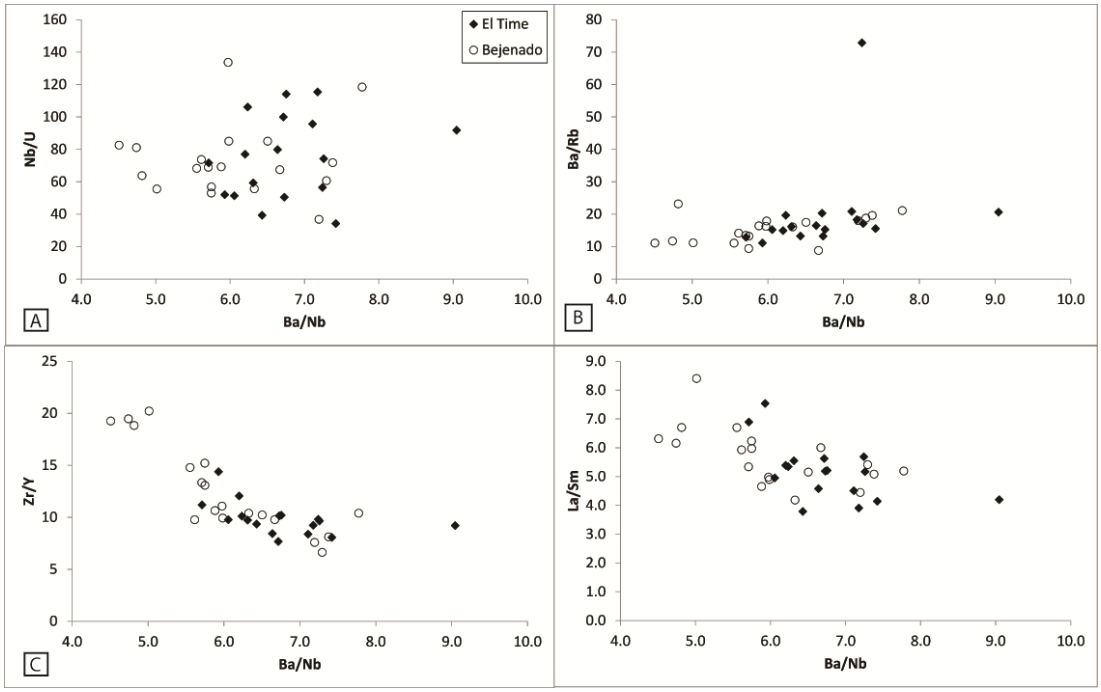

Figure 6-8 Bivariate diagrams of incompatible element ratios of pre-collapse (*El Time*) and post-collapse (*Bejenado*) samples (MgO >3 wt%). A) Ba/Nb vs Nb/U, B) Ba/Nb vs Ba/Rb, C) Ba/Nb vs Zr/Y, D) Ba/Nb vs La/Sm.

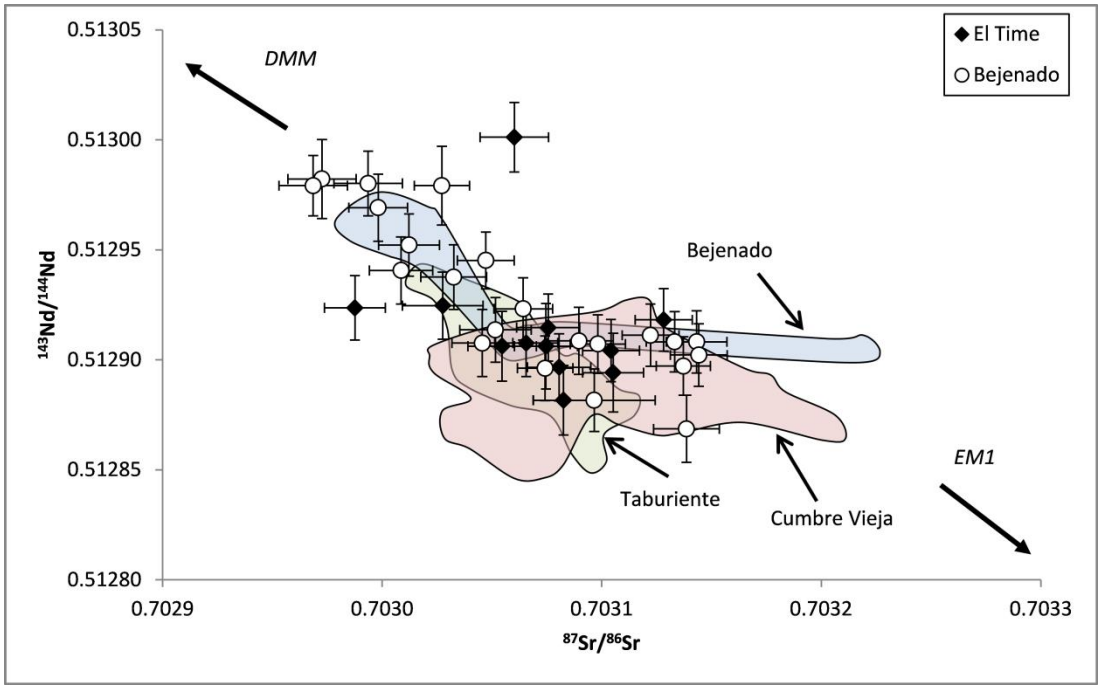

Figure 6-9 $^{87}Sr/^{86}Sr$ versus $^{143}Nd/^{144}Nd$ of *El Time* and *Bejenado* lava samples interpreted in terms of relevant mantle components. Coloured fields indicate data from previous studies of lava samples from major La Palma edifices (Day et al., 2010, Galipp, 2005., Gurenko et al., 2006, Praegel & Holm, 2005, Johansen et al, 2005).

Nb/U of 47 ± 10 (Hofmann et al., 1986), and Ba/Rb of 11.3 (Hofmann and White, 1983). Sample LP13SG31 has an unusually high Ba/Rb (73) indicative of alteration and this sample has not been included in the radiogenic isotope study. Zr/Y and La/Sm both show broad negative correllations with Ba/Nb.

6.4.4 Sr and Nd isotopes

The results of Sr and Nd isotope analyses of lava samples from *El Time* and *Bejenado* are presented in Table 6-2 and Figure 6-9. Both suites form a shared array between a low $^{87}Sr/^{86}Sr$ component with a high $^{143}Nd/^{144}Nd$ and a high $^{87}Sr/^{86}Sr$ component with low $^{143}Nd/^{144}Nd$. The 12 samples of the *El Time* suite exhibit surprising variation in $^{87}Sr/^{86}Sr$, with a larger range than all previous data from the *Taburiente* volcano (Day et al., 2010; Galipp, 2005). Among these samples, LP12SG18 has the highest $^{143}Nd/^{144}Nd$, but with median $^{87}Sr/^{86}Sr$ for our combined suite, together rendering this sample off the main trend shared by our data. The $^{87}Sr/^{86}Sr$ and $^{143}Nd/^{144}Nd$ isotopic ranges of the 22 *Bejenado* samples (0.70297-0.70314, and 0.51290-0.51298 respectively) are similar to that of all published data from the island. These samples form a hyperbolic trend between a cluster with the lowest $^{87}Sr/^{86}Sr$ of any samples analysed from La Palma, and a more radiogenic group with compositions typical of lavas from either the *Cumbre Vieja* or *Taburiente*.

6.4.5 Pb isotopes

The results of Pb isotope analysis of lava samples from *El Time* and *Bejenado* are presented in Table 6-3 and Figure 6-10.

Sample	Locality	Petrology	$^{87}Sr/^{86}Sr$	± 2σ	$^{143}Nd/^{144}Nd$	± 2σ
El Time						
LP13SG05	Barr.Jur.	Bas & prim	0.70299	0.00001	0.51292	0.00001
LP13SG06	Barr.Jur.	Bas & prim	0.70305	0.00002	0.51291	0.00002
LP13SG32	Barr.Jur.	Bas & prim	0.70313	0.00001	0.51292	0.00001
LP13SG07	Barr.Jur.	Amph-teph	0.70310	0.00001	0.51290	0.00001
LP12SG15	Bar. Gomm.	Bas & prim	0.70308	0.00001	0.51288	0.00002
LP12SG10	Surf. Flow	Bas & prim	0.70308	0.00001	0.51291	0.00002
LP12SG14	Surf. Flow	Bas & prim	0.70307	0.00001	0.51291	0.00002
LP12SG18	Surf. Flow	Bas & prim	0.70306	0.00002	0.51300	0.00002
LP12SG22	Surf. Flow	Pho-Teph	0.70303	0.00002	0.51292	0.00002
LP12SG23	Surf. Flow	Ankaramite	0.70307	0.00001	0.51291	0.00002
LP12SG26	Surf. Flow	Amph-teph	0.70308	0.00001	0.51290	0.00002
LP12SG09	Surf. Flow	Amph-teph	0.70311	0.00001	0.51289	0.00002
Bejenado						
LP13SG38	Basal Unit	Ankaramite	0.70297	0.00002	0.51298	0.00002
LP12SG87	West Bej	Bas & prim	0.70306	0.00001	0.51292	0.00001
LP13SG01	West Bej	Bas & prim	0.70312	0.00001	0.51291	0.00001
LP13SG10	West Bej	Bas & prim	0.70310	0.00001	0.51291	0.00001
LP13SG11	West Bej	Bas & prim	0.70314	0.00001	0.51291	0.00001
LP13SG30	LREVP-XPT	Amph-teph	0.70310	0.00003	0.51288	0.00001
LP13SG26	LREVP-XPT	Amph-teph	0.70307	0.00001	0.51290	0.00001
LP13SG29	BEP	Ankaramite	0.70299	0.00002	0.51298	0.00001
LP12SG03	BEP	Ankaramite	0.70300	0.00001	0.51297	0.00002
LP12SG05	BEP	Ankaramite	0.70303	0.00001	0.51298	0.00002
LP12SG82	BEP	Ankaramite	0.70301	0.00001	0.51295	0.00001
LP14SG08	BEP	Ankaramite	0.70297	0.00002	0.51298	0.00001
LP14SG06	BEP	teph	0.70303	0.00001	0.51294	0.00001
LP14SG09	BEP	teph	0.70301	0.00001	0.51294	0.00002
LP14SG04	BEP	Teph-pho	0.70305	0.00001	0.51291	0.00002
LP14SG05	BEP	Teph-pho	0.70305	0.00002	0.51291	0.00001
LP13SG13	TSP	Pho-teph	0.70314	0.00001	0.51290	0.00001
LP13SG16	TSP	Pho-Teph	0.70314	0.00001	0.51290	0.00001
LP13SG28	TSP	Amph-teph	0.70309	0.00002	0.51291	0.00002
LP14SG10	TSP	Amph-teph	0.70305	0.00001	0.51295	0.00001
LP13SG34	Mon L Hie	Pho-teph	0.70313	0.00001	0.51291	0.00001
LP14SG07	Mon L Hie	Pho-teph	0.70314	0.00001	0.51287	0.00002
BCR-2 (measured)					0.51264	0.000008
BCR-2 (published)					0.51263	0.000012

Table 6-2 Sr and Nd isotope data of *El Time* and *Bejenado* lavas determined by TIMS. BCR-2 was prepared and run as an unknown with each Nd sample batch. Locality nomenclature is the same as used in Table 6-1. Uncertaintes are the result of propagating within-run uncertainties and the reproducibility of the standard. Published BCR-2 values taken from Weiss et al., 2006.

Sample	Locality	Petrology	$^{206}Pb/^{204}Pb$	± 2σ	$^{207}Pb/^{204}Pb$	± 2σ	$^{208}Pb/^{204}Pb$	± 2σ	$^{207}Pb/^{206}Pb$	± 2σ	$^{208}Pb/^{206}Pb$	± 2σ
El Time												
LP13SG05	Barr.Jur.	Bas & prim	19.331	0.002	15.584	0.002	39.087	0.005	0.8062	0.00003	2.0221	0.0001
LP13SG06	Barr.Jur.	Bas & prim	19.807	0.003	15.622	0.002	39.673	0.007	0.7887	0.00004	2.0030	0.0001
LP13SG32	Barr.Jur.	Bas & prim	19.979	0.003	15.650	0.002	39.826	0.007	0.7833	0.00003	1.9934	0.0001
LP13SG07	Barr.Jur.	Amph teph	19.693	0.002	15.610	0.002	39.605	0.007	0.7927	0.00003	2.0111	0.0001
LP12SG15	Bar. Gomm.	Bas & prim	19.877	0.002	15.638	0.002	39.709	0.006	0.7867	0.00003	1.9978	0.0001
LP12SG10	Surf. Flow	Bas & prim	19.676	0.002	15.603	0.002	39.510	0.005	0.7930	0.00003	2.0080	0.0001
LP12SG14	Surf. Flow	Bas & prim	19.713	0.002	15.616	0.002	39.491	0.006	0.7922	0.00003	2.0034	0.0001
LP12SG18	Surf. Flow	Bas & prim	19.109	0.003	15.567	0.003	38.835	0.007	0.8146	0.00003	2.0323	0.0001
LP12SG22	Surf. Flow	Pho-Teph	19.459	0.002	15.596	0.002	39.247	0.006	0.8015	0.00003	2.0169	0.0001
LP12SG23	Surf. Flow	Ankaramite	19.883	0.002	15.635	0.002	39.727	0.006	0.7864	0.00003	1.9981	0.0001
LP12SG26	Surf. Flow	Amph teph	19.705	0.002	15.612	0.002	39.626	0.005	0.7923	0.00003	2.0109	0.0001
LP12SG09	Surf. Flow	Amph teph	19.708	0.002	15.612	0.002	39.644	0.007	0.7922	0.00003	2.0115	0.0001
Bejenado												
LP13SG38	Basal Unit	Ankaramite	19.086	0.002	15.564	0.002	38.810	0.005	0.8155	0.00003	2.0334	0.0001
LP12SG87	West Bej	Bas & prim	19.754	0.002	15.626	0.002	39.610	0.007	0.7910	0.00003	2.0052	0.0001
LP13SG01	West Bej	Bas & prim	19.890	0.003	15.635	0.003	39.731	0.007	0.7861	0.00003	1.9976	0.0001
LP13SG10	West Bej	Bas & prim	19.869	0.002	15.632	0.002	39.747	0.007	0.7867	0.00003	2.0004	0.0001
LP13SG11	West Bej	Bas & prim	19.765	0.002	15.624	0.002	39.619	0.007	0.7905	0.00003	2.0045	0.0001
LP13SG30	LREVP	Amph teph	19.782	0.002	15.619	0.002	39.673	0.005	0.7895	0.00003	2.0055	0.0001
LP13SG26	LREVP	Amph teph	19.837	0.002	15.626	0.002	39.725	0.007	0.7877	0.00003	2.0026	0.0001
LP13SG29	BEP	Ankaramite	19.162	0.002	15.569	0.002	38.912	0.006	0.8125	0.00003	2.0307	0.0001
LP12SG03	BEP	Ankaramite	19.170	0.002	15.569	0.002	38.912	0.007	0.8122	0.00003	2.0299	0.0001
LP12SG05	BEP	Ankaramite	19.159	0.002	15.565	0.002	38.893	0.007	0.8124	0.00003	2.0300	0.0001
LP12SG82	BEP	Ankaramite	19.190	0.002	15.574	0.002	38.951	0.007	0.8115	0.00003	2.0297	0.0001
LP14SG08	BEP	Ankaramite	19.176	0.002	15.569	0.002	38.923	0.005	0.8119	0.00003	2.0298	0.0001
LP14SG06	BEP	Tephrite	19.420	0.002	15.590	0.002	39.221	0.005	0.8028	0.00003	2.0197	0.0001
LP14SG09	BEP	Tephrite	19.421	0.002	15.590	0.002	39.225	0.006	0.8028	0.00003	2.0197	0.0001

Table 6-3 Pb isotopic data determined by MC-ICP-MS. BCR-2 was prepared and run as an unknown with each sample batch. Lcality nomenclature is the same as used in Table 6-1.

Sample	Locality	Petrology	$^{206}Pb/^{204}Pb$	± 2σ	$^{207}Pb/^{204}Pb$	± 2σ	$^{208}Pb/^{204}Pb$	± 2σ	$^{207}Pb/^{206}Pb$	± 2σ	$^{208}Pb/^{206}Pb$	± 2σ
Bejenado												
LP14SG04	BEP	Teph-pho	19.532	0.002	15.600	0.002	39.359	0.005	0.79868	0.00003	2.0151	0.0001
LP14SG05	BEP	Teph-pho	19.517	0.002	15.602	0.002	39.351	0.005	0.79942	0.00003	2.0162	0.0001
LP13SG13	TSP	Pho-teph	19.827	0.002	15.625	0.002	39.733	0.007	0.78811	0.00003	2.0041	0.0001
LP13SG16	TSP	Pho-teph	19.829	0.002	15.626	0.002	39.738	0.007	0.78806	0.00003	2.0041	0.0001
LP13SG28	TSP	Amph teph	19.624	0.002	15.610	0.002	39.471	0.005	0.79547	0.00003	2.0114	0.0001
LP14SG10	TSP	Amph teph	19.509	0.002	15.600	0.002	39.334	0.007	0.79960	0.00003	2.0162	0.0001
LP13SG34	Mon L Hie	Pho-Teph	19.830	0.002	15.627	0.002	39.749	0.007	0.78807	0.00003	2.0045	0.0001
LP14SG07	Mon L Hie	Pho-Teph	19.818	0.002	15.623	0.002	39.729	0.005	0.78832	0.00003	2.0046	0.0001
BCR-2 (measured)			18.803	0.002	15.627	0.002	38.83	0.007	0.83109	0.00003	2.0651	0.0001
BCR-2 (published)			18.753	0.020	15.625	0.004	38.724	0.041	N/A	N/A	N/A	N/A

Table 6-3 Pb isotopic data determined by MC-ICP-MS. BCR-2 was prepared and run as an unknown with each sample batch. Locality nomenclature is the same as used in Table 6-1. Published BCR-2 values taken from Weiss et al., 2006. Uncertaintes are the result of propagating within-run uncertainties and the reproducibility of the standard.

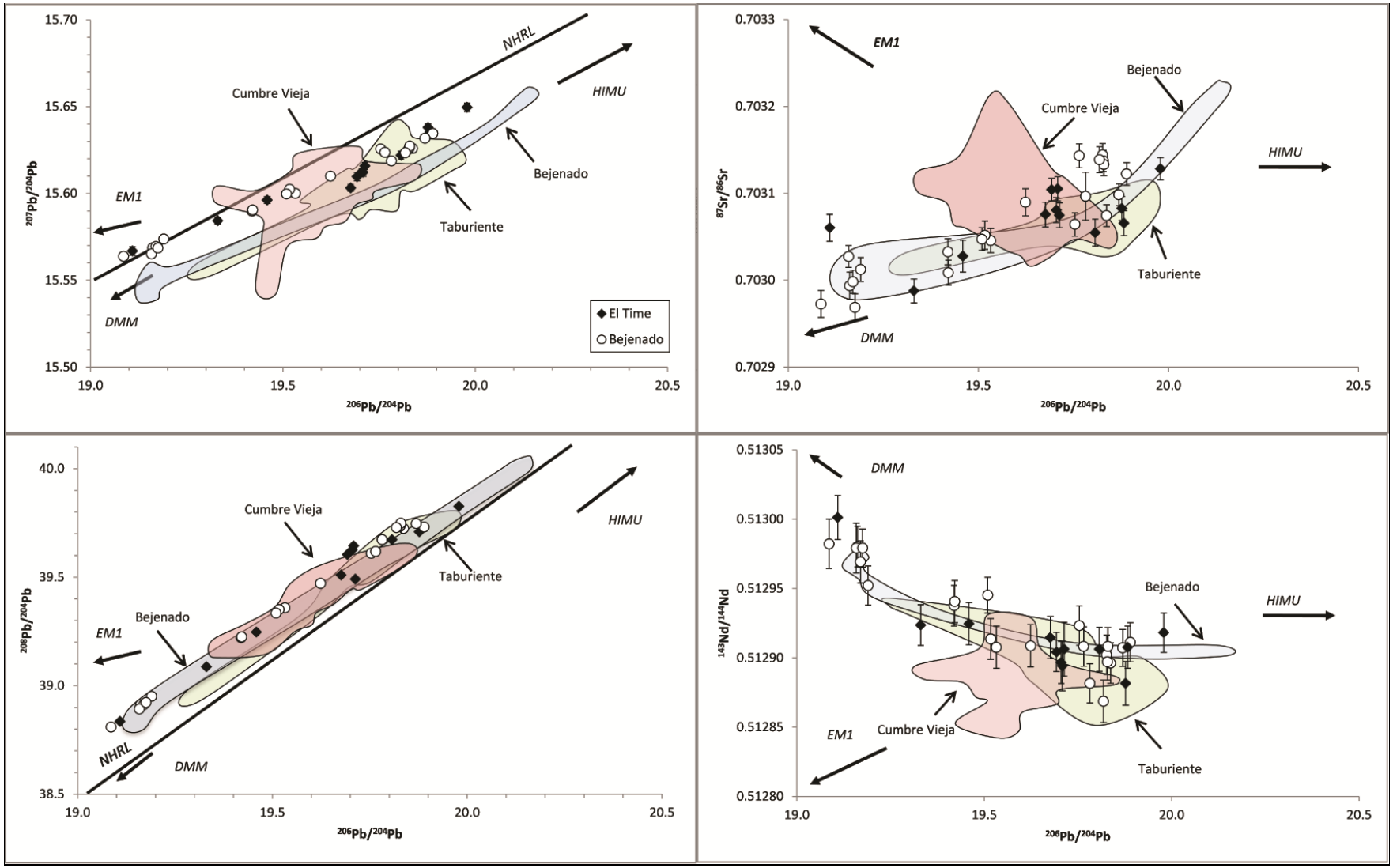

Figure 6-10 Pb, Sr and Nd isotope systematics of *El Time* and *Bejenado* lava samples interpreted in terms of relevant mantle components. Coloured fields indicate data from previous studies of lava samples from major La Palma edifices (Day et al., 2010, Galipp, 2005., Gurenko et al., 2006, Praegel & Holm, 2005, Johansen et al, 2005).

When Pb isotopic data are combined with that for Sr and Nd, the results are consistent with previous studies of western Canary Island lavas (Day et al., 2010; Galipp, 2005; Gurenko et al., 2006). Such studies have described these islands as the result of partial melts from a mixture of a DMM-like component, characterised by more radiogenic Nd and less radiogenic Sr and Pb, and the young-HIMU component with more radiogenic Sr and Pb compositions, and less radiogenic Nd.

Among the *El Time* suite, LP12SG18 has the lowest $^{206}Pb/^{204}Pb$, however the data from this sample should be treated with caution due to the sample's anomalously high $^{87}Sr/^{86}Sr$ (it would benefit from complete re-analysis) and it will not be discussed in further detail. Other than this sample, the data within our *El Time* suite exhibits considerable unstructured scatter. This scatter is of a similar scale to the well-structured isotopic variation within the *Bejenado* suite (Figure 6-15), with which it overlaps, leading us to conclude that this scatter is geological, not analytical, but its nature is unresolved by our sampling. As was observed in $^{87}Sr/^{86}Sr$, the Pb isotopic variation in our *Bejenado* suite extends beyond that previously observed at La Palma's *Taburiente* and *Cumbre Vieja* edifices (Figure 6-10), with considerable variation in $^{206}Pb/^{204}Pb$ (19.086-19.890), $^{207}Pb/^{204}Pb$ (15.564-15.634) and $^{208}Pb/^{204}Pb$ (38.810-39.749). Typically for La Palma basalts, samples generally lie beneath the Northern Hemisphere Reference Line (NHRL) on plots of $^{207}Pb/^{204}Pb$ versus $^{206}Pb/^{204}Pb$, and above it in terms of $^{208}Pb/^{204}Pb$ versus $^{206}Pb/^{204}Pb$. However, the most depleted samples from both *Bejenado* and *El Time* cross this boundary for $^{207}Pb/^{204}Pb$ and $^{206}Pb/^{204}Pb$. Most significantly, no isotopic system provides clear means of discriminating pre-collapse from post-collapse phase lavas.

6.5 Results, part 2: post-collapse variation presented by stratigraphic unit

The following section addresses the same data as the previous section, but by using stratigraphically grouped samples (the "eruptive phases") aims to resolve the specific post-collapse magmatic processes that contributed to *Bejenado*. Detailed petrographic descriptions of samples from the stratigraphic sample groups are included in the appendix[30] .

Samples from *Bejenado's* eruptive phases indicate that these units are often compositionally heterogeneous (Figure 6-11), with the most variation observed in the *Bejenado Effusive Phase*[31] (BEP) and Terminal Sheet Phase (TSP) units from eastern *Bejenado*. TSP lavas are typically silica-poor tephrites and phono-tephrites with variable alkali contents that lie near the foidite field. The primitive, opportunistic samples from *West Bejenado* show unusual variation in SiO_2 forming basalts, basanites and foidites. Samples from the *Los Rodeos Evolved and Volcaniclastic Phase* (LREVP)

[30]Appendix D: Supplementary petrology — petrography of sample groups from *Bejenado* used in Chapter 6. pp.247-255

[31] 5.4.1 Petrography of BEP lava-units.pp.108-110

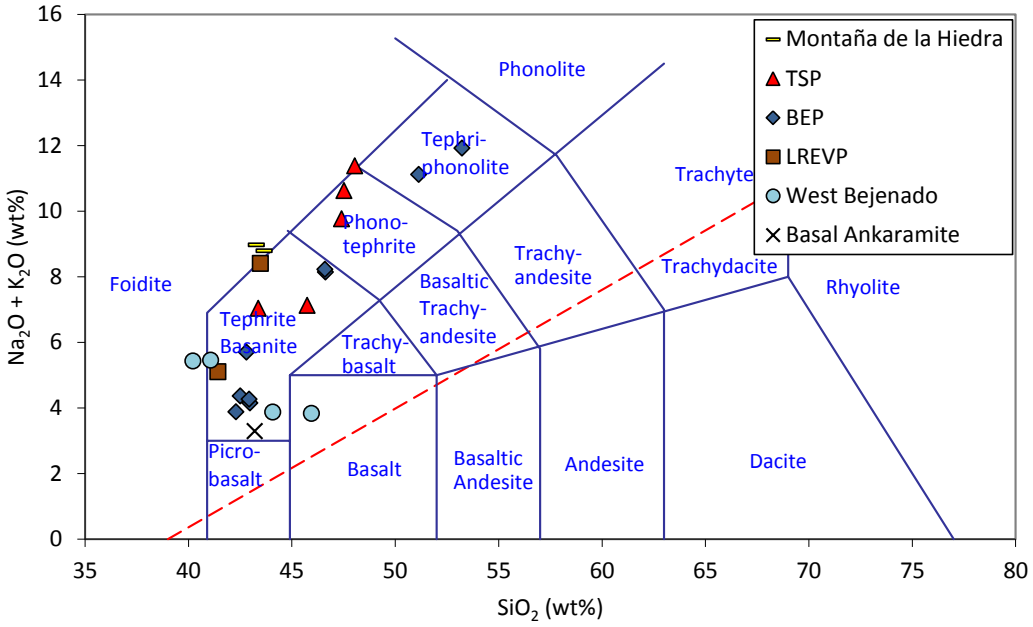

Figure 6-11 A TAS classification diagram of the whole rock compositions of the Bejenado lava flows presented in this chapter and selected BEP lavas, presented by volcano-stratigraphic unit. The TAS diagram is in the style of Le Bas et al. (1986). LREVP = Los Rodeos Evolved and Volcaniclastic Phase, BEP = Bejenado Effusive Phase, TSP = Terminal Sheet Phase.

are both tephritic with considerable differences in alkali content. The most primitive sample (LP13SG38) is a basanitic Basal Ankaramite sample from the *Bejenado Lower Series*.

6.5.2 Whole-rock major and trace element compositions

Since elemental variation diagrams are largely used for determining regional-scale differentiation trends, rather than providing a means of group discrimination, these figures (Figure 6-5, Figure 6-6) have not been re-presented. However, with the aid of stratigraphic groups the combination of primitive mantle-normalised incompatible element diagrams (Figure 6-12) and bivariate plots of incompatible element ratios (Figure 6-13A-D) may provide a means of resolving the scatter observed across the *Bejenado* suite (Figure 6-8A-D).

Samples from the same eruptive phases (BEP, TSP and *Montaña de la Hiedra*) typically form clusters (Figure 6-13A-D), with variation in magmatic evolution providing the most obvious structure found in the *Bejenado* elemental data. The primitive *West Bejenado* samples have complex profiles, usually having positive anomalies in Ba, Sm and Yb and negative anomalies in Rb, Ta and Zr, leading all but LP13SG10 to form a group with high Ba/Rb (18-21, Figure 6-13B) and low Zr/Y (0.10-0.15, Figure 6-13C) compositions. In contrast, the evolved samples of the TSP and *Moñtana de la Hiedra* units exhibit major negative anomalies in P and Ti (likely to reflect the importance of apatite, titanomagnetite and titan-augite crystallisation) and high contents of HFSE elements (Nb and Ta are high, and there is a significant positive anomaly in Zr). Such high HFSE contents (Nb 118.3-214.3 ppm) are likely to

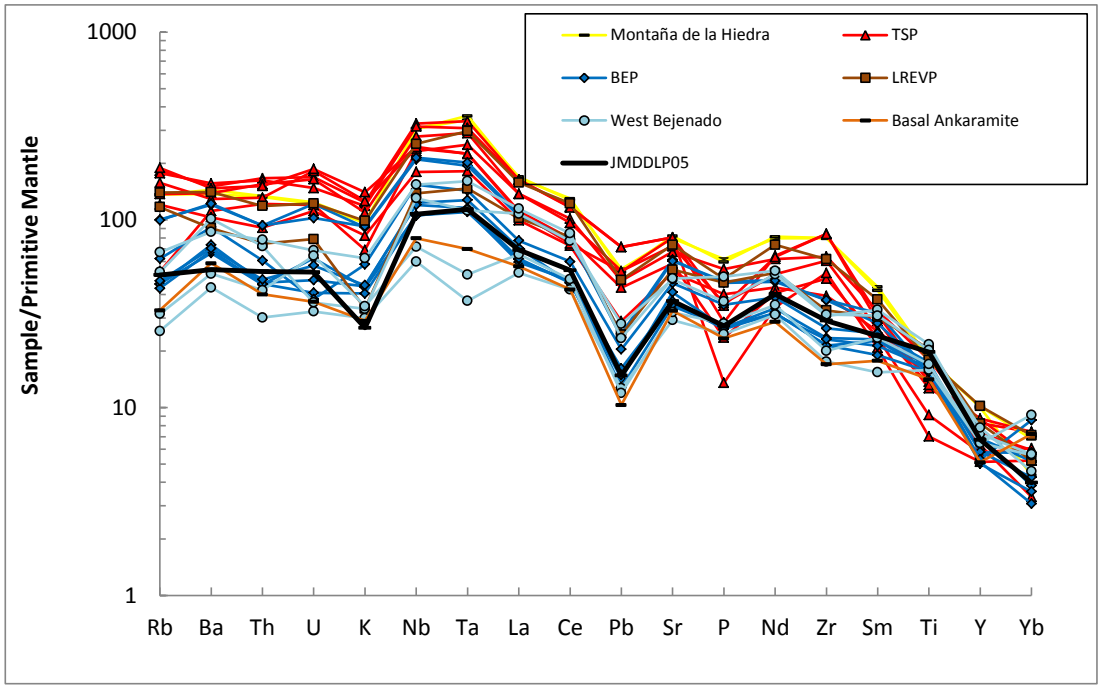

Figure 6-12 Multi-element primitive mantle-normalised diagram (McDonough & Sun, 1995) of samples of primitive lavas (>3 wt% MgO) from post-collapse (*Bejenado*) La Palma grouped by stratigraphic unit. JMDDLP05 is included as a comparative sample from pre-collapse *Taburiente* (Day et al., 2010).

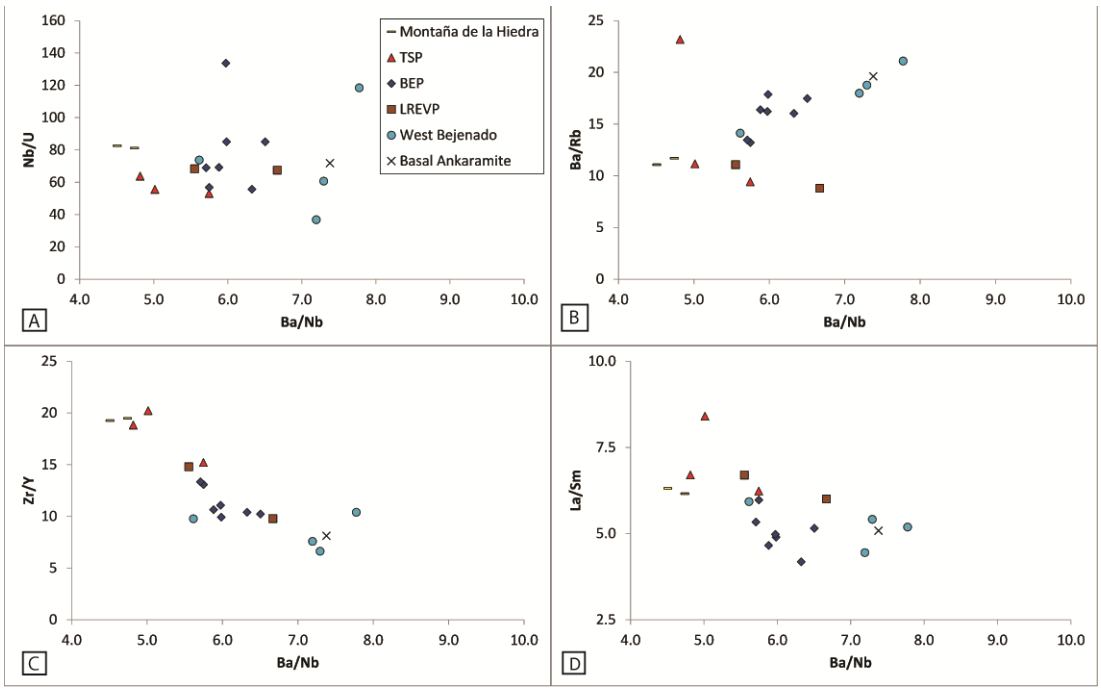

Figure 6-13 Bivariate diagrams of incompatible element ratios of *Bejenado* samples (MgO >3 wt%), plotted by stratigraphic unit. A) Ba/Nb vs Nb/U, B) Ba/Nb vs Ba/Rb, C) Ba/Nb vs Zr/Y, D) Ba/Nb vs La/Sm.

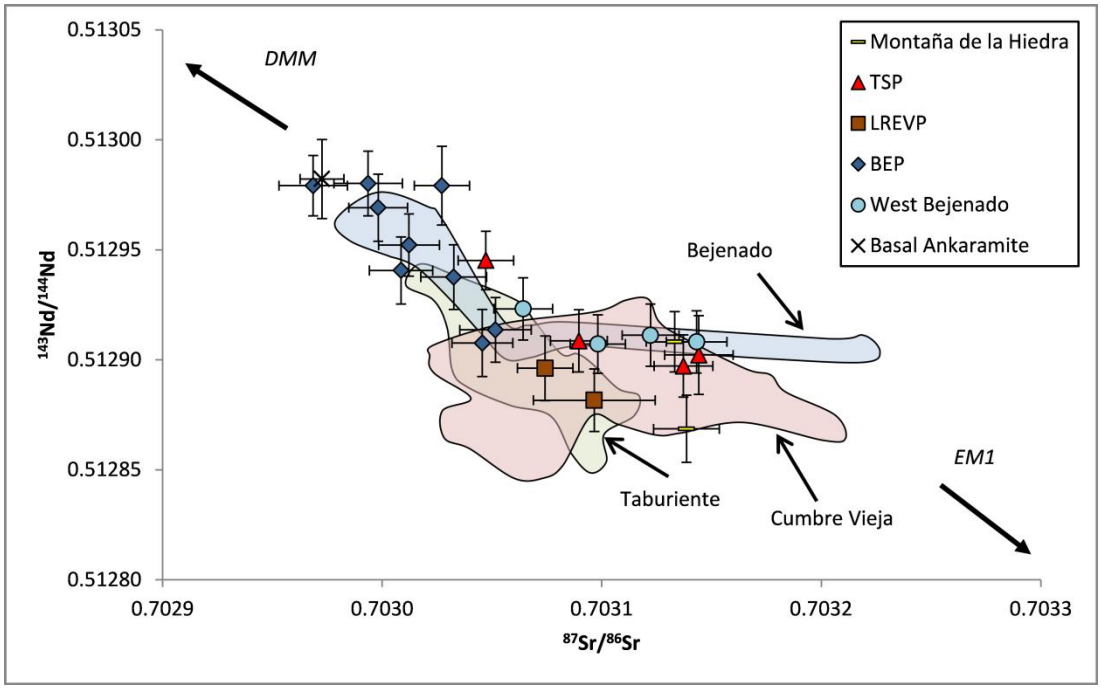

Figure 6-14 $^{87}Sr/^{86}Sr$ versus $^{143}Nd/^{144}Nd$ of *Bejenado* lava samples grouped by stratigraphic unit and interpreted in terms of relevant mantle components. Coloured fields indicate data from previous studies of lava samples from major La Palma edifices (Day et al., 2010, Galipp, 2005, Gurenko et al., 2006, Praegel & Holm, 2005, Johansen et al, 2005).

contribute to the low Ba/Nb of these samples (4.5-5.0), although Nb enrichment is not reflected in the group's Nb/U (53-83, Figure 6-13A) which are near the mean of the *Bejenado* suite. In general samples from the voluminous BEP sequence lie towards the median of all incompatible element ratio diagrams from *Bejenado*.

6.5.3 Sr, Nd and Pb Isotopes

Groups of samples from *Bejenado's* stratigraphic units form meaningful clusters and trends (Figure 6-14, Figure 6-15). Samples with a strong DMM-like, less radiogenic, component are all ankaramites (Basal Ankaramite and the BEP's Glomerocrystic Ankaramite), and together form a cluster in $^{87}Sr/^{86}Sr$ (0.70297 – 0.70303), $^{143}Nd/^{144}Nd$ (0.51296-0.51298) and $^{206}Pb/^{204}Pb$ (19.086-19.190). In contrast, the foidites of *Montaña de la Hiedra* and the TSP have strongly radiogenic Sr (0.70313-0.70314) and surprising variability in Nd isotopes (0.51269-0.52191) together exhibiting the strongest young-HIMU component. The majority of *Bejenado* samples (LREVP, TSP and non-ankaramitic BEP lavas) form shared arrays between these groups. The exceptions are the *West Bejenado* samples, which have elevated radiogenic Nd (0.51291-0.51292) for their Sr and Pb isotopic compositions.

Within the *Bejenado* suite there is a relationship between increasing degree of magmatic evolution and an increasing role for the young-HIMU mantle component. The strongest role for the DMM-like component is observed among samples of primitive basanites (Basal Ankaramite and BEP), while that for the young-HIMU signature is observed in evolved magmas of the TSP and *Montaña de la Hiedra*. Mixing between these components is shown by diagrams of the relationship between $^{206}Pb/^{204}Pb$ and the abundances of individual incompatible

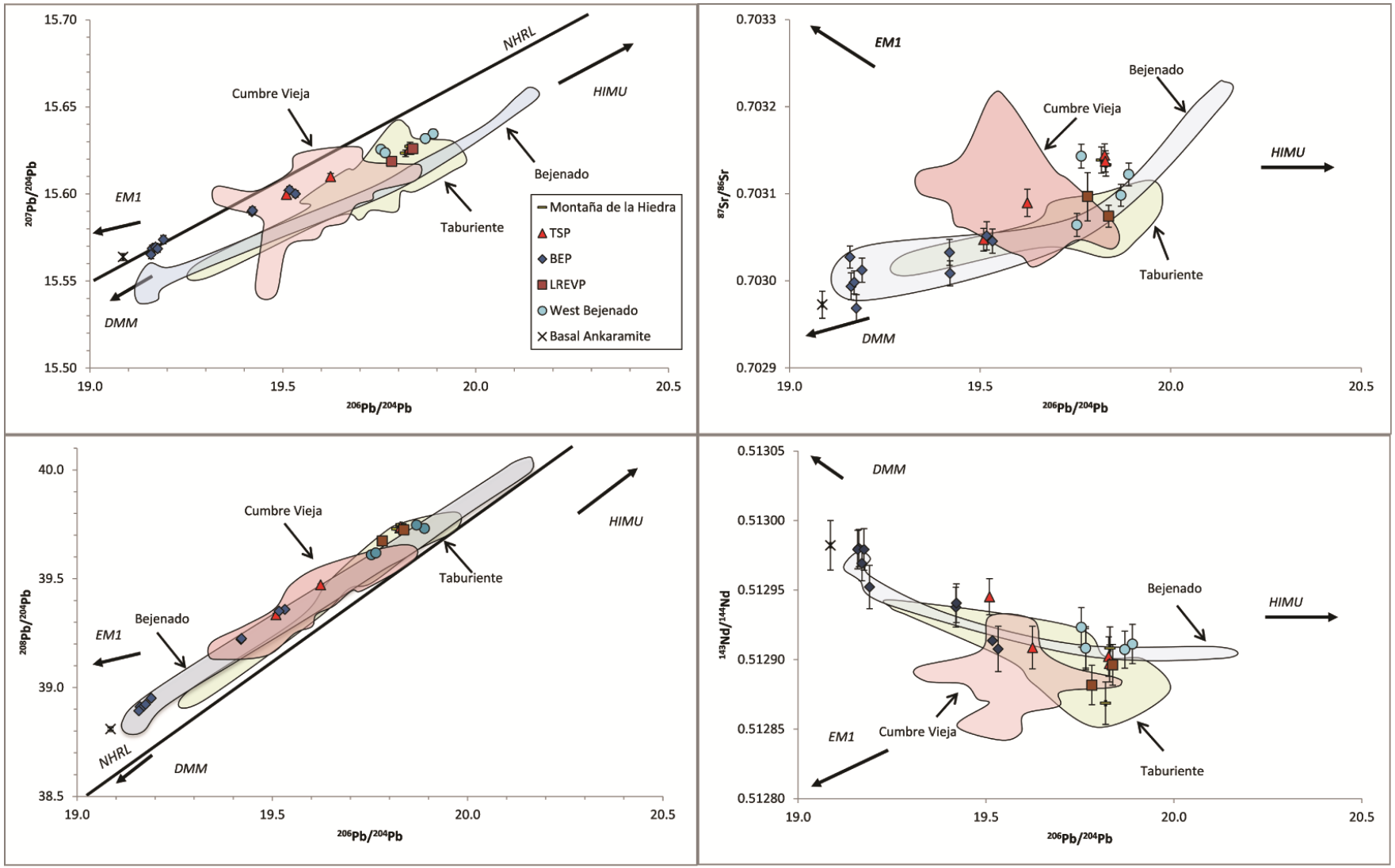

Figure 6-15 Pb, Sr and Nd isotope systematics of Bejenado lava samples grouped by stratigraphic unit and interpreted in terms of relevant mantle components. Coloured fields indicate data from previous studies of lava samples from major La Palma edifices (Day et al., 2010, Galipp, 2005., Gurenko et al., 2006, Praegel & holm, 2005, Johansen et al 2005).

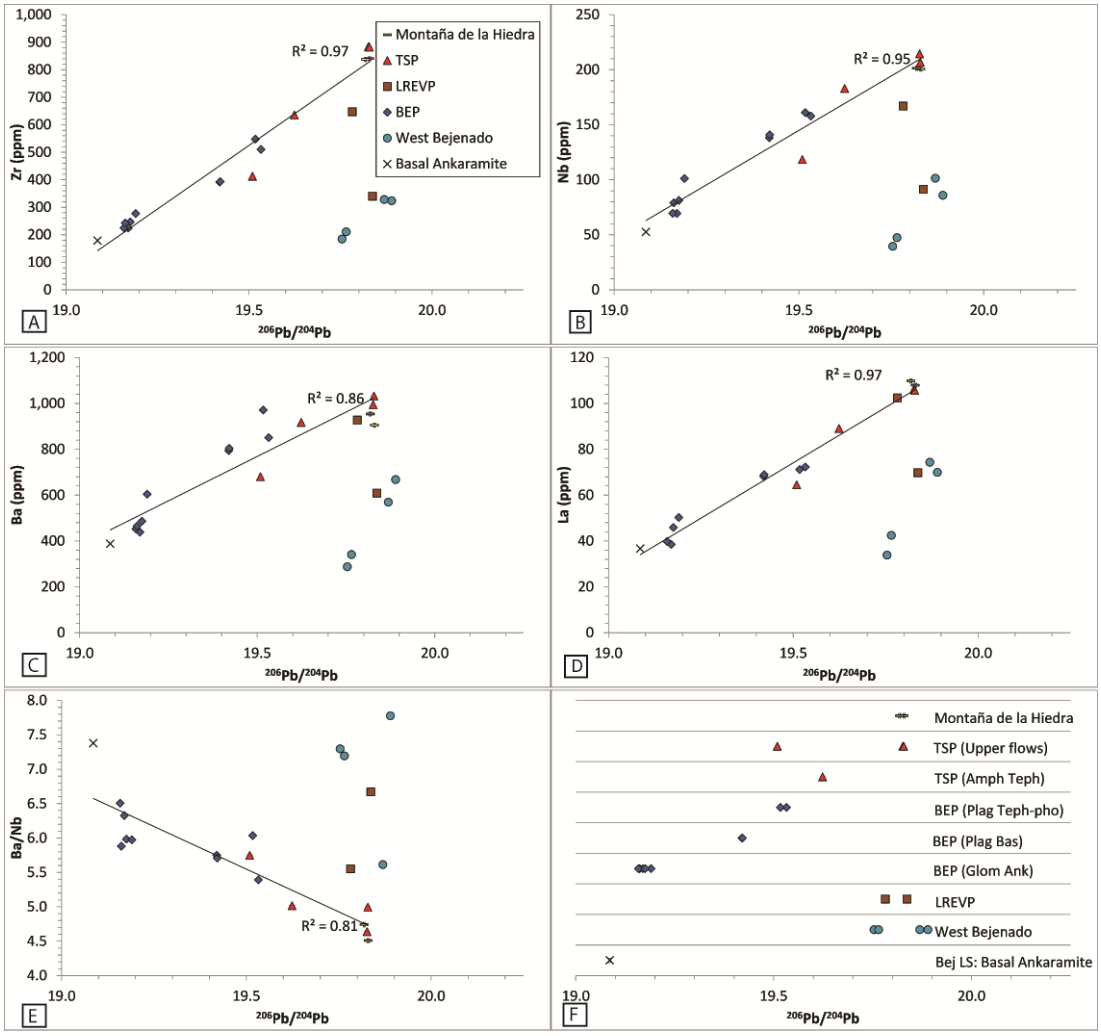

Figure 6-16 Plots of $^{206}Pb/^{204}Pb$ vs the concentrations of characteristic incompatible elements in *Bejenado* samples: A) Zr vs $^{206}Pb/^{204}Pb$, B) Nb vs $^{206}Pb/^{204}Pb$, C) Ba vs $^{206}Pb/^{204}Pb$, D) La vs $^{206}Pb/^{204}Pb$, E) Ba/Nb vs $^{206}Pb/^{204}Pb$. Elements were chosen as to indicate variation among HFSE, LILE and REE, respectively. The data used to derive the trendlines does not include LREVP or *West Bejenado* samples. F) Illustrates $^{206}Pb/^{204}Pb$ by stratigraphic unit from the base of *Bejenado's* extrusive sequences, where TSP upper flows indicate both TSP Phono-tephrite and Amphibole Olivine Tephrite lavas.

elements (Figure 6-16A-D). These groups of samples show strong correlations in terms of Zr and Nb (HFSE elements) and La (a REE element), and a weaker correlation in terms of Ba (a LILE element). As a result of these correlations, these mixtures control Ba/Nb among these groups of samples (Figure 6-16E). The only *Bejenado* samples that do not fit these trends are those from the LREVP unit and *West Bejenado*, which all exhibit high $^{206}Pb/^{204}Pb$ despite the primitive composition of the *West Bejenado* samples.

The relative proportions of the depleted, DMM-like isotopic component and the young-HIMU component in lava-units appears to vary stratigraphically from the base of *Bejenado* (Figure 6-16F). The observed progression is: 1) the least radiogenic $^{206}Pb/^{204}Pb$ erupted at the base of *Bejenado* in the Basal Ankaramite of the *Bejenado Lower Series*, 2) this was followed in both *West Bejenado* group and the LREVP unit by a change to high $^{206}Pb/^{204}Pb$ signatures, 3) low $^{206}Pb/^{204}Pb$ magmas return with the BEP's primitive Glomerocrystic Ankaramite, 4) this is followed by a progressive,

increasing role for the radiogenic $^{206}Pb/^{204}Pb$ component that becomes dominant towards the top of the TSP unit, 5) there is a return of the low $^{206}Pb/^{204}Pb$ component with the TSP's Amphibole Olivine Tephrite, in one of the uppermost flows of the edifice.

6.6 Discussion

Before this thesis there were relatively few studies of whole-rock geochemistry (Hildenbrand et al., 2004; Longpré et al., 2009) that focused on how the deep and sub-lithospheric part of an ocean island's magma supply system interacted with the processes involved in lateral collapses. Within our sample suite, pre-collapse and post-collapse lava samples share petrological groups, lie on shared trends on variation diagrams, and when plotted in terms of incompatible element abundances and radiogenic isotope compositions cannot be discriminated by composition. The only unique post-collapse petrological features are the feldspar-phyric lavas of the *Bejenado Effusive Phase*, while all other mineral assemblages and major features are shared by both pre-collapse and post-collapse units.

The lack of discrimination in composition is surprising, since the *Cumbre Nueva Collapse* is likely to have led to some of the most rapid changes in the conditions within the magmatic system to have occurred over the course of La Palma's growth. Furthermore, previous petrological studies of post-collapse volcanism have identified significant processes resulting from the collapse (Longpré et al., 2008; Manconi et al., 2009) with findings which have been supported by our work on the BEP sequence[32].

We propose that the lack of discrimination largely results from the character of multivariate compositional and isotopic whole-rock data, which is well-suited to identifying subtle but long-lived differences between large groups of samples, but is less well-suited to recognising the significance of major short-lived features which can appear to be analytical outliers. Nonetheless, whole rock data provides the most robust and detailed aggregate view of the magmatic processes that contributed to a volcanic edifice or region. They provide a baseline characterisation of the differentiation and transport processes that acted during the growth of central La Palma which can then be compared with the more specific, petrological interpretation of individual eruptive units. In the section that follows we describe this aggregate view of the magmatic conditions that contributed to central La Palma's eruptive products, and follow it with a detailed specific study of *Bejenado*.

6.6.1 Magmatic evolution and melt production in the period of the *Cumbre Nueva Collapse*

Source characteristics

[32] Chapter 5: Petrology. pp. 98-138.

Previous radiogenic isotope and mantle geochemistry studies of La Palma and neighbouring El Hierro characterised the lavas of these islands as resulting from partially melting a heterogeneous mixture of lithologically and isotopically distinct mantle components. Two competing models proposed different end-members: 1) Gurenko et al. (2009b) proposed that La Palma would be the product of a simple mixture of 70% HIMU-peridotite and 30% DMM-like pyroxenite, in contrast to neighbouring El Hierro with 25% HIMU-peridotite to 75% DMM-like pyroxenite; 2) Day et al. (2010) proposed a mixture of a common component (90%) and a recycled oceanic crustal slab with different starting proportions of oceanic crust components (a mixture of basaltic oceanic crust and a layer 3 unit that was a mixture of gabbro and peridotite) metamorphosed into a heterogeneous mixture of pyroxenite and peridotite. There has been vibrant debate over the specific nature of these source-rock lithologies (Day et al., 2009, 2012, Gurenko et al., 2009b, 2011, 2012). Our samples form a combined group that covers a range of compositions between the otherwise discrete fields formed by each of the two islands' data. All our isotopic compositions would be consistent with the melting of mixtures between La Palma and El Hierro's characteristic magma sources.

Such lithological characterisations of the magma-source are typically based on either Os and O isotope data (Day et al., 2009, 2010; Marcantonio et al., 1995) or trace element phenocryst chemistry (Gurenko et al., 2009a, 2009b), and since neither has been obtained in this study it is difficult to interpret our data in this context. We prefer to treat mantle components largely as vectors in Sr-Nd-Pb isotope diagrams, and lithological components in terms of elemental compositions. Only where our data shows strong correlations between elemental and isotopic evidence are we comfortable uniting lithological and mantle component models.

In elemental studies of mantle source lithology there are ongoing discussions about the role of hydrous phases in the petrogenesis of La Palma magmas. Negative anomalies in Rb, Ba and K on incompatible element diagrams have been used by several authors (Galipp, 2005; Gurenko et al., 2006; Praegel and Holm, 2006) as evidence that amphibole or phlogopite was present in the source, since these minerals would be expected to buffer these elements as the melt formed. Our data shares these Rb and K negative anomalies, although positive Ba anomalies are often present (Figure 6-7, Figure 6-12).

The samples with strong DMM-like signatures at *Bejenado* are unusual for La Palma, and support the results of Galipp (2005), which included five samples from *Bejenado.* That study identified four samples with similar DMM-like signatures to those we have identified, and one sample with a more young-HIMU dominated composition. Such young-HIMU compositions are common among our *Bejenado* samples (Figure 6-15), and this is likely to be part of the reason for the lack of meaningful discrimination in terms of radiogenic isotope compositions of our pre-collapse and post-collapse lava suites. The strongly depleted compositions at *Bejenado* are more characteristic of neighbouring El Hierro than of *Bejenado's* large edifices, and comparable compositions have only been identified in

dredge samples from offshore La Palma (Abratis et al., 2002) for which there is very little stratigraphic constraint.

In contrast, our samples with the strongest young-HIMU signatures form a wider, less stratigraphically distinct spread with less clear groups in terms of incompatible trace element ratios (Figure 6-13). Within our suite young-HIMU compositions are found in an unrelated cluster of samples from *El Time* (LP13SG32, LP12SG15, LP12SG23), as well as among *Bejenado's* more evolved lavas (from the TSP, LREVP and *Montaña de la Hiedra*) and the primitive *West Bejenado* samples.

MAGMA-MIXING AND WALL-ROCK INTERACTION: PETROGRAPHY AND ELEMENTAL GEOCHEMISTRY

Several authors have proposed on the basis of samples with high Nb/U (<88) that La Palma magmas have assimilated amphibole-rich material at depth (Galipp, 2005; Turner et al., 2015). This has been supported by a study of cumulate xenoliths and the phenocryst content of La Palma's 1971 eruption (Barker et al., 2015) which proposed that the combined cargo was the product of assimilated cumulate material acquired in the lower lithosphere. The Nb/U of our analyses ranges from 37-115, extending well beyond the 47 ± 10 determined as canonical for OIB basalts (Hofmann, 1988). Among our samples this ratio does not have a strong correlation with the main indicators of petrogenetic processes, particularly Ba/Nb (Figure 6-8, Figure 6-13), making it difficult to determine the wider relationship of amphibole assimilation to other petrogenetic processes.

Amphibole-assimilation is compatible with our petrographic results from both *El Time* and *Bejenado* where numerous lava-units exhibit embayed amphibole xenocrysts and holocrystalline glomerocrysts that appear to be of cumulate origin (Figure 6-4E). In particular, LREVP samples[33] provide the strongest textural support (although they have median Nb/U) for these assimilation models and contain cumulate xenoliths similar to those described elsewhere on La Palma (Galipp et al., 2006; Schmincke et al., 1998) as well as kaersutite xenocrysts with rounded edges and selvages similar to those described in the lavas from *Teneguia* (Barker et al., 2015) where they have been interpreted as resulting from disequilibrium. In combination, this appears to indicate that a temporally and spatially extensive complex of a kaersutite-rich lithology is present beneath La Palma and may have resulted from underplating. This complex has then been interacting with primitive magmas during their ascent. Amphibole appears to be important, both in terms of the melt source and underplated hornblendite/pyroxenite, in processes in La Palma's deep magma supply system.

In general, the four petrographic groups formed by the majority of our lava samples are surprisingly consistent between *El Time* and *Bejenado*, indicating that the collapse did not fundamentally alter the crystal cargoes characteristic of these lavas. Notably, among our samples xenocrysts are very common (Figure 6-4). The most easily identified xenocrysts are those which have very different

[33]Appendix D: Supplementary petrology — petrography of sample groups from *Bejenado* used in Chapter 6. pp.251-253.

degrees of differentiation to their host magmas. In the primitive magmas we observed embayed ferroan diopside green-core pyroxenes, while in the more evolved magmas we observed relic olivine, both indicating interactions between magmas of very different composition. It is possible that these embayed xenocrysts are the most refractory remnants of a larger mineral suite now resorbed into the host magma. Thus, beyond amphibole-assimilation, La Palma's magma transport processes may be routinely remobilising a varied body of material that originates in stagnant reservoirs, wall-rocks and/or crystal-mushes of varying degrees of evolution.

ELEMENTAL VARIATION - GROSS RESERVOIR SYSTEM PROCESSES

In studies of whole-rock composition, variation between samples in degrees of magmatic evolution is usually ascribed to fractional crystallisation processes that are constrained by elemental variation trends. Our phenocryst assemblages lead us to propose three possible fractionation stages that could explain the trends: 1) a primitive stage controlled by clinopyroxene, olivine and titanomagnetite crystallisation, 2) an intermediate stage controlled by clinopyroxene, kaersutitic amphibole and titanomagnetite crystallisation, 3) an evolved stage where clinopyroxene-dominated (± kaersutitic amphibole) crystallisation is likely to be accompanied by the formation of apatite. Similar fractionation stages have been proposed in previous publications on La Palma lavas (Carracedo et al., 2001; Praegel and Holm, 2006; Turner et al., 2015).

The coherent trends in major and trace elements against MgO (Figure 6-5, Figure 6-6) formed by collapse-related samples, and their linear decrease in Ni, are likely a result of the significant role for olivine in controlling the composition of primitive magmas. Lavas with high-MgO (>10 wt% MgO) can probably be attributed to olivine accumulation, since these are commonly phenocryst-rich ankaramites. The linear decrease in Ni contents below 10 wt% MgO should be attributed to olivine fractional crystallisation, although this trend's point of inflection at 6 wt% MgO is accompanied by the disappearance of olivine in thin section. This initial olivine crystallisation would be accompanied by clinopyroxene and titanomagnetite crystallisation, producing negative linear trends in Fe_2O_3T, TiO_2 and CaO that continue beneath 6 wt% MgO. While kaersutitic amphibole is common in evolved magmas (<6 wt% MgO), its compositional similarity to the ubiquitous clinopyroxene is likely to mask its role in fractional crystallisation. The most evolved magmas (<3.5 wt% MgO) show decreasing P_2O_5 contents, likely to result from fractionation of apatite. The linear increase in Sr with decreasing MgO appears to indicate that feldspar fractionation has not played a major role in the evolution of these magmas. However, while fractional crystallisation is the aggregate control on magmatic evolution over the combined period of interest, on the basis of petrographic textures we propose that the position of individual lava samples on such trends are more likely to result from discrete stages (particularly magma-mixing events) within their magma batch's process of transport, ponding and migration.

6.6.2 THE MAGMATIC EVOLUTION OF POST-COLLAPSE *BEJENADO*

Previous studies have suggested that oceanic island collapses may have an impact on the process of melt production. On Tahiti-Nui, Hildenbrand et al. (2004) described changes in mantle source signature following a collapse at ≈870 ka, with the eruption of post-collapse lavas with more radiogenic Nd and less radiogenic Sr (i.e a more DMM-like compositon). This provides an interesting parallel to the DMM-like magmas observed at *Bejenado*. Furthermore, in a study on Tenerife, Longpré et al. (2009) proposed that the effect of a collapse on an oceanic island would result in a process comparable to the post-glacial unloading of Iceland at the end of the Pleistocene (≈12 ka), where it has been widely observed (Gee et al., 1998; Jull and McKenzie, 1996) that deglaciation was accompanied by eruption rates 30-50 times higher than in more recent times.

There are therefore precedents for interpreting our results from *Bejenado* in the context of decompression-related disruption of the deepest part of the magma supply. However, these previous studies both suggested that decompression-related melt production would be the key process responsible for unusual features, but after a lateral collapse these may be explained by at least two possible processes: 1) as the product of melt production processes, where decompression resulted in unusual conditions of partial melting, such as affecting separate lithologies in a heterogeneous source differently, or 2) as the product of reservoir and transport processes, where decompression may have resulted in unusual transport and ascent conditions, potentially allowing the products of the deep magma supply system to be erupted without the homogenisation that would otherwise be likely in a gradual ascent process.

In the following section we discuss the petrological observations from *Bejenado* and provide a possible explanation for the geochemical stratigraphy of *Bejenado*.

GEOCHEMICAL COMPONENTS WITHIN THE *BEJENADO* SUITE

On combined diagrams of incompatible element abundance and $^{206}Pb/^{204}Pb$ (Figure 6-16) the shared trends formed by samples from the Basal Ankaramite, BEP, TSP and *Montaña de la Hiedra* are most simply explained by treating these lava-units as the product of two compositional components: 1) an isotopically DMM-like component with low incompatible element contents, and 2) an isotopically young-HIMU component with high incompatible element contents (particularly HFSE). This is also consistent with the results of Sr, Nd and other Pb isotope systems (Figure 6-14, Figure 6-15) where they also form shared arrays. In addition to the products of these components, the primitive *West Bejenado* group and intermediate LREVP samples also have young-HIMU signatures, potentially being the product of two further compositional components.

The strongest signature of the DMM-like and incompatible element poor component is in samples from the Basal Ankaramites as well as the BEP's Glomerocrystic Ankaramite lava-unit. On La Palma magmas with such strong DMM-like signatures are almost exclusively associated with post-collapse volcanism, so it is worth considering how this component may be causally associated with the

collapse. If the causal process responsible for the unusual features of these magmas had been decompression in the zone of melt production then it would be likely to have resulted in a higher degree of partial melting. Changes in degree of partial melting can be studied through the abundances of moderately incompatible elements (MICE) relative to very incompatible elements (VICE). Within a group of magmatic samples sourced from a common parent lithology, a suitable VICE/MICE ratio should decrease with increasing degree of partial melting as the relative contribution of the MICE component to the magma increases. Among *Bejenado* rocks (Figure 6-13C+D) these DMM-like samples have low Zr/Y (a HFSE MICE/MICE) and form a group with the lowest La/Sm (a REE VICE/MICE). It is difficult to argue that these DMM-like rocks are the product of unusually high degrees of partial melting for La Palma when their results are compared with samples from pre-collapse *El Time* (Figure 6-8C+D) since many of these have similarly low Zr/Y and La/Sm. We have no reason to expect these *El Time* samples to be the product of unusual partial melting conditions. Alternatively, if the causal process responsible for these magmas' unusual characteristics had been the preferential melting of a specific lithology wihin a heterogeneous source, then it is surprising that the Ba/Nb, Nb/U and Ba/Rb (Figure 6-13A+B) of these DMM-like magmas all lie towards the median of the *Bejenado* suite. Such canonical "constant ratio" incompatible element pairs would be expected to provide an indication of differences in source lithology (Hofmann, 2014), but these magmas show typical compositions for their region. It therefore appears unlikely that the DMM-like, incompatible element poor magma was the product of an extreme change in either melt-forming conditions or source-lithology as a result of decompression.

The isotopically young-HIMU component with high incompatible element contents is strongest in samples from the TSP eruptive phase and *Montaña de la Hiedra*. These samples fall within typical isotopic ranges for lavas from northern and central La Palma (*Taburiente,* Figure 6-15*)*, but have unusual incompatible element profiles for our study. Their HFSE contents are proportionately high compared to LILE contents (Figure 6-12), a feature that results in low Ba/Nb (Figure 6-8, Figure 6-13). Conversely, their Zr/Y and La/Sm are among the highest of the suite.

The opportunistic group of primitive *West Bejenado* samples and the combined products of the intermediate LREVP eruptive phase are a small and stratigraphically poorly-constrained suite so it is difficult to resolve whether these form two separate components or are the combined product of a mixing trend. Both possess similar young-HIMU isotopic signatures to the previously discussed component (compared to which the $^{143}Nd/^{144}Nd$ of LREVP lavas is slightly low, and of *West Bejenado* lavas is slightly high), but have lower incompatible element contents. They do not generally form a combined cluster in terms of pairs of incompatible elements (Figure 6-13), although among them are the samples with the highest Ba/Nb and lowest Zr/Y and La/Sm.

THE ROLE OF MAGMA SUPPLY SYSTEM PROCESSES IN CONTROLLING THE GEOCHEMISTRY OF *BEJENADO* MAGMAS

The numerous correllations that exist between radiogenic isotopes and the absolute concentrations of individual elements (Figure 6-16A-E) are among the most surprising results of this geochemical study, since they indicate that the samples in the middle of these trends must have formed through hybridisation in the magma transport system. On the TAS diagram (Figure 6-11) the strongly DMM-like rocks with low incompatible element contents are all primitive basanites, while the young-HIMU incompatible element rich rocks of the TSP are all evolved phono-tephrites. In order to have produced the linear trends between radiogenic isotopes and absolute element concentrations the end-members must have mixed together after the more evolved (phono-tephritic) component had differentiated. These end-compositions are therefore best interpreted as two discrete magma batches with contrasting radiogenic isotope signatures. These contrasts allow the determination of each batch's contribution to each sample. The linear trends include samples from both the earliest and latest stages of *Bejenado's* growth, indicating that these magma batches were involved in reservoir system processes throughout the post-collapse phase of volcanism.

This does not preclude these magmas having each originated through separate melt production processes in an isotopically heterogeneous mantle — this must have occurred — but indicates that a major magma-hybridisation process has overprinted much of the petrological information about their origins. However, the young-HIMU magma batch had an evolved composition before hybridisation began and therefore it cannot be assumed that its relative incompatible element abundances, or those resulting from mixing it with other magma batches, are purely the result of melt production (Figure 6-12). In contrast, the characteristic incompatible element contents of the primitive DMM-like magma batch are more likely to reflect their initial source and melt production profile.

Petrographic study of the hybrid magmas that result is therefore revealing, since at the point of mixing they had distinctive mineralogies and characteristics[34]. Both units of strongly DMM-like magmas are ankaramitic with a crystal cargo that probably originated in a cumulate disruption process before mixing began, while the most evolved rocks from the TSP and those from *Montaña de la Hiedra* contain abundant crystal clots of tabular pyroxene, this batch may previously have been an evolved crystal mush. The TSP's Amphibole Olivine Tephrite lava-unit lies at the midpoint of the linear mixing trends and contains both euhedral olivine and near euhedral amphibole. Since these two minerals would not usually be found in equilibrium with the same magma their joint presence illustrates this sample's origin as a hybrid.

There is also significant evidence of wall rock assimilation in the LREVP and *West Bejenado* groups of samples. Both units contain xenoliths, micro-xenoliths and abundant disaggregated crystals sourced from a lithology rich in kaersutite amphibole and pyroxene, typically hosted in a primitive basanitic

[34] Appendix D: Supplementary petrology — petrography of sample groups from *Bejenado* used in Chapter 6. pp. 247-255.

magma. The presence of mechanically re-worked crystals and evidence for resorption of amphibole indicates that assimiliation contributed to the magmatic evolution of these units. If these magmas were crystallising at this point then this is likely to have been accompanied by fractional crystallisation (AFC processes). Further study would be required to determine the contribution of wall rock material to the whole rock composition of the resulting samples. Isotopically, these two groups of samples may reflect one or possibly two further magma batches produced from La Palma's young-HIMU dominated source component.

POST-COLLAPSE MAGMATIC ACTIVITY ON LA PALMA

This evidence of two mineralogically distinctive magma batches contributing to eruptions throughout *Bejenado's* stratigraphy leads us to suggest that throughout the post-collapse phase there was an ongoing major reservoir system process beneath La Palma. The relative contribution of each of these batches to the products tapped by the volcano oscillated from its earliest to its latest stratigraphic units (Figure 6-13F), with a minor contribution at an early stage by the potentially different magmas tapped by the LREVP and *West Bejenado* units. *Bejenado* was therefore either a single continuous eruption or a single intermittent eruptive cycle.

A characteristic feature of *Bejenado* volcanism is the eruption of extremely heterogeneous magmatic units. All units we have studied are either the product of the main magma hybridisation process or they contain abundant mafic xenoliths. In some cases both heterogeneities are observed. The volcano therefore provides a rare opportunity to study the varied and tangible contents of an ocean island's deep magma supply. It is reasonable to attribute much of this complexity to post-collapse disruption, since decompression may have led to unusually favourable ascent conditions, allowing material to be erupted without complete hybridisation or assimilation.

In spite of the presence of isotopically unusual DMM-like basanites, there is relatively little evidence preserved of post-collapse melt production. The role of highly evolved magmas and presence of wall-rock in the units with more young-HIMU compositions indicates that they formed well before the major reservoir-system hybridisation process, and are therefore likely to have undergone partial melting before the *Cumbre Nueva Collapse*. Detailed study of the DMM-like basanites may potentially provide insights into post-collapse melt source processes but even among these samples there is abundant evidence of incorporated xenocrystic material. The unusual isotopic composition of the DMM-like magma batch appears to hold out the tantalising prospect of the collapse having affected the deep melt producing region of the Canarian hotspot, but there is surprisingly little information preserved about this process in the petrological record. As a result, we propose that post-collapse disruption of the magma transport system played a larger role in controlling the composition of these eruptive products than any changes in the melt source.

6.8 CONCLUSIONS

The results of this study lead us to emphasise the importance of detailed field relations and petrography to whole-rock petrogenetic studies of oceanic island lavas. Without geological constraints there is potential for both sampling artefacts and the noise resulting from magma transport processes to mask petrologically meaningful differences that would be readily observeable in field studies through changes in lithology. This study indicates that the *Cumbre Nueva Collapse* was followed by a brief period of intense volcanism that involved isotopically unusual and intensely mixed magmas. Our key findings are:

1) Comparative study of samples from *El Time* and *Bejenado*, the two edifices whose volcanism most closely brackets the *Cumbre Nueva Collapse*, show no meaningful discrimination in terms of petrographic groups, incompatible trace element compositions or Sr, Nd and Pb radiogenic isotope data.
2) *Bejenado* is a petrologically complex volcano and its best exposed, upper, eruptive units show strong evidence of being isotopically heterogeneous, with evidence for the involvement of both a DMM-like component and a young-HIMU component with high incompatible element contents.
3) Most *Bejenado* lavas lie on geochemical trends between a specific DMM-like component with low incompatible element contents, and a specific young-HIMU component with high incompatible element contents. Since these form linear trends when radiogenic isotopes are plotted against absolute element concentrations and the resulting end-members show very different degrees of differentiation, these trends appear to be the product of erupting mixtures of two isotopically contrasting magma batches.
4) The isotopic composition of the DMM-like magma batch is extremely unusual on La Palma. The resulting lavas tend to be primitive basanites that form *Bejenado's* most voluminous, ankaramitic, lava-units. The presence in the post-collapse phase of such an isotopically unusual magma batch is probably the result of the collapse and may have been the product of melt production after collapse-related decompression. Nonetheless, there is little petrological information preserved about this process.
5) The young-HIMU dominated magma batch with high incompatible element contents had an evolved composition before mixing. Its presence is strongest in *Bejenado's* late eruptive units and is dominant in the lavas found at the TSP and *Montaña de la Hiedra* vent cluster. This magma batch has particularly high HFSE contents, and tends to form pyroxene dominated crystal clots. This magma batch is likely to have existed before the *Cumbre Nueva Collapse*.
6) The resulting linear trends include samples from both the earliest and latest stages of Bejenado's growth, indicating that these magma batches were involved in a major reservoir system process that persisted throughout the post-collapse phase of volcanism.

Chapter 7 : SYNTHESIS

7.1 INTRODUCTION

This thesis was intended to investigate the magmatic products linked to La Palma's *Cumbre Nueva Collapse* using a multi-disciplinary approach that combined field volcanology, lava-flow petrology and whole rock magmatic geochemistry. It was aimed at determining whether this combination would yield more insights than each sub-discipline was likely to produce on its own. It has presented detailed new field evidence, $^{40}Ar/^{39}Ar$ geochronology data, detailed petrographic characterisations, mineral chemistry (EPMA), cpx-melt thermobarometry and whole rock elemental (XRF) and radiogenic isotope analysis (Sr, Nd, Pb).

Each results chapter of this thesis was intended as a self-contained body of work, with its own discussion, literature review and conclusions, and this choice reduces the need for a final thesis discussion. This synthesis therefore has two main aims: 1) to review the strengths and weaknesses of an integrated geological approach to oceanic island magmatism, 2) to review in combination the results from our study of the magmatic products linked to the *Cumbre Nueva Collapse*. Sections addressing these issues will be followed by a summary of our interpretation of collapse-related magmatism and then a suggestion of further work. In some sections this synthesis necessitates the use of a more informal voice than was used in earlier chapters.

OVERVIEW OF THE MAIN RESULTS FROM PREVIOUS CHAPTERS

In studying the magmatic products of this period, the study has: 1) conducted detailed fieldwork on the post-collapse *Bejenado* volcano, as well as reconnaissance field study and sampling of *Taburiente's* pre-collapse *El Time* region, and supported this with new $^{40}Ar/^{39}Ar$ dates, 2) studied samples from the newly identified Bejenado Effusive Phase (BEP) lava flow-field to reconstruct processes in the island's magmatic reservoir system in the period after the *Cumbre Nueva Collapse*, 3) performed elemental and radiogenic isotope analysis on two suites of lava samples from *El Time* and *Bejenado*. This was conducted with an opportunistic approach in which each method was focused on the local features that were regarded as having the greatest research potential.

In combination, the findings of the three results chapters enable us to interpret them beyond their individual conclusions:

1. *Bejenado* is comprised of a remarkably small number (≈7) of petrologically distinctive units and stratigraphic 'eruptive phases': The *Bejenado Lower Series*, *West Bejenado*, *Los Rodeos Evolved and Volcaniclastic Phase,* the *Bejenado Effusive Phase*, the Terminal Sheet Phase and *Montaña de la Hiedra*. The difference between $^{40}Ar/^{39}Ar$ dates of samples from the earlier of these indicates *Bejenado* was emplaced sufficiently rapidly that our radiometric determinations likely provide an upper limit for its duration, and the period of volcanism is difficult to constrain within the limits of current instrumental precision.

2. Samples from the petrologically very distinctive rocks of the Bejenado Effusive Phase indicate that all the products of this eruptive phase were the result of tapping different stages of a progressive, ongoing process in the magma reservoir system.
3. The shared linear trends formed by samples from Basal Ankaramite, BEP, TSP and *Montaña de la Hiedra* units on whole rock diagrams[35] that combine incompatible element abundances and $^{206}Pb/^{204}Pb$ compositions indicates that throughout *Bejenado's* eruptive sequences eruptions were the product of hybridisation between a primitive isotopically DMM-like magma batch and an isotopically young-HIMU magma batch with an evolved composition. Together these results lead us to propose that *Bejenado* was largely the product of tapping a continuous magma reservoir system process that was directly related to the collapse.
4. The scarcity of palaeosols across the volcano, combined with the brief duration of activity determined by geochronology, lead us to suggest that this volcano may best be interpreted as one continuous complex eruption or a single eruptive cycle.
5. Therefore, following the *Cumbre Nueva Collapse,* a major continuous reservoir system process began that subsequently contributed to most *Bejenado* eruptions. This *Bejenado* phase of post-collapse volcanism was characterised by dynamic magmatic processes at all depths, with rapid emplacement of large lava flow-fields, intense mixing in the reservoir system, and isotopically unusual magmas emerging from deep within the magma supply system.

These are striking results, and put the author of this study in a difficult position. While we believe this interpretation is robust, a number of sections presented in this thesis are inevitably weak due to the limitations of a work conducted for a PhD thesis. If these processes occur as we describe, with post-collapse disruption leading to unusual activity throughout an island's magma supply system, and being best observed through study of the products of the intense eruptive activity that results, then this has potential to impact on our wider understanding of Canarian-type volcanism. As a result, these claims should be treated as provisional, and require confirmation through further study.

7.2 Integrated study of an oceanic island's magma supply system

Field volcanology and whole rock geochemistry (particularly the study of Sr, Nd and Pb isotopes) provide two almost completely independent frameworks (Self et al., 1998; Zindler and Hart, 1986) for studying the eruptive products of oceanic islands. These either treat processes downwards from the top, by interpreting results in terms of a single edifice's specific features, or upwards from the bottom, by interpreting results in terms of mantle components and melt-producing lithologies. This

[35] 6.5 Results, part 2: post-collapse variation presented by stratigraphic unit. pp.166-169

thesis was intended to determine if sufficiently detailed integrated study could produce one combined framework anchored in field relationships.

THE VALUE OF HAVING CONDUCTED AN INTEGRATED STUDY

It would not have been reasonable to have made the previous claims without providing all the forms of evidence used in this study, indicating that integrated study has some merit. However, several fortuitous features of *Bejenado* meant it was unusually suitable for this combined multi-disciplinary approach.

The relatively unstudied nature of the *Bejenado* edifice, and the relatively extreme radiogenic isotope compositions observed in some samples previously taken from it, were recognised before fieldwork began and on this basis we expected a combined field and geochemical study to be rewarding. This has proved to be the case. Detailed field volcanology and whole rock geochemistry have provided independent, but generally mutually supportive, means of determining the relationships between eruptive units. Prior to field study, *Bejenado's* unusual radiogenic isotope geochemistry had to be treated in terms of opportunistic sampling with ambiguous age relationships, while prior to geochemical study it was unclear that four of its stratigraphic units (*Bejenado Lower Series*, BEP, TSP and *Montaña de la Hiedra*) were the product of a shared reservoir system process. In particular, the petrological similarities of some samples from the TSP and *Montaña de la Hiedra* are sufficient that they were both likely to have been the products of erupting the same magma, providing a significant constraint on the potentially ambiguous field relationships observed between these units. This independently confirms the field interpretation and trends in the geochemical study and demonstrates the value of evidence drawn from opposite ends of the magma supply system.

But, the small number of stratigraphically distinct eruptive phases identified made mapping and representative sampling of this volcano much less demanding than would be the case on a larger shield volcano such as the *Cumbre Vieja* or *Taburiente*. Furthermore, the diversity present among *Bejenado's* eruptive products, with porphyritic lava-units of both primitive and highly evolved composition found throughout its stratigraphy, was unexpected and both made field-study easier (it led to very distinctive lithologies) and provided material for a petrological study of the island's magma reservoir system.

Combining whole rock geochemistry and detailed petrography has proved rewarding, and we believe this is because the shared processes in the magma reservoir system have allowed the common textures observed in the multiple resulting lava-units to give physical, observational context to abstract geochemical trends. Whether this shared petrological context is because *Bejenado* is the result of a single continuous eruption, or a longer episodic eruptive cycle that resulted from the collapse, in the Canary Islands the best parallel to such shared source-reservoir-eruption relationships is likely to be the heterogeneous products of individual eruptions. Previous

studies of La Palma's historic eruptions (Barker et al., 2015; Johansen et al., 2005; Klügel et al., 2000) indicated that individual eruptions provide a natural scale at which to study deep processes within oceanic islands since they are each the product of a discrete series of events in the reservoir system (Klügel et al., 2005). Studies focused on the products of shared reservoir system processes potentially provide a means of eliminating the non-analytical compositional scatter that has been observed in previous studies of La Palma and the western Canary Islands (Day et al., 2010; Galipp, 2005). Sources of uncertainty traditionally invoked in whole rock studies of mantle geochemistry – such as the role of crustal contamination – can potentially be eliminated if petrology can provide a sufficiently detailed understanding of processes in the reservoir system.

THE DISADVANTAGES OF A MULTI-DISCIPLINARY APPROACH

Conducting all three approaches concurrently inevitably led to difficulties, despite being central to our method. Early strategic decisions shaped the application of each approach, while in combination the project became logistically demanding.

In having initially selected the *El Time* inland headland and the *Bejenado* edifice as the scale of study, the specific field relations of these areas inevitably dictated the shape of research, and the opportunistic approach to fieldwork in a study of this type (only conducting focused work in areas where field study was likely to resolve a regional geological issue) resulted in some areas of central La Palma being neglected. This inevitably weakened other parts of the study. For instance, the complete sample suite for both our geochronological age determinations and geochemical analyses would have benefitted from unambiguous age-relationships. This would ideally have involved mapping *El Time* and logging and sketching of the *Barranco Jurado* lava sequence (although extensive cultivation means that *El Time* is not quite as suitable as *Bejenado* for fieldwork). Combined with analytical data, this could potentially have provided as detailed an understanding of the pre-collapse period as we have obtained for the post-collapse period. But, producing such a flow-field scale map of *El Time* would not have represented a worthwhile self-contained research project. Similar problems occurred with western *Bejenado*, an area in which focused fieldwork appeared to be unfeasible due to its formidable terrain.

Furthermore, collecting samples for whole rock geochemistry before a full stratigraphy of each region had been determined often led to multiple samples being collected unintentionally from the more laterally extensive eruptive units. This increased the sample size for geochemical study, increasing the labour and laboratory costs of the project, and subsequently made it difficult to justify the selection of only one sample from each group without giving the appearance of cherry-picking. We hope that by presenting all data in an appendix, we have sufficiently justified why these samples were not used in graphs or interpretation.

As a result of such strategic and logistical difficulties, we would suggest that an integrated approach requires a team effort and should not in future be largely implemented by a single researcher.

SOME CONSIDERATIONS FOR ANY FUTURE INTEGRATED STUDIES

In light of these methodological findings, we propose a number of guidelines for studies of this type:

1. The products of discrete magma reservoir system processes provide a natural scale at which to sample and study deeper magmatic processes within individual Canarian-type islands. Such processes may be most easily recognised by studying the products of individual petrologically heterogeneous eruptions (composed of multiple porphyritic lava-units).
2. Each disciplinary component of the study should be as self-contained as possible. This particularly benefits whole rock magmatic geochemistry, since the likelihood of structured variation in radiogenic isotope composition is difficult to determine before analysis.
3. Geological mapping using 1: 10 000 scale field slips remains the best way of determining a volcanic stratigraphy, and the resulting unambiguous age relationships can benefit geochemical, petrological and geochronological studies. Where this stratigraphic resolution is insufficient for addressing the research problems, combined morphological and petrological logging of lava flows can also provide robust age relationships.
4. Detailed textural description of multiple samples from porphyritic lava-units in a well-mapped lava flow-field can provide a means of determining subtle changes in the magmatic reservoir system processes that contributed to an eruption, and can potentially tie field relationships to the geochemical trends that emerge from deeper in the system.
5. Determining Sr, Nd and Pb radiogenic isotope compositions remains a necessary part of an oceanic island whole rock magmatic geochemistry study, since such data provides context to other geochemical relationships by allowing it to be interpreted in terms of mantle component models.

7.3 THE MAGMATIC PRODUCTS LINKED TO THE *CUMBRE NUEVA COLLAPSE*

In this section we address each chapter's main conclusions in the context of the findings as an integrated study, to determine how each sub-discipline impacts on our understanding of the period of interest.

A REVIEW OF THE RESULTS OF FIELDWORK AND GEOCHRONOLOGY IN THE CONTEXT OF OF AN INTEGRATED STUDY

The main conclusions presented in chapter 4:

1) We provided a new age estimate of ≈530ka for the *Cumbre Nueva Collapse*, based on $^{40}Ar/^{39}Ar$ dating of stratigraphically-sourced lava flows.
2) We presented a reconnaissance map and detailed stratigraphy for the eastern sector of *Bejenado*, accompanied by the first systematic description of this volcano's eruptive units.

3) On the grounds of reconnaissance mapping and unit-by-unit descriptions, *Bejenado* is composed of ≈5-7 eruptive units. New $^{40}Ar/^{39}Ar$ age determinations indicate that *Bejenado's* activity ended after 496 ±16 ka. Together, these results mean *Bejenado* was emplaced rapidly after the collapse.
4) We presented the first identification and description of the major Bejenado Effusive Phase (BEP) and *Los Rodeos Evolved and Volcaniclastic Phase* (LREVP) eruptive units. The BEP is a major, morphologically complex, flow-field composed of multiple lava-units. The pyroclastic LREVP is a complex, tephritic, eruptive unit with multiple strombolian vents and is associated with a major phreatomagmatic deposit.

These substantial findings largely remain robust when combined with our petrological and magmatic geochemical studies. In general, the results of petrological study have clarified the relationship between the lava-units observed in the BEP, while whole rock geochemistry has provided independent confirmation of the number of stratigraphic units identified in the field (such as the flows sampled opportunistically from *West Bejenado*).

However, in the context of the shared reservoir system processes determined in petrological and geochemical studies, many features of *Bejenado* may need to be reinterpreted. There are few known precedents for eruptive cycles in the Canary Islands, and thus shared reservoir system processes have previously only been observed in the products of individual eruptions, such as the 1730-1736 eruption on Lanzarote (Solana et al., 2004). This and any similar eruptions (the ongoing long-lived eruption of *Kilauea* may also share some characteristics with this) may provide the best parallel to what we observe at *Bejenado*.

In mapping a topographically complex shield volcano, the most natural stratigraphic units are the products of separate eruptions bounded by eruptive hiatuses. At *Bejenado* it was initially assumed that the major differences observed in lava petrology, morphology and lithological characteristics were the result of different eruptions with considerable intervals between them. However, without observed palaeosols and in the context of a brief eruptive cycle or one continuous eruption, the differences between individual petrological and morphological units are more likely to reflect changes in eruptive style caused by either changes in magma reservoir processes or changes in surface volcanism. If this is the case the contacts between them would ideally now be re-assessed in the field. The significance of such a change in interpretation is best illustrated by the boundary between LREVP and BEP units at *Los Rodeos*, where a fine-grained laminar lapilli tuff of phreatomagmatic origin (LREVP) is overlain by effusive aa flows (BEP) and no paleosol has been observed. If the LREVP unit is phreatomagmatic, then a surface process involving the presence or absence of water must have had a role in this lithological change. Further work would be beneficial in determining whether these two eruptive units are both the products of a common magma-batch.

A single-eruption or eruptive cycle interpretation of *Bejenado* also has implications for understanding the wider the geology of central La Palma. Previous gradual, erosional, models (Carracedo et al., 1999a; Colmenero et al., 2012; Roa, 2003) for the early stages of growth of *Caldera de Taburiente* will need to be revised if *Bejenado* was emplaced in a single episode of volcanism. How erosion began at the *El Riachuelo* canyon to *Bejenado's* east and the *Caldera de Taburiente* to its north will need to be reassessed if rapid resurfacing was taking place in the *Valle de Aridane,* shortly after a multi-vent, explosive, phreatomagmatic phase.

A REVIEW OF THE PETROLOGICAL RESULTS WITHIN THE CONTEXT OF AN INTEGRATED STUDY

The main conclusions presented in chapter 5:

1) The Bejenado Effusive Phase flow-field was the product of at least three magma-batches that crystallised and mixed in reservoirs located between the lithospheric mantle and the oceanic crust in the period when this system was disrupted after the *Cumbre Nueva Collapse*.
2) The Glomerocrystic Ankaramite lava-unit, a highly porphyritic, large volume lava forming the base of the BEP sequence, is likely to be the result of a pulse of primitive magma that disrupted a pre-existing olivine-diopside lithology located in the lithospheric mantle.
3) The Plagioclase Basalt lava-unit, a porphyritic and unusually feldspar-phyric lava, appears to be the result of super-saturated crystallisation of this primitive magma under dynamic conditions.
4) The Plagioclase Tephri-phonolite lava-unit, an evolved unit showing strong petrographic evidence of mixing between multiple magma-batches, may have resulted from mixing of these two early magma-batches with a more evolved, phonolitic, crustal reservoir during its ascent.
5) Magmatic degassing may have been involved in these processes. This would help explain both the mobilisation and disruption of the olivine-diopside lithology, as well as the super-saturation of plagioclase and clinopyroxene. If this occurred it is also likely to have resulted from post-collapse decompression.

These results largely remain robust in the context of field relations. The BEP flow-field was selected for focused study and sampled at the end of the last field campaign and therefore its context cannot be changed by subsequent field results. It was chosen because the continuous pahoehoe sequence and the multiple lava-units present within it appeared ideal for allowing any petrological results to be interpreted stratigraphically.

However, this was before the field relations of *Bejenado* had been fully interpreted. Subsequent results from whole rock geochemistry indicate that the distinction between the BEP unit and the overlying TSP sequence was largely morphological, and the results of combined study indicate that all of *Bejenado* appears to be the product of one petrological process. The BEP flow-field, rather

than being one discrete eruptive unit, may be a middle-stage in a larger sequence and therefore a petrological study that addresses just this eruptive phase is inherently incomplete. Resolving this would ideally involve adapting the petrological chapter to include the three lava-units of the TSP, now known to lie on the same hybridisation trend (Figure 6-16). Unfortunately, this would require both further fieldwork (to determine the nature of the transition between the BEP's late Plagioclase Tephri-phonolite lava-unit and the TSP's early Amphibole Tephrite lava-unit) as well as further microanalysis to determine mineral chemistry within TSP samples.

Furthermore, the BEP sequence is separated from the base of the post-collapse lava succession by a considerable thickness (>150m) of earlier erupted lavas. These sequences are practically inaccessible, and have not been studied to the same resolution as the later sequences. However, this separation limits our ability to interpret the BEP unit's petrological and geochemical complexity in terms of the collapse.

The results of whole rock magmatic geochemistry also raise concerns about the interpretion of petrological units. We adopted the convention of identifying lithological units in the field as "lava-units" and those that petrographic study indicated were likely to be the product of discrete reservoir processes as "magma batches". The result was a model (Figure 5-15) that treated the Plagioclase Tephri-phonolite as a distinct magma batch stored at shallower depth than the complex Glomerocrystic Ankaramite and Plagioclase Basalt reservoir process. However, the trends identified between primitive, DMM-like and evolved, incompatible element rich, young-HIMU magmas indicate that all three BEP petrological units lie on a single shared isotopic mixing trend that persists into the overlying TSP. A distinctive radiogenic isotope signature probably provides the best genetic means for identifying magmatic units from the melt-source, and in that case there would only be two magma-batches involved in this part of the *Bejenado* eruptive sequence. We believe there may be a meaningful distinction to be drawn between "source magma batches" as isotopic units that originate from the melt source and feed reservoirs, and "reservoir magma batches" as those with shared textural characeristics that ascend and feed eruptions. However, resolving the differences that emerge between whole rock and petrological perspectives on reservoir system processes is a major task and requires significant further work.

A REVIEW OF THE RESULTS OF MAGMATIC GEOCHEMISTRY IN THE CONTEXT OF AN INTEGRATED STUDY:

The main conclusions presented in chapter 6:

1) Comparative study of samples from *El Time* and *Bejenado*, the two edifices whose volcanism most closely brackets the *Cumbre Nueva Collapse*, showed no meaningful discrimination in terms of petrographic groups, incompatible trace element compositions or Sr, Nd and Pb radiogenic isotope data.

2) *Bejenado* is a petrologically complex volcano and its best exposed, upper, eruptive units show strong evidence of being isotopically heterogeneous, with roles for a DMM-like component and a young-HIMU component with high incompatible element contents.
3) Most samples of *Bejenado* lavas lie on geochemical trends between a specific DMM-like component with low incompatible element contents, and a specific young-HIMU component with high incompatible element contents. Since these form linear trends when radiogenic isotopes are plotted against absolute element concentrations and the resulting end-members show very different degrees of differentiation, these trends appear to be the product of erupting mixtures of two isotopically contrasting magma batches.
4) The isotopic composition of the DMM-like magma batch is almost unique on La Palma. The resulting lavas tend to be primitive basanites that form *Bejenado's* most voluminous, ankaramitic, lava-units. The presence in the post-collapse phase of such an isotopically unusual magma batch is probably the result of the collapse and may have been the product of melt production after collapse-related decompression. Nonetheless, there is little petrological information preserved about this process.
5) The young-HIMU dominated magma batch with high incompatible element contents had an evolved composition before mixing. Its presence is strongest in *Bejenado's* late eruptive units and is dominant in the lavas found at the TSP and *Montaña de la Hiedra* vent cluster. This magma batch has particularly high HFSE contents, and tends to form pyroxene dominated crystal clots. This magma batch is likely to have existed before the *Cumbre Nueva Collapse*.
6) The resulting linear trends include samples from both the earliest and latest stages of Bejenado's growth, indicating that these magma batches were involved in a major reservoir system process that persisted throughout the post-collapse phase of volcanism.

As the last of the results chapters to be presented, there is little here that needs to be re-assessed in terms of the combined results of integrated study. However, the structure of this chapter itself is a result of the integrated approach, with the contrast between regional suites of whole rock geochemical samples (which would have led to a negative result) being supplemented by a stratified edifice-scale study where samples are plotted in terms of stratigraphic unit. The more informative edifice-scale study was the result of plotting opportunistically collected samples in terms of their later-constrained stratigraphic position.

One of the aims of this study was to determine whether integrated study has the potential to take the results of a study of whole rock magmatic geochemistry, a discipline usually interpreted in terms of source lithologies and mantle component models, and anchor its findings to unambiguous field and age relationships. Unfortunately mantle geochemistry is best at determining compositional differences that are known to be independent of transport processes, and thus in order to integrate

its findings with petrological studies of reservoir systems the petrological models must be unusually robust. Our study is not yet sufficiently comprehensive to allow our source geochemical processes to be anchored to the more detailed reservoir system processes. Nonetheless, hybridisation trends observed in radiogenic isotope data can be linked to sequences observed in field relationships, and a textural record exists of this hybridisation process. We believe that integrated study should be able to eliminate issues that blur between source and transport processes, such as "crustal contamination" which coud be identified as an assimilated component in the petrological record. Generally, it would require a study with tightly constrained stratigraphic units, detailed petrographic descriptions and extremely robust geochemical data to allow all parts of this system to be integrated.

Nonetheless, if we regard *Bejenado* as the product of an ongoing post-collapse progressive reservoir system processes and its most primitive magma-batch was the DMM-like basanites, it becomes increasingly reasonable to argue that this magma batch was the result of partial melting soon after the collapse, with this context resulting in its unusual isotopic signature. Further work needs to be done to investigate this process, but we propose that the effects of collapse-related decompression may have penetrated into the melt source.

7.4 A SUMMARY OF COLLAPSE-RELATED VOLCANISM ON LA PALMA

Prior to this study, La Palma's lava sequences most closely related to the *Cumbre Nueva Collapse* had been relatively poorly studied. The geometry of the collapse structure had been debated (Ancochea et al., 1994; Carracedo et al., 1999a) and samples from flows bracketing the collapse had been dated (Guillou et al., 2001), but the flow-fields exposed at *El Time* and *Bejenado* had not been subject to focused work. The structural model for Canarian-type volcanism (Carracedo, 1994) suggested that the collapse resulted from endogenous processes within the edifice, as the accretion of lava flows caused the flank to become increasingly unstable. *Bejenado* was commonly described as the remains of a stratovolcano (Roa, 2003) constructed over a period of "a few tens of thousands of years" (Carracedo et al., 2001).

This study leads us to suggest that the collapse ended a period of relatively typical volcanic re-surfacing along the *Paleo-Cumbre Nueva Rift,* consistent with an endogenous collapse model. However, the collapse was followed, after a brief hiatus when sedimentary processes dominated, by focused volcanism within the collapse structure above the remains of the *Paleo-Cumbre Nueva Rift's* dyke swarm. The result was the major, possibly continuous, *Bejenado* episode, an intensely complex magmatic period resulting from an ongoing process in the reservoir system and dynamic activity in all parts of the magma supply system.

At the surface, the result was an eruptive episode focused at numerous vents, with explosive periods of phreatomagmatic activity as well as prolonged, large volume, effusive phases. The

characteristics of the episode were in-part controlled by considerable variations in magmatic composition, including a range of degrees of differentiation from basanites to tephri-phonolites. This variation was a result of equally dynamic and complex processes in the island's magma reservoir system, located in the shallow lithospheric mantle. Reservoir processes included the disruption of olivine-clinopyroxene lithologies, super-saturated crystallisation of feldspar and clinopyroxene, mixing between primitive and evolved magmas, as well as assimilation of amphibole-bearing lithologies. The most primitive of these magmas possessed a radiogenic isotope signature almost uniquely depleted for La Palma lavas, indicating the effects of the collapse penetrated into the deepest part of the magma-supply system. The initial ascent of this magma appears to have been the earliest event in the post-collapse phase, and led to all that followed. The lava flow-fields of the resulting volcano provide a unique opportunity to study the products of deep magma-supply system processes on a Canarian-type oceanic island.

When this focused and complex eruption ended, volcanism migrated southwards to begin forming the currently active *Cumbre Vieja* volcano.

7.5 FURTHER WORK

Many of the findings of this study would benefit from confirmation through further work. If true, our rapid interpretation of the *Bejenado* edifice as the product of a small number of large eruptive episodes changes the regional context in which erosion initiated in *Caldera de Taburiente.* We suggest that the relationship of *Bejenado* to *Caldera de Taburiente* needs to be investigated, with a particular focus on the post-collapse volcanic units exposed within the basin's interior such as the *Roques* studied by Roa (2003). Furthermore, we believe that it needs to be determined whether this may have been a continuous eruption with a duration similar to Lanzarote's 1730-1736 episode or a longer eruptive cycle, and this is best determined through careful study of the contacts between eruptive phases.

The detailed petrological study of the Bejenado Effusive Phase would ideally be extended into the lavas of the Terminal Sheet Phase, allowing a complete reconstruction of the reservoir system processes that contributed to this late effusive period. There is considerable potential in this sequence for the application of modern quantitative petrological techniques (determining magmatic H_2O, magma-mixing timescales, and the rates of magmatic ascent) to determine the chemical characteristics of the reservoir system processes that contributed to these lavas.

The unusual degree of reservoir-system context we have for the isotopically unusual, porphyritic, DMM-like basanites of *Bejenado* makes this magma batch a significant opportunity to study La Palma's mantle source, particularly focusing on the contrast with the the evolved, HFSE-rich, young-HIMU magmatic unit. Therefore, we suggest there may be benefits to extending our geochemical study into more radiogenic isotope systems (Hf, Os) and stable isotope systems (O, He). Anchoring

our magma-system lithologies to modern source lithology models would best be achieved through microanalytical studies of olivine chemistry and any melt inclusions hosted within them. This may allow us to determine whether this unit originated from pyroxenite or peridotite partial melting.

However, if the results of this study prove robust then this volcano is likely to provide an opportunity for research well into the future.

BIBLIOGRAPHY

Abdel-Monem, A., Watkins, N.D., Gast, P.W., 1972. Potassium-argon ages, volcanic stratigraphy, and geomagnetic polarity history of the Canary Islands; Tenerife, La Palma and Hierro. Am J Sci 272, 805–825. doi:10.2475/ajs.272.9.805

Abratis, M., Schmincke, H.-U., Hansteen, T., 2002. Composition and evolution of submarine volcanic rocks from the central and western Canary Islands. International Journal of Earth Sciences 91, 562–582. doi:10.1007/s00531-002-0286-7

Allard, P., Behncke, B., D'Amico, S., Neri, M., Gambino, S., 2006. Mount Etna 1993–2005: Anatomy of an evolving eruptive cycle. Earth-Science Reviews 78, 85–114. doi:10.1016/j.earscirev.2006.04.002

Ancochea, E., Hernán, F., Cendrero, A., Cantagrel, J.M., Fúster, J., Ibarrola, E., Coello, J., 1994. Constructive and destructive episodes in the building of a young Oceanic Island, La Palma, Canary Islands, and genesis of the Caldera de Taburiente. Journal of Volcanology and Geothermal Research 60, 243–262. doi:10.1016/0377-0273(94)90054-X

Anguita, F., Hernán, F., 2000. The Canary Islands origin: a unifying model. Journal of Volcanology and Geothermal Research 103, 1–26. doi:10.1016/S0377-0273(00)00195-5

Anguita, F., Hernán, F., 1975. A propagating fracture model versus a hot spot origin for the Canary islands. Earth and Planetary Science Letters 27, 11–19. doi:10.1016/0012-821X(75)90155-7

Barker, A.K., Troll, V.R., Carracedo, J.C., Nicholls, P.A., 2015. The magma plumbing system for the 1971 Teneguía eruption on La Palma, Canary Islands. Contributions to Mineralogy and Petrology 170, 1–21. doi:10.1007/s00410-015-1207-7

Blundy, J., Cashman, K., 2005. Rapid decompression-driven crystallization recorded by melt inclusions from Mount St. Helens volcano. Geology 33, 793–796. doi:10.1130/G21668.1

Blundy, J., Cashman, K., Humphreys, M., 2006. Magma heating by decompression-driven crystallization beneath andesite volcanoes. Nature 443, 76–80. doi:10.1038/nature05100

Branney, M.J., Kokelaar, B.P., 2002. Pyroclastic density currents and the sedimentation of ignimbrites, Memoir 27. Geological Society, London.

Burgisser, A., Bergantz, G.W., 2011. A rapid mechanism to remobilize and homogenize highly crystalline magma bodies. Nature 471, 212–215. doi:10.1038/nature09799

Carracedo, J.C., 1999. Growth, structure, instability and collapse of Canarian volcanoes and comparisons with Hawaiian volcanoes. Journal of Volcanology and Geothermal Research 94, 1–19. doi:16/S0377-0273(99)00095-5

Carracedo, J.C., 1994. The Canary Islands: An example of structural control on the growth of large oceanic-island volcanoes. Journal of Volcanology and Geothermal Research 60, 225–241. doi:10.1016/0377-0273(94)90053-1

Carracedo, J.C., Badiola, E.R., Guillou, H., De la Nuez, J., Pérez Torrado, F.J., 2001. Geology and vulcanology of La Palma and El Hierro, Western Canaries. Estud. geol. 57. doi:10.3989/egeol.01575-6134

Carracedo, J.C., Badiola, E.R., Guillou, H., Paterne, M., Scaillet, S., Torrado, F.J.P., Paris, R., Fra-Paleo, U., Hansen, A., 2007. Eruptive and structural history of Teide Volcano and rift zones of Tenerife, Canary Islands. Geological Society of America Bulletin 119, 1027–1051. doi:10.1130/B26087.1

Carracedo, J.C., Day, S., Guillou, H., Rodriguez Badiola, E., Canas, J.A., Perez Torrado, F.J., 1998. Hotspot volcanism close to a passive continental margin; the Canary Islands. Geological Magazine 135, 591–604.

Carracedo, J.C., Day, S.J., Guillou, H., Gravestock, P., 1999a. Later stages of volcanic evolution of La Palma, Canary Islands: Rift evolution, giant landslides, and the genesis of the Caldera de Taburiente. Geological Society of America Bulletin 111, 755–768. doi:10.1130/0016-7606(1999)111<0755:LSOVEO>2.3.CO;2

Carracedo, J.C., Day, S.J., Guillou, H., Perez Torrado, F.J., 1999b. Giant Quaternary landslides in the evolution of La Palma and El Hierro, Canary Islands. Journal of Volcanology and Geothermal Research 94, 169–190. doi:10.1016/S0377-0273(99)00102-X

Carracedo, J.C., Guillou, H., Perez-Torrado, F.J., Rodríguez-Badiola, E., 2013. Volcanic history and stratigraphy of the Teide volcanic complex, in: Carracedo, J.C., Troll, V.R. (Eds.), Teide Volcano, Active Volcanoes of the World. Springer Berlin Heidelberg, pp. 105–128.

Carracedo, J.C., Paris, R., 2001. Formation d'une caldera d'érosion et instabilité récurrente d'une île de point chaud : La Caldera de Taburiente, La Palma, îles Canaries. morfo 7, 93–105. doi:10.3406/morfo.2001.1093

Carracedo, J.C., Troll, V.R., 2013. Structural and Geological Elements of Teide Volcanic Complex: Rift Zones and Gravitational Collapses, in: Carracedo, J.C., Troll, V.R. (Eds.), Teide Volcano, Active Volcanoes of the World. Springer Berlin Heidelberg, pp. 57–74.

Cashman, K.V., Sparks, R.S.J., 2013. How volcanoes work: A 25 year perspective. Geological Society of America Bulletin 125, 664–690. doi:10.1130/B30720.1

Clague, D., Dalrymple, G.B., 1988. Age and petrology of alkalic postshield and rejuvenated-stage lava from Kauai, Hawaii. Contributions to Mineralogy and Petrology 99, 202–218. doi:10.1007/BF00371461

Clarke, H., Troll, V.R., Carracedo, J.C., 2009. Phreatomagmatic to Strombolian eruptive activity of basaltic cinder cones: Montaña Los Erales, Tenerife, Canary Islands. Journal of Volcanology and Geothermal Research 180, 225–245. doi:10.1016/j.jvolgeores.2008.11.014

Coe, A.L. (Ed.), 2010. Geological field techniques. Wiley-Blackwell in association with the Open University, Milton Keynes.

Colmenero, J.R., de la Nuez, J., Casillas, R., Castillo, C., 2012. Epiclastic deposits associated with large-scale landslides and the formation of erosive calderas in oceanic islands: The example of the La Palma Island (Canary Archipelago). Geomorphology 177–178, 108–127. doi:10.1016/j.geomorph.2012.07.019

Day, J.M.D., Macpherson, C.G., Lowry, D., Pearson, D.G., 2012. Oxygen isotope heterogeneity of the mantle beneath the Canary Islands: a discussion of the paper of Gurenko et al. Contributions to Mineralogy and Petrology 164, 177–183. doi:10.1007/s00410-012-0755-3

Day, J.M.D., Pearson, D.G., Macpherson, C.G., Lowry, D., Carracedo, J.C., 2010. Evidence for distinct proportions of subducted oceanic crust and lithosphere in HIMU-type mantle beneath El Hierro and La Palma, Canary Islands. Geochimica et Cosmochimica Acta 74, 6565–6589. doi:10.1016/j.gca.2010.08.021

Day, J.M.D., Pearson, D.G., Macpherson, C.G., Lowry, D., Carracedo, J.C., 2009. Pyroxenite-rich mantle formed by recycled oceanic lithosphere: Oxygen-osmium isotope evidence from Canary Island lavas. Geology 37, 555–558. doi:10.1130/G25613A.1

Day, S.J., Carracedo, J.C., Guillou, H., Gravestock, P., 1999. Recent structural evolution of the Cumbre Vieja volcano, La Palma, Canary Islands: volcanic rift zone reconfiguration as a precursor to volcano flank instability? Journal of Volcanology and Geothermal Research 94, 135–167. doi:10.1016/S0377-0273(99)00101-8

Deniel, C., Pin, C., 2001. Single-stage method for the simultaneous isolation of lead and strontium from silicate samples for isotopic measurements. Analytica Chimica Acta 426, 95–103. doi:10.1016/S0003-2670(00)01185-5

Duke, J.M., 1976. Distribution of the Period Four Transition Elements among Olivine, Calcic Clinopyroxene and Mafic Silicate Liquid: Experimental Results. J Petrology 17, 499–521. doi:10.1093/petrology/17.4.499

Edmonds, M., 2008. New geochemical insights into volcanic degassing. Philosophical Transactions of the Royal Society of London A: Mathematical, Physical and Engineering Sciences 366, 4559–4579. doi:10.1098/rsta.2008.0185

Elliott, T.., 1991. Element fractionation in the Petrogenesis of Ocean Island Basalts. The Open University, Milton Keynes.

Galipp, K., 2005. Geochemical and petrological evolution of La Palma (Canary Islands) and its rift zone during the last 1.0 Ma (PhD Thesis). University of Bremen, Bremen.

Galipp, K., Klügel, A., Hansteen, T.H., 2006. Changing depths of magma fractionation and stagnation during the evolution of an oceanic island volcano: La Palma (Canary Islands). Journal of Volcanology and Geothermal Research 155, 285–306. doi:10.1016/j.jvolgeores.2006.04.002

Gee, M.A.M., Taylor, R.N., Thirlwall, M.F., Murton, B.J., 1998. Glacioisostacy controls chemical and isotopic characteristics of tholeiites from the Reykjanes Peninsula, SW Iceland. Earth and Planetary Science Letters 164, 1–5. doi:10.1016/S0012-821X(98)00246-5

Geldmacher, J., Hoernle, K., 2000. The 72 Ma geochemical evolution of the Madeira hotspot (eastern North Atlantic): recycling of Paleozoic (≤500 Ma) oceanic lithosphere. Earth and Planetary Science Letters 183, 73–92. doi:10.1016/S0012-821X(00)00266-1

Geldmacher, J., Hoernle, K., Bogaard, P. v. d., Duggen, S., Werner, R., 2005. New 40Ar / 39Ar age and geochemical data from seamounts in the Canary and Madeira volcanic provinces: Support for the mantle plume hypothesis. Earth and Planetary Science Letters 237, 85–101. doi:10.1016/j.epsl.2005.04.037

Geldmacher, J., Hoernle, K., Hanan, B.B., Blichert-Toft, J., Hauff, F., Gill, J.B., Schmincke, H.-U., 2010. Hafnium isotopic variations in East Atlantic intraplate volcanism. Contributions to Mineralogy and Petrology 162, 21–36. doi:10.1007/s00410-010-0580-5

González, P.J., Bagnardi, M., Hooper, A.J., Larsen, Y., Marinkovic, P., Samsonov, S.V., Wright, T.J., 2015. The 2014–2015 eruption of Fogo volcano: Geodetic modeling of Sentinel-1 TOPS interferometry. Geophysical Research Letters 42, 2015GL066003. doi:10.1002/2015GL066003

Grieken, R.V., Markowicz, A., 2001. Handbook of X-Ray Spectrometry, Second Edition,. CRC Press.

Guest, J.E., Murray, J.B., 1979. An analysis of hazard from Mount Etna volcano. Journal of the Geological Society 136, 347–354.

Guillou, H., Carracedo, J.., Duncan, R.., 2001. K–Ar, 40Ar–39Ar ages and magnetostratigraphy of Brunhes and Matuyama lava sequences from La Palma Island. Journal of Volcanology and Geothermal Research 106, 175–194. doi:10.1016/S0377-0273(00)00294-8

Guillou, H., Carracedo, J.C., Day, S.J., 1998. Dating of the Upper Pleistocene-Holocene volcanic activity of La Palma using the unspiked K-Ar technique. Journal of Volcanology and Geothermal Research 86, 137–149. doi:16/S0377-0273(98)00074-2

Gurenko, A.A., Bindeman, I.N., Chaussidon, M., 2012. Reply to “Oxygen isotope heterogeneity of the mantle beneath the Canary Islands: a discussion of the paper of Gurenko et al.” Contributions to Mineralogy and Petrology 164, 185–189. doi:10.1007/s00410-012-0756-2

Gurenko, A.A., Bindeman, I.N., Chaussidon, M., 2011. Oxygen isotope heterogeneity of the mantle beneath the Canary Islands: insights from olivine phenocrysts. Contributions to Mineralogy and Petrology 162, 349–363. doi:10.1007/s00410-010-0600-5

Gurenko, A.A., Hoernle, K.A., Hauff, F., Schmincke, H.-U., Han, D., Miura, Y.N., Kaneoka, I., 2006. Major, trace element and Nd–Sr–Pb–O–He–Ar isotope signatures of shield stage lavas from the central and western Canary Islands: Insights into mantle and crustal processes. Chemical Geology 233, 75–112. doi:10.1016/j.chemgeo.2006.02.016

Gurenko, A.A., Hoernle, K.A., Sobolev, A.V., Hauff, F., Schmincke, H.-U., 2009a. Source components of the Gran Canaria (Canary Islands) shield stage magmas: evidence from olivine composition and Sr–Nd–Pb isotopes. Contributions to Mineralogy and Petrology 159, 689–702. doi:10.1007/s00410-009-0448-8

Gurenko, A.A., Sobolev, A.V., Hoernle, K.A., Hauff, F., Schmincke, H.-U., 2009b. Enriched, HIMU-type peridotite and depleted recycled pyroxenite in the Canary plume: A mixed-up mantle. Earth and Planetary Science Letters 277, 514–524. doi:10.1016/j.epsl.2008.11.013

Hammer, J., Jacob, S., Welsch, B., Hellebrand, E., Sinton, J., 2015. Clinopyroxene in postshield Haleakala ankaramite: 1. Efficacy of thermobarometry. Contributions to Mineralogy and Petrology 171, 1–23. doi:10.1007/s00410-015-1212-x

Hansteen, H.T., Klügel, A., Schmincke, H.-U., 1998. Multi-stage magma ascent beneath the Canary Islands: evidence from fluid inclusions. Contributions to Mineralogy and Petrology 132, 48–64. doi:10.1007/s004100050404

Hansteen, T.H., Klügel, A., 2008. Fluid inclusion thermobarometry as a tracer for magmatic processes. Reviews in Mineralogy and Geochemistry 69, 143–177. doi:10.2138/rmg.2008.69.5

Hildenbrand, A., Gillot, P.-Y., Le Roy, I., 2004. Volcano-tectonic and geochemical evolution of an oceanic intra-plate volcano: Tahiti-Nui (French Polynesia). Earth and Planetary Science Letters 217, 349–365. doi:16/S0012-821X(03)00599-5

Hildenbrand, A., Gillot, P.-Y., Soler, V., Lahitte, P., 2003. Evidence for a persistent uplifting of La Palma (Canary Islands), inferred from morphological and radiometric data. Earth and Planetary Science Letters 210, 277–289. doi:10.1016/S0012-821X(03)00133-X

Hildner, E., Klügel, A., Hansteen, T.H., 2012. Barometry of lavas from the 1951 eruption of Fogo, Cape Verde Islands: Implications for historic and prehistoric magma plumbing systems. Journal of Volcanology and Geothermal Research 217–218, 73–90. doi:10.1016/j.jvolgeores.2011.12.014

Hilton, D.., Macpherson, C.., Elliott, T.., 2000. Helium isotope ratios in mafic phenocrysts and geothermal fluids from La Palma, the Canary Islands (Spain): implications for HIMU mantle sources. Geochimica et Cosmochimica Acta 64, 2119–2132. doi:10.1016/S0016-7037(00)00358-6

Hoernle, K., Schmincke, H.-U., 1993. The petrology of the tholeiites through melilite nephelinites on Gran Canaria, Canary Islands: crystal fractionation, accumulation, and depths of melting. Journal of Petrology 34, 573–597. doi:10.1093/petrology/34.3.573

Hoernle, K., Zhang, Y.-S., Graham, D., 1995. Seismic and geochemical evidence for large-scale mantle upwelling beneath the eastern Atlantic and western and central Europe. Nature 374, 34–39. doi:10.1038/374034a0

Hofmann, A.W., 2014. 3.3 - Sampling Mantle Heterogeneity through Oceanic Basalts: Isotopes and Trace Elements A2 - Holland, Heinrich D., in: Turekian, K.K. (Ed.), Treatise on Geochemistry (Second Edition). Elsevier, Oxford, pp. 67–101.

Hofmann, A.W., 1988. Chemical differentiation of the Earth: the relationship between mantle, continental crust, and oceanic crust. Earth and Planetary Science Letters 90, 297–314. doi:10.1016/0012-821X(88)90132-X

Hofmann, A.W., Jochum, K.P., Seufert, M., White, W.M., 1986. Nb and Pb in oceanic basalts: new constraints on mantle evolution. Earth and Planetary Science Letters 79, 33–45. doi:10.1016/0012-821X(86)90038-5

Hofmann, A.W., White, W.M., 1983. Ba, Rb and Cs in the Earth's Mantle. Zeitschrift für Naturforschung A 38, 256–266. doi:10.1515/zna-1983-0225

Hofmann, A.W., White, W.M., 1982. Mantle plumes from ancient oceanic crust. Earth and Planetary Science Letters 57, 421–436. doi:10.1016/0012-821X(82)90161-3

Hon, K., Kauahikaua, J., Denlinger, R., Mackay, K., 1994. Emplacement and inflation of pahoehoe sheet flows: Observations and measurements of active lava flows on Kilauea Volcano, Hawaii. Geological Society of America Bulletin 106, 351–370. doi:10.1130/0016-7606(1994)106<0351:EAIOPS>2.3.CO;2

Huber, C., Bachmann, O., Manga, M., 2010. Two competing effects of volatiles on heat transfer in crystal-rich magmas: thermal insulation vs defrosting. J. Petrology 51, 847–867. doi:10.1093/petrology/egq003

Hunt, J.E., Wynn, R.B., Masson, D.G., Talling, P.J., Teagle, D.A.H., 2011. Sedimentological and geochemical evidence for multistage failure of volcanic island landslides: A case study from Icod landslide on north Tenerife, Canary Islands. Geochemistry, Geophysics, Geosystems 12, Q12007. doi:10.1029/2011GC003740

Hunt, J.E., Wynn, R.B., Talling, P.J., Masson, D.G., 2013a. Multistage collapse of eight western Canary Island landslides in the last 1.5 Ma: Sedimentological and geochemical evidence from subunits in submarine flow deposits. Geochemistry, Geophysics, Geosystems 14, 2159–2181. doi:10.1002/ggge.20138

Hunt, J.E., Wynn, R.B., Talling, P.J., Masson, D.G., 2013b. Turbidite record of frequency and source of large volume (>100 km3) Canary Island landslides in the last 1.5 Ma: Implications for landslide triggers and geohazards. Geochemistry, Geophysics, Geosystems 14, 2100–2123. doi:10.1002/ggge.20139

Johannes, W., 1989. Melting of plagioclase-quartz assemblages at 2 kbar water pressure. Contributions to Mineralogy and Petrology 103, 270–276. doi:10.1007/BF00402914

Johansen, T.S., Hauff, F., Hoernle, K., Klügel, A., Kokfelt, T.F., 2005. Basanite to phonolite differentiation within 1550-1750 yr: U-Th-Ra isotopic evidence from the A.D. 1585 eruption on La Palma, Canary Islands. Geology 33, 897–900. doi:10.1130/G21663.1

Jull, M., McKenzie, D., 1996. The effect of deglaciation on mantle melting beneath Iceland. J. Geophys. Res. 101, 21815–21828. doi:10.1029/96JB01308

Kilburn, C., R.J., 2000. Lava flows and flow fields, in: Encyclopedia of Volcanoes. Academic Press, San Diego, pp. 291–305.

King, S.D., Ritsema, J., 2000. African Hot Spot Volcanism: Small-Scale Convection in the Upper Mantle Beneath Cratons. Science 290, 1137–1140. doi:10.1126/science.290.5494.1137

Klügel, A., 1999. Chronology and volcanology of the 1949 multi-vent rift-zone eruption on La Palma (Canary Islands). Journal of Volcanology and Geothermal Research 94, 267–282. doi:10.1016/S0377-0273(99)00107-9

Klügel, A., 1998. Reactions between mantle xenoliths and host magma beneath La Palma (Canary Islands): constraints on magma ascent rates and crustal reservoirs. Contributions to Mineralogy and Petrology 131, 237–257. doi:10.1007/s004100050391

Klügel, A., Hansteen, T.H., Galipp, K., 2005. Magma storage and underplating beneath Cumbre Vieja volcano, La Palma (Canary Islands). Earth and Planetary Science Letters 236, 211–226. doi:10.1016/j.epsl.2005.04.006

Klügel, A., Hansteen, T.H., Schmincke, H.-U., 1997. Rates of magma ascent and depths of magma reservoirs beneath La Palma (Canary Islands). Terra Nova 9, 117–121. doi:10.1046/j.1365-3121.1997.d01-15.x

Klügel, A., Hoernle, K.A., Schmincke, H.-U., White, J.D.L., 2000. The chemically zoned 1949 eruption on La Palma (Canary Islands): Petrologic evolution and magma supply dynamics of a rift zone eruption. Journal of Geophysical Research 105, 5997–6016. doi:200010.1029/1999JB900334

Klügel, A., Longpré, M.-A., García-Cañada, L., Stix, J., 2015. Deep intrusions, lateral magma transport and related uplift at ocean island volcanoes. Earth and Planetary Science Letters 431, 140–149. doi:10.1016/j.epsl.2015.09.031

Kovalenko, V.I., Naumov, V.B., Girnis, A.V., Dorofeeva, V.A., Yarmolyuk, V.V., 2007. Volatiles in basaltic magmas of ocean islands and their mantle sources: I. Melt compositions deduced from melt inclusions and glasses in the rocks. Geochemistry International 45, 105.

Lesne, P., Kohn, S.C., Blundy, J., Witham, F., Botcharnikov, R.E., Behrens, H., 2011. Experimental Simulation of Closed-System Degassing in the System Basalt–H2O–CO2–S–Cl. J Petrology 52, 1737–1762. doi:10.1093/petrology/egr027

Lisle, R.J., Brabham, P., Barnes, J.W., 2011. Basic geological mapping, 5th ed. Wiley-Blackwell.

Longpré, M.-A., Klügel, A., Diehl, A., Stix, J., 2014. Mixing in mantle magma reservoirs prior to and during the 2011–2012 eruption at El Hierro, Canary Islands. Geology 42, 315–318. doi:10.1130/G35165.1

Longpré, M.-A., Troll, V.R., Hansteen, T.H., 2008. Upper mantle magma storage and transport under a Canarian shield-volcano, Teno, Tenerife (Spain). Journal of Geophysical Research 113, 11. doi:200810.1029/2007JB005422

Longpré, M.-A., Troll, V.R., Walter, T.R., Hansteen, T.H., 2009. Volcanic and geochemical evolution of the Teno massif, Tenerife, Canary Islands: Some repercussions of giant landslides on ocean island magmatism. Geochemistry Geophysics Geosystems 10, 31. doi:2009 10.1029/2009GC002892 [Citation]

Lyell, C., 1855. A manual of elementary geology. D. Appleton.

Mader, H.M., Llewellin, E.W., Mueller, S.P., 2013. The rheology of two-phase magmas: A review and analysis. Journal of Volcanology and Geothermal Research 257, 135–158. doi:10.1016/j.jvolgeores.2013.02.014

Manconi, A., Longpré, M.-A., Walter, T.R., Troll, V.R., Hansteen, T.H., 2009. The effects of flank collapses on volcano plumbing systems. Geology 37, 1099–1102. doi:10.1130/G30104A.1

Marcantonio, F., Zindler, A., Elliott, T., Staudigel, H., 1995. Os isotope systematics of La Palma, Canary Islands: Evidence for recycled crust in the mantle source of HIMU ocean islands. Earth and Planetary Science Letters 133, 397–410. doi:10.1016/0012-821X(95)00092-Q

Mark, D.F., Barfod, D., Stuart, F.M., Imlach, J., 2009. The ARGUS multicollector noble gas mass spectrometer: Performance for 40Ar/39Ar geochronology. Geochemistry, Geophysics, Geosystems 10, Q0AA02. doi:10.1029/2009GC002643

Martí, J., Gudmundsson, A., 2000. The Las Cañadas caldera (Tenerife, Canary Islands): an overlapping collapse caldera generated by magma-chamber migration. Journal of Volcanology and Geothermal Research 103, 161–173. doi:10.1016/S0377-0273(00)00221-3

Martí, J., Hurlimann, M., Ablay, G.J., Gudmundsson, A., 1997. Vertical and lateral collapses on Tenerife (Canary Islands) and other volcanic ocean islands. Geology 25, 879–882. doi:10.1130/0091-7613(1997)025<0879:VALCOT>2.3.CO;2

Masotta, M., Mollo, S., Freda, C., Gaeta, M., Moore, G., 2013. Clinopyroxene–liquid thermometers and barometers specific to alkaline differentiated magmas. Contributions to Mineralogy and Petrology 166, 1545–1561. doi:10.1007/s00410-013-0927-9

Masson, D.G., 1996. Catastrophic collapse of the volcanic island of Hierro 15 ka ago and the history of landslides in the Canary Islands. Geology 24, 231–234. doi:10.1130/0091-7613(1996)024<0231:CCOTVI>2.3.CO;2

McDonough, W.F., Sun, S. -s., 1995. The composition of the Earth. Chemical Geology 120, 223–253. doi:10.1016/0009-2541(94)00140-4

Morgan, W.J., 1971. Convection Plumes in the Lower Mantle. Nature 230, 42–43. doi:10.1038/230042a0

Navarro, J.M., Coello, J., 1994. Mapa geológico del Parque Nacional de Caldera de Taburiente. ICONA (in Spanish).

Nikogosian, I.K., Elliott, T., Touret, J.L.., 2002. Melt evolution beneath thick lithosphere: a magmatic inclusion study of La Palma, Canary Islands. Chemical Geology 183, 169–193. doi:10.1016/S0009-2541(01)00387-4

Ovchinnikova, G.V., Belyatskii, B.V., Vasil'eva, I.M., Levskii, L.K., Grachev, A.F., Araña, V., Mitjavila, I.J., 1995. Sr-Nd-Pb isotopes of mantle sources of basalts from the Canary Islands. Petrologiya 3, 195–206.

Paulatto, M., Annen, C., Henstock, T.J., Kiddle, E., Minshull, T.A., Sparks, R.S.J., Voight, B., 2012. Magma chamber properties from integrated seismic tomography and thermal modeling at Montserrat. Geochemistry, Geophysics, Geosystems 13, Q01014. doi:10.1029/2011GC003892

Pinel, V., Jaupart, C., 2005. Some consequences of volcanic edifice destruction for eruption conditions. Journal of Volcanology and Geothermal Research 145, 68–80. doi:10.1016/j.jvolgeores.2005.01.012

Pinel, V., Jaupart, C., 2003. Magma chamber behavior beneath a volcanic edifice. Journal of Geophysical Research: Solid Earth 108, 2072. doi:10.1029/2002JB001751

Pinel, V., Jaupart, C., 2000. The effect of edifice load on magma ascent beneath a volcano. Philosophical Transactions of the Royal Society of London. Series A: Mathematical, Physical and Engineering Sciences 358, 1515–1532. doi:10.1098/rsta.2000.0601

Praegel, N.-O., 1986. The petrology and geochemistry of Volcan Teneguia, La Palma, Canary Islands. Institute of Petrology, University of Copenhagen.

Praegel, N.-O., Holm, P.M., 2006. Lithospheric contributions to high-MgO basanites from the Cumbre Vieja Volcano, La Palma, Canary Islands and evidence for temporal variation in plume influence. Journal of Volcanology and Geothermal Research 149, 213–239. doi:10.1016/j.jvolgeores.2005.07.019

Putirka, K., 1999. Clinopyroxene + liquid equilibria to 100 kbar and 2450 K. Contributions to Mineralogy and Petrology 135, 151–163. doi:10.1007/s004100050503

Putirka, K., Johnson, M., Kinzler, R., Longhi, J., Walker, D., 1996. Thermobarometry of mafic igneous rocks based on clinopyroxene-liquid equilibria, 0–30 kbar. Contributions to Mineralogy and Petrology 123, 92–108. doi:10.1007/s004100050145

Putirka, K.D., 2008. Thermometers and barometers for volcanic systems. Reviews in Mineralogy and Geochemistry 69, 61–120. doi:10.2138/rmg.2008.69.3

Putirka, K.D., Mikaelian, H., Ryerson, F., Shaw, H., 2003. New clinopyroxene-liquid thermobarometers for mafic, evolved, and volatile-bearing lava compositions, with applications to lavas from Tibet and the Snake River Plain, Idaho. American Mineralogist 88, 1542–1554. doi:10.2138/am-2003-1017

Renne, P.R., Balco, G., Ludwig, K.R., Mundil, R., Min, K., 2011. Response to the comment by W.H. Schwarz et al. on "Joint determination of 40K decay constants and 40Ar∗/40K for the Fish Canyon sanidine standard, and improved accuracy for 40Ar/39Ar geochronology" by P.R. Renne et al. (2010). Geochimica et Cosmochimica Acta 75, 5097–5100. doi:10.1016/j.gca.2011.06.021

Riker, J.M., Cashman, K.V., Rust, A.C., Blundy, J.D., 2015. Experimental Constraints on Plagioclase Crystallization during H2O- and H2O–CO2-Saturated Magma Decompression. Journal of Petrology egv059. doi:10.1093/petrology/egv059

Roa, K., 2003. Nature and origin of toreva remnants and volcaniclastics from La Palma, Canary Islands. Journal of Volcanology and Geothermal Research 125, 191–214. doi:10.1016/S0377-0273(03)00069-6

Schmincke, H.-U., Klügel, A., Hansteen, T.H., Hoernle, K., van den Bogaard, P., 1998. Samples from the Jurassic ocean crust beneath Gran Canaria, La Palma and Lanzarote (Canary Islands). Earth and Planetary Science Letters 163, 343–360. doi:10.1016/S0012-821X(98)00168-X

Self, S., Keszthelyi, L., Thordarson, T., 1998. The importance of pāhoehoe. Annual Review of Earth and Planetary Sciences 26, 81–110. doi:10.1146/annurev.earth.26.1.81

Simonsen, S.L., Neumann, E.-R., Seim, K., 2000. Sr–Nd–Pb isotope and trace-element geochemistry evidence for a young HIMU source and assimilation at Tenerife (Canary Island). Journal of Volcanology and Geothermal Research 103, 299–312. doi:10.1016/S0377-0273(00)00228-6

Smith, J.R., 2000. Isostatic consequences of giant landslides on the Hawaiian ridge. Pure and Applied Geophysics 157, 1097–1114. doi:10.1007/s000240050019

Sobolev, A.V., Hofmann, A.W., Kuzmin, D.V., Yaxley, G.M., Arndt, N.T., Chung, S.-L., Danyushevsky, L.V., Elliott, T., Frey, F.A., Garcia, M.O., Gurenko, A.A., Kamenetsky, V.S., Kerr, A.C., Krivolutskaya, N.A., Matvienkov, V.V., Nikogosian, I.K., Rocholl, A., Sigurdsson, I.A., Sushchevskaya, N.M., Teklay, M., 2007. The amount of recycled crust in sources of mantle-derived melts. Science 316, 412–417. doi:10.1126/science. 1138113

Sobolev, A.V., Hofmann, A.W., Sobolev, S.V., Nikogosian, I.K., 2005. An olivine-free mantle source of Hawaiian shield basalts. Nature 434, 590–597. doi:10.1038/nature03411

Solana, M.C., Kilburn, C.R.J., Rodriguez Badiola, E., Aparicio, A., 2004. Fast emplacement of extensive pahoehoe flow-fields: the case of the 1736 flows from Montaña de las Nueces, Lanzarote. Journal of Volcanology and Geothermal Research 132, 189–207. doi:10.1016/S0377-0273(03)00345-7

Sparks, R.S.J., Folkes, C.B., Humphreys, M.C.S., Barfod, D.N., Clavero, J., Sunagua, M.C., McNutt, S.R., Pritchard, M.E., 2008. Uturuncu volcano, Bolivia: Volcanic unrest due to mid-crustal magma intrusion. American Journal of Science 308, 727–769. doi:10.2475/06.2008.01

Staudigel, H., Schmincke, H.-U., 1984. The Pliocene seamount series of La Palma/Canary Islands. Journal of Geophysical Research: Solid Earth 89, 11195–11215. doi:10.1029/JB089iB13p11195

Sun, S., McDonough, W.F., 1989. Chemical and isotopic systematics of oceanic basalts: implications for mantle composition and processes. Geological Society, London, Special Publications 42, 313–345. doi:10.1144/GSL.SP.1989.042.01.19

Thirlwall, M.F., 2002. Multicollector ICP-MS analysis of Pb isotopes using a 207Pb-204Pb double spike demonstrates up to 400 ppm/amu systematic errors in Tl-normalization. Chemical Geology 184, 255–279. doi:16/S0009-2541(01)00365-5

Thirlwall, M.F., 1997. Pb isotopic and elemental evidence for OIB derivation from young HIMU mantle. Chemical Geology 139, 51–74. doi:10.1016/S0009-2541(97)00033-8

Thirlwall, M.F., Jenkins, C., Vroon, P.Z., Mattey, D.P., 1997. Crustal interaction during construction of ocean islands: Pb---Sr---Nd---O isotope geochemistry of the shield basalts of Gran Canaria, Canary Islands. Chemical Geology 135, 233–262. doi:10.1016/S0009-2541(96)00118-0

Thirlwall, M.F., Singer, B.., Marriner, G.., 2000. 39Ar–40Ar ages and geochemistry of the basaltic shield stage of Tenerife, Canary Islands, Spain. Journal of Volcanology and Geothermal Research 103, 247–297. doi:10.1016/S0377-0273(00)00227-4

Thomas, L.E., Hawkesworth, C.J., Van Calsteren, P., Turner, S.P., Rogers, N.W., 1999. Melt generation beneath ocean islands: a U-Th-Ra isotope study from Lanzarote in the Canary Islands. Geochimica et Cosmochimica Acta 63, 4081–4099. doi:10.1016/S0016-7037(99)00310-5

Thordarson, T., Self, S., 1998. The Roza Member, Columbia River Basalt Group: A gigantic pahoehoe lava flow field formed by endogenous processes? Journal of Geophysical Research: Solid Earth 103, 27411–27445. doi:10.1029/98JB01355

Truby, J.M., Mueller, S.P., Llewellin, E.W., Mader, H.M., 2015. The rheology of three-phase suspensions at low bubble capillary number. Proc. R. Soc. A 471, 20140557. doi:10.1098/rspa.2014.0557

Turner, S., Hoernle, K., Hauff, F., Johansen, T.S., Klügel, A., Kokfelt, T., Lundstrom, C., 2015. 238U–230Th–226Ra Disequilibria constraints on the magmatic rvolution of the Cumbre Vieja volcanics on La Palma, Canary Islands. Journal of Petrology 56, 1999–2024. doi:10.1093/petrology/egv061

Turner, S.J., Izbekov, P., Langmuir, C., 2013. The magma plumbing system of Bezymianny Volcano: Insights from a 54 year time series of trace element whole-rock geochemistry and amphibole compositions. Journal of Volcanology and Geothermal Research 263, 108–121. doi:10.1016/j.jvolgeores.2012.12.014

Urgeles, R., Masson, D.G., Canals, M., Watts, A.B., Le Bas, T., 1999. Recurrent large-scale landsliding on the west flank of La Palma, Canary Islands. Journal of Geophysical Research: Solid Earth 104, 25331–25348. doi:10.1029/1999JB900243

Walter, T.R., Troll, V.R., 2003. Experiments on rift zone evolution in unstable volcanic edifices. Journal of Volcanology and Geothermal Research 127, 107–120. doi:10.1016/S0377-0273(03)00181-1

Waters, L.E., Lange, R.A., 2015. An updated calibration of the plagioclase-liquid hygrometer-thermometer applicable to basalts through rhyolites. American Mineralogist 100, 2172–2184. doi:10.2138/am-2015-5232

Weis, F.A., Skogby, H., Troll, V.R., Deegan, F.M., Dahren, B., 2015. Magmatic water contents determined through clinopyroxene: Examples from the Western Canary Islands, Spain. Geochemistry, Geophysics, Geosystems 16, 2127–2146. doi:10.1002/2015GC005800

White, W.M., 2015. Probing the Earth's Deep Interior Through Geochemistry.

Widom, E., Hoernle, K.A., Shirey, S.B., Schmincke, H.-U., 1999. Os isotope systematics in the Canary Islands and Madeira: lithospheric contamination and mantle plume signatures. Journal of Petrology 40, 279–296. doi:10.1093/petroj/40.2.279

Wiesmaier, S., Deegan, F.M., Troll, V.R., Carracedo, J.C., Chadwick, J.P., Chew, D.M., 2011. Magma mixing in the 1100 AD Montaña Reventada composite lava flow, Tenerife, Canary Islands: interaction between rift zone and central volcano plumbing systems. Contributions to Mineralogy and Petrology 162, 651–669. doi:10.1007/s00410-010-0596-x

Wilson, J.T., 1963. A possible origin of the Hawaiian Islands. Canadian Journal of Physics 41, 863–870. doi:10.1139/p63-094

Zaczek, K., Troll, V.R., Cachao, M., Ferreira, J., Deegan, F.M., Carracedo, J.C., Soler, V., Meade, F.C., Burchardt, S., 2015. Nannofossils in 2011 El Hierro eruptive products reinstate plume model for Canary Islands. Scientific Reports 5. doi:10.1038/srep07945

Zindler, A., Hart, S., 1986. Chemical geodynamics. Annual Review of Earth and Planetary Sciences 14, 493–571. doi:10.1146/annurev.ea.14.050186.002425

APPENDICES

APPENDIX A: SAMPLE INDEX AND SOURCING INFORMATION

This thesis includes the results of analysing 72 samples collected over the course of three annual field campaigns (2012-2014). All have been given sample numbers based on the 8 character USGS system, using 2 characters each for *case study, year, collecting geologist* and *sample number*. We include only samples which have been analysed in the course of this project, although thin sections and hand specimens were produced from a larger sample suite.

The tables that follow include GPS co-ordinates, locality or stratigraphic unit, and an index of which chapters the data is presented in and which analytical techniques have been used on each sample.

Abbreviations used in appendices:

Barr. Jur	Barranco Jurado
Barr. Gom	Barranco de los Gomeros
Surf. Flow	Surface Flow
Bej LS	Bejenado Lower Series
LREVP-XPT	Los Rodeos Evolved and Volcaniclastic Phase, Xenolithic Pyroxene Tephrite
BEP: Glom Ank	Bejenado Effusive Phase: Glomerocrystic Ankaramite
BEP: Plag Basalt	Bejenado Effusive Phase: Plagioclase Basalt
BEP: Plag Teph-pho	Bejenado Effusive Phase: Plagioclase Tephri-phonolite
TSP: Amph Teph	Terminal Sheet Phase: Amphibole Tephrite
TSP: Pho-teph	Terminal Sheet Phase: Phono-tephrite
TSP: Amph Ol Teph	Terminal Sheet Phase: Amphibole Olivine Tephrite
Mña de la Hiedra	Moñtana de la Hiedra

Appendix A: Sample index and sourcing

	Locality information		*Data presented in:*				*Analytical techniques used:*			
Sample	Strat Unit /Source	UTM Co-ordinates	Chapter 4	Chapter 5	Chapter 6	Appendix 3	$^{40}Ar/^{39}Ar$	XRF	EDS-EPMA (mineralogy)	Sr/Nd/Pb isotopes
El Time										
LP13SG04	Barr. Jur.	211817 / 3179037				X		X		
LP13SG05	Barr. Jur.	211817 / 3179037	X		X		X	X		X
LP13SG06	Barr. Jur.	211507 / 3178865	X		X		X	X		X
LP13SG07	Barr. Jur.	211361 / 3178591			X			X		X
LP13SG17	Barr. Jur.	211675 / 3178819				X		X		
LP13SG08	Barr. Jur.	211636 / 3178815				X		X		
LP13SG31	Barr. Jur.	210454 / 3179090			X			X		
LP13SG32	Barr. Jur.	209753 / 3178602						X		
LP13SG33	Barr. Jur.	210006 / 3178625						X		
LP12SG09	Surf. Flow	212381 / 3174101			X			X		X
LP12SG10	Surf. Flow	212715 / 3175923	X		X		X	X		X
LP12SG11	Surf. Flow	213130 / 3176292			X			X		
LP12SG13	Surf. Flow	213092 / 3176729				X		X		
LP12SG14	Surf. Flow	212981 / 3177133	X		X		X	X		X
LP12SG15	Barr Gom.	212938 / 3177872	X		X		X	X		X
LP12SG16	Barr Gom.	212885 / 3177808			X			X		
LP12SG17	Barr Gom.	212835 / 3177744				X		X		
LP12SG18	Barr Gom.	212765 / 3177703			X			X		X
LP12SG19	Barr Gom.	212984 / 3177898			X			X		
LP12SG20	Surf. Flow	213542 / 3178833				X		X		
LP12SG21	Surf. Flow	213347 / 3178706				X		X		
LP12SG22	Surf. Flow	213091 / 3178334			X			X		X
LP12SG23	Surf. Flow	213097 / 3178399			X			X		X
LP12SG24	Surf. Flow	213016 / 3178187				X		X		
LP12SG26	Surf. Flow	212558 / 3178354			X			X		X
LP12SG27	Taburiente (other)	208623 / 3188126				X		X		
LP12SG28	Taburiente (other)	208515 / 3184642				X		X		

Appendix A: Sample index and sourcing

	Locality information		*Data presented in:*				*Analytical techniques used:*			
Sample	Strat Unit /Source	UTM Co-ordinates	Chapter 4	Chapter 5	Chapter 6	Appendix 3	$^{40}Ar/^{39}Ar$	XRF	EDS-EPMA (mineralogy)	Sr/Nd/Pb isotopes
Bejenado										
LP14SG03	Bejenado Sill	219017 / 3177771				X		X		
LP13SG02	Bej LS: Ankaramite	217960 / 3173996				X		X		
LP13SG36	Bej LS: Ankaramite	219266 / 3177265				X		X		
LP13SG38	Bej LS: Ankaramite	219352 / 3177094	X		X		X	X		X
LP12SG80	West Bejenado	217048 / 3174597				X		X		
LP12SG81	West Bejenado	216787 / 3173651				X		X		
LP12SG87	West Bejenado	216636 / 3174613			X		X	X		X
LP13SG01	West Bejenado	217570 / 3173821			X			X		X
LP13SG10	West Bejenado	215226 / 3175800			X			X		X
LP13SG11	West Bejenado	216021 / 3174999			X			X		X
LP13SG18	LREVP-XPT	220804 / 3177634				X		X		
LP13SG19	LREVP-XPT	220709 / 3177574				X		X		
LP13SG20	LREVP-XPT	220504 / 3177403				X		X		
LP13SG22	LREVP-XPT	220310 / 3177277				X		X		
LP13SG24	LREVP-XPT	221716 / 3176567				X		X		
LP13SG25	LREVP-XPT	221801 / 3175765				X		X		
LP13SG26	LREVP-XPT	221786 / 3175536			X			X		X
LP13SG30	LREVP-XPT	218968 / 3177399	X		X		X	X		X
LP14SG02	LREVP-XPT	219936 / 3174918				X	X	X		

Appendix A: Sample index and sourcing

	Locality information		*Data presented in:*				*Analytical techniques used:*			
Sample	Strat Unit /Source	UTM Co-ordinates	Chapter 4	Chapter 5	Chapter 6	Appendix 3	$^{40}Ar/^{39}Ar$	XRF	EDS-EPMA (mineralogy)	Sr/Nd/Pb isotopes
Bejenado										
LP12SG01	BEP: Glom Ank	221250 / 3175955		X				X		
LP12SG03	BEP: Glom Ank	220946 / 3175709		X				X		X
LP12SG04	BEP: Glom Ank	221093 / 3175507		X				X		
LP12SG05	BEP: Glom Ank	220948 / 3174777		X				X		X
LP12SG07	BEP: Glom Ank	221061 / 3174271		X				X		
LP12SG82	BEP: Glom Ank	219983 / 3173618		X				X		X
LP13SG21	BEP: Glom Ank	220412 / 3177354		X				X		
LP13SG23	BEP: Glom Ank	220379 / 3177201		X				X		
LP13SG29	BEP: Glom Ank	219300 / 3177095	X	X			X	X	X	X
LP13SG40	BEP: Glom Ank	219898 / 3176244		X				X		
LP14SG08	BEP: Glom Ank	221038 / 3175654		X				X	X	X
LP13SG12	BEP: Plag Bas	219275 / 3176221		X				X		
LP14SG06	BEP: Plag Bas	219437 / 3176214		X				X	X	X
LP14SG09	BEP: Plag Bas	221038 / 3175654	X	X			X	X	X	X
LP14SG04	BEP: Plag Teph-Pho	219437 / 3176214		X				X	X	
LP14SG05	BEP: Plag Teph-Pho	219437 / 3176214		X				X	X	
LP12SG02	TSP: Amph Teph	221214 / 3175822	X		X		X	X		
LP13SG14	TSP: Amph Teph	219643 / 3176220				X		X		
LP13SG27	TSP: Amph Teph	220283 / 3176307				X		X		
LP13SG28	TSP: Amph Teph	220585 / 3176163			X			X		X
LP13SG13	TSP: Pho-teph	219255 / 3176189			X			X		X
LP13SG15	TSP: Pho-teph	219699 / 3176107				X		X		
LP13SG16	TSP: Pho-teph	219783 / 3176117	X		X		X	X		X
LP14SG10	TSP: Amph Ol Teph	220618 / 3177334			X			X		X
LP13SG34	Mña de la Hiedra	219589 / 3174676			X			X		X
LP13SG35	Mña de la Hiedra	218899 / 3173623				X		X		
LP14SG07	Mña de la Hiedra	219093 / 3174203	X		X		X	X		X

APPENDIX B: ANALYTICAL METHODS AND HISTORY

Analyses towards this thesis were produced in laboratories located at:

Technique	*Laboratory*	*Dates samples prepared/analysed*
Energy Dispersive Electron Probe Micro-Analysis (EDS-EPMA)	Birkbeck, University of London	25/2/2016 – 27/2/2016
X-Ray Fluorescence (XRF) - major and trace elements	Royal Holloway, University of London	4 batches: 02/2013 - 06/2013, 02/2015 - 04/2015, 02/2014 – 06/2014, 02/2016-07/2016
$^{40}Ar/^{39}Ar$ geochronology	The Scottish Universities Environmental Research Centre (SUERC), East Kilbride	2 batches: 02/2014, 10/2015
Radiogenic isotope analysis (Sr-Nd-Pb)	The NERC Isotope Geosciences Laboratory, British Geological Survey, Keyworth	2 batches: 06/2015, 10/2015
cpx-melt thermobarometry (Wavelength Dispersive EPMA & Laser Ablation Inductively Coupled Mass Spectrometry)	Department of Geosciences, University of Bremen	1 batch: 12/2015

Arrangements for analysis were different in each laboratory. For EDS-EPMA, thin sections were polished and analyses were run entirely by Simon Groom, while all stages of cpx-melt thermobarometry analysis were conducted by Dr. Andreas Klügel. However, for the remaining techniques initial preparation was typically conducted by Simon Groom and samples were run at a later date by facility staff.

The exceptions to this were for the second batch of Pb samples which were digested and prepared by Dr. Ian Millar, and a batch of XRF pellets discussed below. Detailed protocols for all sample preparation procedures are held at Birkbeck, University of London.

ENERGY DISPERSIVE ELECTRON PROBE MICRO-ANALYSIS (EDS-EPMA)

All analytical data were collected over the course of one weekend, with repeat analyses of standard BCR-2 run both at the beginning and end of this session. Differences in values obtained from this standard are likely to be a result of instrumental drift over the course of the second day. Standards data were taken from individual point analyses of polished areas of the BCR-2 glass.

X-RAY FLUORESCENCE (XRF)

Samples were prepared as fusions and pellets with analytical data collected between 2013 and 2016, a period that includes a change in instrument X-ray tube during preparation and analysis of the second batch of samples (2013-2014). Preparatory and analytical precision was determined on samples originally run in the 2015 batch, in combination with new replicates prepared in 2016, demonstrating long-term precision from this period. Co, Cl and Br were analysed but the results

have not been presented since the samples were milled in WC pots (where Co is used as a binder and its presence is a known source of contamination), and pellets were prepared in close proximity to an area where HCl was used for cleaning platinumware.

Some concerns were raised in April 2016 about the quality of powder grinding, with 17 samples among the full suite (72) identified as being sub-optimal ("gritty textures"), a problem which could potentially result in poorly homogenised powders and mineralogical effects in pellets (Grieken and Markowicz, 2001). To resolve these issues, these 17 samples were re-ground from crushate, pelleted (by Dr. Christina Manning) and re-analysed with the resulting pressed pellet data used in all graphs and tables. Nonetheless, major element precision has been determined on a sample (LP14SG08) that had been identified as among those with the coarsest grind-quality of all 72 (prior to re-grinding) and trace element precision has been determined on a sample (LP14SG04) that had been identified as among those with the coarsest grind-quality that remained after re-grinding. Therefore, the effect of grind quality on analytical results can be assumed to be less than reported precision. Extensive documentation on this issue is held at Birkbeck, University of London.

^{40}Ar/^{39}Ar and Radiogenic isotope data.

All analytical information recommended by the facilities to support preparation and instrumentation for these techniques is provided in preceding chapters.

Replicate Pb isotope analyses of standard NBS981 from the instrumental runs used are held at Birkbeck, University of London but were not considered necessary (Pers. Comm. Ian Millar) for supporting this thesis.

In accordance with standard NIGL procedures a basalt standard (Columbia River Basalt, BCR-2) was run as an unknown with each batch of Nd and Pb isotope data. With the first batch this standard returned values that were anomalously low when compared to other repeat-runs of this standard over the year of analysis, and when compared to the normalisation standards JND-i and NBS 981. This was believed to have resulted from mistakenly leaching this standard in 6M HCl along with the samples, when protocol suggests it should just have been digested. The standard was not leached in the course of the second batch and the resulting values are included in data tables.

Appendix B: Analytical methods and history

EDS-EPMA: Instrumental precision and accuracy

Sample	Recomm	Results of replicate analyses of standard BCR-2										
Date		27/02/16	27/02/16	27/02/16	27/02/16	27/02/16	27/02/16	28/02/16	28/02/16	28/02/16	28/02/16	28/02/16
SiO_2	54.1	55.2	54.3	55.7	55.0	55.6	54.7	56.2	56.5	56.1	56.2	55.9
Al_2O_3	13.5	14.0	14.0	14.2	14.0	14.2	13.9	14.6	14.6	14.6	14.6	14.4
FeO	12.42	12.4	12.4	12.5	12.2	12.5	12.0	12.0	12.8	12.2	12.3	12.8
MgO	3.59	3.8	3.6	3.7	3.7	3.7	3.6	3.8	3.8	3.9	3.7	3.7
CaO	7.12	7.2	7.1	7.3	7.3	7.2	7.1	7.6	7.4	7.5	7.2	7.3
Na_2O	3.16	3.1	3.2	3.3	2.8	3.2	3.0	3.1	3.2	3.2	3.1	3.0
K_2O	1.79	1.9	1.8	1.8	1.8	1.8	1.9	1.8	1.9	1.9	1.9	1.8
TiO_2	2.26	2.4	2.6	2.5	2.3	2.3	2.3	2.4	2.5	2.6	2.5	2.3
MnO	0.2	0.2	0.2	0.2	0.1	0.2	0.1	0.2	0.2	0.3	0.1	0.2
P_2O_5	0.35	0.4	0.2	0.6	0.8	0.6	0.6	0.7	0.7	0.9	0.7	0.6
Total		100.4	99.4	101.5	100.2	101.1	99.1	102.5	103.8	103.1	102.3	102.1

Sample	Recomm	Mean	2 sd
Date			
SiO_2	54.1	55.6	1.4
Al_2O_3	13.5	14.3	0.6
FeO	12.42	12.4	0.6
MgO	3.59	3.7	0.2
CaO	7.12	7.3	0.3
Na_2O	3.16	3.1	0.2
K_2O	1.79	1.8	0.1
TiO_2	2.26	2.4	0.2
MnO	0.2	0.2	0.1
P_2O_5	0.35	0.6	0.4
Total		101.4	3.0

Appendix B: Analytical methods and history

XRF: instrumental precision, accuracy and detection limit

	BCR-2	BCR-2			Results for five replicate XRF preparations of LP14SG04						
	Recommended	Measured	% error	LOD						Mean	2 sdev
Date prep		May/June 2013			26/11/2014	18/04/2016	18/04/2016	18/04/2016	18/04/2016		
Ni	12	13	4.4	0.6	8	7	8	7	8	8	1
Cr	18	18	2.4	1.5	16	13	14	12	16	14	4
V	416	406	2.5	1.4	81	78	80	79	79	79	2
Sc	33	31	6.2	1.5	2	3	2	2	2	2	1
Cu	19	20	3.5	0.3	10	10	10	10	10	10	0
Zn	127	121	4.4	0.4	108	108	108	108	107	108	1
As	1	1	39.1	0.2	1	1	1	1	1	1	1
S	160	321	100.7	2	121	100	98	97	95	102	21
Ga	23.0	22.6	1.8	0.4	25.4	25.6	25.5	25.3	25.3	25.4	0.3
Pb	11.0	10.7	3.0	0.4	6.5	7.4	7.3	6.9	7.0	7.0	0.7
Sr	343.0	339.9	0.9	0.2	1160.9	1152.3	1155.7	1153.8	1149.1	1154.4	8.7
Rb	47.0	47.5	1.0	0.1	94.6	94.8	95.0	95.0	94.3	94.7	0.6
Ba	680.0	693.5	2.0	1.5	850.5	848.2	848.1	843.7	837.7	845.7	10.2
Zr	186.0	186.5	0.3	0.1	510.2	510.0	511.3	510.5	507.4	509.9	2.9
Nb	12.6	12.5	0.9	0.1	157.8	157.7	157.7	158.0	156.9	157.6	0.8
Ta	0.7	0.6	17.0	0.6	8.3	8.3	8.2	8.2	7.8	8.2	0.4
Mo	250.0	221.2	11.5	0.15	5.9	6.3	6.3	6.4	6.5	6.3	0.5
Th	5.9	6.5	9.5	0.3	10.5	10.0	9.9	9.8	9.9	10.0	0.5
U	1.7	1.7	0.6	0.3	3.6	2.8	2.4	2.5	2.9	2.8	1.0
Y	37.0	36.0	2.6	0.2	24.8	25.3	25.2	25.3	25.0	25.1	0.5
La	25.0	28.4	13.5	1.8	72.2	71.3	71.5	71.8	70.0	71.3	1.7
Ce	53.0	55.6	4.9	2.2	133.3	129.4	129.2	130.8	130.0	130.5	3.3
Nd	28.3	28.9	2.1	1.5	51.1	50.4	50.6	49.9	50.9	50.6	0.9
Sm	6.6	7.1	8.2	2	9.6	7.9	7.7	9.4	8.0	8.5	1.8
Yb	3.4	3.2	6.0	0.8	2.7	2.5	1.8	1.8	1.9	2.1	0.9
Hf	4.85	4.5	7.8	5	5.5	10.5	9.5	9.8	9.0	8.9	4.0
Cs	1.1	2.2	1.0	1.5	1	1	0	1	1	1	1

Appendix B: Analytical methods and history

XRF: instrumental precision and accuracy

	BCR-2	BCR-2		Results for four replicate XRF preparations of LP14SG08				Mean	2 sdev
	Recommended	Measured	% error						
Date prep		May/June 2013		05/03/2015	29/01/2016	29/01/2016	29/01/2016		
SiO_2	54.10	54.10	0.03	42.94	43.09	43.10	42.98	43.03	0.16
Al_2O_3	13.50	13.52	0.12	12.60	12.71	12.59	12.57	12.62	0.12
Fe_2O_3	13.80	13.69	0.03	13.45	13.49	13.63	13.58	13.54	0.16
MgO	3.59	3.57	0.07	10.28	10.20	10.36	10.23	10.27	0.14
CaO	7.12	7.17	0.27	11.18	11.25	11.30	11.24	11.24	0.09
Na_2O	3.16	3.12	0.03	2.98	3.00	2.96	2.96	2.97	0.03
K_2O	1.79	1.78	0.86	1.28	1.30	1.28	1.29	1.29	0.02
TiO_2	2.26	2.28	0.01	3.37	3.39	3.40	3.39	3.39	0.03
MnO	0.20	0.20	0.02	0.18	0.18	0.18	0.18	0.18	0.00
P_2O_5	0.35	0.36	0.13	0.55	0.55	0.54	0.55	0.55	0.01
Total	99.87	99.80	0.02	98.83	99.25	99.46	99.08	99.15	0.54

APPENDIX C: SUPPORTING ANALYTICAL DATA

Analytical techniques (Ar-Ar, XRF, radiogenic isotopes and EPMA) used in this thesis all resulted in the production of additional data that was not included in individual chapters.

^{40}AR/^{39}AR GEOCHRONOLOGY

Multiple analyses of individual samples were combined to produce composite plateau from which age determinations were taken. Composite plateau of all samples are presented. Calculating this data as isochrons allows the composition of any trapped argon component to be determined. Isochrons for all samples are presented. Data is presented in stratigraphic order.

EDS-EPMA

Complete EDS-EPMA data for all mineral analyses used in Chapter 5 is presented.

X-RAY FLUORESCENCE (XRF)

Complete major and trace element data of all samples not included in the main body thesis are presented. In the majority of cases these are alternate samples from the same lava-units as those previously presented, and the most similar sample is indicated under "alternate".

CPX-MELT THERMOBAROMETRY

All data was collected by Andreas Klügel. New LA-ICP-MS and EPMA data is presented along with *Bejenado* data collected and presented previously in Galipp et al. (2006) but now presented in the context of *Bejenado's* new stratigraphy..

LP13SG05 Isochron

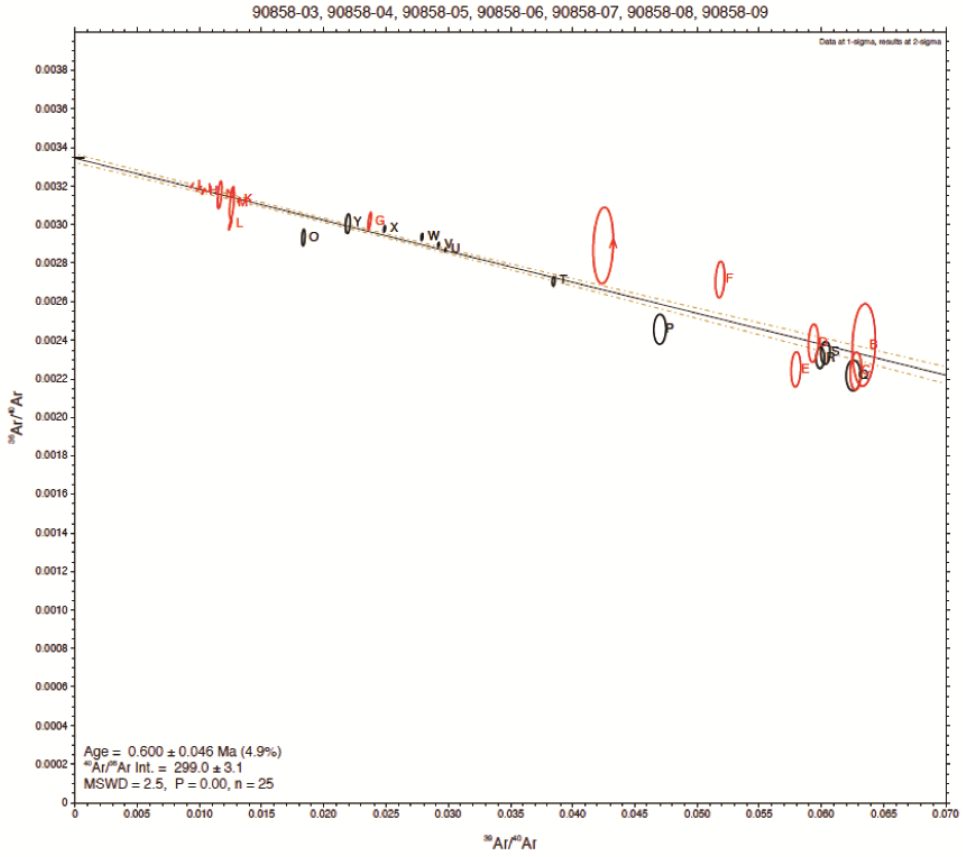

Plateau age determination

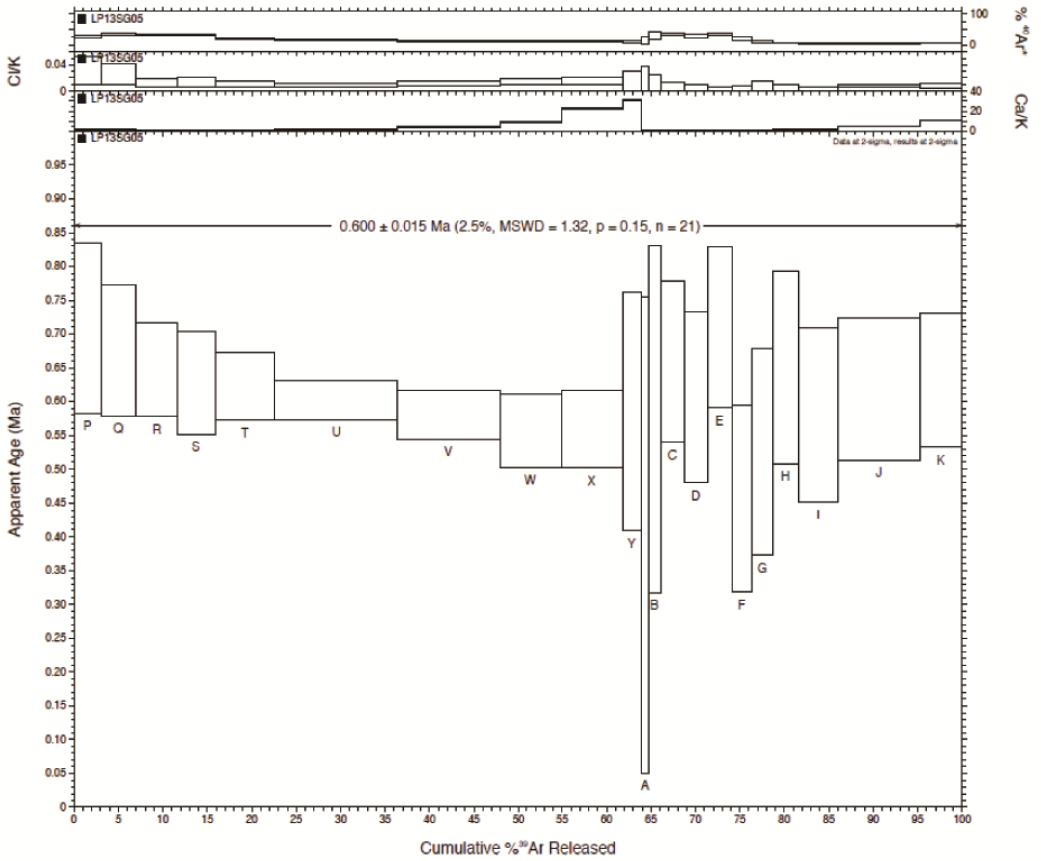

El Time: LP13SG06

Isochron

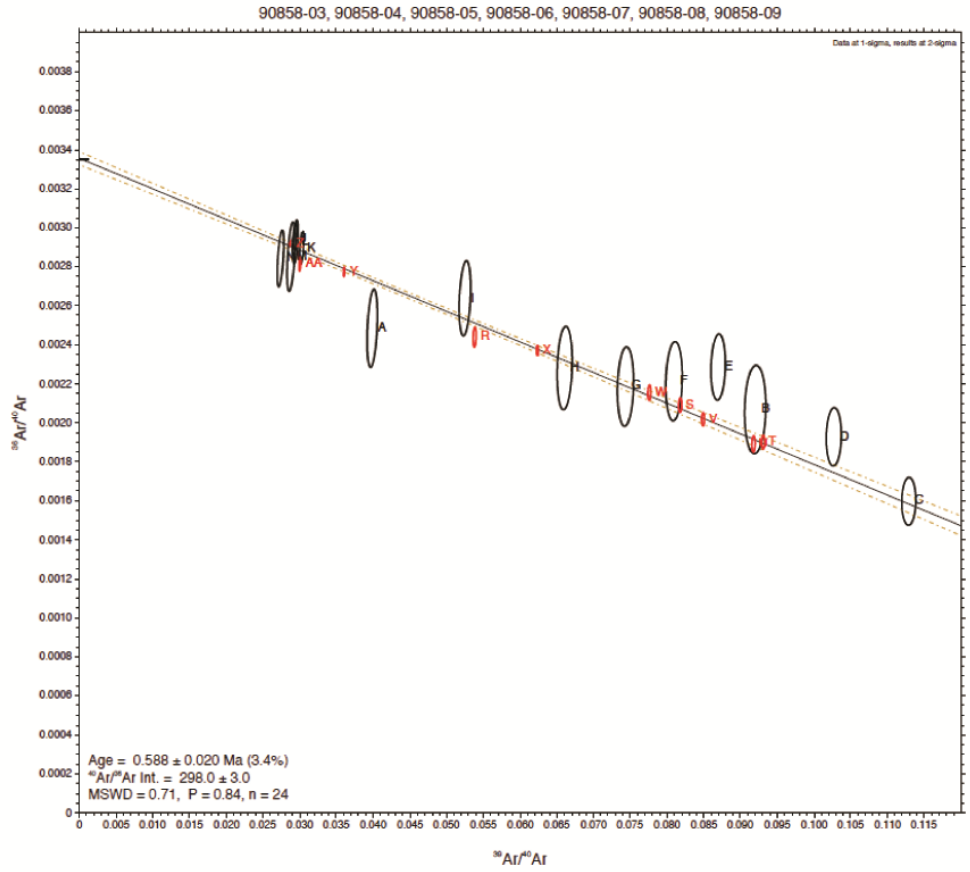

Plateau age determination

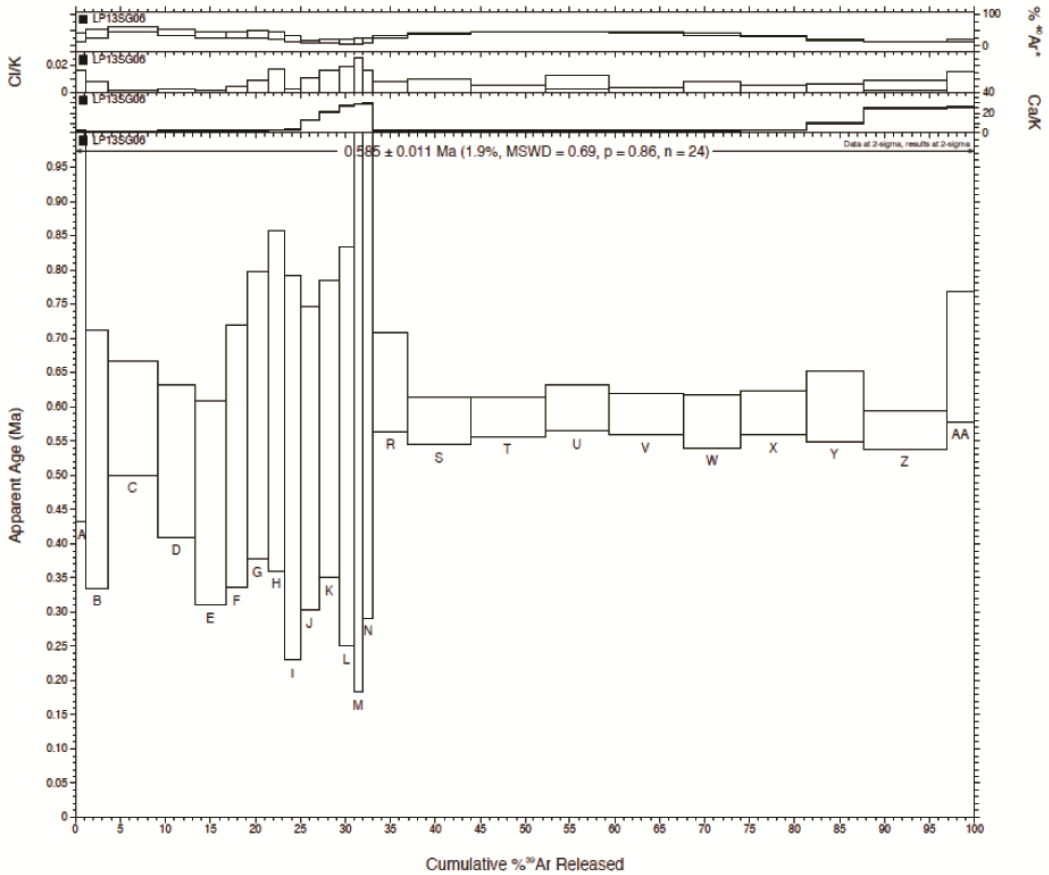

El Time: LP12SG15 Isochron

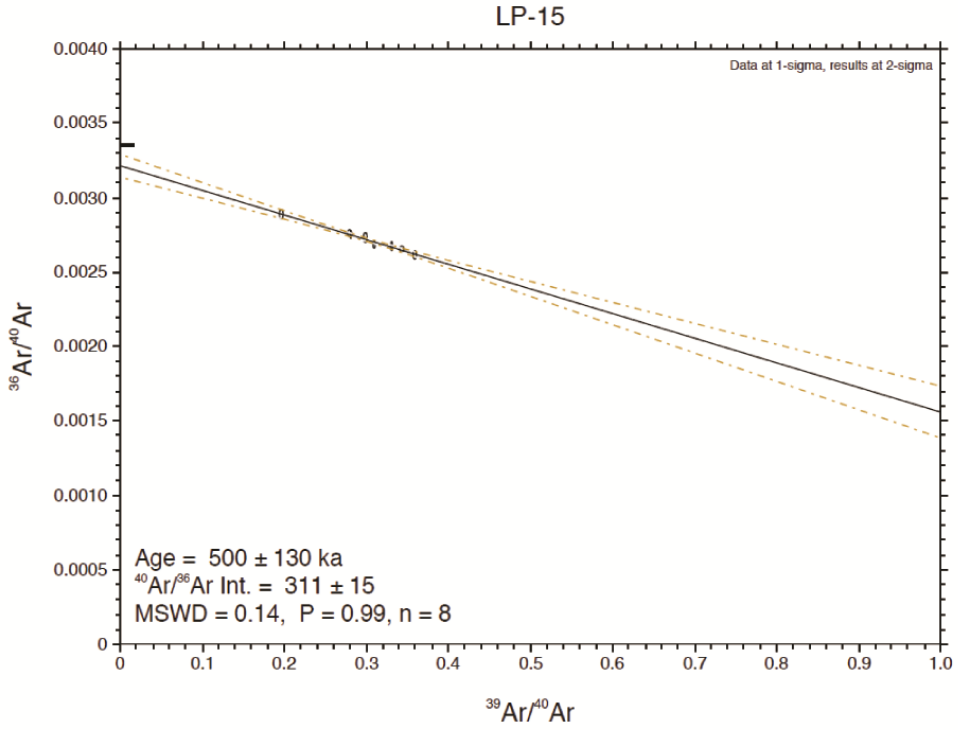

Plateau age determination

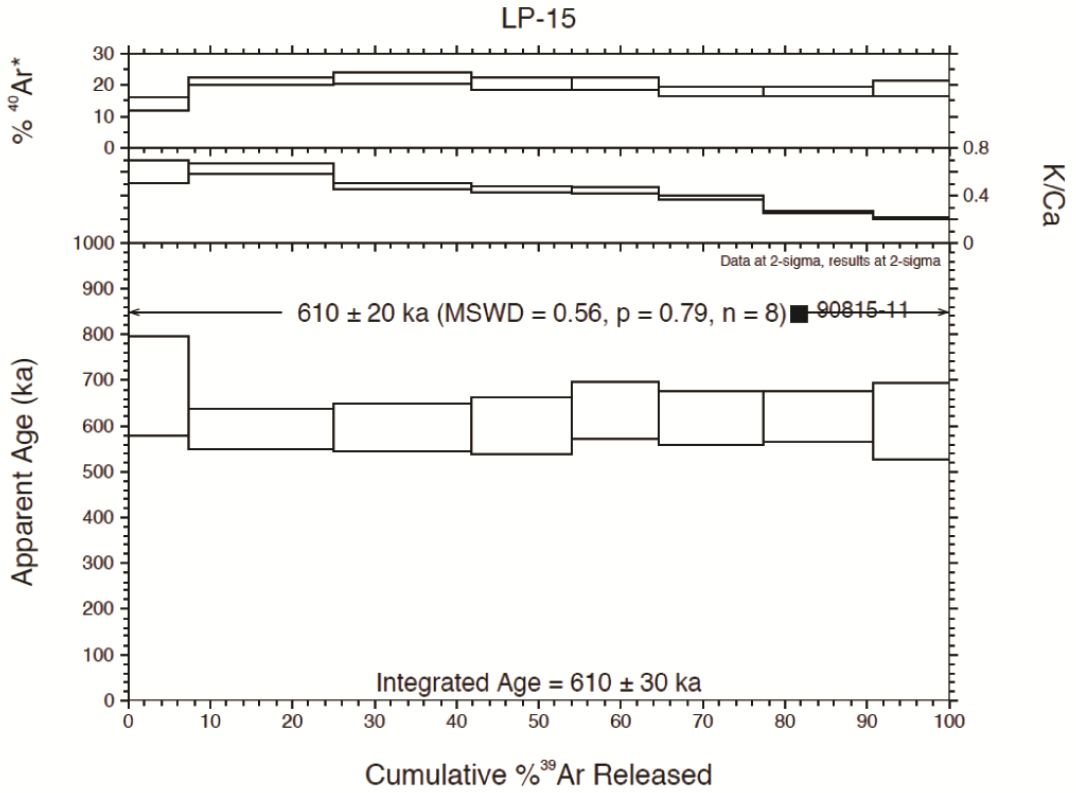

El Time: LP12SG10 Isochron

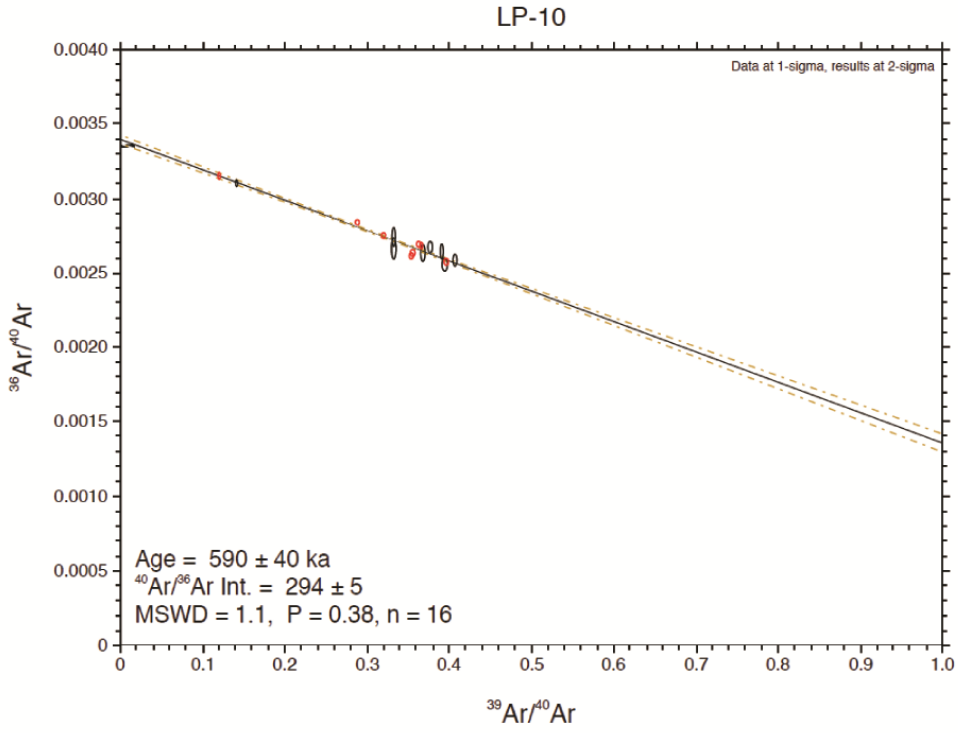

Plateau age determination

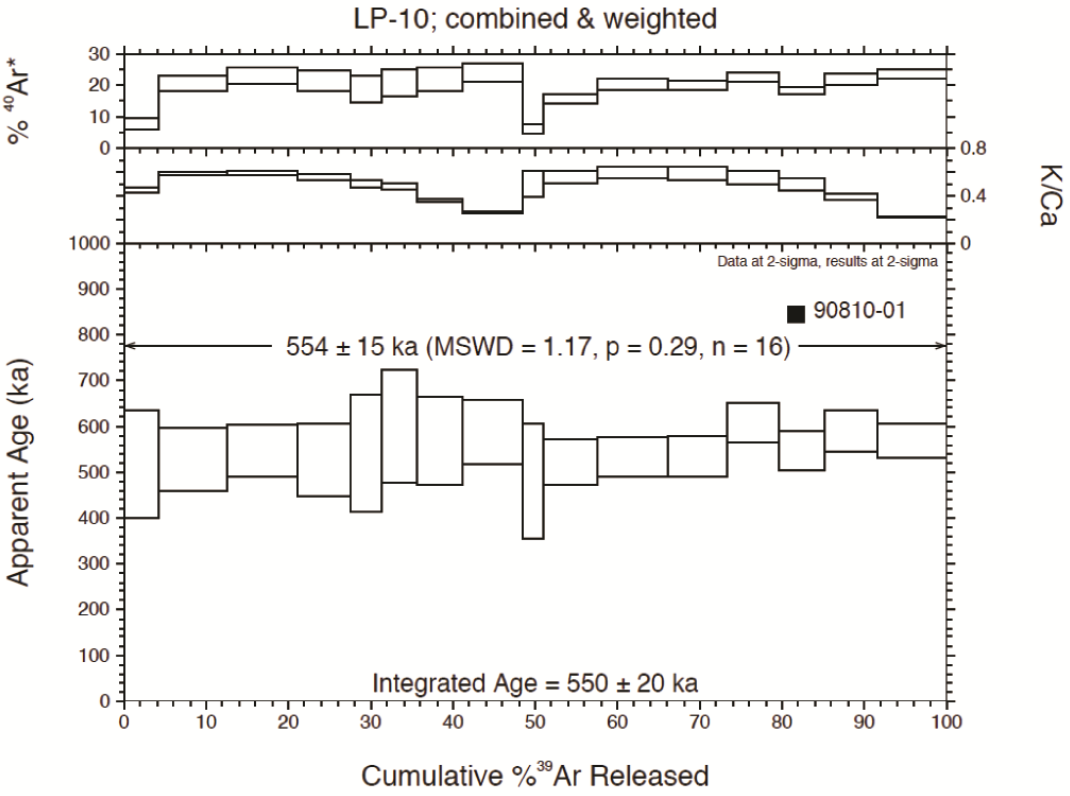

El Time: LP12SG14 Isochron

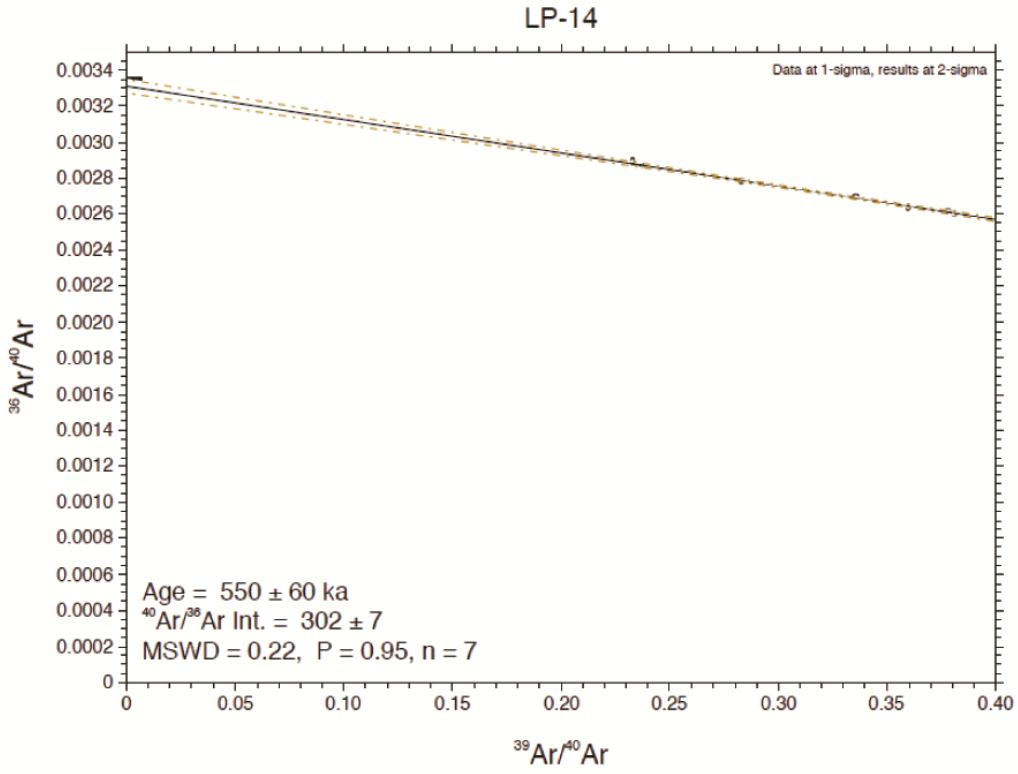

Plateau age determination

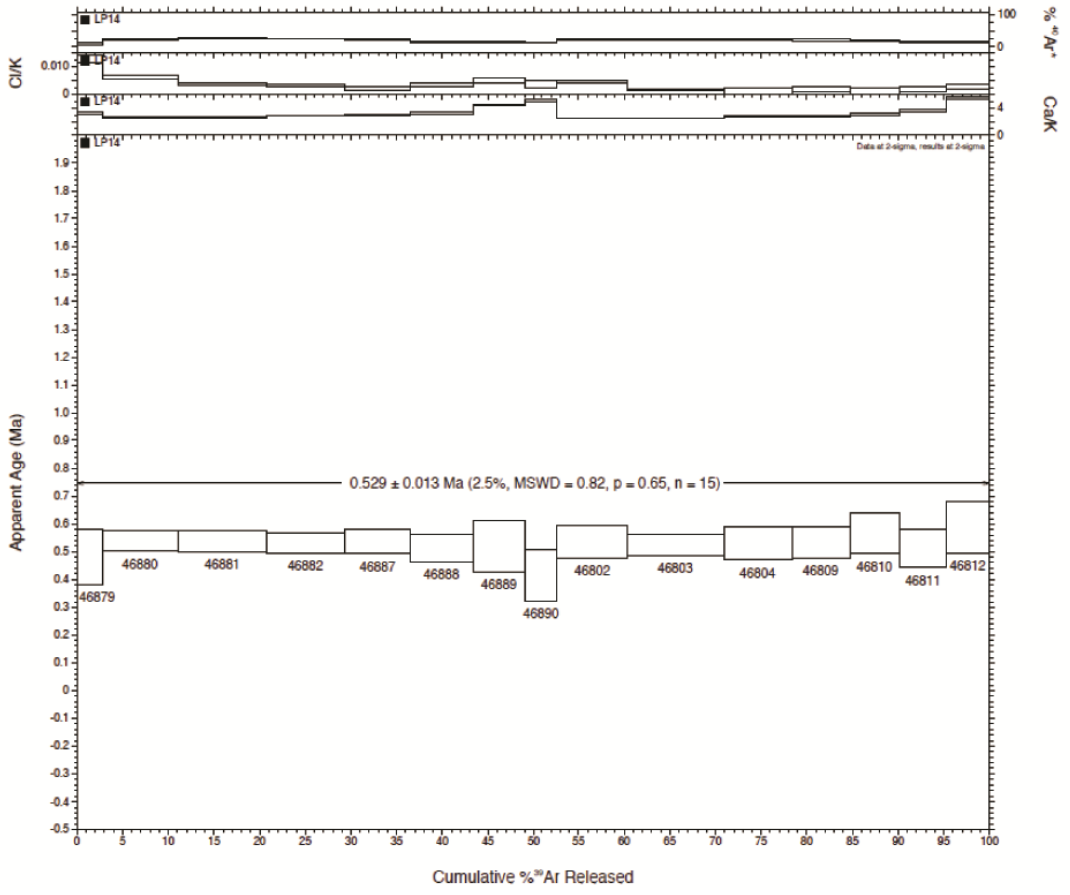

Bejenado: LP13SG38 Isochron

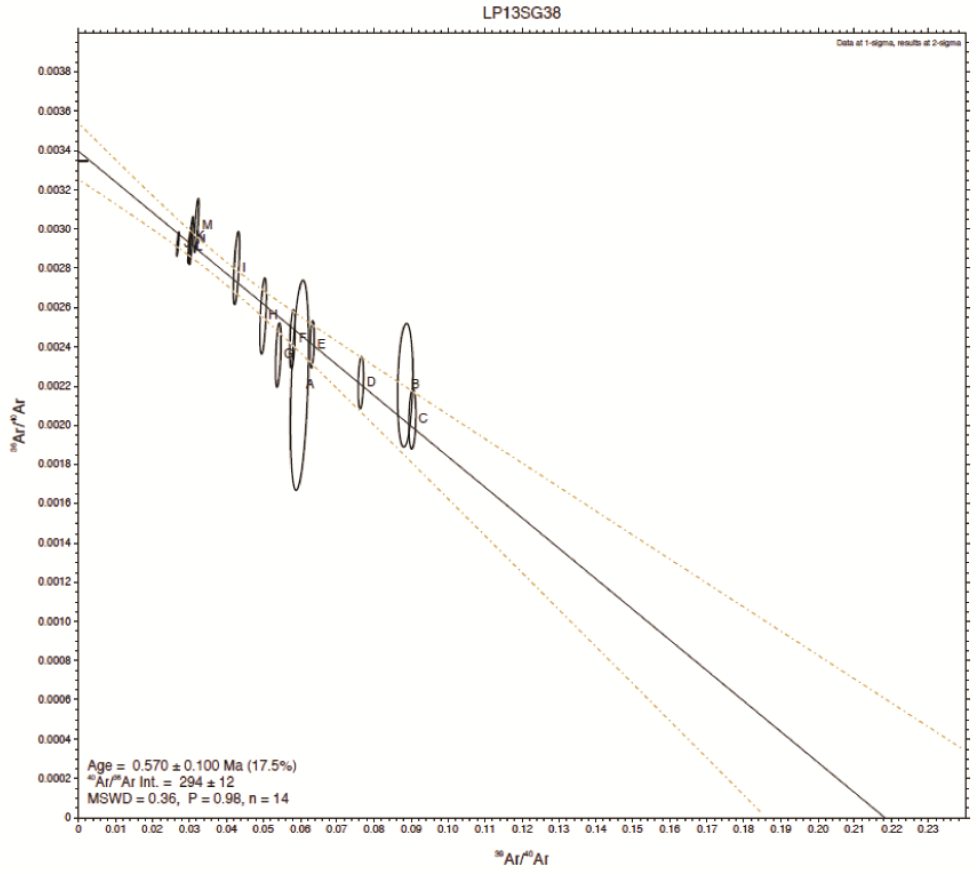

Plateau age determination

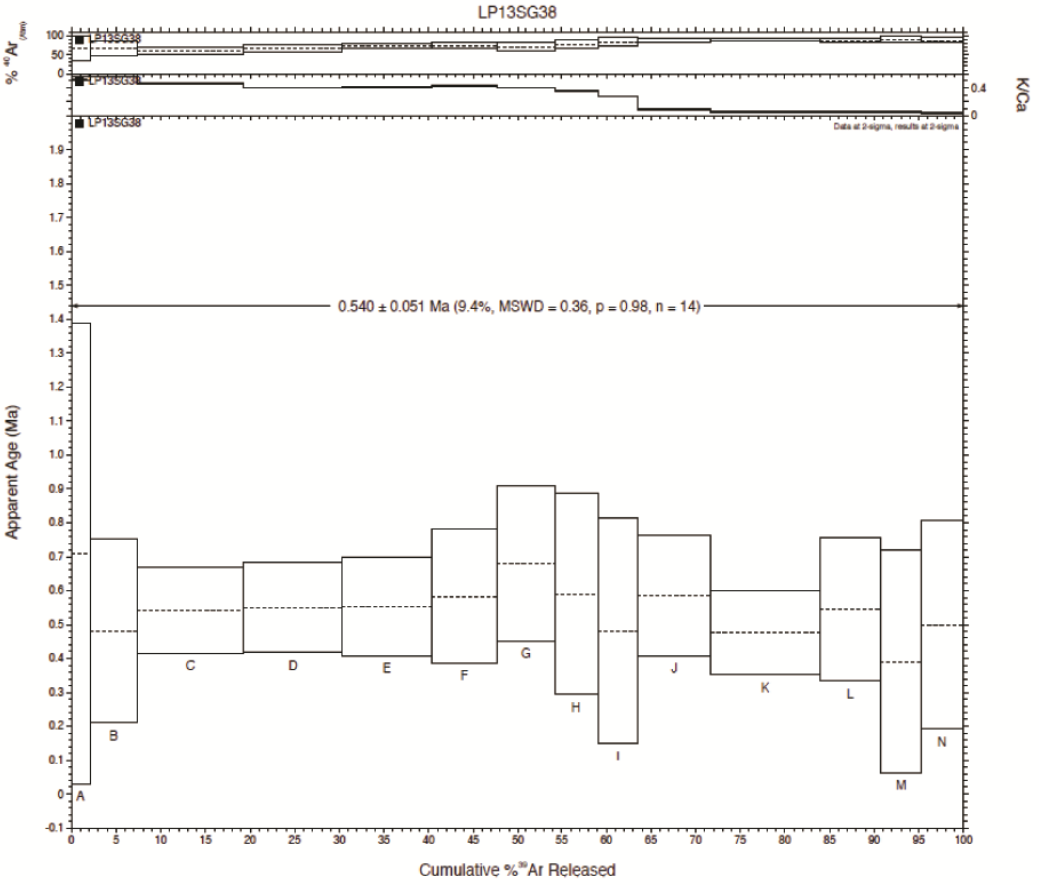

Bejenado: LP12SG87 Isochron

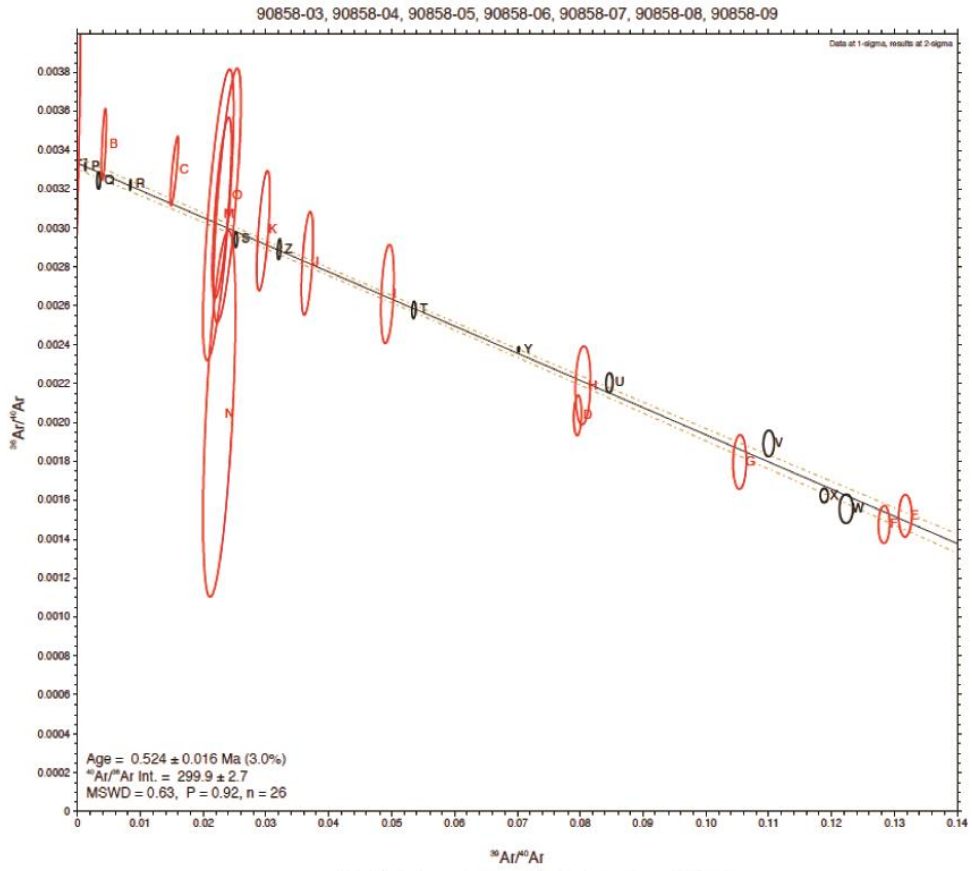

Plateau age determination

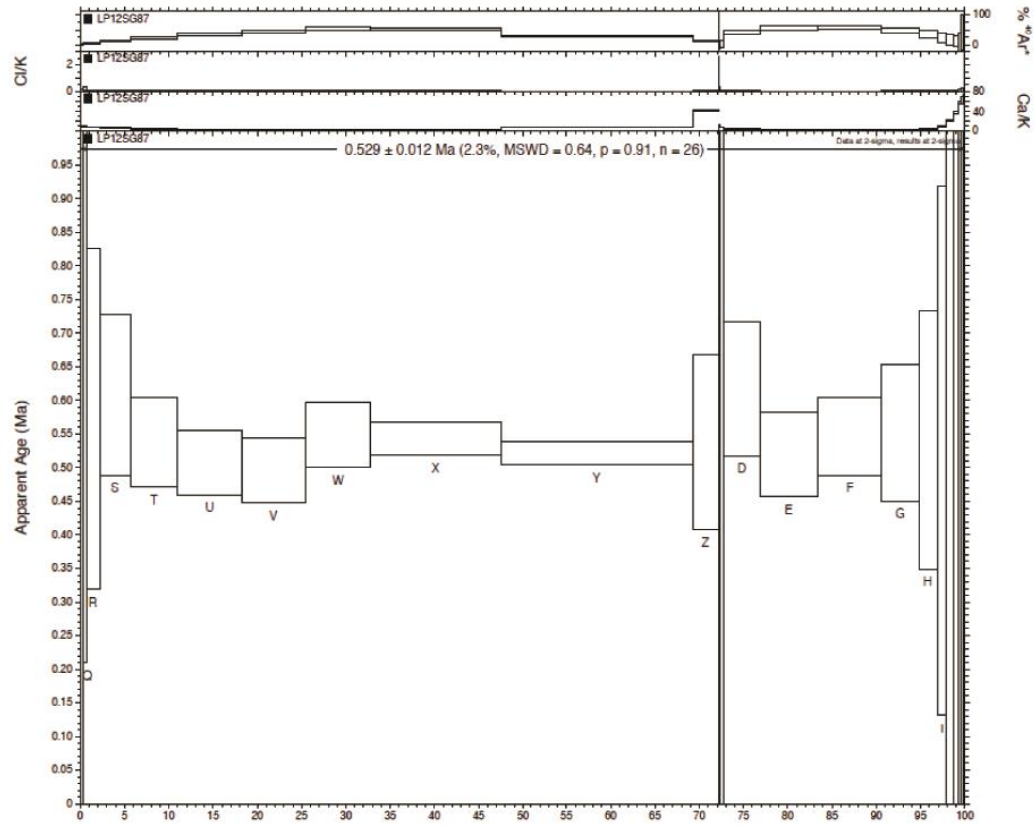

Bejenado: LP14SG02 Isochron

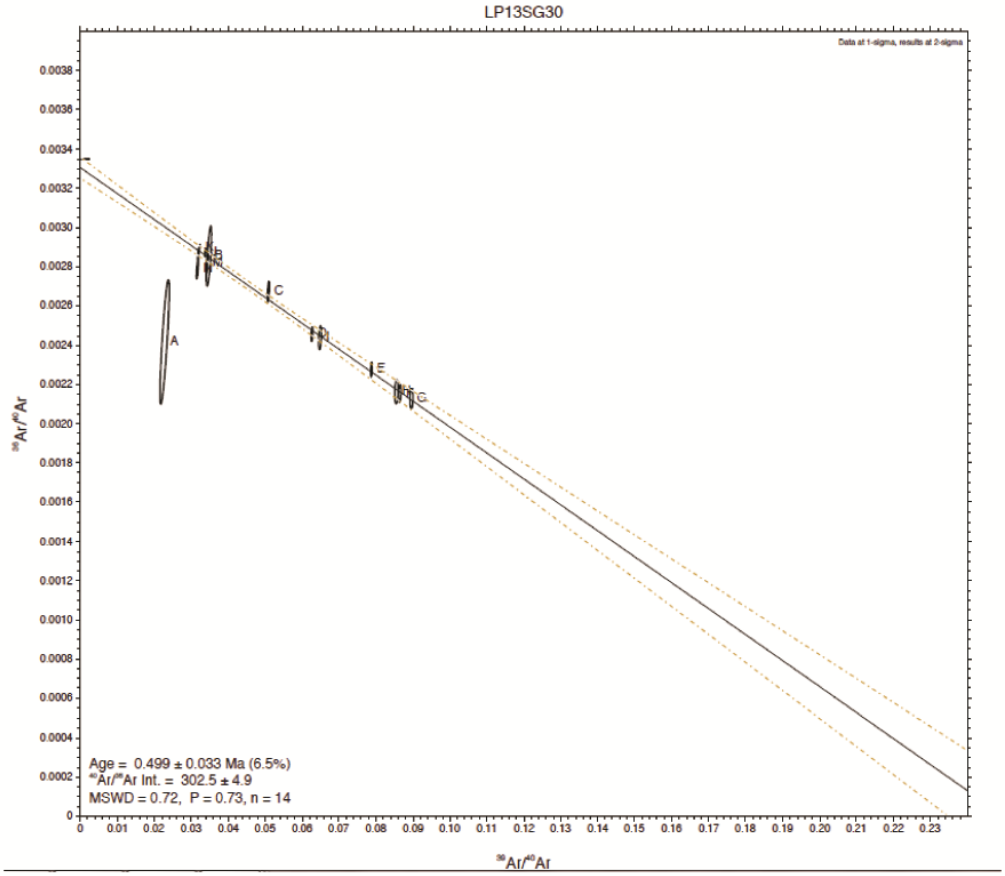

Plateau age determination

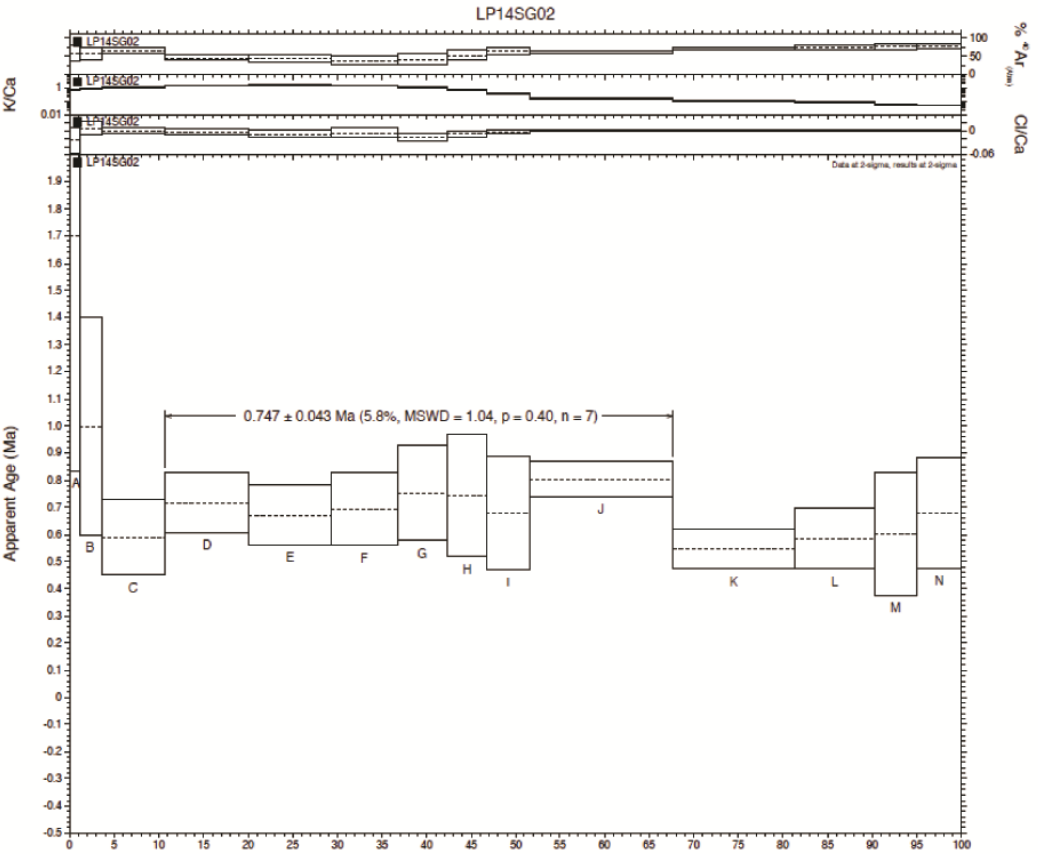

Bejenado: LP13SG30 Isochron

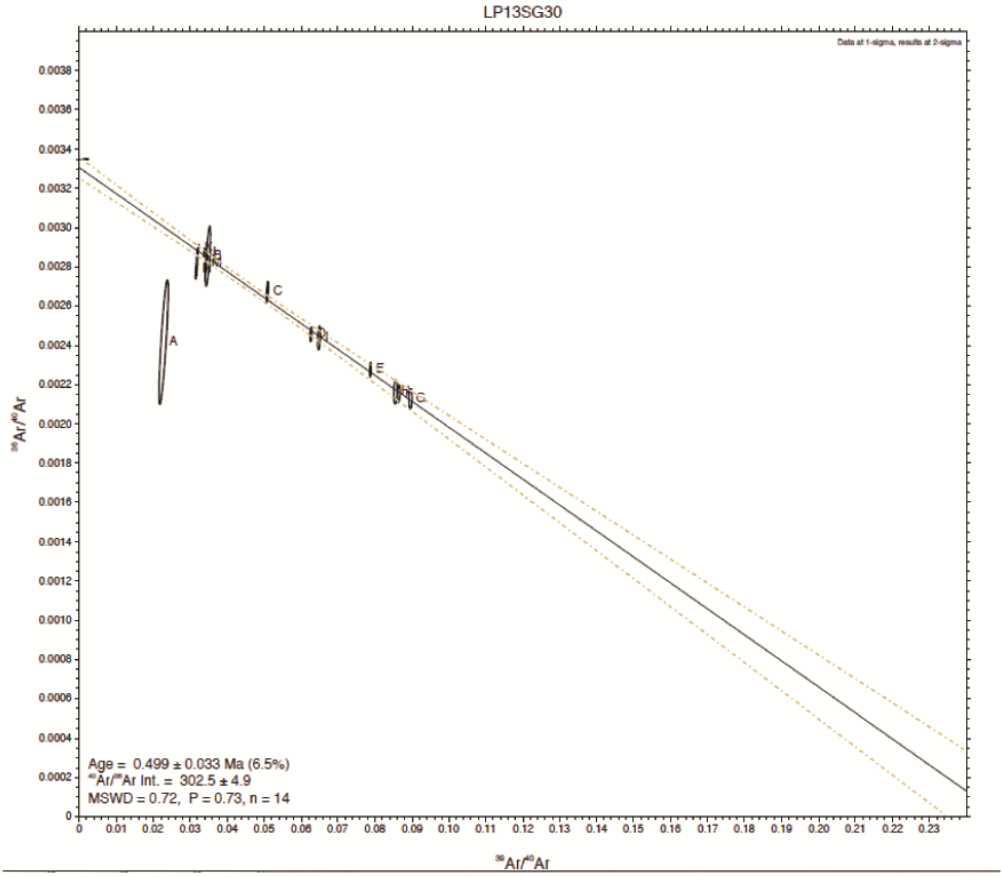

Plateau age determination

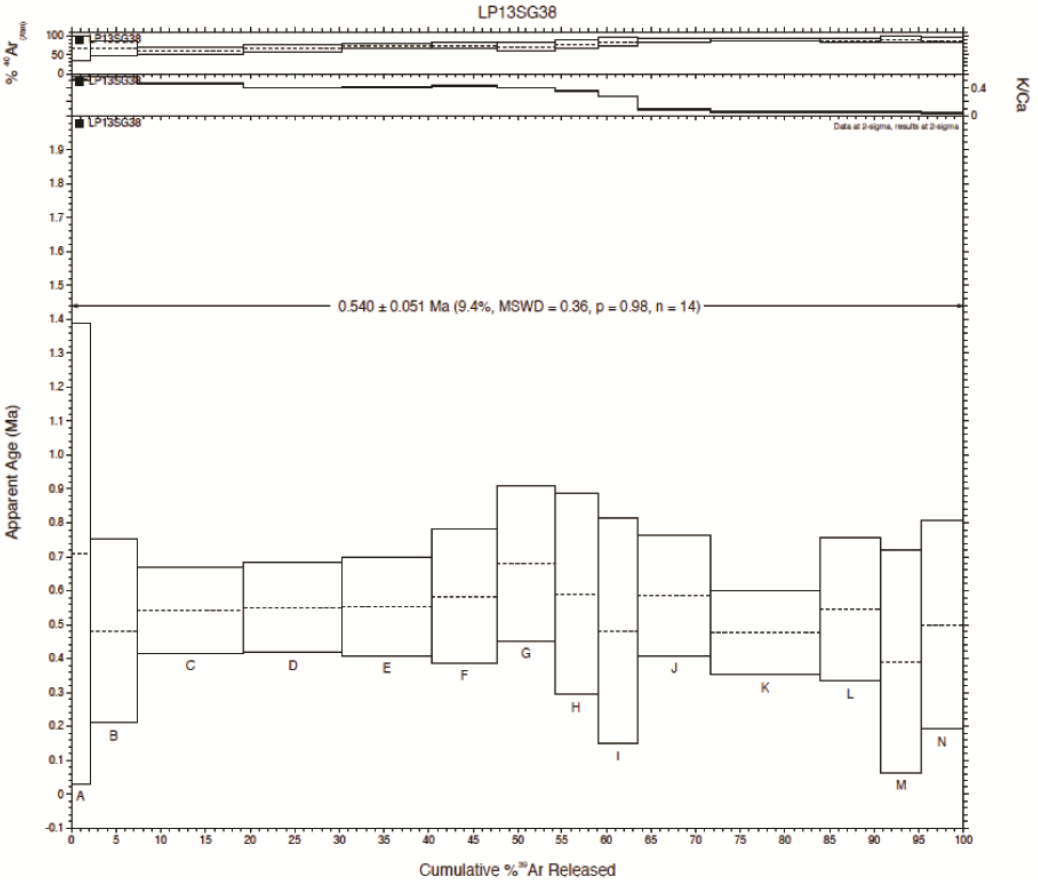

Bejenado: LP13SG29 Isochron

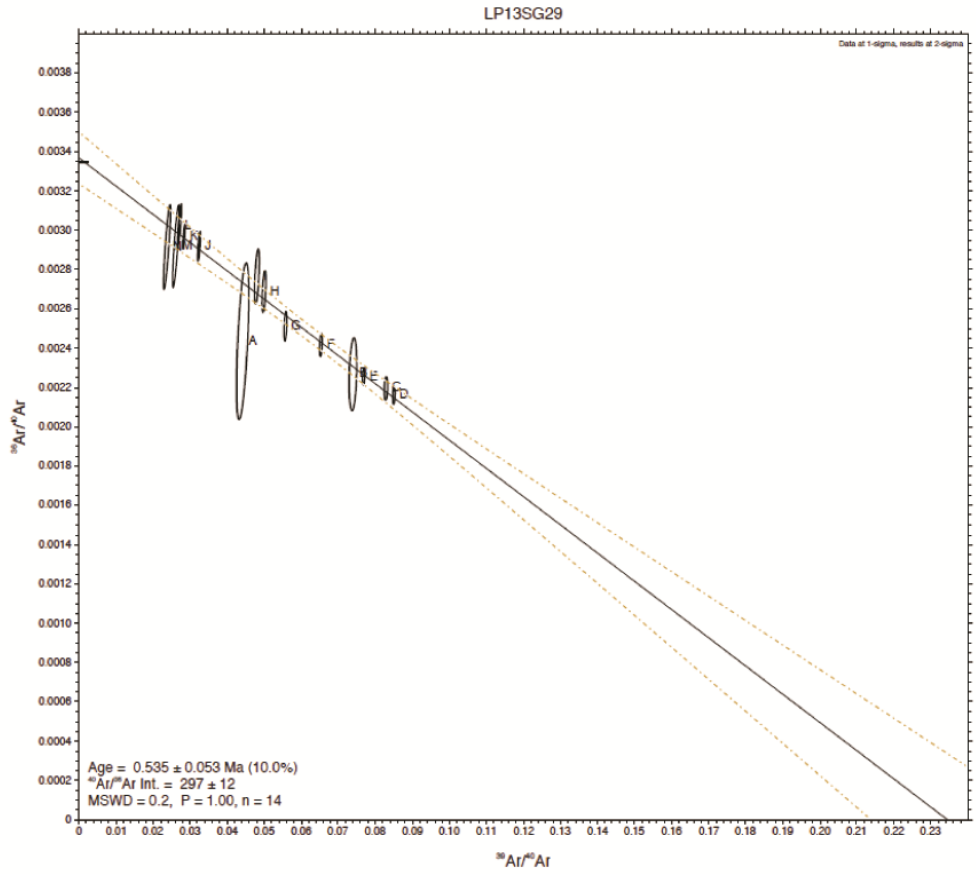

Plateau age determination

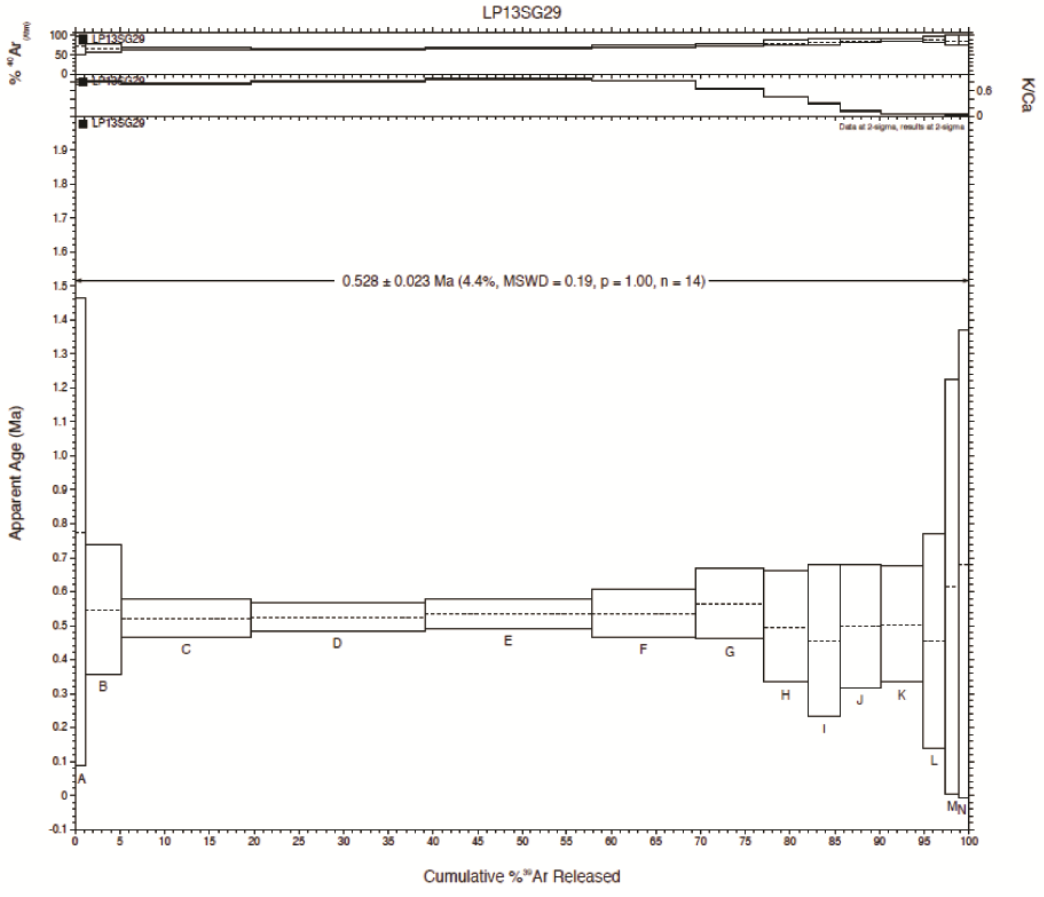

Bejenado: LP14SG09 Isochron

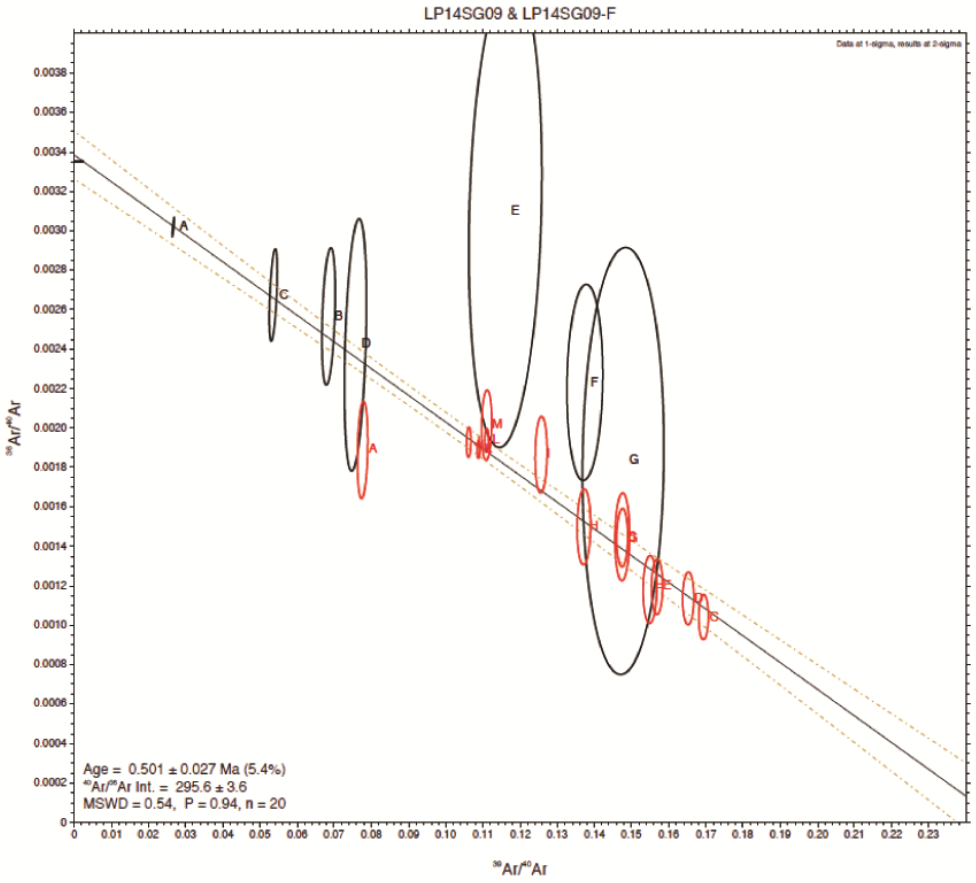

Plateau age determination

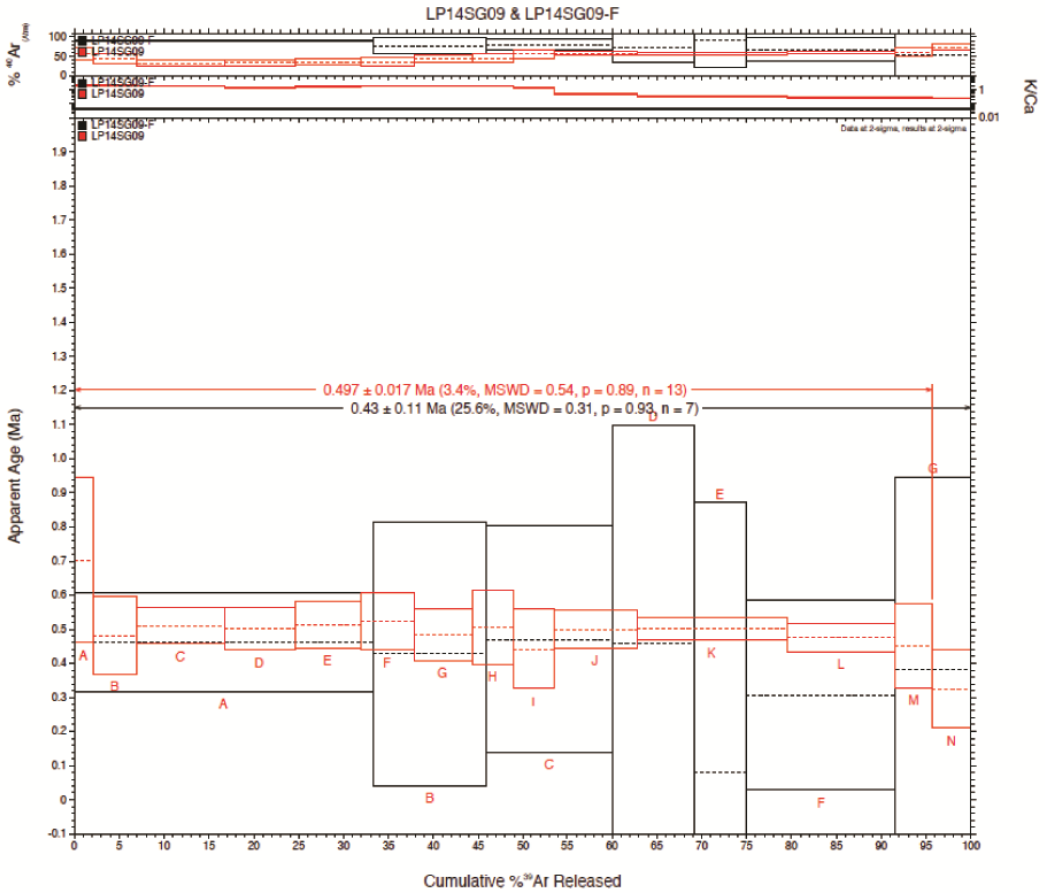

Bejenado: LP12SG02 Isochron

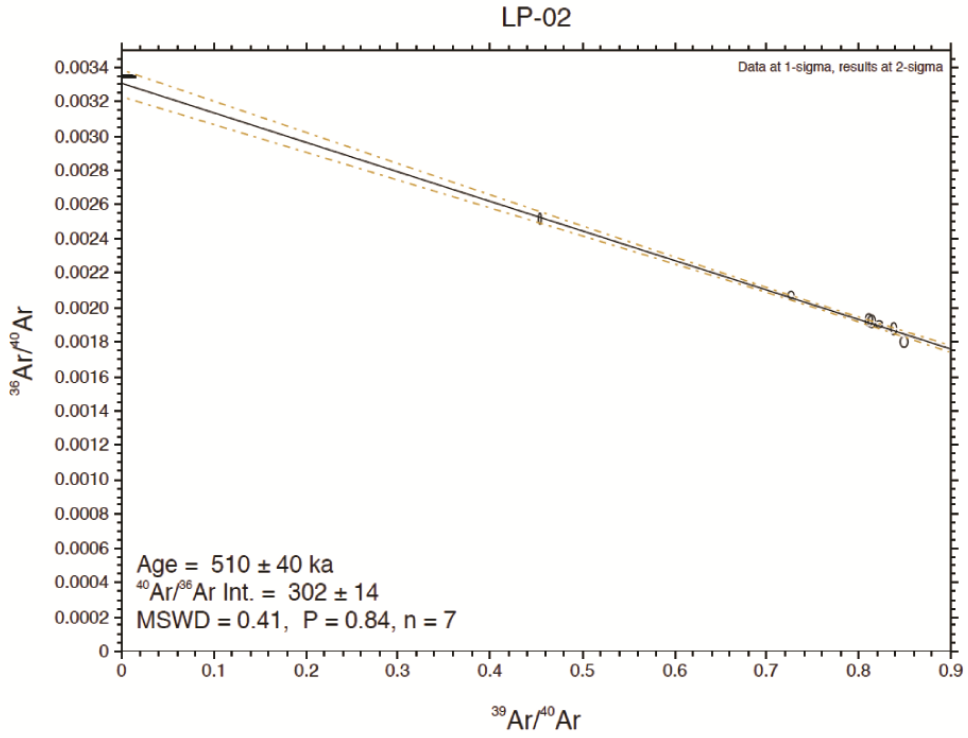

Plateau age determination

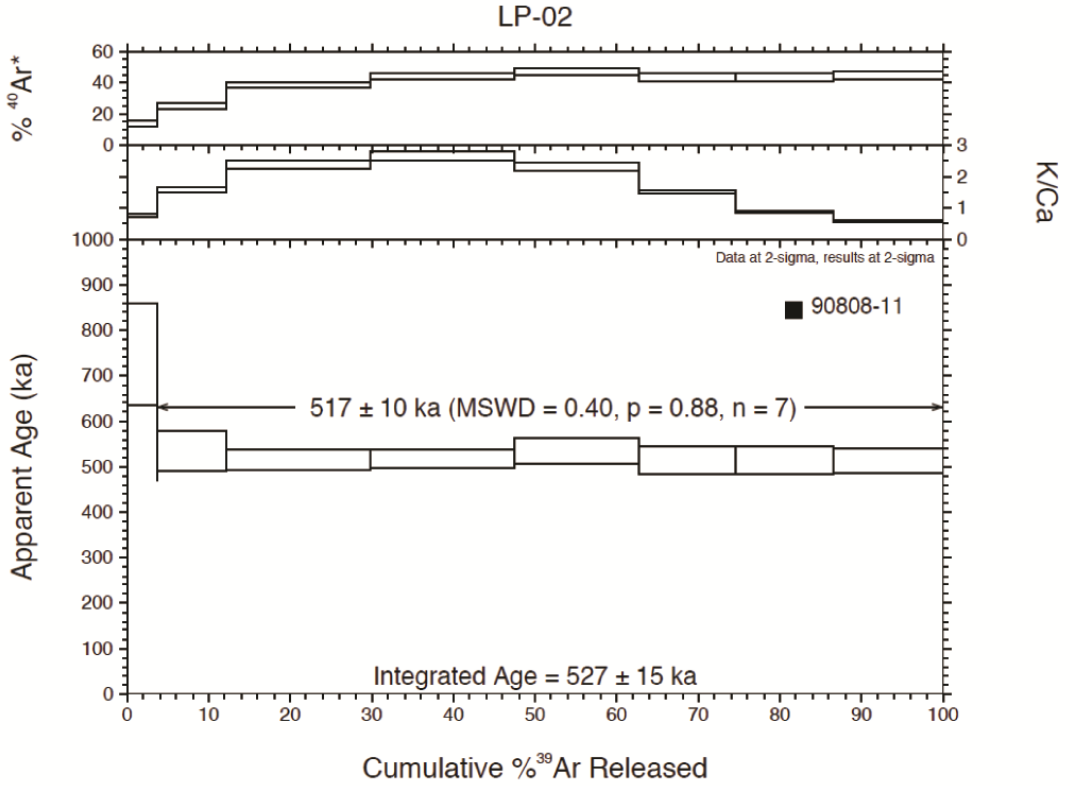

Bejenado: LP13SG16 Isochron

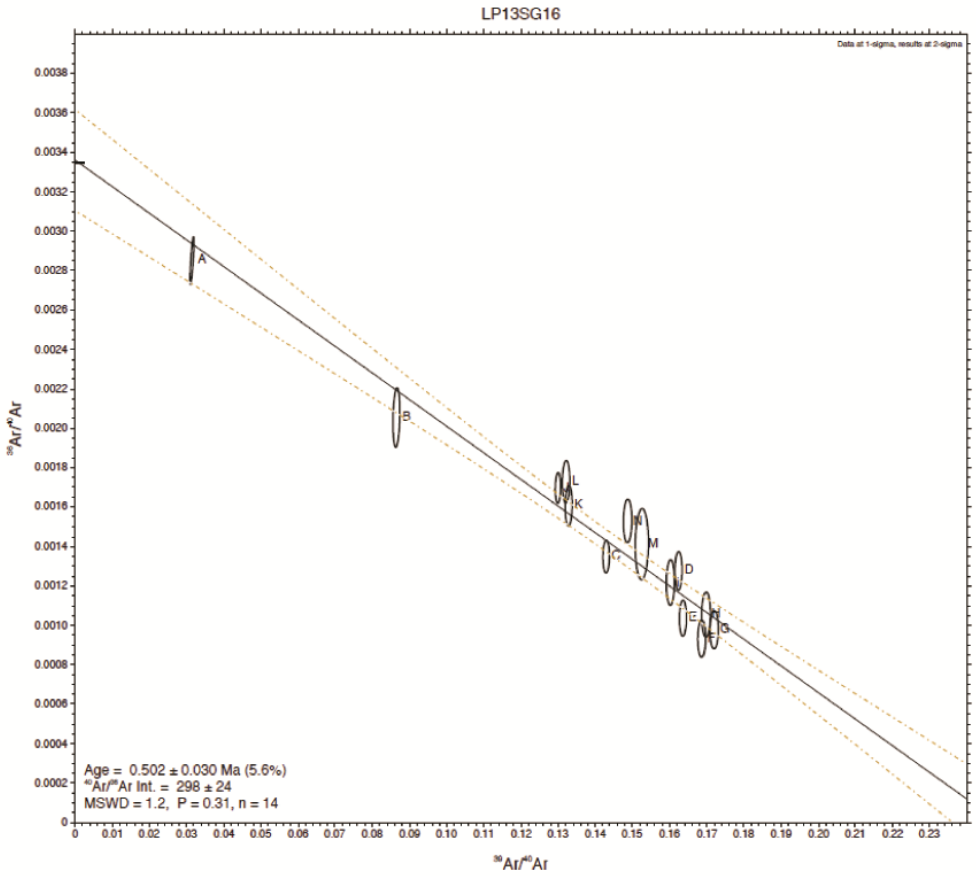

Plateau age determination

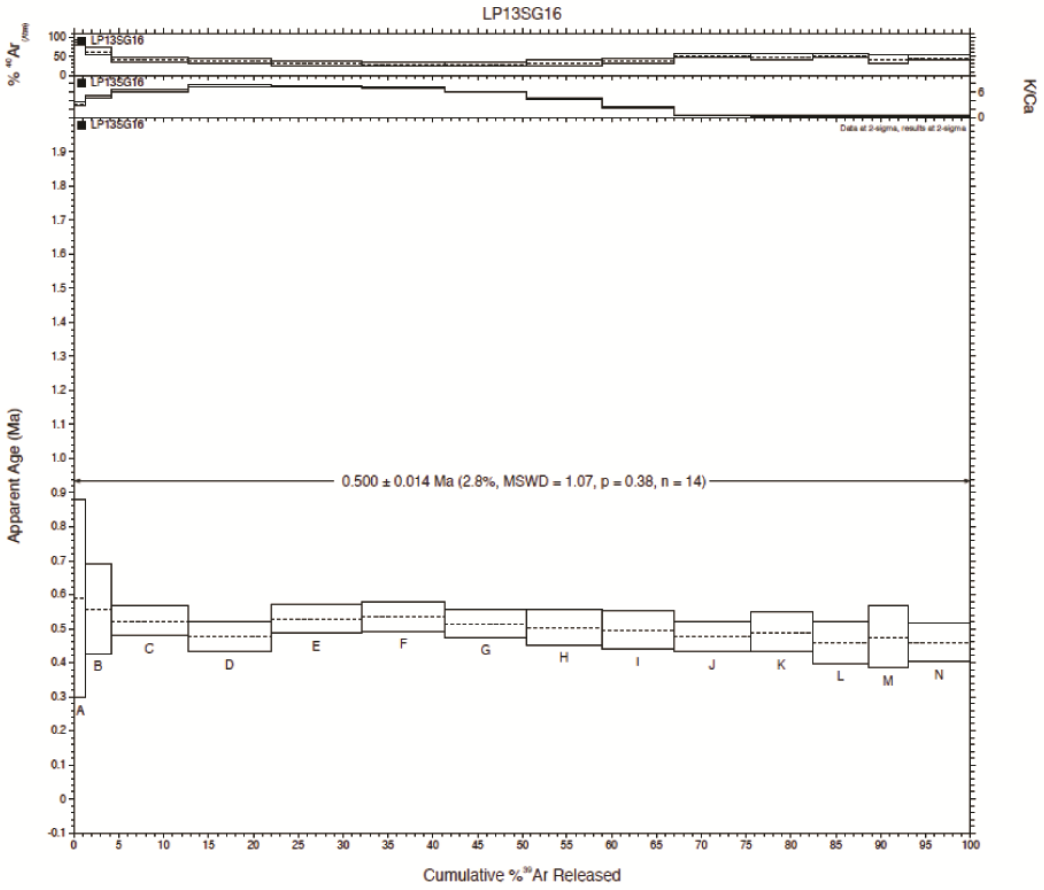

Bejenado: LP14SG07 Isochron

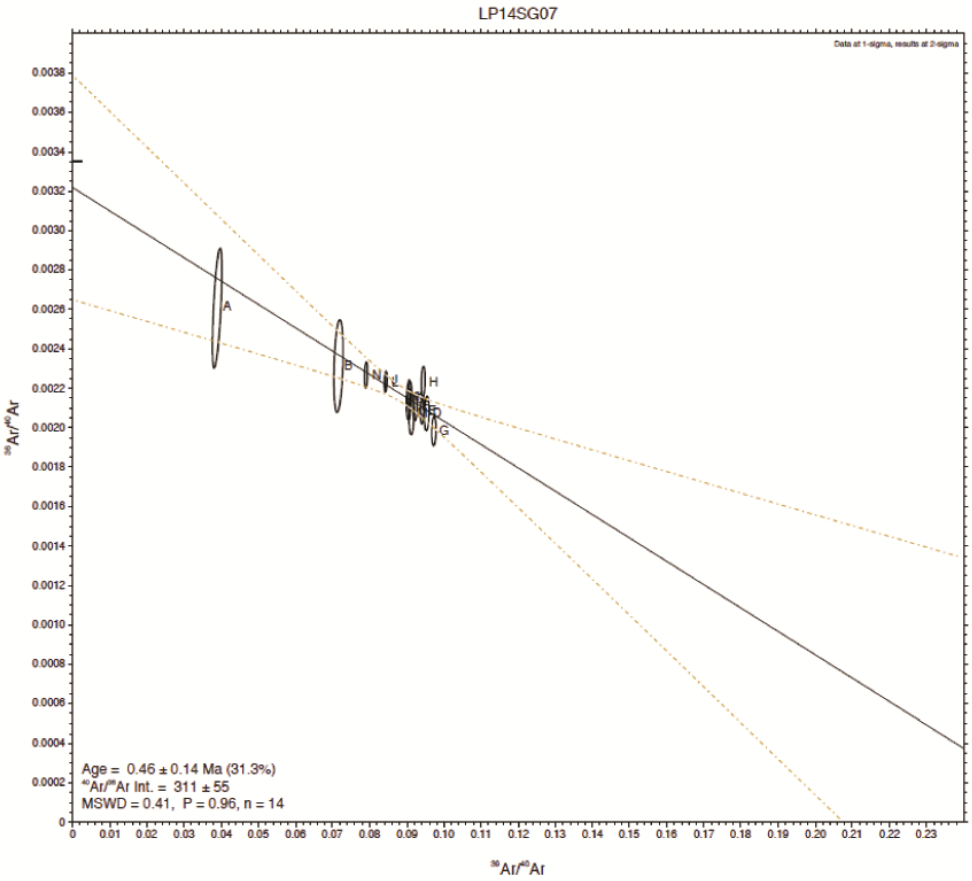

Plateau age determination

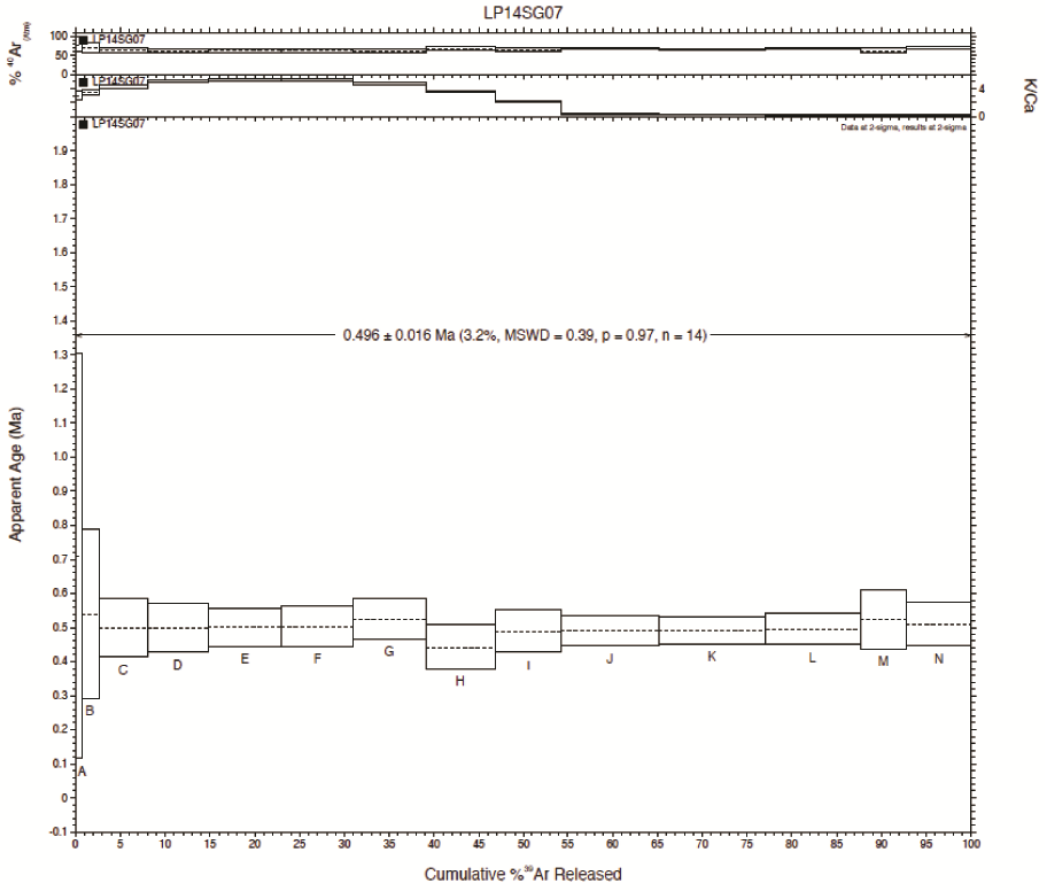

Pyroxenes

Lava-unit	Glomerocrystic Ankaramite									
Sample	LP13SG29	LP13SG29	LP13SG29	LP13SG29	LP13SG29	LP13SG29	LP13SG29	LP14SG08	LP14SG08	LP14SG08
Mineral ID	CPX_1	CPX_2	CPX_3	CPX_4	CPX_5	CPX_6	CPX_7	CPX_1	CPX_2	CPX_3
Mineral Population	Aggregate Core	Aggregate Core	Aggregate Core	Aggregate Core	Aggregate Core	Aggregate Core	Aggregate Core	Aggregate Core	Aggregate Core	Aggregate Core
SiO_2	47.4	47.8	47.6	48.3	47.8	46.8	47.1	48.1	47.2	47.2
TiO_2	2.3	2.4	2.3	2.2	1.8	2.8	2.5	1.9	1.8	2.0
Al_2O_3	7.7	6.8	7.1	7.0	7.0	6.9	6.5	6.3	6.6	6.6
FeO	6.6	6.4	6.5	6.4	6.2	7.0	5.9	5.8	5.9	6.2
MnO	0.1	0.1	0.0	0.2	0.1	0.2	0.1	0.1	0.1	0.1
Cr_2O_3	0.7	0.4	0.2	0.4	0.4	0.1	0.7	0.6	0.8	0.8
MgO	13.5	13.6	13.5	13.9	13.7	13.1	13.5	14.1	13.6	13.7
CaO	22.0	22.2	22.2	22.3	21.8	22.5	23.0	22.0	21.7	21.8
Na_2O	0.7	0.6	0.7	0.6	0.6	0.6	0.5	0.6	0.7	0.6
K_2O	0.0	0.0	0.0	0.0	0.0	0.1	0.0	0.0	0.0	0.0
Total	100.9	100.3	100.2	101.1	99.6	99.9	99.7	99.4	98.5	99.0
mg #	0.78	0.79	0.79	0.80	0.80	0.77	0.80	0.81	0.80	0.80

All presented concentrations are in oxide wt% with O_2 determined by stoichiometry, all Fe is determined as FeO

Pyroxenes

Lava-unit	Glomerocrystic Ankaramite									
Sample	LP14SG08	LP14SG08	LP13SG29	LP13SG29	LP13SG29	LP13SG29	LP13SG29	LP13SG29	LP13SG29	LP14SG08
Mineral ID	CPX_4	CPX_5	CPX_1	CPX_2	CPX_3	CPX_4	CPX_5	CPX_6	CPX_7	CPX_1
Mineral	Aggregate	Aggregate	Overgrowth	Overgrowth	Overgrowth	Overgrowth	Overgrowth	Overgrowth	Overgrowth	Overgrowth
Population	Core	Core	Rim	Rim	Rim	Rim	Rim	Rim	Rim	Rim
SiO_2	46.7	47.6	43.2	45.4	44.8	46.1	43.4	44.4	44.9	45.3
TiO_2	2.4	1.9	4.1	3.5	3.9	3.7	4.3	3.9	3.4	3.3
Al_2O_3	7.7	6.6	10.1	8.7	9.5	8.5	9.8	9.8	8.4	8.3
FeO	6.2	5.9	7.7	7.1	7.8	7.4	7.7	7.6	7.3	7.1
MnO	0.2	0.1	0.2	0.0	0.1	0.1	0.2	0.1	0.2	0.1
Cr_2O_3	0.1	0.7	0.1	0.2	0.1	0.1	0.0	0.1	0.1	0.1
MgO	13.2	13.8	11.2	12.4	11.7	12.6	11.5	11.8	12.1	12.1
CaO	22.0	21.6	22.1	22.3	22.5	23.0	22.0	22.3	22.0	21.9
Na_2O	0.7	0.6	0.7	0.7	0.7	0.6	0.6	0.6	0.6	0.7
K_2O	0.0	0.0	0.0	0.0	0.0	0.0	0.0	0.0	0.0	0.0
Total	99.3	98.9	99.4	100.4	101.0	102.1	99.4	100.7	98.9	99.0
mg #	0.79	0.81	0.72	0.76	0.73	0.75	0.73	0.73	0.75	0.75

All presented concentrations are in oxide wt% with O_2 determined by stoichiometry, all Fe is determined as FeO

Pyroxenes

Lava-unit	Glomerocrystic Ankaramite				Plagioclase Basalt				
Sample	LP14SG08	LP14SG08	LP14SG08	LP14SG08	LP14SG09	LP14SG09	LP14SG09	LP14SG09	LP14SG09
Mineral ID	CPX_2	CPX_3	CPX_4	CPX_5	CPX_1	CPX_2	CPX_3	CPX_4	CPX_5
Mineral	Overgrowth	Overgrowth	Overgrowth	Overgrowth					
Population	Rim	Rim	Rim	Rim	Core	Core	Core	Core	Core
SiO_2	43.4	44.1	44.0	46.3	45.2	43.2	47.9	47.9	48.0
TiO_2	4.3	3.9	3.7	3.0	4.1	4.8	3.1	2.8	3.0
Al_2O_3	9.3	9.2	8.9	6.6	8.6	10.1	6.2	6.2	5.3
FeO	7.6	7.5	7.3	7.0	7.1	7.7	6.7	6.6	7.0
MnO	0.1	0.1	0.1	0.2	0.3	0.1	0.2	0.2	0.3
Cr_2O_3	0.0	0.1	0.1	0.0	0.1	0.1	0.1	0.1	0.0
MgO	11.4	11.6	11.6	12.7	12.1	11.3	13.2	13.6	13.2
CaO	22.0	22.0	22.0	21.9	22.7	22.3	22.7	22.8	22.7
Na_2O	0.7	0.7	0.6	0.6	0.6	0.7	0.7	0.6	0.6
K_2O	0.0	0.0	0.0	0.0	0.0	0.0	0.0	0.0	0.0
Total	98.9	99.2	98.3	98.4	100.9	100.2	100.6	100.6	100.0
mg #	0.73	0.73	0.74	0.76	0.75	0.75	0.78	0.79	0.77

All presented concentrations are in oxide wt% with O_2 determined by stoichiometry, all Fe is determined as FeO

Pyroxenes

Lava-unit	Plagioclase Basalt									
Sample	LP14SG09	LP14SG06	LP14SG06	LP14SG06	LP14SG06	LP14SG06	LP14SG06	LP14SG09	LP14SG09	LP14SG09
Mineral ID	CPX_6	CPX_1	CPX_2	CPX_3	CPX_4	CPX_5	CPX_6	CPX_1	CPX_2	CPX_3
Mineral Population	Core	Core	Core	Core	Core	Core	Core	Rim	Rim	Rim
SiO_2	48.2	47.7	48.2	48.2	44.0	48.1	46.5	47.5	45.1	45.5
TiO_2	3.0	2.8	3.0	2.6	4.3	3.0	3.2	3.2	4.4	4.5
Al_2O_3	5.3	5.7	5.5	6.1	9.3	5.8	7.2	5.4	8.3	8.2
FeO	6.6	6.7	6.6	6.7	7.3	6.9	6.7	6.7	7.1	7.2
MnO	0.2	0.2	0.2	0.2	0.3	0.2	0.1	0.2	0.2	0.2
Cr_2O_3	0.0	0.1	0.0	0.1	0.1	0.1	0.0	0.1	0.0	0.1
MgO	13.5	13.4	13.3	13.5	11.6	13.5	12.9	13.1	11.8	12.0
CaO	22.6	22.4	22.8	22.6	22.6	22.6	22.6	22.5	22.7	22.6
Na_2O	0.5	0.6	0.6	0.6	0.6	0.6	0.6	0.5	0.6	0.6
K_2O	0.0	0.0	0.0	0.0	0.0	0.0	0.0	0.0	0.0	0.0
Total	99.9	99.6	100.3	100.6	100.1	100.7	99.9	99.3	100.1	101.0
mg #	0.79	0.78	0.78	0.78	0.74	0.78	0.77	0.78	0.75	0.75

All presented concentrations are in oxide wt% with O_2 determined by stoichiometry, all Fe is determined as FeO

Pyroxenes

Lava-unit	Plagioclase Basalt									
Sample	LP14SG09	LP14SG09	LP14SG09	LP14SG06	LP14SG06	LP14SG06	LP14SG06	LP14SG06	LP14SG06	LP14SG06
Mineral ID	CPX_4	CPX_5	CPX_6	CPX_1	CPX_2	CPX_3	CPX_4	CPX_5	CPX_6	CPX_7
Mineral Population	Rim	Rim	Rim	Rim	Rim	Rim	Rim	Rim	Rim	Rim
SiO_2	45.3	44.0	44.5	47.2	46.2	45.2	47.5	44.6	45.8	48.9
TiO_2	4.6	4.9	3.9	3.7	4.0	4.2	3.3	4.7	3.5	3.1
Al_2O_3	8.6	8.9	9.0	6.5	7.4	9.0	6.0	9.7	7.9	5.7
FeO	7.1	7.1	7.1	7.6	7.0	7.1	6.7	7.4	6.8	7.0
MnO	0.2	0.2	0.1	0.2	0.1	0.2	0.2	0.1	0.1	0.1
Cr_2O_3	0.0	0.1	0.0	0.0	0.0	0.0	0.1	0.1	0.0	0.0
MgO	12.1	11.5	12.0	12.2	12.3	12.1	13.0	11.8	12.4	13.5
CaO	22.8	22.4	22.4	22.5	22.9	22.6	22.7	22.8	22.7	23.1
Na_2O	0.7	0.7	0.7	0.6	0.6	0.6	0.6	0.7	0.7	0.6
K_2O	0.0	0.0	0.0	0.0	0.1	0.0	0.0	0.0	0.0	0.0
Total	101.4	99.7	99.7	100.7	100.6	100.9	100.1	101.9	100.0	102.0
mg #	0.75	0.74	0.75	0.74	0.76	0.75	0.78	0.74	0.76	0.77

All presented concentrations are in oxide wt% with O_2 determined by stoichiometry, all Fe is determined as FeO

Pyroxenes

Lava-unit			Plag Tephri-phonolite						
Sample	LP14SG06	LP14SG06	LP14SG05	LP14SG05	LP14SG05	LP14SG05	LP14SG05	LP14SG05	LP14SG05
Mineral ID	CPX_8	CPX_9	CPX_3	CPX_5	CPX_7	CPX_1	CPX_2	CPX_3	CPX_4
Mineral	Aggregate	Aggregate							
Population	Core	Core	Xeno-Core	Xeno-Core	Xeno-Core	Rim (S-Zone)	Rim (S-Zone)	Rim (S-Zone)	Rim (S-Zone)
SiO_2	50.0	47.7	45.0	45.9	45.7	45.8	44.0	43.8	45.8
TiO_2	1.8	1.8	3.2	2.9	3.1	3.3	3.7	3.9	3.1
Al_2O_3	4.4	5.9	7.6	7.2	7.5	8.1	9.2	9.2	7.8
FeO	5.3	5.7	12.4	10.1	12.4	9.2	9.3	9.3	8.9
MnO	0.1	0.1	0.5	0.3	0.5	0.3	0.3	0.3	0.2
Cr_2O_3	0.6	0.6	0.1	0.0	0.0	0.0	0.1	0.0	0.1
MgO	14.9	13.9	8.2	10.4	8.7	11.0	10.2	10.1	10.6
CaO	23.5	21.9	22.0	22.4	22.2	22.9	22.4	22.4	22.7
Na_2O	0.4	0.6	1.2	1.0	1.2	1.0	0.9	1.0	0.9
K_2O	0.0	0.0	0.0	0.0	0.0	0.0	0.0	0.0	0.0
Total	101.0	98.2	100.3	100.3	101.3	101.4	100.1	99.9	100.1
mg #	0.83	0.81	0.54	0.65	0.56	0.68	0.66	0.66	0.68

All presented concentrations are in oxide wt% with O_2 determined by stoichiometry, all Fe is determined as FeO

Pyroxenes

Lava-unit	Plagioclase Tephri-phonolite									
Sample	LP14SG05	LP14SG05	LP14SG05	LP14SG05	LP14SG05	LP14SG05	LP14SG05	LP14SG05	LP14SG05	LP14SG05
Mineral ID	CPX_5	CPX_6	CPX_7	CPX_1	CPX_3	CPX_4	CPX_5	CPX_6	CPX_7	CPX_7
Mineral Population	Rim (S-Zone)	Rim (S-Zone)	Rim (S-Zone)	Rim (S-Zone)	Rim (S-Zone)	Rim (S-Zone)	Rim (S-Zone)	Rim (S-Zone)	Rim (S-Zone)	Rim (S-Zone)
SiO_2	45.1	45.3	44.4	46.5	47.4	46.8	46.8	46.2	47.9	44.3
TiO_2	3.2	3.3	3.8	2.6	2.5	2.5	2.7	2.9	2.4	3.9
Al_2O_3	8.4	8.3	9.1	6.7	6.4	6.6	7.0	7.5	5.9	8.7
FeO	9.4	9.0	9.5	8.6	8.6	8.7	8.6	8.9	8.9	10.1
MnO	0.3	0.3	0.2	0.3	0.3	0.4	0.3	0.2	0.3	0.3
Cr_2O_3	0.1	0.0	-0.1	0.0	0.0	0.0	0.0	0.1	0.0	0.0
MgO	10.4	10.7	10.3	11.3	11.5	11.4	11.3	11.0	11.6	9.7
CaO	22.4	22.7	22.6	22.6	22.9	22.8	22.8	22.6	23.0	22.2
Na_2O	0.9	0.9	0.9	0.9	0.9	0.9	0.9	0.9	0.8	1.1
K_2O	0.0	0.0	0.0	0.0	0.0	0.0	0.0	0.0	0.0	0.0
Total	100.2	100.4	101.0	99.4	100.5	100.2	100.4	100.4	101.0	100.3
mg #	0.66	0.68	0.66	0.70	0.71	0.70	0.70	0.69	0.70	0.63

All presented concentrations are in oxide wt% with O_2 determined by stoichiometry, all Fe is determined as FeO

Pyroxenes

Lava-unit	Plagioclase Tephri-phonolite									
Sample	LP14SG04	LP14SG04	LP14SG04	LP14SG04	LP14SG04	LP14SG04	LP14SG04	LP14SG04	LP14SG04	LP14SG04
Mineral ID	CPX_1	CPX_2	CPX_1	CPX_1	CPX_1	CPX_2	CPX_3	CPX_3	CPX_4	CPX_4
Mineral Population	Xeno-Core	Xeno-Core	Rim (S-Zone)	Rim (S-Zone)	Rim (S-Zone)	Rim (S-Zone)	Rim (S-Zone)	Rim (S-Zone)	Rim (S-Zone)	Rim (S-Zone)
SiO_2	47.8	48.0	45.1	45.7	47.4	45.5	43.9	45.8	44.4	46.7
TiO_2	2.4	2.2	3.8	3.4	2.6	3.5	4.1	3.2	3.9	2.8
Al_2O_3	5.0	5.5	9.2	8.2	7.1	8.4	9.3	7.8	9.4	7.2
FeO	11.5	10.6	9.3	8.9	8.4	9.5	9.4	9.2	9.4	8.7
MnO	0.4	0.6	0.3	0.3	0.3	0.3	0.3	0.3	0.3	0.2
Cr_2O_3	0.1	0.0	0.1	0.0	-0.1	0.0	0.1	0.0	0.0	0.0
MgO	9.8	10.3	10.6	11.1	11.9	10.6	10.0	11.1	10.3	11.5
CaO	22.6	22.0	22.9	22.9	23.2	22.7	22.6	22.8	22.8	22.9
Na_2O	1.0	1.3	0.9	0.9	0.8	1.0	1.0	0.9	1.0	0.9
K_2O	0.0	0.0	0.0	0.0	0.0	0.0	0.0	0.0	0.1	0.0
Total	100.5	100.5	102.1	101.3	101.7	101.5	100.7	101.0	101.4	101.0
mg #	0.60	0.63	0.67	0.69	0.72	0.67	0.65	0.68	0.66	0.70

All presented concentrations are in oxide wt% with O_2 determined by stoichiometry, all Fe is determined as FeO

Pyroxenes

Lava-unit	
Sample	LP14SG04
Mineral ID	CPX_2
Mineral Population	Rim (S-Zone)
SiO_2	44.6
TiO_2	3.9
Al_2O_3	9.3
FeO	9.3
MnO	0.3
Cr_2O_3	0.0
MgO	10.1
CaO	22.7
Na_2O	1.0
K_2O	0.0
Total	101.1
mg #	0.66

All presented concentrations are in oxide wt% with O_2 determined by stoichiometry, all Fe is determined as FeO

Feldspars

Lava-unit	Glomerocrystic Ankaramite												
Sample	LP13SG29	LP13SG29	LP13SG29	LP13SG29	LP13SG29	LP13SG29	LP13SG29	LP13SG29	LP14SG08	LP14SG08	LP14SG08	LP14SG08	LP14SG08
Mineral ID	Plag_1	Plag_2	Plag_3	Plag_4	Plag_5	Plag_6	Plag_7	Plag_8	Plag_1	Plag_2	Plag_3	Plag_4	Plag_5
SiO_2	52.0	51.9	52.0	51.7	52.4	52.6	51.3	51.2	52.2	52.3	51.8	52.4	51.6
TiO_2	0.2	0.2	0.2	0.2	0.2	0.3	0.2	0.2	0.2	0.2	0.2	0.2	0.1
Al_2O_3	30.1	30.5	30.6	30.5	30.8	29.8	30.2	30.1	30.1	30.4	29.9	30.7	30.1
FeO	0.7	0.7	0.6	0.6	0.4	0.7	0.6	0.5	0.5	0.5	0.5	0.5	0.6
CaO	12.9	13.5	13.4	13.5	13.4	12.6	13.2	13.4	13.0	13.1	12.9	13.5	13.0
Na_2O	3.9	3.8	3.8	3.8	3.7	4.2	3.8	3.8	4.1	4.0	4.1	3.9	3.9
K_2O	0.4	0.3	0.3	0.3	0.3	0.4	0.3	0.3	0.3	0.3	0.4	0.3	0.3
Total	100.2	100.8	101.0	100.5	101.3	100.5	99.7	99.4	100.4	100.9	99.6	101.5	99.7
An (Mol%)	64.5	66.3	66.2	66.6	66.5	62.4	65.9	66.1	63.8	64.3	63.7	65.9	64.9

Lava-unit	Glomerocrystic Ankaramite	Plagioclase Basalt										
Sample	LP14SG08	LP14SG09	LP14SG09	LP14SG09	LP14SG09	LP14SG09	LP14SG09	LP14SG09	LP14SG09	LP14SG06	LP14SG06	LP14SG06
Mineral ID	Plag_6	Plag_1	Plag_2	Plag_3	Plag_4	Plag_5	Plag_6	Plag_7	Plag_8	Plag_1	Plag_2	Plag_3
SiO_2	52.4	53.0	53.6	53.2	53.9	53.2	53.3	52.7	53.1	53.2	53.9	53.9
TiO_2	0.2	0.2	0.3	0.1	0.2	0.3	0.2	0.2	0.1	0.2	0.2	0.1
Al_2O_3	30.6	29.4	29.9	29.6	29.9	29.6	29.4	29.2	29.5	29.6	30.1	29.9
FeO	0.6	0.3	0.4	0.3	0.4	0.4	0.3	0.2	0.3	0.3	0.3	0.4
CaO	13.3	12.0	12.2	12.2	12.0	12.1	12.1	12.1	12.0	12.1	12.2	12.1
Na_2O	3.9	4.5	4.5	4.4	4.6	4.5	4.6	4.4	4.5	4.4	4.5	4.6
K_2O	0.3	0.5	0.4	0.4	0.4	0.4	0.4	0.3	0.4	0.4	0.4	0.4
Total	101.3	99.8	101.2	100.2	101.3	100.4	100.4	99.2	100.0	100.3	101.6	101.3
An (Mol%)	65.2	59.6	59.9	60.6	59.2	59.5	59.4	60.2	59.7	60.4	60.2	59.5

All presented concentrations are in oxide wt% with O_2 determined by stoichiometry, all Fe is determined as FeO

Feldspars

Lava-unit	Plagioclase Basalt					Plagioclase Tephri-phonolite						
Sample	LP14SG06	LP14SG06	LP14SG06	LP14SG06	LP14SG06	LP14SG05	LP14SG05	LP14SG05	LP14SG05	LP14SG05	LP14SG05	LP14SG05
Mineral ID	Plag_4	Plag_5	Plag_6	Plag_7	Plag_8	Plag_1	Plag_2	Plag_3	Plag_4	Plag_5	Plag_6	Plag_7
SiO_2	53.0	53.4	52.4	53.4	53.0	57.1	54.7	58.6	55.6	60.3	57.5	55.4
TiO_2	0.2	0.2	0.2	0.2	0.2	0.1	0.1	0.1	0.1	0.1	0.2	0.2
Al_2O_3	29.1	29.2	29.5	29.8	29.6	26.7	28.0	26.0	28.0	25.3	25.9	27.9
FeO	0.3	0.4	0.3	0.4	0.3	0.4	0.3	0.3	0.4	0.2	0.5	0.3
CaO	11.8	11.8	12.4	12.3	12.0	8.3	10.4	7.5	9.8	6.7	7.4	10.0
Na_2O	4.5	4.5	4.3	4.4	4.4	6.3	5.4	6.8	5.7	7.3	6.6	5.5
K_2O	0.4	0.4	0.4	0.4	0.4	0.6	0.4	0.7	0.4	0.8	0.7	0.4
Total	99.3	99.9	99.4	100.9	99.9	99.5	99.3	99.9	100.1	100.7	98.6	99.8
An (Mol%)	59.3	59.2	61.5	60.6	60.1	42.2	51.8	38.1	48.5	33.6	38.3	50.0
						52.9	10.73					

Lava-unit	Plagioclase Tephri-phonolite								
Sample	LP14SG05	LP14SG04	LP14SG04	LP14SG04	LP14SG04	LP14SG04	LP14SG04	LP14SG04	LP14SG04
Mineral ID	Plag_8	Plag_1	Plag_2	Plag_3	Plag_4	Plag_5	Plag_6	Plag_7	Plag_8
SiO_2	55.8	55.6	55.9	54.8	55.5	54.8	56.1	55.4	54.0
TiO_2	0.1	0.0	0.2	0.1	0.1	0.1	0.1	0.1	0.1
Al_2O_3	28.3	28.6	28.2	29.4	28.5	29.3	28.7	29.1	29.8
FeO	0.3	0.4	0.4	0.4	0.4	0.4	0.4	0.3	0.4
CaO	10.1	10.6	10.1	11.2	10.5	11.4	10.5	10.9	11.8
Na_2O	5.6	5.4	5.6	5.0	5.4	4.9	5.4	5.2	4.7
K_2O	0.4	0.4	0.4	0.4	0.4	0.4	0.4	0.4	0.4
Total	100.6	101.1	100.7	101.4	100.8	101.1	101.6	101.3	101.1
An (Mol%)	50.1	52.0	50.0	55.4	51.9	56.0	51.6	53.8	58.2

All presented concentrations are in oxide wt% with O_2 determined by stoichiometry, all Fe is determined as FeO

Olivines

Lava-Unit	Glomerocrystic Ankaramite									
Samples	LP13SG29_	LP13SG29_	LP13SG29_	LP13SG29_	LP13SG29_	LP14SG08_	LP14SG08_	LP14SG08_	LP14SG08_	LP14SG08_
Mineral ID	OL_1	OL_2	OL_3	OL_4	OL_5	OL_1	OL_2	OL_3	OL_4	OL_5
Analysis Label	Aggregate Core	Aggregate Core	Aggregate Core	Aggregate Core	Aggregate Core	Aggregate Core	Aggregate Core	Aggregate Core	Aggregate Core	Aggregate Core
SiO_2	40.5	40.9	41.1	40.8	40.1	40.6	40.7	40.5	41.3	40.5
FeO	18.4	18.7	17.9	17.8	18.4	17.1	18.1	19.3	16.7	17.9
MnO	0.3	0.5	0.3	0.3	0.3	0.3	0.3	0.4	0.3	0.3
MgO	41.3	41.9	42.5	42.5	40.6	42.1	41.9	41.2	43.7	41.7
CaO	0.5	0.3	0.4	0.3	0.3	0.5	0.4	0.3	0.1	0.4
Ni	0.2	0.3	0.3	0.3	0.2	0.1	0.2	0.2	0.3	0.2
Total	101.2	102.5	102.5	102.0	100.0	100.5	101.5	102.0	102.4	100.9
mg #	0.80	0.80	0.81	0.81	0.80	0.81	0.80	0.79	0.82	0.81

Lava-Unit	Glomerocrystic Ankaramite									
Samples	LP13SG29_	LP13SG29_	LP13SG29_	LP13SG29_	LP13SG29_	LP14SG08_	LP14SG08_	LP14SG08_	LP14SG08_	LP14SG08_
Mineral ID	OL_1	OL_2	OL_3	OL_4	OL_5	OL_1	OL_2	OL_3	OL_4	OL_5
Analysis Label	Overgrowth Rim	Overgrowth Rim	Overgrowth Rim	Overgrowth Rim	Overgrowth Rim	Overgrowth Rim	Overgrowth Rim	Overgrowth Rim	Overgrowth Rim	Overgrowth Rim
SiO_2	40.0	40.3	40.2	39.1	40.2	39.9	39.8	39.6	40.5	39.2
FeO	21.0	21.5	21.8	21.7	19.7	21.4	21.7	22.2	20.9	21.3
MnO	0.4	0.4	0.5	0.3	0.3	0.4	0.4	0.3	0.4	0.4
MgO	39.7	39.5	38.5	37.1	40.5	38.8	38.8	38.2	40.4	38.2
CaO	0.4	0.5	0.4	0.5	0.4	0.5	0.4	0.5	0.3	0.4
Ni	0.1	0.2	0.3	0.0	0.2	0.1	0.0	0.1	0.1	0.1
Total	101.6	102.4	101.7	98.7	101.2	101.2	101.1	100.9	102.6	99.7
mg #	0.77	0.77	0.76	0.75	0.79	0.76	0.76	0.75	0.78	0.76

All presented concentrations are in oxide wt% with O_2 determined by stoichiometry, all Fe is determined as FeO

Olivines

Lava-Unit	Plagioclase Basalt								
Samples	LP14SG09_	LP14SG09_	LP14SG09_	LP14SG09_	LP14SG09_	LP14SG09_	LP14SG09_	LP14SG09_	LP14SG09_
Mineral ID	OL_1	OL_2	OL_3	OL_4	OL_5	OL_6	OL_7	OL_8	OL_9
Analysis Label	Core	Core	Core	Core	Core	Core	Core	Core	Core
SiO_2	39.6	39.6	39.6	39.3	39.2	39.5	39.4	39.4	39.6
FeO	25.2	24.9	25.1	24.6	25.2	25.1	24.7	24.9	23.6
MnO	0.6	0.5	0.4	0.6	0.6	0.4	0.7	0.5	0.4
MgO	36.0	36.6	36.4	36.5	36.5	36.7	36.8	36.4	37.4
CaO	0.5	0.5	0.5	0.5	0.5	0.5	0.5	0.5	0.4
Ni	0.1	0.1	0.1	0.1	0.2	0.1	0.0	0.0	0.1
Total	102.0	102.2	102.1	101.6	102.1	102.4	102.1	101.8	101.5
mg #	0.72	0.72	0.72	0.73	0.72	0.72	0.73	0.72	0.74

All presented concentrations are in oxide wt% with O_2 determined by stoichiometry, all Fe is determined as FeO

Spinel group minerals

Lava-unit	Glomerocrystic Ankaramite											
Sample	LP13SG29	LP13SG29	LP13SG29	LP13SG29	LP13SG29	LP13SG29	LP13SG29	LP13SG29	LP13SG29	LP14SG08	LP14SG08	LP14SG08
Mineral ID	Spin_1	Spin_2	Spin_3	Spin_4	Spin_5	Spin_6	Spin_7	Spin_8	Spin_9	Spin_1	Spin_2	Spin_3
TiO_2	18.2	18.7	18.6	19.0	19.5	19.5	17.8	20.1	15.5	18.6	19.4	21.5
Al_2O_3	9.1	9.0	9.6	8.5	8.0	9.5	9.5	7.8	10.6	8.6	8.2	7.8
Cr_2O_3	1.1	1.1	1.3	1.4	0.9	4.8	2.8	1.1	6.0	1.2	0.4	0.7
FeO	60.4	61.0	60.7	61.9	61.8	57.5	60.3	62.2	57.8	60.6	61.2	58.8
MnO	0.5	0.5	0.4	0.6	0.7	0.7	0.4	0.7	0.6	0.5	0.5	0.7
MgO	7.3	7.5	7.7	6.8	6.4	3.9	6.6	5.9	6.9	8.0	7.3	5.8
Total	96.6	97.8	98.3	98.2	97.3	95.9	97.5	97.8	97.4	97.4	97.0	95.3

Lava-unit	Glomerocrystic Ankaramite							Plagioclase Basalt			
Sample	LP14SG08	LP14SG08	LP14SG08	LP14SG08	LP14SG08	LP14SG08	LP14SG08	LP14SG09	LP14SG09	LP14SG09	LP14SG09
Mineral ID	Spin_4	Spin_5	Spin_6	Spin_7	Spin_8	Spin_9	Spin_10	Spin_1	Spin_2	Spin_3	Spin_4
TiO_2	19.5	18.6	18.7	19.5	19.0	20.2	20.0	24.8	24.6	25.0	24.6
Al_2O_3	8.1	8.8	8.6	8.1	8.4	7.9	7.2	5.5	5.8	5.6	5.7
Cr_2O_3	0.6	1.0	1.0	0.9	1.0	0.6	0.8	0.1	0.2	0.2	0.2
FeO	61.0	59.0	59.7	60.7	61.6	61.1	62.6	59.8	60.6	59.8	59.9
MnO	0.4	0.5	0.5	0.4	0.4	0.7	0.5	0.5	0.5	0.6	0.7
MgO	6.7	8.1	8.1	7.7	7.2	6.4	6.2	6.8	6.7	6.7	7.4
Total	96.3	96.0	96.5	97.3	97.5	96.8	97.1	97.4	98.4	98.0	98.3

All presented concentrations are in oxide wt% with O_2 determined by stoichiometry, all Fe is determined as FeO

Spinel group minerals

Lava-unit	Plagioclase Basalt											
Sample	LP14SG09	LP14SG09	LP14SG09	LP14SG09	LP14SG09	LP14SG06	LP14SG06	LP14SG06	LP14SG06	LP14SG06	LP14SG06	LP14SG06
Mineral ID	Spin_5	Spin_6	Spin_7	Spin_8	Spin_9	Spin_1	Spin_2	Spin_3	Spin_4	Spin_5	Spin_6	Spin_7
TiO_2	24.0	24.2	24.3	24.3	24.4	24.6	25.5	25.2	25.5	25.4	19.9	26.1
Al_2O_3	5.6	5.6	5.7	5.7	5.5	5.8	5.7	5.5	5.1	5.6	7.6	5.5
Cr_2O_3	0.1	0.1	0.1	0.0	0.1	0.1	0.1	0.1	0.0	0.1	0.1	0.1
FeO	59.1	59.5	59.6	59.4	59.5	59.7	61.0	60.8	60.1	60.4	61.6	61.3
MnO	0.5	0.6	0.5	0.5	0.5	0.6	0.7	0.7	0.7	0.6	0.4	0.9
MgO	7.1	6.9	7.1	7.4	7.1	6.1	5.5	4.8	5.2	4.8	8.2	4.3
Total	96.5	97.0	97.3	97.3	97.2	96.9	98.4	97.1	96.6	96.8	97.7	98.1

Lava-unit	Plagioclase Basalt	Plagioclase Tephri-phonolite								
Sample	LP14SG06	LP14SG05	LP14SG05	LP14SG05	LP14SG05	LP14SG05	LP14SG05	LP14SG05	LP14SG05	LP14SG04	LP14SG04
Mineral ID	Spin_8	Spin_1	Spin_2	Spin_3	Spin_4	Spin_5	Spin_6	Spin_7	Spin_8	Spin_1	Spin_2
TiO_2	23.7	15.9	15.9	16.4	16.2	16.7	16.0	16.2	16.4	16.3	16.4
Al_2O_3	7.5	2.6	2.6	2.6	2.5	4.3	4.2	4.3	4.5	4.9	5.0
Cr_2O_3	0.1	0.0	0.0	0.1	0.0	0.1	0.0	0.1	0.0	0.0	0.1
FeO	59.3	72.7	72.9	73.5	72.4	70.3	69.9	70.2	69.7	70.3	70.4
MnO	0.7	1.5	1.3	1.4	1.7	1.1	0.9	1.1	1.2	0.9	0.9
MgO	6.0	2.0	2.6	2.1	1.6	3.6	3.6	3.6	3.6	4.3	4.1
Total	97.3	94.8	95.2	96.1	94.4	96.0	94.6	95.4	95.4	96.6	96.7

All presented concentrations are in oxide wt% with O_2 determined by stoichiometry, all Fe is determined as FeO

Spinel group minerals

Lava-unit	Plagioclase Tephri-phonolite					
Sample	LP14SG04	LP14SG04	LP14SG04	LP14SG04	LP14SG04	LP14SG04
Mineral ID	Spin_3	Spin_4	Spin_5	Spin_6	Spin_7	Spin_8
TiO_2	17.1	17.1	17.4	16.9	16.7	17.1
Al_2O_3	5.6	5.6	5.8	6.0	6.4	5.7
Cr_2O_3	0.1	0.0	0.0	0.0	0.1	0.1
FeO	67.6	67.5	67.6	68.2	67.0	67.3
MnO	0.8	0.9	0.9	0.8	0.8	0.9
MgO	5.3	5.6	5.6	5.3	5.7	5.4
Total	96.5	96.6	97.2	97.3	96.5	96.4

All presented concentrations are in oxide wt% with O_2 determined by stoichiometry, all Fe is determined as FeO

El Time

Sample ID	LP13SG04	LP13SG17	LP13SG08	LP12SG13	LP12SG24	LP12SG17
Source	Barr. Jur.	Barr. Jur.	Barr. Jur.	Surf. Flow	Surf. Flow	Surf. Flow
Alternate	LP13SG33	LP13SG07	LP13SG07	LP12SG18	LP12SG18	LP12SG18
SiO_2	45.74	41.18	42.70	42.40	40.76	40.96
Al_2O_3	17.00	14.03	14.57	13.75	13.54	13.56
Fe_2O_3T	11.40	15.14	13.89	14.99	15.03	15.03
MgO	4.24	6.57	6.33	6.36	6.37	6.40
CaO	9.30	11.96	10.60	12.49	13.00	12.98
Na_2O	4.65	3.46	4.36	4.04	3.85	4.23
K_2O	1.92	0.69	1.06	0.82	1.20	0.83
TiO_2	3.42	4.31	3.84	4.30	4.27	4.28
MnO	0.21	0.21	0.22	0.20	0.20	0.20
P_2O_5	0.92	0.90	1.09	0.74	0.78	0.79
Total	99.34	99.11	99.32	100.68	99.74	99.88
LOI (%)	-0.12	0.50	1.10	0.06	0.37	0.36
Ni	5	51	51	68	71	71
Cr	3	58	63	45	35	34
V	221	305	315	407	438	446
Sc	13	18	18	25	23	23
Cu	23	81	82	110	147	146
Zn	114	127	126	119	122	117
As	1	1	1			1
S	41	138	136	181	467	144
Ga	22.3	24.2	24.0	23.4	23.6	23.8
Pb	4.1	5.4	4.5	2.6	3.1	3.6
Sr	1062	1116.0	1076.2	897	1152	973.7
Rb	40.4	22.7	17.5	12.5	35.6	30.5
Ba	556	595.6	595.7	499	666	597.4
Zr	345.5	461.8	443.2	299.1	276.2	280.1
Nb	91.7	111.1	106.2	81.1	87.0	85.5
Ta	4.7	6.0	6.5	4.6	5.2	4.5
Mo	1.7	2.9	2.7	2.2	2.7	1.5
Th	5.9	7.7	7.1	4.6	5.2	5.3
U	1.3	1.9	2.1	1.1	1.2	0.8
Y	34.8	37.8	35.2	28.6	28.3	29.1
La	69.1	77.3	76.0	55.0	56.1	56.8
Ce	133.7	152.7	154.2	108.7	109.3	109.3
Nd	62.2	74.8	72.1	55.4	54.4	57.6
Sm	12.8	13.8	13.2	11.1	11.0	11.4
Yb	2.7	3.0	3.6	2.0	2.1	2.0
Hf	7	7	6	7	6	7
Cs	2			1	1	

Major element (wt %) and trace element (ppm) compositions of samples from central La Palma lava-suites, determined by XRF. Barr. Jur. = Barranco Jurado, Surf. Flow = Surface Flow Barr. *= sample that did not originate from area of final study

El Time

Sample ID	LP12SG20	LP12SG21	LP12SG27	LP12SG28
Source	Surf. Flow	Surf. Flow	Taburiente	Taburiente
Alternate	LP12SG26	LP12SG27	*	*
SiO_2	41.90	41.08	43.41	43.15
Al_2O_3	14.87	13.68	11.93	11.77
Fe_2O_3T	14.61	14.84	13.91	14.03
MgO	6.10	7.19	10.52	10.85
CaO	11.54	11.85	12.02	11.87
Na_2O	3.98	4.12	2.58	2.77
K_2O	1.43	0.81	0.96	1.06
TiO_2	4.22	4.32	3.40	3.38
MnO	0.21	0.21	0.18	0.18
P_2O_5	1.00	0.88	0.55	0.54
Total	100.47	99.59	100.01	100.12
LOI (%)	0.00	0.43	0.17	-0.13
Ni	31	76	240	253
Cr	19	89	460	471
V	340	396	342	339
Sc	20	23	32	32
Cu	55	73	115	137
Zn	117	117	109	108
As				
S	423	93	75	46
Ga	22.2	23.1	19.7	19.5
Pb	4.3	4.6	3.1	2.3
Sr	981.8	1035.6	682.1	671.3
Rb	28.2	19.6	20.9	21.4
Ba	538.4	616.1	387.6	359.0
Zr	328.7	377.3	228.4	223.5
Nb	77.2	96.5	56.3	54.9
Ta	5.0	6.4	3.5	3.2
Mo	1.4	1.9	2.0	1.8
Th	4.9	6.4	3.4	3.4
U	0.5	1.0	0.5	0.4
Y	33.6	33.2	25.6	24.7
La	58.0	72.3	41.5	39.6
Ce	118.9	137.6	78.3	81.3
Nd	62.1	68.1	41.3	42.0
Sm	13.0	13.0	9.3	8.6
Yb	1.9	2.3	1.9	2.5
Hf	8	9	6	6
Cs		1	1	

Major element (wt %) and trace element (ppm) compositions of samples from central La Palma lava-suites, determined by XRF. Surf, Flow = Surface Flow Barr. *= sample that did not originate from area of final study

Bejenado

Sample ID	LP13SG36	LP13SG02	LP12SG80	LP12SG81	LP13SG18	LP13SG19
Source	Basal Ank	West Bej	West Bej	West Bej	LREVP-XPT	LREVP-XPT
Alternate	LP13SG38	LP13SG38?	LP13SG01	LP13SG01	LP13SG26	LP13SG26
SiO_2	42.56	43.39	42.08	41.98	42.77	44.89
Al_2O_3	12.04	11.37	14.18	12.74	14.49	16.65
Fe_2O_3T	14.72	13.64	13.59	13.93	13.71	11.69
MgO	11.08	11.83	7.13	9.24	6.15	4.23
CaO	11.40	11.02	11.49	11.08	10.45	10.00
Na_2O	2.25	3.09	4.63	4.19	4.53	4.25
K_2O	1.02	0.90	0.97	0.92	1.58	2.10
TiO_2	3.46	2.86	4.42	4.09	3.79	3.75
MnO	0.19	0.18	0.18	0.19	0.21	0.22
P_2O_5	0.57	0.51	0.76	0.79	1.09	0.85
Total	99.88	99.63	100.07	100.05	99.32	99.31
LOI (%)	0.23	0.50	0.76	0.73	0.50	1.50
Ni	283	320	77	182	63	25
Cr	439	508	100	261	65	31
V	333	287	396	364	390	313
Sc	28	24	23	24	24	11
Cu	34	106	122	107	102	44
Zn	115	105	98	115	109	119
As		1			1	
S	67	158	95	67	54	189
Ga	20.1	19.1	21.5	21.6	21.3	24.7
Pb	2.0	1.3	4.0	3.3	2.5	5.5
Sr	730	615.3	982.0	881.4	878.6	1510.3
Rb	19.2	20.8	38.0	26.6	82.0	80.3
Ba	346	367.6	684.8	499.4	562.2	826.2
Zr	227.9	178.2	320.5	347.5	316.2	485.0
Nb	56.9	51.6	80.8	82.2	80.1	157.3
Ta	3.0	2.0	4.3	4.7	5.3	10.2
Mo	1.2	1.7	2.4	2.4	2.0	2.4
Th	3.0	3.3	6.2	4.5	5.0	8.7
U	0.6	0.8	1.0	1.0	1.4	1.7
Y	23.6	21.8	27.9	27.7	30.2	42.7
La	38.0	33.6	71.2	52.1	62.8	98.0
Ce	76.8	69.5	130.0	107.5	123.0	188.2
Nd	40.6	35.6	61.8	56.4	61.0	84.3
Sm	7.8	6.1	12.3	11.4	10.1	15.1
Yb	2.6	3.6	2.3	1.4	2.6	3.0
Hf	4	4			7	8
Cs						2

Major element (wt %) and trace element (ppm) compositions of samples from central La Palma lava-suites, determined by XRF. Surf, Flow = Surface Flow Barr. Bas. Ank. = Basal Ankaramite, West Bej = West Bejenado LREVP = LREVP Xenolithic Pyroxene Tephrite. ? = slight uncertainty if sample is a duplicate

Bejenado

Sample ID	LP13SG20	LP13SG22	LP13SG24	LP13SG25	LP14SG03	LP13SG27
Source	LREVP-XPT	LREVP-XPT	LREVP-XPT	LREVP-XPT	LREVP-XPT	TSP A Teph
Alternate	LP13SG26	LP13SG30	LP13SG30	LP13SG26	LP13SG30	LP13SG28
SiO_2	47.07	48.97	47.43	42.02	42.51	48.49
Al_2O_3	18.32	18.37	17.77	15.01	11.86	18.37
Fe_2O_3T	8.98	8.29	9.78	13.70	14.45	9.47
MgO	3.35	2.19	2.90	5.65	11.98	3.70
CaO	7.60	7.15	8.40	11.44	11.56	7.10
Na_2O	6.30	6.40	5.58	3.91	2.58	6.06
K_2O	3.40	3.57	2.29	1.24	0.71	2.98
TiO_2	2.77	2.41	2.88	3.88	3.13	2.37
MnO	0.19	0.23	0.24	0.21	0.19	0.18
P_2O_5	0.81	0.55	0.80	1.02	0.55	0.93
Total	99.53	98.91	98.71	98.73	99.37	100.28
LOI (%)	0.42	0.42	1.01	0.84	0.80	0.33
Ni	18	9	9	32	304	24
Cr	16	10	9	27	545	28
V	218	151	185	305	321	169
Sc	5	5	6	17	31	7
Cu	35	16	19	77	138	25
Zn	109	129	134	112	103	112
As	1	1	1		1	
S	406	285	21	172	248	110
Ga	27.0	27.3	25.9	22.5	18.3	26.0
Pb	7.5	8.7	7.9	4.8	1.6	6.3
Sr	1358	1545.6	1476	1180.0	635	1234
Rb	97.9	114.3	69.2	61.5	18.5	82.6
Ba	910	1003.9	868	727.8	317	773
Zr	597.3	631.1	570.6	398.4	208.7	502.7
Nb	176.6	175.5	180.3	105.6	50.0	144.8
Ta	10.4	10.8	11.0	6.0	2.6	7.9
Mo	2.6	4.3	4.2	2.3	1.3	2.9
Th	11.0	11.6	11.4	7.4	3.0	9.5
U	2.9	3.1	2.7	1.8	0.6	2.2
Y	32.0	41.9	44.3	37.7	23.7	29.1
La	91.2	105.3	115.7	80.5	41.7	77.2
Ce	165.5	197.5	222.4	161.6	83.7	144.2
Nd	67.2	81.2	92.0	74.6	41.7	61.3
Sm	10.4	12.7	15.3	15.2	11.8	10.0
Yb	2.6	3.4	3.0	3.3	3.1	1.9
Hf	10	11	10	7	6	8
Cs	1	2	1	1		3

Major element (wt %) and trace element (ppm) compositions of samples from central La Palma lava-suites, determined by XRF. LREVP = LREVP Xenolithic Pyroxene Tephrite. TSP A Teph = Terminal Sheet Phase, Amphibole Tephrite, ? = there is uncertainty if sample is a duplicate

Bejenado

Sample ID	LP13SG14	LP13SG15	LP13SG35	LP14SG02
Source	TSP A Teph	TSP P-teph	Mon L Hie	Bej Sill
Alternate	LP13SG28	LP13SG16	LP14SG07	*
SiO_2	45.68	47.59	48.67	41.95
Al_2O_3	16.16	17.74	18.46	14.40
Fe_2O_3T	11.03	9.13	8.94	14.12
MgO	5.92	2.63	3.52	5.22
CaO	9.10	7.17	6.97	11.73
Na_2O	4.49	7.24	6.46	4.33
K_2O	2.27	3.48	2.09	1.40
TiO_2	3.04	2.74	2.33	4.16
MnO	0.19	0.22	0.18	0.25
P_2O_5	0.82	0.72	0.95	1.28
Total	99.30	99.53	99.18	99.58
LOI (%)	0.44	0.50	0.70	2.45
Ni	80	10	20	26
Cr	151	5	20	16
V	228	184	160	330
Sc	13	5	5	16
Cu	47	35	23	67
Zn	108	133	108	136
As	1	1	1	1
S	101	445	105	185
Ga	23.9	32.2	25.5	26.0
Pb	4.2	11.0	5.8	5.6
Sr	1070	1609.2	1195	1348.4
Rb	55.5	104.2	54.9	91.7
Ba	729	1090.9	776	763.3
Zr	400.9	883.1	496.8	579.8
Nb	120.8	207.2	142.3	141.0
Ta	6.6	10.9	7.6	8.6
Mo	1.9	2.8	3.2	1.8
Th	6.6	12.9	9.1	8.7
U	1.3	2.7	2.4	2.6
Y	29.2	38.0	29.4	38.1
La	68.0	105.7	78.5	91.3
Ce	121.5	191.4	141.9	184.4
Nd	57.9	77.9	61.0	90.3
Sm	9.8	14.5	11.6	17.7
Yb	1.7	2.5	2.2	2.9
Hf	7	14	8	7
Cs	2	2	1	1

Major element (wt %) and trace element (ppm) compositions of samples from central La Palma lava-suites, determined by XRF. TSP A Teph = TSP Amphibole Tephrite, TSP P-Teph = TSP Phono-tephrite, Mon L Hie = Montaña de la Hiedra, * = this sample is not a lava flow

cpx-melt thermobarometry: new data, LA-ICPMS analyses of groundmass, 22 May 2015, normalized to 100% (wt%)

Compositions of melts used for clinopyroxene-melt thermobarometry, directly determined from thin section of one clinopyroxene phenocryst. P and T calculated after Masotta et al. 2013

Sample	Melt comp.	SiO_2	TiO_2	Al_2O_3	FeO	MnO	MgO	CaO	Na_2O	K_2O	P_2O_5	Total
004_LP14SG05		54.66	1.31	20.83	4.50	0.16	0.99	3.64	8.94	4.74	0.23	100.00
005_LP14SG05		55.25	1.37	20.08	4.63	0.16	0.98	3.56	9.15	4.56	0.26	100.00
006_LP14SG05		54.68	1.45	20.23	4.92	0.16	1.04	4.24	8.56	4.44	0.28	100.00
007_LP14SG05		54.99	1.41	20.03	4.85	0.16	0.95	3.93	8.78	4.64	0.26	100.00
Average	Phonolite	54.90	1.39	20.30	4.73	0.16	0.99	3.84	8.86	4.59	0.26	100.00
RSD%		0.5	4.3	1.8	4.1	2.4	3.8	8.0	2.8	2.8	7.8	
010_LP14SG04		52.27	1.87	20.13	6.19	0.18	1.67	5.16	8.29	3.81	0.44	100.00
011_LP14SG04		52.89	1.79	20.05	6.01	0.17	1.62	5.19	8.09	3.75	0.43	100.00
012_LP14SG04		52.31	1.87	19.94	6.18	0.18	1.72	5.15	8.35	3.83	0.46	100.00
Average	Tephriphonolite	52.49	1.84	20.04	6.13	0.17	1.67	5.17	8.24	3.80	0.45	100.00
RSD%		0.7	2.6	0.5	1.7	1.9	2.8	0.4	1.6	1.1	3.7	
015_KLP5		54.29	1.42	20.57	4.90	0.17	1.00	3.58	9.28	4.55	0.24	100.00
016_KLP5		54.93	1.33	20.46	4.58	0.16	0.94	3.51	9.37	4.49	0.23	100.00
017_KLP5		54.25	1.33	20.91	4.55	0.16	0.95	3.74	9.24	4.51	0.35	100.00
Average	Phonolite	54.49	1.36	20.65	4.68	0.16	0.96	3.61	9.30	4.52	0.28	100.00
RSD%		0.7	3.7	1.2	4.2	3.0	3.3	3.2	0.7	0.6	24.8	
019_KLP6B		55.61	1.38	20.24	4.96	0.16	1.06	3.45	8.37	4.53	0.23	100.00
020_KLP6B		55.28	1.44	20.28	4.99	0.16	1.12	3.72	8.29	4.43	0.29	100.00
021_KLP6B		55.03	1.45	20.22	5.07	0.16	1.04	3.89	8.53	4.34	0.26	100.00
022_KLP6B		55.67	1.32	20.76	4.72	0.15	0.95	3.61	8.08	4.51	0.23	100.00
023_KLP6B		55.37	1.42	20.72	4.98	0.18	1.06	3.93	7.65	4.45	0.24	100.00
Average	Phonolite	55.39	1.40	20.45	4.94	0.16	1.05	3.72	8.18	4.45	0.25	100.00
RSD%		0.5	3.7	1.3	2.7	5.8	5.6	5.4	4.2	1.6	9.9	

All data in wt% with O_2 calculated by stoichiometry, all Fe is determined as FeO

cpx-melt thermobarometry: new data

Compositions of clinopyroxene rims used for cpx-melt thermobarometry. Each sample comprises the mean value of 5-20 analysed points of one clinopyroxene phenocryst. P and T calculated after Masotta et al. 2013

Sample	SiO_2	TiO_2	Al_2O_3	FeO	MnO	MgO	CaO	Na_2O	K_2O	Cr_2O_3	Total
KLP5-Cpx6-aver.	44.61	3.47	8.32	9.25	0.31	10.37	22.34	0.95	0.03	0.04	99.69
KLP5-Cpx8-aver.	44.82	3.44	8.25	9.30	0.28	10.40	22.42	0.90	0.03	0.08	99.92
KLP5-Cpx4-aver.	44.48	3.45	8.24	9.42	0.31	10.47	22.28	0.93	0.02	0.35	99.95
KLP5-Cpx5-aver.	44.85	3.38	8.34	9.35	0.33	10.39	22.36	0.94	0.04	0.04	100.02
KLP5-Cpx3-aver.	44.20	3.50	8.32	9.52	0.35	10.26	21.92	1.00	0.06	0.23	99.36
KLP5-Cpx1-aver.	44.97	3.25	8.02	9.14	0.29	10.39	22.18	0.91	0.03	0.53	99.69
KLP5-Cpx2-aver.	44.87	3.12	7.89	9.20	0.37	10.36	22.01	1.00	0.09	0.38	99.29
KLP5-Cpx7-aver.	45.02	3.32	8.32	9.70	0.34	10.31	22.23	0.97	0.04	0.48	100.73
LP14SG05-Cpx2-aver.	44.42	3.72	8.81	9.65	0.24	10.17	22.32	0.90	0.04	0.03	100.30
LP14SG05-Cpx3-aver.	47.36	2.36	5.82	10.38	0.40	10.32	22.10	1.13	0.04	0.04	99.94
LP14SG05-Cpx4-aver.	45.03	3.38	8.23	9.31	0.25	10.49	22.37	0.93	0.05	0.02	100.05
LP14SG05-Cpx5-aver.	45.12	3.46	8.09	9.46	0.26	10.60	22.36	0.92	0.03	0.03	100.33
LP14SG05-Cpx6-aver.	46.29	2.87	7.39	9.01	0.26	11.05	22.55	0.90	0.03	0.02	100.36
LP14SG05-Cpx7-aver.	45.96	2.99	7.53	9.12	0.24	10.93	22.57	0.91	0.03	0.02	100.31
LP14SG05-Cpx8-aver.	44.62	3.57	8.52	9.51	0.26	10.35	22.25	0.92	0.03	0.02	100.05
LP14SG05-Cpx10-aver.	46.69	2.72	6.78	9.24	0.28	11.09	22.41	0.87	0.04	0.03	100.13
KLP6B-Cpx1-aver.	46.06	2.84	7.38	9.22	0.28	10.98	22.34	0.88	0.01	0.00	99.99
KLP6B-Cpx2-aver.	46.21	3.02	6.63	10.63	0.41	10.01	21.85	1.09	0.02	0.01	99.88
KLP6B-Cpx3-aver.	45.23	3.35	8.24	9.54	0.29	10.51	22.30	0.92	0.02	0.01	100.40
KLP6B-Cpx4-aver.	44.96	2.94	7.17	11.47	0.44	9.06	22.16	1.11	0.03	0.01	99.36
KLP6B-Cpx5-aver.	45.87	2.85	6.78	11.58	0.48	9.22	21.78	1.16	0.02	0.00	99.73
KLP6B-Cpx6-aver.	45.25	3.26	7.99	9.33	0.28	10.50	22.25	0.91	0.02	0.00	99.80
LP14SG04-Cpx1-aver.	44.44	3.71	8.60	9.07	0.24	10.41	22.53	0.86	0.02	0.01	99.89
LP14SG04-Cpx2-aver.	43.76	4.01	9.03	9.73	0.29	9.95	22.12	0.89	0.02	0.00	99.80
LP14SG04-Cpx5-aver.	45.36	3.27	7.85	8.92	0.27	10.59	22.41	0.94	0.02	0.02	99.66
LP14SG04-Cpx3-aver.	45.64	3.21	7.43	9.23	0.27	10.77	22.50	0.94	0.02	0.01	100.01
LP14SG04-Cpx4-aver.	44.44	3.77	9.20	8.49	0.22	10.75	22.46	0.83	0.02	0.01	100.19

All data in wt% with O_2 calculated by stoichiometry

cpx-melt thermobarometry: published cpx compositions of Bejenado lavas (Gallip et al., 2006)interpreted by BEP stratigraphy

Sample	Strat Unit	SiO_2	TiO_2	Al_2O3	FeOt	MnO	MgO	CaO	Na_2O	K_2O	Cr_2O_3	Sum	Mg#	P(kbar)	P(GPa)	Temp °C
KLP6_Cpx5	Plag Basalt	45.52	3.98	8.63	7.62	0.10	11.87	22.10	0.60	0.0116	0.0068	100.4	73.5	5.69	0.57	1064.1
KLP6_Cpx1	Plag Basalt	45.63	4.00	7.39	7.70	0.16	11.96	21.95	0.58	0.0018	0.0110	99.4	73.5	5.50	0.55	1060.2
KLP6_Cpx6	Plag Basalt	46.69	3.53	6.60	7.48	0.14	12.44	21.77	0.53	0.0045	0.0160	99.2	74.8	5.04	0.50	1056.3
KLP6_Cpx2	Plag Basalt	44.15	4.12	8.97	7.77	0.14	11.54	21.57	0.57	0.0014	0.0098	98.8	72.6	5.59	0.56	1065.0
KLP6_Cpx3	Plag Basalt	47.56	3.45	6.67	7.69	0.18	12.66	21.90	0.56	0.0063	0.0173	100.7	74.6	5.25	0.53	1058.4
KLP6A_Cpx2	Plag Basalt	44.81	4.00	7.95	7.64	0.13	12.01	22.13	0.61	0.0033	0.0215	99.3	73.7	5.18	0.52	1063.2
KLP6A_Cpx9	Plag Basalt	45.53	3.91	7.07	7.63	0.14	12.21	22.07	0.62	0.0107	0.0115	99.2	74.1	4.61	0.46	1057.8
KLP6A_Cpx8	Plag Basalt	43.86	4.69	8.48	7.65	0.14	11.57	21.96	0.60	0.0035	0.0038	99.0	72.9	5.18	0.52	1064.5
KLP6A_Cpx3	Plag Basalt	44.53	3.96	8.47	7.51	0.14	11.87	22.04	0.62	0.0041	0.0063	99.2	73.8	5.31	0.53	1065.4
KLP6A_Cpx5	Plag Basalt	44.12	4.56	8.47	7.67	0.13	11.57	22.00	0.65	0.0043	0.0100	99.2	72.9	5.54	0.55	1067.0
KLP6A_Cpx6	Plag Basalt	45.82	3.92	7.08	7.42	0.16	12.24	22.16	0.58	0.0007	0.0197	99.4	74.6	4.88	0.49	1059.6
KLP6A_Cpx7	Plag Basalt	44.95	4.19	7.99	7.71	0.12	11.82	22.01	0.62	0.0043	0.0187	99.4	73.2	5.27	0.53	1064.5
KLP6A_Cpx4	Plag Basalt	44.79	3.86	8.41	7.65	0.13	12.03	22.06	0.61	0.0068	0.0112	99.6	73.7	5.22	0.52	1064.8
KLP6A_Cpx1	Plag Basalt	45.06	4.12	7.77	7.62	0.12	12.04	22.06	0.60	0.0128	0.0052	99.4	73.8	5.10	0.51	1062.6
KLP106_Cpx2	Trans GA to PB	43.86	4.05	9.22	8.11	0.11	11.51	21.76	0.62	0.0037	0.0258	99.3	71.7	6.47	0.65	1131.7
KLP106_Cpx1	Trans GA to PB	45.31	3.44	7.97	7.81	0.10	12.21	21.73	0.58	0.0045	0.0342	99.2	73.6	6.03	0.60	1126.2
KLP106_Cpx3	Trans GA to PB	45.06	3.47	8.26	7.84	0.11	12.16	21.67	0.59	0.0072	0.1422	99.3	73.4	6.15	0.61	1128.1
KLP106_Cpx4	Trans GA to PB	44.50	3.66	8.51	7.88	0.12	11.84	21.76	0.59	0.0059	0.0591	98.9	72.8	6.17	0.62	1127.9
KLP112_Cpx1	Glom Ank	44.60	3.57	9.21	7.60	0.08	11.54	21.88	0.67	0.0073	0.0400	99.2	73.0	6.17	0.62	1092.5
KLP112_Cpx2	Glom Ank	45.35	3.32	7.98	7.29	0.08	12.06	22.19	0.58	0.0072	0.0505	98.9	74.7	5.39	0.54	1083.2
KLP112_Cpx3	Glom Ank	45.60	3.21	7.90	7.42	0.09	12.08	21.99	0.58	0.0087	0.0247	98.9	74.4	5.36	0.54	1083.6
KLP112_Cpx4	Glom Ank	44.75	3.46	8.91	7.32	0.08	11.71	21.97	0.65	0.0082	0.0454	98.9	74.0	5.98	0.60	1090.1
KLP112_Cpx5	Glom Ank	45.82	3.36	7.89	7.48	0.10	12.11	22.21	0.60	0.0107	0.0268	99.6	74.3	5.49	0.55	1084.1
KLP113_Cpx2	Glom Ank	46.56	3.31	7.70	7.45	0.13	12.22	21.66	0.73	0.0047	0.0315	99.8	74.5	7.02	0.70	1109.0
KLP113_Cpx3	Glom Ank	44.61	3.64	8.72	7.70	0.11	11.79	21.41	0.70	0.0115	0.0585	98.8	73.2	6.96	0.70	1110.9
KLP113_Cpx1	Glom Ank	45.21	3.63	8.55	7.74	0.13	11.75	21.38	0.76	0.0066	0.0313	99.2	73.0	7.35	0.73	1113.7
KLP113_Cpx4_5	Glom Ank	45.22	3.58	8.10	7.70	0.12	11.94	21.51	0.70	0.0151	0.0389	98.9	73.4	6.89	0.69	1108.8
KLP113_Cpx6	Glom Ank	44.69	3.67	8.87	7.72	0.12	11.70	21.52	0.73	0.0046	0.0500	99.1	73.0	7.16	0.72	1112.4

Data in oxide wt%, O2 calculated by stoichiometry

cpx-melt thermobarometry: published melt compositions of Bejenado lavas (Gallip et al., 2006)interpreted by BEP stratigraphy

Sample	Loc.	SiO_2	TiO_2	Al_2O3	FeOt	MnO	MgO	CaO	Na_2O	K_2O	Total	Mg#
KLP6	Plag Basalt	48.06	3.40	18.02	9.55	0.19	3.01	7.70	6.53	3.16	99.6	36.0
KLP6A	Plag Basalt	49.48	3.32	18.40	8.94	0.20	2.86	7.38	5.69	2.82	99.1	36.3
KLP106	Trans GA to PB	46.98	4.09	16.83	11.01	0.19	3.99	9.72	4.12	2.26	99.2	39.2
KLP112	Glom Ank	46.31	3.79	16.93	10.05	0.13	3.21	8.47	5.44	3.00	97.3	36.3
KLP113	Glom Ank	46.67	3.72	17.24	10.84	0.19	3.70	8.95	5.19	2.56	99.1	37.8

Data in oxide wt%, O2 calculated by stoichiometry

APPENDIX D: SUPPLEMENTARY PETROLOGY — PETROGRAPHY OF SAMPLE GROUPS FROM *BEJENADO* USED IN CHAPTER 6

At *Bejenado*, the four petrological mineral assemblage groups described in Chapter 6 ("basanites and primitive lavas", "ankaramites", "amphibole tephrites" and "phono-tephrites and evolved foidites") were usually the product of combined descriptions of samples from two stratigraphically distinct eruptive units. This appendix is intended to provide detailed petrographic descriptions and interpretations of these individual units. Samples from the Bejenado Effusive Phase have not been included since these were described in detail in Chapter 5.

Samples that fall within to the "ankaramite" group have been identified both in the *Bejenado Lower Series* (the Basal Ankaramite) and in the BEP sequence's Glomerocrystic Ankaramite. Notably, the "basanites and primitive lavas" group is the only group with a single source, all having been taken from *West Bejenado*. Samples that correspond to the "amphibole tephrite" group have been identified within the LREVP unit and in samples from the less evolved TSP units. The "phono-tephrites and evolved foidites" correspond to the most evolved lavas from the TSP unit and those from the *Montaña de la Hiedra* vent cluster.

GROUPS OF SAMPLES FROM STRATIGRAPHIC ERUPTIVE PHASES:

1. Bejenado Lower Series: Basal Ankaramite ["ankaramites" group]
2. West Bejenado: opportunistic samples ["basanites and primitive lavas" group]
3. Los Rodeos Evolved and Volcaniclastic Phase ["amphibole tephrites" group]
4. Terminal Sheet Phase [both "amphibole tephrites" and "phono-tephrites and evolved foidites" group]
5. Montaña de la Hiedra ["phono-tephrites and evolved foidites" group]

1) BEJENADO LOWER SERIES: BASAL ANKARAMITE

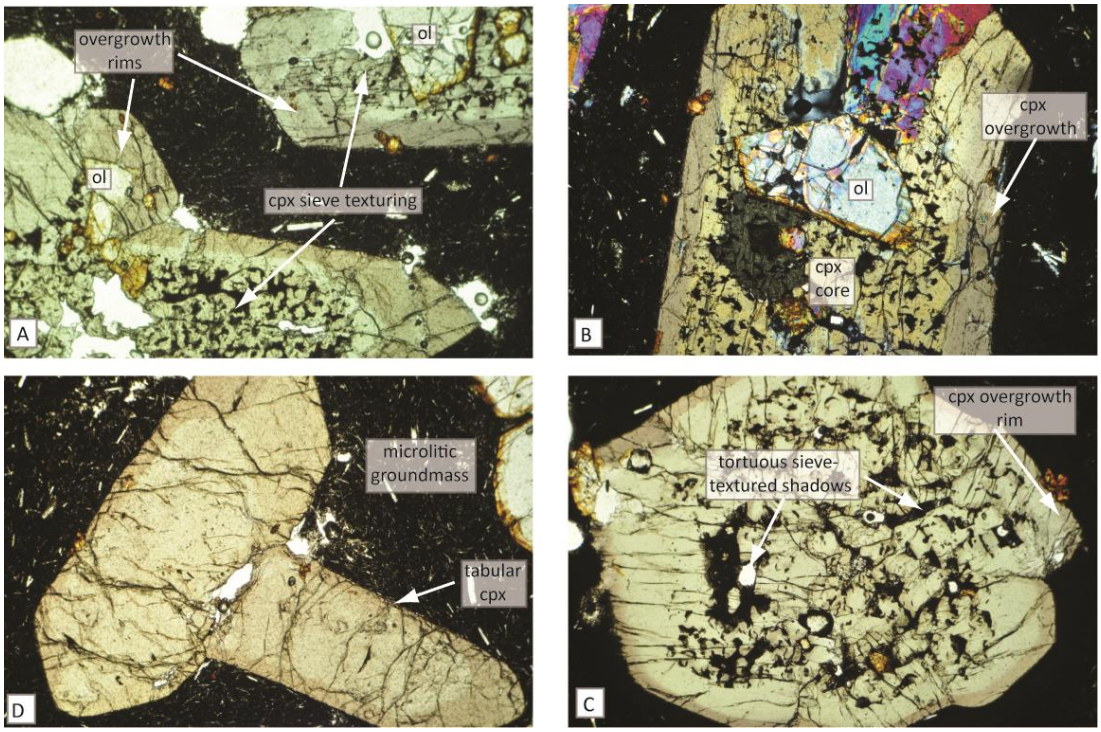

Figure A-1 Photomicrographs of textural variation in the sample of the Basal Ankaramite. A. Ankaramite with multiple glomerocrysts each with diopside cores enclosed in augite rims (PPL, FOV = 4.4mm). B. Glomerocryst formed of large, tabular, intensely sieve-textured, cpx enclosing euhedral olivine (XPL, FOV = 4.4mm). C. Glomerocryst formed of large tabular cpx crystals (PPL, FOV = 4.4mm). D. Cpx with intense, tortuous sieve-texturing (PPL, FOV = 4.4mm). PPL = plane polarised light, FOV = field of view, cpx = clinopyroxene, ol = olivine.

Samples: (LP13SG38)

DESCRIPTION

The lower of *Bejenado's* two ankaramitic lava-units, this was sampled close to the base of the post-collapse extrusive sequences in *Caldera de Taburiente*. The unit has many textural similarities to the later-erupted Glomerocrystic Ankaramite of the BEP flow-field. The characteristic feature of the Glomerocrystic Ankaramite is the presence of crystal aggregates where cores of multiple sieve-textured diopside crystals[36] are enclosed in well-preserved augite rims, and such aggregates are also common in the Basal Ankaramite (Figure A-1A-D). However the aggregates of this lower-most unit tend to be composed of tabular crystals that are generally larger (<5mm diameter), fewer in number (Figure A-1D) and better preserved than those of the Glomerocrystic Ankaramite. Sieve-texturing in this unit results in opaque shadows with amorphous tortuous shapes (< 40% of diopside area, Figure A-1A-B+D).

The groundmass enclosing these aggregates is microlitic and relatively crystal-poor. Plagioclase contents are low with smaller crystals than is typical in Glomerocrystic Ankaramite samples, while titanomagnetite is virtually absent.

[36] 5.4.1 Petrography of BEP lava-units. pp.108-110.

INTERPRETATION

This unit shares two key petrological features with the BEP's Glomerocrystic Ankaramite: 1) this is an ankaramite in which aggregates with augitic overgrowth rims enclose earlier-formed cores, 2) this unit exhibits an unusually strong DMM-like mantle-component signature, with the lowest radiogenic Pb and highest radiogenic Nd contents of all La Palma lavas so far studied (Figure 6-16). The aggregates mean that the same process model developed for the Glomerocrystic Ankaramite[37] can be used to explain the textures observed in this unit, having similarly resulted from the disruption of an olivine-diopside lithology by a pulse of primitive magma.

Since this unit shares both of these exotic features there is likely to be a common genetic relationship (either shared formation process, or resulting from a shared magma-batch) between the Glomerocrystic Ankaramite and the Basal Ankaramite. The depleted isotopic compositions, almost unique on sub-aerial La Palma, indicate that both ankaramites are likely to be the product of exotic processes that are only observed after the *Cumbre Nueva Collapse*.

[37] 5.5.1 Interpreting textures of individual BEP lava-units. pp.124-126.

2) *West Bejenado*: opportunistic samples

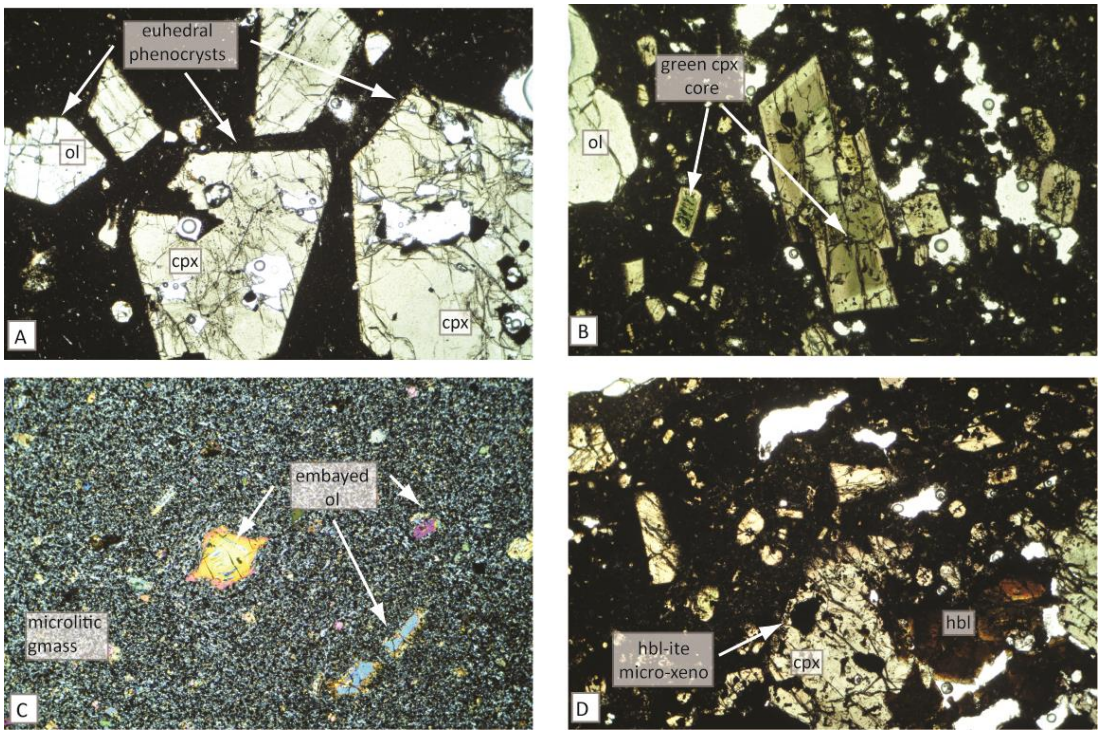

Figure A-2 Photomicrographs of textural variation among *West Bejenado* samples. A. Euhedral single crystals of ol and cpx in a microlitic groundmass (PPL, FOV = 4.4mm). B. Basanite with ol and green core cpx (PPL, FOV = 4.4mm). C. Embayed ol phenocrysts in microlitic groundmass (XPL, FOV = 4.4mm). D. Mafic micro-xenolith (probably hornblendite) in a microlitic groundmass (PPL, FOV = 4.4mm). PPL = plane polarised light, XPL = crossed polarised light, FOV = field of view, cpx = clinopyroxene, ol = olivine, hbl = kaersutitic amphibole, gmass = groundmass, micro-xeno = micro xenolith.

Samples: (LP12SG87, LP13SG01, LP13SG10, LP13SG11)

Description

In this group samples are largely primitive porphyritic lavas with clinopyroxene and titanomagnetite. Glomerocrysts are relatively rare with individual phenocrysts dominating mineral assemblages (Figure A-2A). Pyroxenes with evolved green cores are very common (Figure A-2B). Olivine content is variable, with euhedral crystals common in some samples while in others crystals are often embayed indicating resorption into the host magma (Figure A-2C). In spite of the absence of glomerocrysts, holocrystalline mafic micro-xenoliths of hornblendite/pyroxenite are often present (Figure A-2D). In all samples groundmasses are typically microlitic and plagioclase is largely absent.

Interpretation

While it cannot be verified without further field evidence, the compositional and petrological similarities shared by the opportunistic samples from *West Bejenado* leads us to interpret them all as the product of one laterally extensive eruptive unit. This proposed unit would be the only basanitic lava-flow on *Bejenado* with a young-HIMU isotopic signature. Within it, green core pyroxenes and cumulate-hornblendite micro-xenoliths provide strong evidence of magma mixing but otherwise this group is broadly characteristic of primitive lavas on La Palma.

3) Los Rodeos Evolved and Volcaniclastic Phase (LREVP)

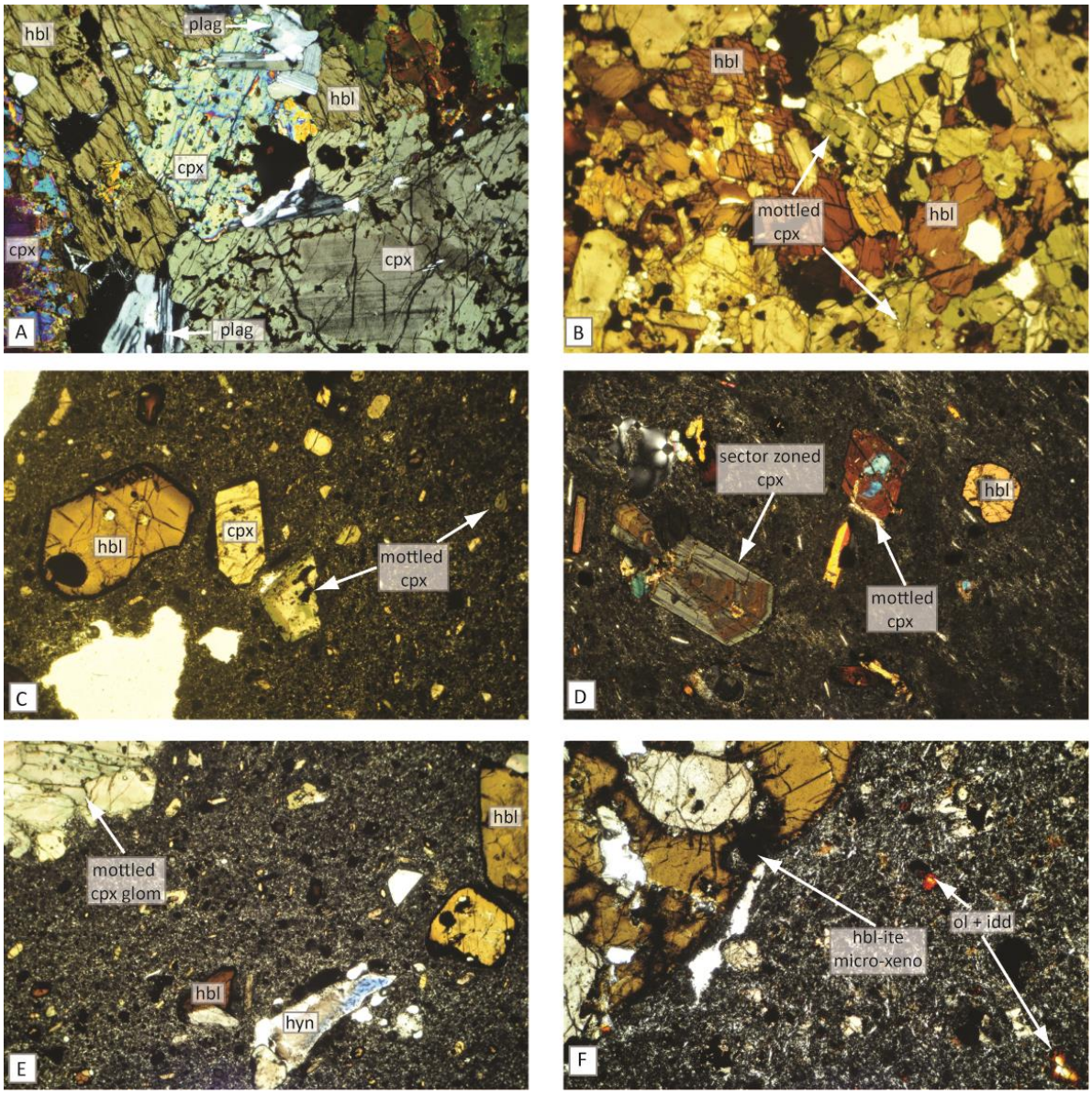

Figure A-3 Photomicrographs of textural variation among samples from Los Rodeos Evolved and Volcaniclastic Phase (*LREVP)* lavas and xenoliths. A. Granular, mafic hornblendite/pyroxenite xenolith containing hbl, cpx and plag (XPL, FOV = 4.4mm). B. Granular, mafic hornblendite/pyroxenite xenolith containing mottled cpx (PPL, FOV = 4.4mm). C. Tephrite with angular mottled cpx crystal and re-worked hbl (PPL, FOV = 4.4mm). D. Tephrite with sector zoned and mottled cpx (XPL, FOV = 4.4mm). E. Evolved tephrite with hyn and mottled cpx glomerocryst (PPL, FOV = 4.4mm). F Primitive tephrite with mafic micro-xenolith hosted in ol-containing groundmass (PPL, FOV = 4.4mm). PPL = plane polarised light, XPL = crossed polarised light, FOV = field of view, cpx = clinopyroxene, ol = olivine, hyn = hauyne, hbl = kaersutitic amphibole, idd = iddingsite, glom = glomerocryst, plag = plagioclase.

Samples: (LP13SG26, LP13SG30)

Description

The Xenolithic Pyroxene Tephrite lava-unit is characterised by lava flows with abundant mafic cumulate xenoliths (<5% volume). While these xenoliths have not been sampled and studied systematically, they are often mafic, granular clinopyroxene, kaersutitic amphibole lithologies (Figure A-3A-B) with titanomagnetite and accessory titanite and plagioclase feldspar.

Samples from the lava-units are porphyritic (<20% crystals) clinopyroxene, amphibole tephrites with minor olivine present in a microlitic groundmass. Clinopyroxenes often have angular surfaces and fractures and are a combination of augite and ferroan-diopside (Figure A-3C). However, rather than simple green-core pyroxenes these are often mottled between zones (Figure A-3C-D), a feature shared by pyroxenes in cumulate xenoliths (Figure A-3B). Furthermore, some pyroxenes show intense pyroxene sector zoning (Figure A-3D), while amphiboles are normally zoned with amber cores enclosed in darker rims. Accessory sodalite-group feldspathoids are present in the more evolved sample (Figure A-3E). Across the sample suite there is variation in proportions of amphibole to olivine. In the more primitive samples, amphibole is largely absent (although it remains present in micro-xenoliths) while phenocryst olivine shows heavy iddingsite formation (Figure A-3F).

INTERPRETATION

The varying amounts of olivine and amphibole between samples indicates that interaction between primitive and evolved magmatic units occurred somewhere in the magma supply system and contributed to this unit.

In this case, the xenoliths and evidence for mechanical re-working of crystals lead us to suggest that the assimilation of wall-rock material contributed to the unit's final composition. The population of mottled clinopyroxenes found in both the xenoliths and often within the lava samples appears to provide insights into these issues. Their presence in the pyroxenitic xenoliths indicates that they must have been the product of a specific secondary geological process (possibly metasomatism) that affected this wall-rock material at some point in its history, and they are sufficiently unusual as to provide us with a petrographic signature of this lithology. That these same mottled pyroxenes occur as fragmentary crystals within the LREVP lava-unit indicates that they are the product of material incorporated from the wall-rock. Furthermore, these clinopyroxene crystals are present in the most primitive LREVP lava samples without the amphibole that accompanies them in the hornblendite/pyroxenite, which we interpret as evidence that this mineral has been resorbed.

4) Terminal Sheet Phase (TSP)

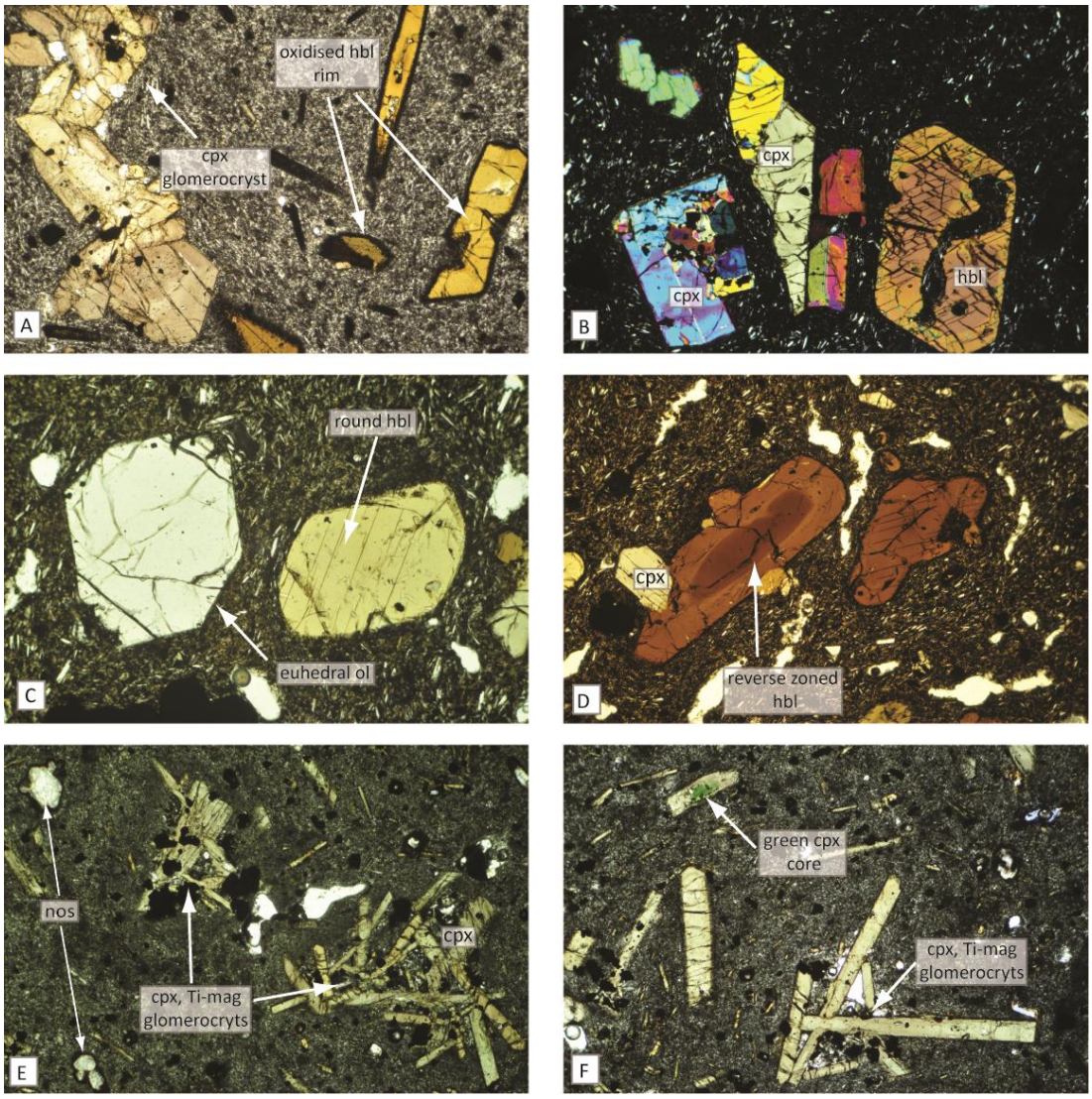

Figure A-4 Photomicrographs of textural variation among Terminal Sheet Phase (TSP) samples. A. TSP Amph Tephrite sample with non-holocrystalline glomerocryst and oxidised rims on hbl (PPL, FOV = 4.4mm).B. Amph Ol Tephrite sample with euhedral hbl and cpx phenocrysts (XPL, FOV = 4.4mm). C. Amph Ol Teph sample with euhedral ol and round hbl (PPL, FOV=2.2mm). D. Amph Ol Tephrite with reverse zoned hbl (PPL, FOV = 2.2mm). E. TSP Phono-tephrite sample with non-holocrystalline glomerocrysts of tabular cpx (PPL, FOV = 4.4mm). F. Green-core cpx and glomerocryst formed of tabular cpx crystals (PPL, FOV = 4.4mm). PPL = plane polarised light, XPL = crossed polarised light, FOV = field of view, cpx = clinopyroxene, ol = olivine, hbl = kaersutitic amphibole, nos = nosean, Ti-mag = titanomagnetite.

Description

Composed of three lava-units:

1. The TSP Amphibole Tephrite (LP12SG02, LP13SG28)
2. The Amphibole Olivine Tephrite (LP14SG10)
3. The TSP Phono-tephrite (LP13SG13, LP13SG16)

The three TSP lava-units are all characterised by mineralogies with clinopyroxene, titanomagnetite and accessory apatite. In addition, the Amphibole Tephrite (Figure A-4A) and the Amphibole Olivine Tephrite (Figure A-4B) each contain varying amounts of amphibole and olivine, although these

minerals are both absent from the feldspathoid-rich TSP Phono-tephrite. In all TSP lava-units mafic xenoliths are present but less abundant than in the LREVP lavas. Non-holocrystalline glomerocrysts are characteristic of all units (Figure A-4A+E-F).

Across all TSP lava-units there is a complicated relationship between the abundances of amphibole and olivine, since these mafic minerals are generally found and considered to be mutually exclusive but here appear to be jointly most common where there is the least clinopyroxene. This relationship is best observed in the samples from the Amphibole Olivine Tephrite (LP14SG10) where euhedral olivines are accompanied by round amphiboles (Figure A-4C), indicating both are broadly stable within their shared host magma, although in many other samples olivine is embayed. Reverse zoned amphiboles are present in LP14SG10 (Figure A-4D) indicating that at a late stage amphibole crystallisation occurred. In the Amphibole Tephrite samples where olivine is much less abundant, the amphiboles tend to be enclosed in fine iron oxide crystals (Figure A-4A).

Throughout all TSP lava-units clinopyroxenes are well-preserved, euhedral, augites that are either normally zoned or sector zoned. These are the most common mineral in the TSP Phono-tephrite, where they are often small and tabular with xenocrystic green cores (Figure A-4F). In this unit, non-holocrystalline glomerocrysts primarily composed of clinopyroxene are common and best described as crystal clots (Figure A-4E). While not present in these clots, phenocryst feldspathoid is abundant in the TSP Phono-tephrite and includes both sodalite-group minerals and square nepheline. In all samples, groundmasses can be either microlitic or plagioclase-rich with trachytic flow textures.

INTERPRETATION

The presence within this unit of both olivine and amphibole, each showing complex textural relationships to their host magmas, provides a mineralogical illustration of the hybridisation process between a primitive magma batch and an evolved magma batch (Figure 6-16) characteristic of this unit. For both primitive and evolved mineral populations the mixing process must have involved episodes of growth, resorption and re-crystallisation. Three mineral suites can be identified whose relative significance in samples is probably dependant on the differences in crystallisation conditions: 1) olivine-rich and basanitic, 2) tephritic and amphibole dominated and 3) clinopyroxene and feldspathoid dominated. It is notable that the glomerocryst population is non-holocrystalline, providing an indication that interstitial spaces were common in the evolved magma batch late in its crystallisation.

Of the TSP samples, the late-erupted Amphibole Olivine Tephrite has the most DMM-like and primitive composition. This leads us to suggest that throughout the eruption of the TSP there were variable proportions of the mingling components, and that this final lava-unit was the product of a greater proportion of the primitive DMM-like batch. This is strong evidence that the TSP was genetically related to the BEP flow-field and all were the product of a shared reservoir-system process.

5) *Montaña de la Hiedra*

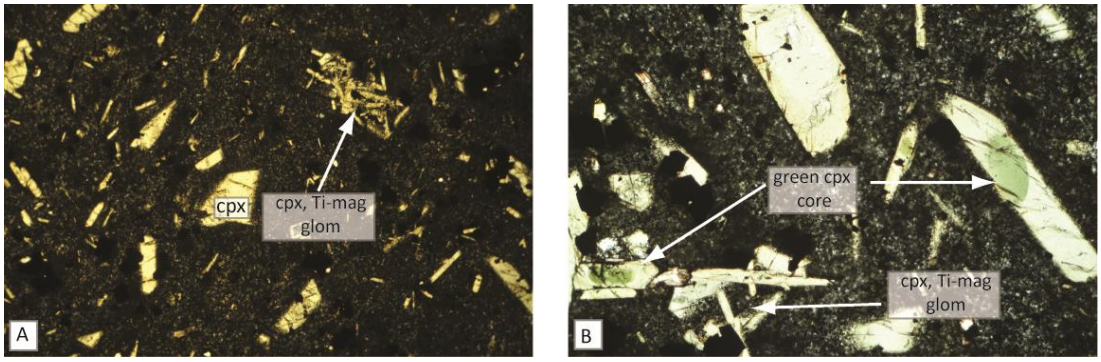

Figure A-5 Photomicrographs of textural variation among *Mantaña de la Hiedra* samples. A. Tephrite with seriate textured cpx and cpx glomerocryst (PPL, FOV = 4.4mm). B. Tephrite with green-core tabular cpx and glomerocryst (PPL, FOV = 2.2mm). PPL = plane polarised light, FOV = field of view, cpx = clinopyroxene, Ti-mag = titanomagnetite.

Samples: (LP13SG34, LP14SG10)

Description

Samples from this vent cluster are texturally very similar to samples from the TSP Phono-tephrite. *Montaña de la Hiedra* lavas also contain abundant clinopyroxene (Figure A-5A) with minor titanomagnetite and accessory apatite. Clinopyroxenes are often tabular with reverse zoned green cores common (Figure A-4B). Apatite is largely found enclosed in clinopyroxene or within the groundmass. Non-holocrystalline glomoerocrysts or crystal clots are common in this unit. These crystals are hosted in a microlitic groundmass. The only major difference between samples from these cones and those of the TSP Phono-tephrite is that feldspathoids are virtually absent in this unit.

Interpretation

Since these magmas are petrographically very similar to those of the TSP Phono-tephrite, and plot close to each other on *Bejenado's* main magma-hybridisation trend (Figure 6-16) it is reasonable to assume these are the product of separate vents erupting the same magma. If this is the case, then both units were likely the product of the same eruptive episode, providing further support for the model that *Bejenado* was the product of one continuous eruption or a single eruptive cycle.